Imperial College
London

Centre for Petroleum Studies

Department of Earth Science and Engineering

Well Test Analysis in Volatile Oil Reservoirs

Moshood Olajide Sanni

A Dissertation Submitted in Fulfilment of the Requirements for the
Degree of Doctor of Philosophy of the University of London
and the Diploma of Imperial College London

September 2008

ABSTRACT

This thesis discusses characterization of volatile oil reservoirs using well test analysis. For this purpose, typical well test behaviours were simulated with a one-dimensional single well compositional reservoir model, for different production rates; fluid composition and relative permeability curves, with bottomhole pressures above and below the bubble point pressure.

It was found that, when the bottomhole pressure falls below the bubble point pressure during a drawdown, a high gas saturation zone is created around the wellbore with two-phase (oil and gas) flow, whereas single phase (oil) with the initial gas saturation remains away from the wellbore. During the subsequent build-up, the gas created around the wellbore during the preceding drawdown condenses into the oil and the saturation in the near-wellbore region returns to the initial gas saturation. The log-log pressure-derivative behaviours below the bubble point correspond to a two-zone radial composite model, with decreasing mobility during drawdowns and increasing mobilities during build-ups. The log-log pressure derivative plot of the build-up reflects oil mobility distribution of the reservoir at the end of the preceding drawdown.

Knowledge obtained from the study was applied to the analysis of a well test in an actual volatile oil reservoir. Analysis results were validated with compositional reservoir simulation that included the effect of capillary number and non-Darcy flow.

Finally, factors affecting well deliverability in volatile oil reservoirs producing at flowing bottomhole pressure below bubble point pressure were studied. The result shows that end point relative permeability of oil phase and oil fluid composition are the most important factors affecting productivity of volatile oil reservoirs producing below bubble point pressure. This study suggests in volatile oil reservoirs, both vertical hydraulic fractures and horizontal wells are best implemented early in the wells life to delay the time when the flowing bottomhole pressure drops below the bubble point pressure, hence improving ultimate recovery.

ACKNOWLEDGMENT

I would like to express my gratitude to my supervisor, Professor A. C. Gringarten for his support and guidance during this project work.

I would also like to thank my colleagues in Joint Industry Project in Well Test Analysis group: Dr. Manijeh Bozorgzadeh, Dr. Thomas von Schroeter, Lekan Aluko, Amin Aram, Thabo Kgogo, Aliki Mavromoustaki, Ahmed Dahroug and Ioannis Papagiannakopoulos, for their valuable comments and assistance during this work.

Further, I would like to acknowledge the support of the Joint Industry Project funded by the UK Department of Trade and Industry, Total, ENI, Petrom, BG, PetroSA, Burlington and ConocoPhillips.

My sincere appreciation to my financial sponsor, Petroleum Technology Development Fund (PTDF) Nigeria.

Finally, I would like to dedicate this effort to my family, parents, brothers and all my friends too numerous to mention.

CONTENTS

LIST OF TABLES

LIST OF FIGURES

NOMENCLATURE AND ABBREVIATIONS

A cross sectional area

a empirical constant in $\frac{k_o}{\mu_o B_o} = ap$ relationship

BHP bottomhole pressure

B_α formation volume factor for phase α

BU build-up. This flow period corresponds to zero production rate. The preceding number is the flow period during well test

c compressibility

C_A shape factor

DD drawdown. This flow period correspond to production period. The preceding number represent the flow period during well test.

EOF engineering oil field

EOS equation of state. This shows relationship of state properties (pressure, volume and temperature) of the reservoir fluid

FBHP flowing bottomhole pressure

GOR gas to oil ratio

h formation thickness

IPR inflow performance relationship

K absolute permeability

K_{eff} effective reservoir pressure

K_r relative permeability

K_α effective permeability of phase α

$K_{r\alpha}$ relative permeability of phase α

$K_{r\alpha max}$ maximum relative permeability of phase α

K_r* end point relative permeability

l length

L well length

m slope of the infinite acting semilog straight line

MCN multiple carbon number

MW molecular weight

N_c capillary number. This is as defined as $\frac{k\|\nabla \Phi\|}{\phi\sigma}$ for this project.

N_g number of pseudo components

N last carbon group number

Q_i production rate for flow period i

P pressure

P_{av} average reservoir pressure

P_i initial reservoir pressure

PI productivity index

P_{bub} bubble point pressure

P_c critical pressure

P_D dimensionless pressure change

P-T pressure temperature

PVT pressure volume temperature

R_s solution gas /oil ratio

r_i radius of Investigation

r_l radius of composite discontinuity

R_v dissolved oil/gas ratio

S skin

S_α saturation of α phase

S_{gc} critical gas saturation

S_r residual saturation

S_t total skin

$S_{r\alpha}$ residual saturation of α phase

t_D dimensionless elapsed time

T_r reservoir temperature

W total volume of injected fluid/water

Greek

μ viscosity

v velocity

ϕ porosity

ρ density

β factor representing the inertia/turbulence or non-Darcy flow effect.

ε Corey exponent that fixes the curvature of the relative permeability function

λ_α mobility ratio of α phase defined as $\left(\frac{k_{r\alpha}}{\mu_\alpha}\right)$

σ interfacial tension

Subscripts

α phase

g gas

I immiscible

M miscible

o oil

t total

eff effective

const-cumm constant cumulative production

CHAPTER 1
INTRODUCTION

Well tests have been used for many years to assess well condition and obtain reservoir parameters. They remain a very important component of the reservoir management process for reservoir characterization and evaluation of well performance.

As hydrocarbon exploration moves to deeper geological formations, volatile oil and gas condensate reservoirs have become increasingly more common. Well tests in volatile oil reservoirs below the bubble point pressure, and in gas condensate reservoirs below the dew point pressure, however, are usually difficult to interpret, because they add the complexity of the fluid behaviour to the complexities of the geology and of the well (Gringarten *et al.*, 2006). Two important characteristics of fluid behaviour are multiphase flow and capillary number effects.

A better understanding of well test behaviours in volatile oil reservoirs is therefore required to better manage production in such reservoirs. This research work uses numerical compositional simulations to identify typical well test behaviours in volatile oil reservoirs below the bubble point pressure. Results are then applied to actual well test data.

1.1 Multiphase Well Test Analysis

Definitions of volatile oil from different authors are summarized in *Table 1-1*. Volatile crude oils contain relatively few heavy hydrocarbon molecules and more intermediate ones compared to black oil. Quality lines in volatile crude oils are closer to one another near the bubble point and more widely spaced at lower pressures than in black oils, hence, volatile oils produce more gas than black oil for the same pressure drop below the bubble point (*Figure 1-1*). They are also characterized by high liquid shrinkage immediately below the bubble point (*Figure 1-2*). In a constant temperature depletion experiment, oil viscosity decreases with decreasing pressure due to the volumetric expansion of oil, until it reaches a minimum value at the bubble point pressure.

Reducing the pressure below the bubble point leads to a net increase in oil viscosity due to liberation of the solution gas until dead oil viscosity is reached at atmospheric pressure (Khan, 1987).

Table 1-1 Literature definitions of volatile oil

Author	Definition	API	GOR (scf/stb)	Bo (rb/stb)	Colour
Whitson and Brulé (2000)	High GOR, High shrinkage to 50%	Greater than 35°	Between 1,000 and 3,000	Greater than 1.5	
Moses (1986)	High shrinkage immediately below the bubble point pressure. Shrinkage can go as high as 45%	Usually 40° or higher	Between 2,000 and 3,500	2.0 or Higher	
Ahmed (1989)	Produce more gas than black oil for same pressure drop	Between 45° to 55°	Between 2,000 and 3,500	Approxi mately 2.0	Greenish to orange colour
McCain (1990)	Relatively fewer heavy molecules and more intermediates	Greater than or equal 40°	Between 2,000 and 3,300	Greater than or equal to 2.0	Brown, Orange or green

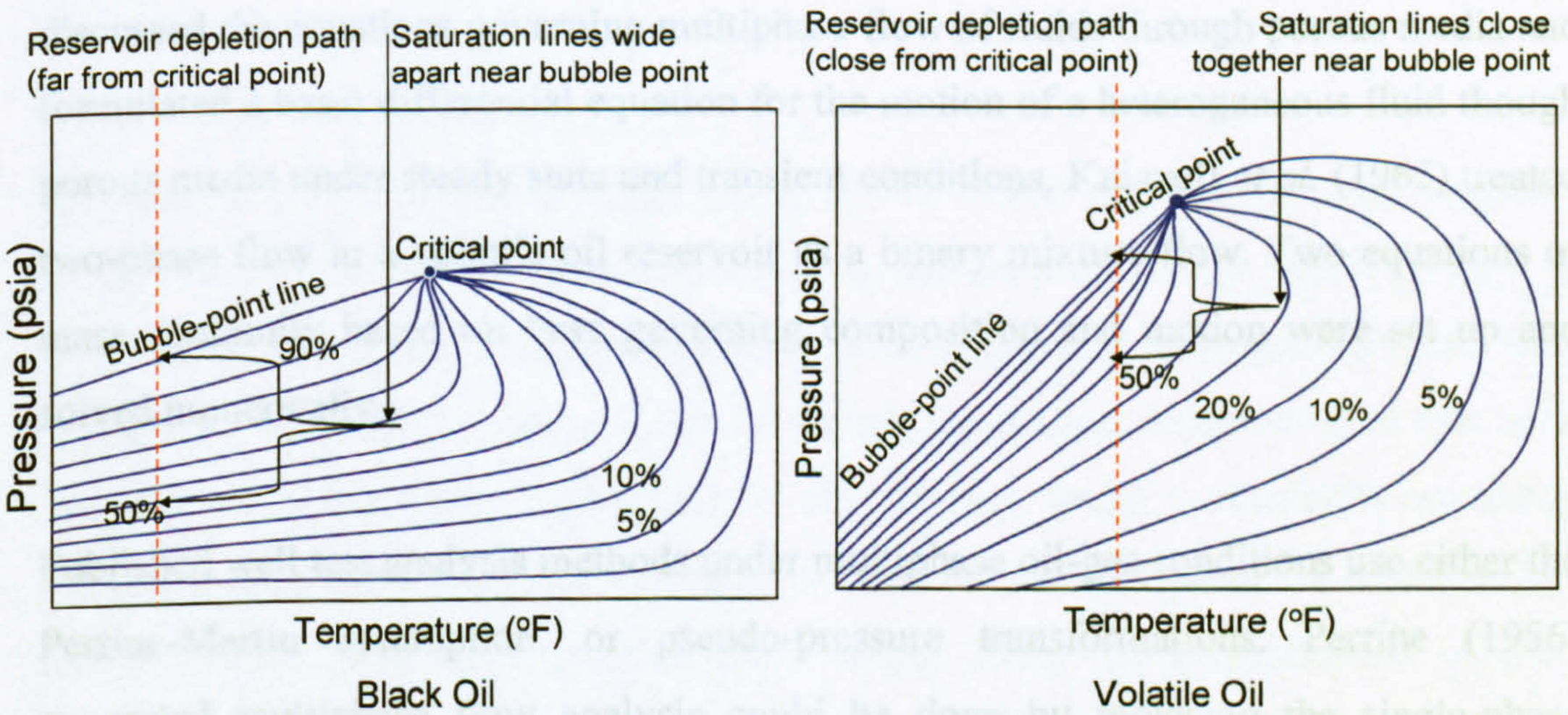

Figure 1-1 Pressure-temperature phase envelope for black oil and volatile oil (Ahmed, 1989)

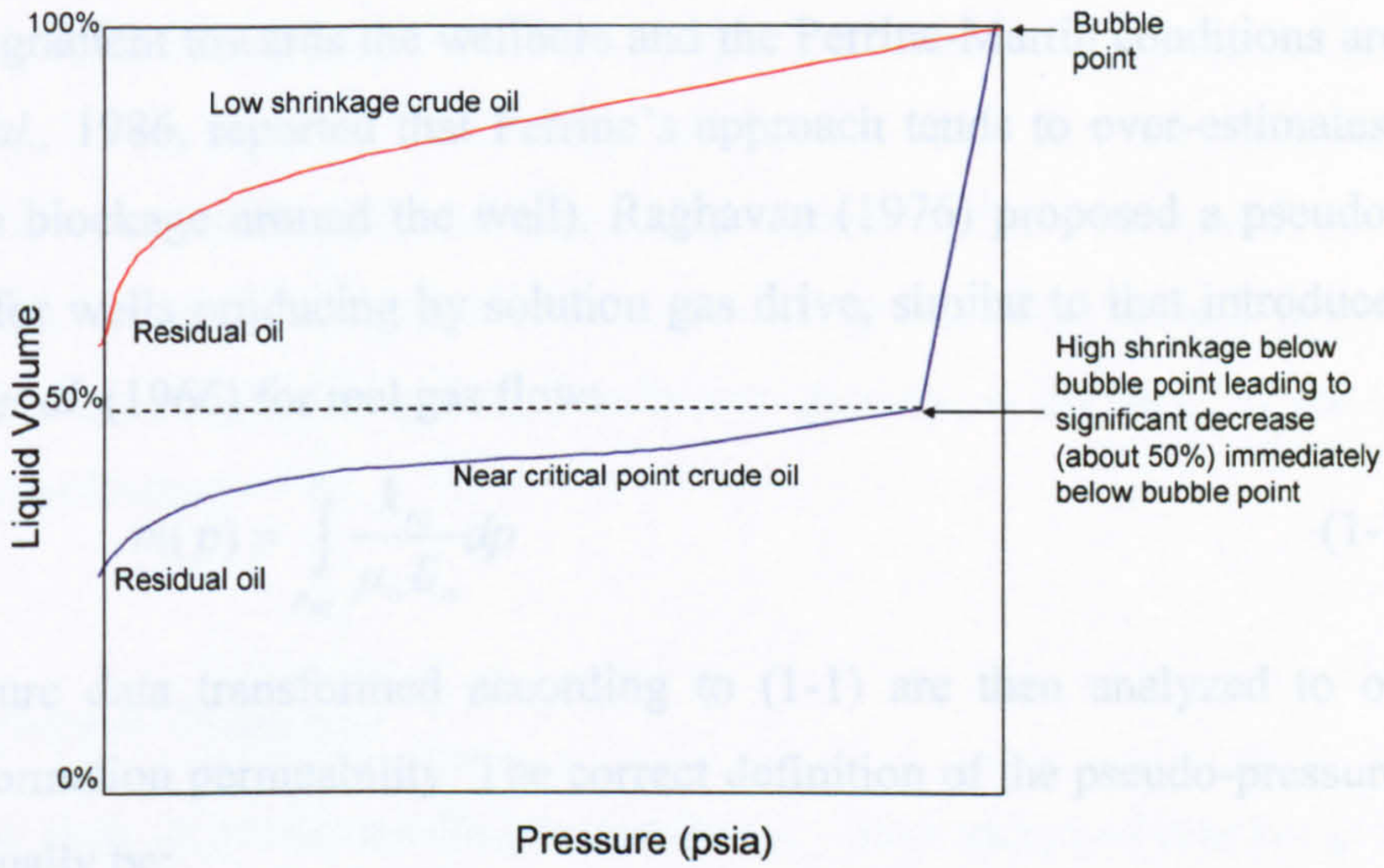

Figure 1-2 Shrinkage curve for crude oil system (Ahmed, 1989)

Below the bubble point pressure, multiphase flow dominates, and fluid relative mobility and reservoir heterogeneities control the performance (Archer and Wall, 1999). Relative mobility depends on the relative permeability curve, phase viscosity and average saturation (Cobenas and Crotti, 1999). Muskat and Meres (1963) discussed the equations governing multiphase flow of fluids through porous media and formulated a basic differential equation for the motion of a heterogeneous fluid though porous media under steady state and transient conditions. Kniazeff *et al.* (1965) treated two-phase flow in a volatile oil reservoir as a binary mixture flow. Two equations of mass continuity based on laws governing composition and motion were set up and solved numerically.

Published well test analysis methods under multiphase oil-gas conditions use either the Perrine-Martin assumption, or pseudo-pressure transformations. Perrine (1956) suggested multiphase flow analysis could be done by replacing the single-phase compressibility and mobility with the sum of compressibilities and mobilities for each phase, respectively. Perrine's method, based on empirical observations, assumes that the different phases are uniformly distributed, with uniform saturations and permeabilities for each phase. Martin (1959) verified Perrine's hypothesis in the case of small saturation gradients.

In the case of a volatile oil below the bubble point pressure, however, there is a high saturation gradient towards the wellbore and the Perrine-Martin conditions are not met (Ayan *et al.,* 1986, reported that Perrine's approach tends to over-estimates the skin due to gas blockage around the well). Raghavan (1976) proposed a pseudo-pressure approach for wells producing by solution gas drive, similar to that introduced by Al-Hussainy *et al.* (1966) for real gas flow:

$$m(p) = \int_{p_{ref}}^{p} \frac{k_{ro}}{\mu_o B_o} dp \qquad (1\text{-}1)$$

The pressure data transformed according to (1-1) are then analyzed to obtain the absolute formation permeability. The correct definition of the pseudo-pressure integral should actually be:

$$m(p) = \int_{P_{ref}}^{P_i} \frac{k_o \rho_o}{\mu_o} dp \qquad (1\text{-}2)$$

to obtain a valid Darcy continuity equation:

$$\frac{1}{r}\frac{\partial}{\partial r}\left(\frac{k_o \rho_o}{\mu_o} r \frac{\partial p}{\partial r}\right) = \phi c_t \rho_o \frac{\partial p}{\partial t} \qquad (1\text{-}3)$$

where Darcy flow velocity is defined as:

$$u = \frac{k_o}{\mu_o}\frac{\partial p}{\partial r} \qquad (1\text{-}4)$$

Raghavan's pseudo-pressure transformation was based on Evinger and Muskat's multiphase flow equation for calculating a theoretical productivity factor. Evinger *et al.*'s solution (1942) assumed steady state flow conditions for heterogeneous fluid flow in order to simplify their formulation (although the authors acknowledged that such conditions did not exist in practice). It also used a single permeability-saturation relationship, because of the unavailability of other data at the time of the research. The authors warned that these simplifications might affect the generalization of their formulation. Al-Khalifah *et al.* (1987) developed a diffusivity equation for multiphase well testing in terms of pressures squared:

$$\frac{\partial^2 p^2}{\partial r^2} + \frac{1}{r}\frac{\partial p^2}{\partial r} = \frac{\phi c_t}{\lambda_t}\frac{\partial p^2}{\partial t} \qquad (1\text{-}5)$$

which was then linearised using Raghavan's pseudo-pressure by assuming a linear relationship between pressure (p) and ($k_{ro}/\mu_o B_o$), which is only approximately true (Fetkovich, 1973). Serra *et al.* (1990a, 1990b) also used flowing wellbore pressure squared and semilog analysis for estimating effective phase permeabilities and skin effects. This approach is limited to low producing time and invalid for volatile oil reservoir below the bubble point, due to the continuous increase in gas saturation around the wellbore.

1.2 Capillary Number

Multiphase flow in porous media commonly uses the concept of relative permeability functions. When fluid is near-critical, the multiphase flow relative permeabilities depend on interfacial tension and superficial velocity (Blom *et al.*, 2000). Bardon *et al.* (1980) considered the impact of very low interfacial tension on relative permeability. They found that during displacement of gas in an oil-bearing formation, multiple transfers occur between the liquid and vapour phases so that complete miscibility may be achieved. As this occurs, the interfacial tension between the two phases reduces progressively to zero.

Fulcher *et al.* (1985) studied the effect of the capillary number, a dimensionless group representing the ratio of viscous to capillary forces, on two-phase relative permeability curves. They also verified the shift of the relative permeability from immiscibility towards miscibility as interfacial tension reduces to zero. Blom *et al.* (2000) re-defined the capillary number (N_c) as:

$$N_c = \frac{k\|\nabla \Phi\|}{\phi\sigma} \qquad (1\text{-}6)$$

Their experiments, using methanol/n-hexane to represent a near-critical gas/condensate or gas/volatile oil system, showed that the near-critical relative permeability depends on the capillary number at the pore scale (Blom *et al.* 2000). As initial reservoir conditions in gas condensate and volatile oil reservoirs are often near critical, the physical properties of the oil and gas phases are very similar and the interfacial tension between the phases is very low.

Blom *et al.* (1998) suggested that this may have an important bearing on the multi-phase flow characteristics in the reservoir during production.

In gas condensate reservoirs with bottomhole pressure below the dew point pressure, high capillary numbers, obtained for high flow rate or low interfacial tension, have been shown to compensate for the productivity losses due to the creation of a condensate bank around the wellbore (Gondouin *et al.* 1967).

There has been no study, however, on the effect of the capillary number in volatile oil reservoirs. A number of published papers show that capillary number effects may exist with two-phase hydrocarbons other than gas condensate and volatile oil reservoirs.

Talabi *et al.* (2003) examined the effect of depletion rate and oil viscosity on gas mobility during solution-gas drive in three viscous oils. They showed that relative permeability to gas was a function of both gas saturation and oil viscosity; and that gas mobility was low and decreased as oil viscosity or depletion rate (combined in a depletion index) increased. They did not consider the interaction between rate and viscosity.

Ostos *et al.* (2004) conducted an experiment to investigate the capillary number effect in heavy oil solution gas drive and its relationship to gas-oil relative permeability. They showed that the oil produced was a unique function of the capillary number and observed no additional improvement beyond a critical value. They also found that the oil relative permeability increases and gas relative permeability decreases with increasing capillary number. Their research suggested that gas-oil relative permeability correlations should incorporate the effect of capillary number in order to predict production in heavy oil solution gas drive.

Bardon *et al.* (1980) found that a reduction in interfacial tension increases the oil relative permeability at constant gas saturation in an oil-gas drainage cycle of the Fontainebleau formation (*Figure 1-3)*

Rowlison *et al.* (1982) described similarities in thermodynamics of near-critical fluids, hence creating a strong basis to investigate effect of capillary number in volatile oil reservoirs. Definitions of capillary number from different authors are summarized *Table 1-2.*

Table 1-2 Literature definition of the capillary number (N_c) ((Blom *et al.* 2000)

Leverett (1939)	$N_c = \sqrt{\frac{k}{\phi}\frac{\|\nabla p\|}{p_c}}$
Brownell and Katz (1947)	$N_c = \frac{k\|\nabla p + \rho g\|}{\sigma \cos\theta}$
Ehrlich *et al.* (1974)	$N_c = \frac{k\|\nabla p\|}{\phi\sigma}$
Larson *et al.* (1981)	$N_c = \frac{k\|\nabla p\|}{\sigma}$
Moore and Slobod (1956)	$N_c = \frac{\mu\|u\|}{\sigma \cos\theta}$
Saffman and Taylor (1958)	$N_c = \frac{\mu\|u\|}{\sigma}$
Foster (1973)	$N_c = \frac{\mu\|u\|}{\phi\sigma}$

This research investigates the existence of effect of capillary number and non-Darcy flow in volatile oil reservoirs below the bubble point pressure.

To study the saturation and mobility distributions around the well when the bottomhole pressure falls below the bubble point pressure, well test behaviours were simulated with a one-dimensional single well compositional reservoir model, for different production rates; fluid composition and relative permeability curves, with bottomhole pressures above and below the bubble point pressure

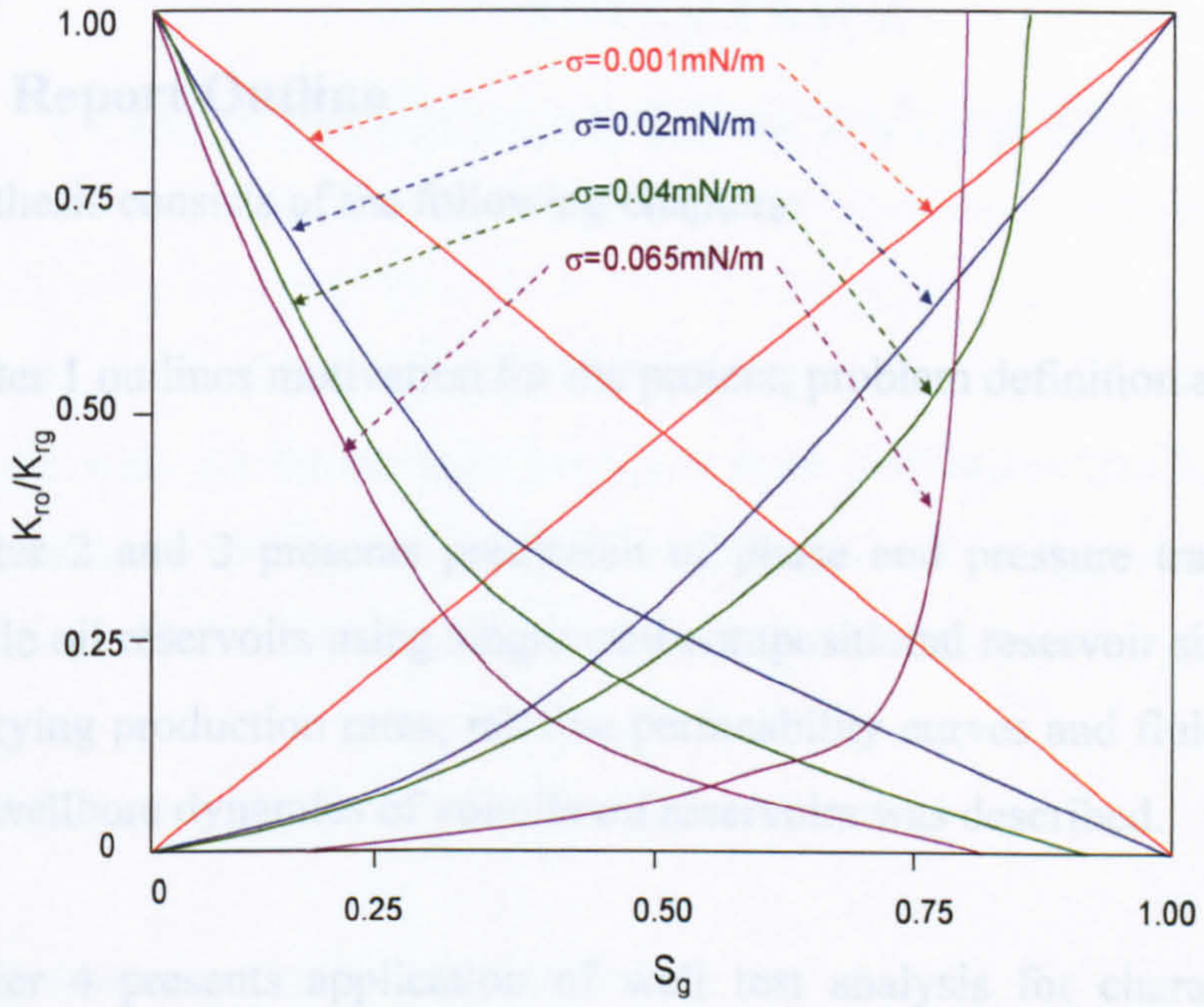

Figure 1-3 Effect of interfacial tension on oil relative permeability in an oil-gas drainage cycle (Bardon *et al.* 1980).

Knowledge obtained from the study was applied to the analysis of a well test and well deliverability forecast in an actual volatile oil reservoir.

This research work is expected to develop a better understanding, of near-wellbore effects in volatile oil reservoirs from well testing, hence leading to better reservoir management practice in volatile oil reservoirs.

The list of publications as a result of this thesis is as follows:

1. Moshood Sanni and Alain C. Gringarten: "Well-Test Analysis in Volatile Oil Reservoirs" SPE 116239, paper submitted for presentation at the SPE Annual Technical Conference and Exhibition held in Denver, Colorado, USA, 21 - 24 Sep 2008.

2. Moshood Sanni and Alain C. Gringarten: "Application of Well Testing for Well Deliverability Forecasting in Volatile Oil Reservoirs", SPE 118377, paper submitted for presentation at the Abu Dhabi International Petroleum Exhibition & Conference to be held in Abu Dhabi, UAE, 3 - 6 Nov 2008.

1.3 Report Outline

This thesis consists of the following chapters:

Chapter 1 outlines motivation for the project; problem definition and objectives.

Chapter 2 and 3 presents prediction of phase and pressure transient behaviours of volatile oil reservoirs using single well compositional reservoir simulation. The effects of varying production rates; relative permeability curves and fluid composition on the near-wellbore dynamics of volatile oil reservoirs was described.

Chapter 4 presents application of well test analysis for characterization of actual volatile oil wells: DST-Well15 from a field in Pur-Taz region of Western Siberia.

Chapter 5 presents application of well test analysis for well performance prediction in volatile oil reservoirs.

Chapter 6 presents conclusions and recommendations on "Well Test Analysis of Volatile Oil Reservoirs" and "Well Deliverability Forecasting in Volatile Oil Reservoirs".

CHAPTER 2
COMPOSITIONAL RESERVOIR SIMULATION

Reservoir simulations were performed to generate well test data in a volatile oil reservoir with the bottomhole pressure above and below the bubble point pressure. Two fluids, A and B, with different properties and compositions were used in the simulations (*Table 2-1*). Data for the simulation model are summarized in *Table 2-2*.

Appendix A describes details of the fluid properties.

.

Table 2-1 Summary of fluid properties

Fluid Samples		
	A	**B**
Fluid Type	Very Volatile Oil	Moderately Volatile Oil
P_{bub} (psia)	4,475 at 176°F	4,076 at 189°F
R_s (scf/bbl)	3,377 at 176°F	1,786 at 189°F
B_o(bbl/stb) at P_{bub}	2.92	2.02
Source	*Coats and Smart 1982*	*Western Siberia*

Table 2-2 Reservoir model characteristics

	Sample	
Parameter	**A**	**B**
Porosity Ø, %	15	15
Absolute permeability k, mD	10	10
Net to-Gross ratio N/G	1	1
Wellbore radius r_w, ft	0.2	0.2
Top depth, ft	10,000	10,000
Reservoir thickness, ft	100	100
Reservoir temperature, °F	176	189
Initial reservoir pressure Pi	5260	4861
$P_i - P_{bub}$, psia	785	785

2.1 Grid Description

A one-layer radial simulation model was built with 40 cells (*Figure 2-1*). The cell widths increase logarithmically in the radial direction, with finer grid cells around the wellbore and larger grids further away, in order to capture pressure and fluid behaviours around the wellbore. The large outer radius of 12000ft ensures that outer boundary effects are not felt during the simulated well tests.

Sensitivity analysis was carried out using different grid sizes to ensure that the grid size used has no effect on the results from the reservoir simulation (*Appendix A-15*)

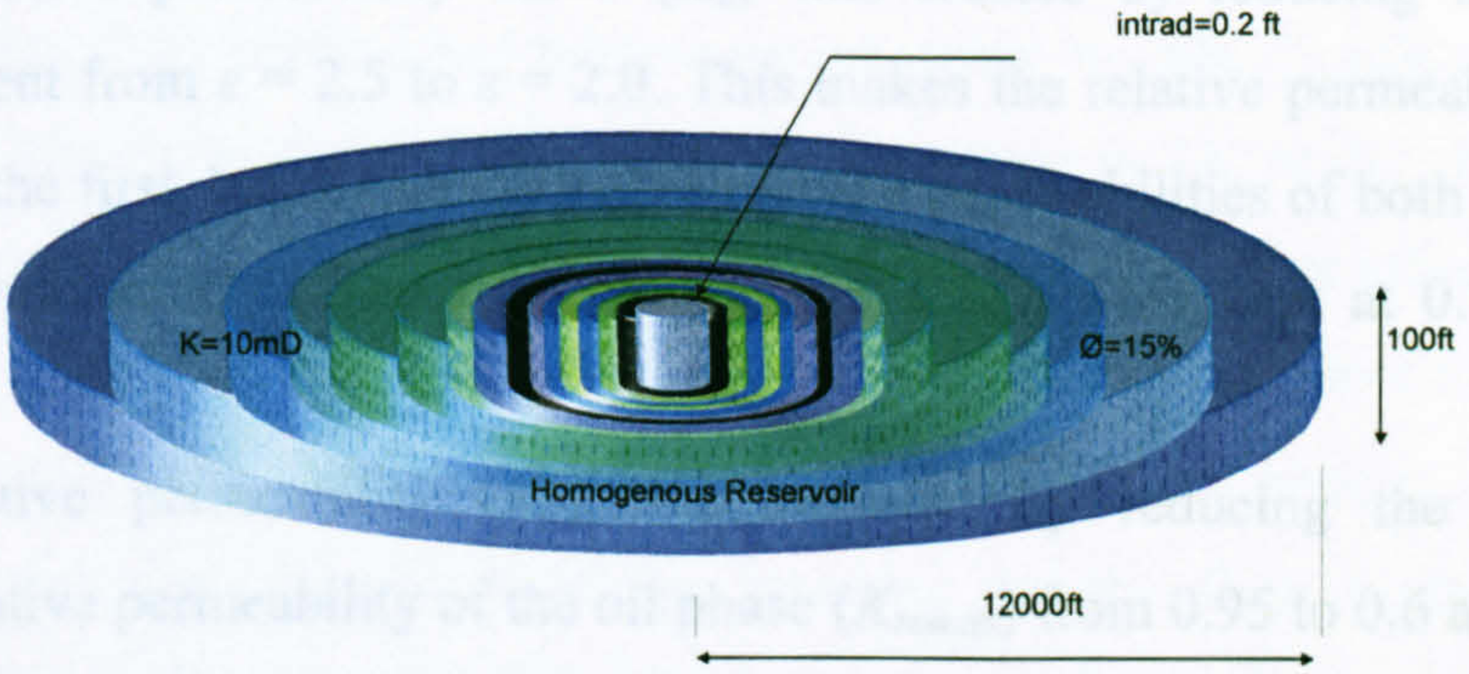

Figure 2-1 Radial simulation grid model (40 x 1 x 1)

2.2 Fluid Characterisation and Modelling

The Modified Peng-Robinson equation of state (*EOS*) with 3 parameters was used for modelling *PVT* properties of the reservoir fluids[1]. Regression was performed on molecular weight (*MW*) of heavy components; critical pressure (P_c) and critical temperature (T_c) of the pseudo-components; and binary interaction coefficients between light and heavy components. *Appendix A* shows comparison between observed and simulated fluid experiments.

The Lorentz-Bray-Clark viscosity correlation gives the best match for fluid sample A, while the Pedersen viscosity correlation gives the best match for fluid sample B. The match error is less than 10% in each case.

[1] Schlumberger: "PVTi Reference Manual version 2001A", 2001

2.3 Relative Permeability Modelling

A Corey type relative permeability model (Blom *et al.* 2000):

$$k_{r\alpha}(S_\alpha, N_c) = k^*_{r\alpha}(N_c)\left[\frac{S_\alpha - S_{r\alpha}(N_c)}{1 - S_{r\alpha}(N_c)}\right]^{\varepsilon\alpha(Nc)} \qquad (1\text{-}6)$$

was used to generate three different relative permeability curves (*Figure 2-2*). The first relative permeability curve (K_1) has a critical gas saturation (S_{gc}) of 0.0, an end point (maximum) gas relative permeability (K_{rgmax}) of 0.7, an end point (maximum) oil relative permeability (K_{romax}) of 0.95, a connate water saturation (S_{wc}) of 0.15 and a Corey's function exponent (ε) of 2.5.

The second relative permeability curve (K_2) was created by reducing the Corey's function exponent from $\varepsilon = 2.5$ to $\varepsilon = 2.0$. This makes the relative permeability curve less steep than the first, hence increasing the relative permeabilities of both oil and gas phases at a given value of saturation. K_{rgmax} and K_{romax} were kept at 0.7 and 0.95 respectively.

The third relative permeability (K_3) was modeled by reducing the end point (maximum) relative permeability of the oil phase (K_{romax}) from 0.95 to 0.6 and keeping K_{rgmax} and ε at 0.7.and 2.5, respectively.

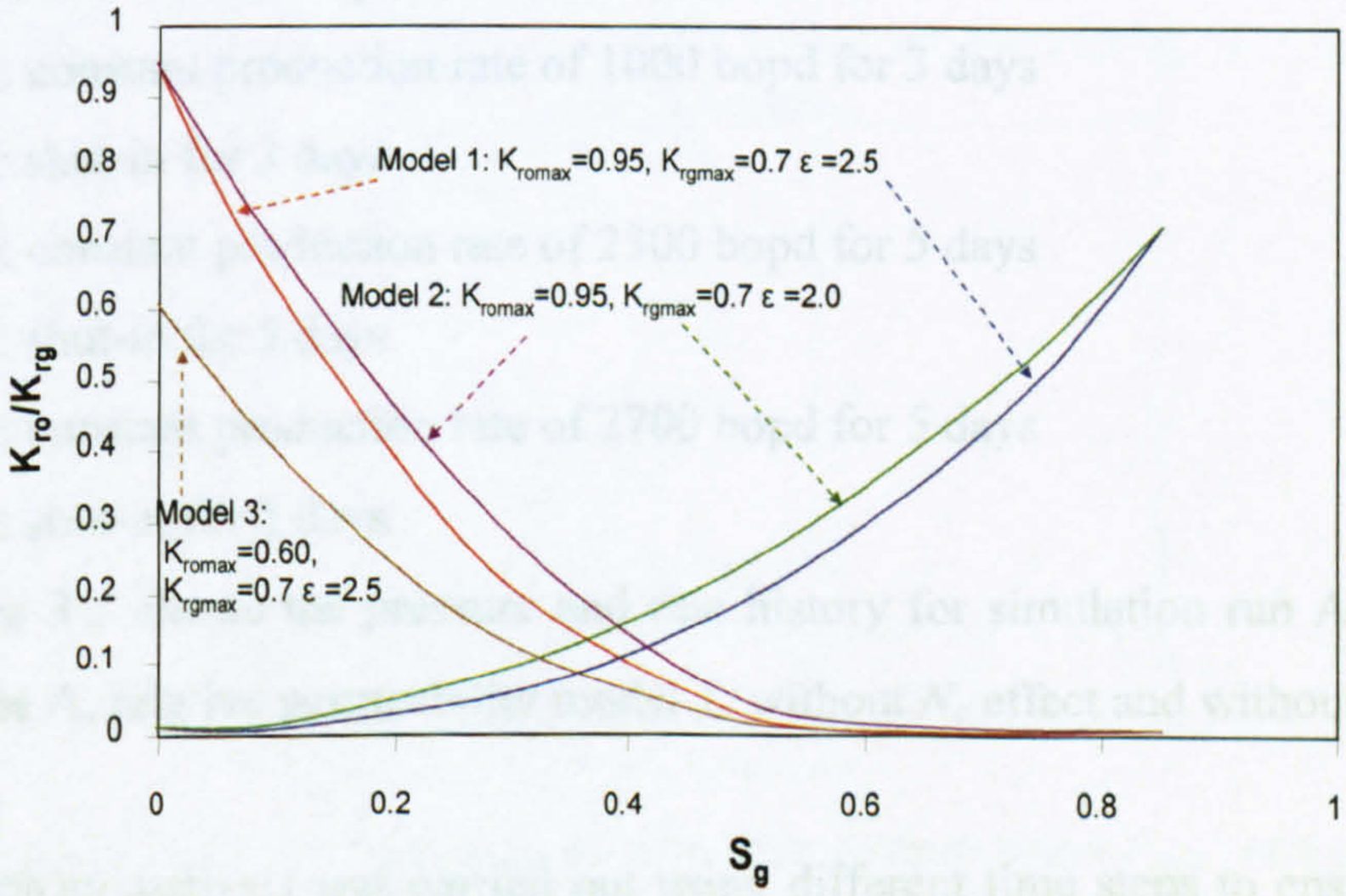

Figure 2-2 Corey's model relative permeability

CHAPTER 3
SIMULATION RESULTS

This chapter presents the prediction of phase and pressure transient behaviours of volatile oil reservoirs using single well compositional reservoir simulation. The effects of varying production rates; relative permeability curves and fluid composition on the near-wellbore dynamics of volatile oil reservoirs were also investigated.

Simulation runs, consisting of a series of drawdowns (*DD*) and build-ups (*BU*), were designed to investigate the impact on well test behaviour of different reservoir conditions, such as fluid samples and relative permeability models. Simulation runs are defined by alphanumeric digits indicating the fluid sample (A or B); the relative permeability models (K_1, K_2, or K_3); the existence of capillary number effect N_c (N_0 or N_1 for simulations without and with N_c, respectively) and the existence of turbulence β (D_0 or D_1 for simulations without and with β, respectively). Flow periods are labelled *DD* for drawdown and *BU* for build-up, preceded by the flow period number. Subscript "*const-cumm*" is used for runs with constant cumulative production.

Definition of the flow periods are shown below:

1 DD: constant production rate of 1000 bopd for 3 days

2 BU: shut-in for 3 days

3 DD: constant production rate of 2300 bopd for 5 days

4 BU: shut-in for 5 days

5 DD: constant production rate of 2700 bopd for 5 days

6 BU: shut-in for 5 days

Figure 3-1 shows the pressure and rate history for simulation run A-K_1-N_0-D_0 (fluid sample A, relative permeability model 1, without N_c effect and without β effect)

Sensitivity analysis was carried out using different time steps to ensure that the time steps used have no effect on the results of the reservoir simulation.

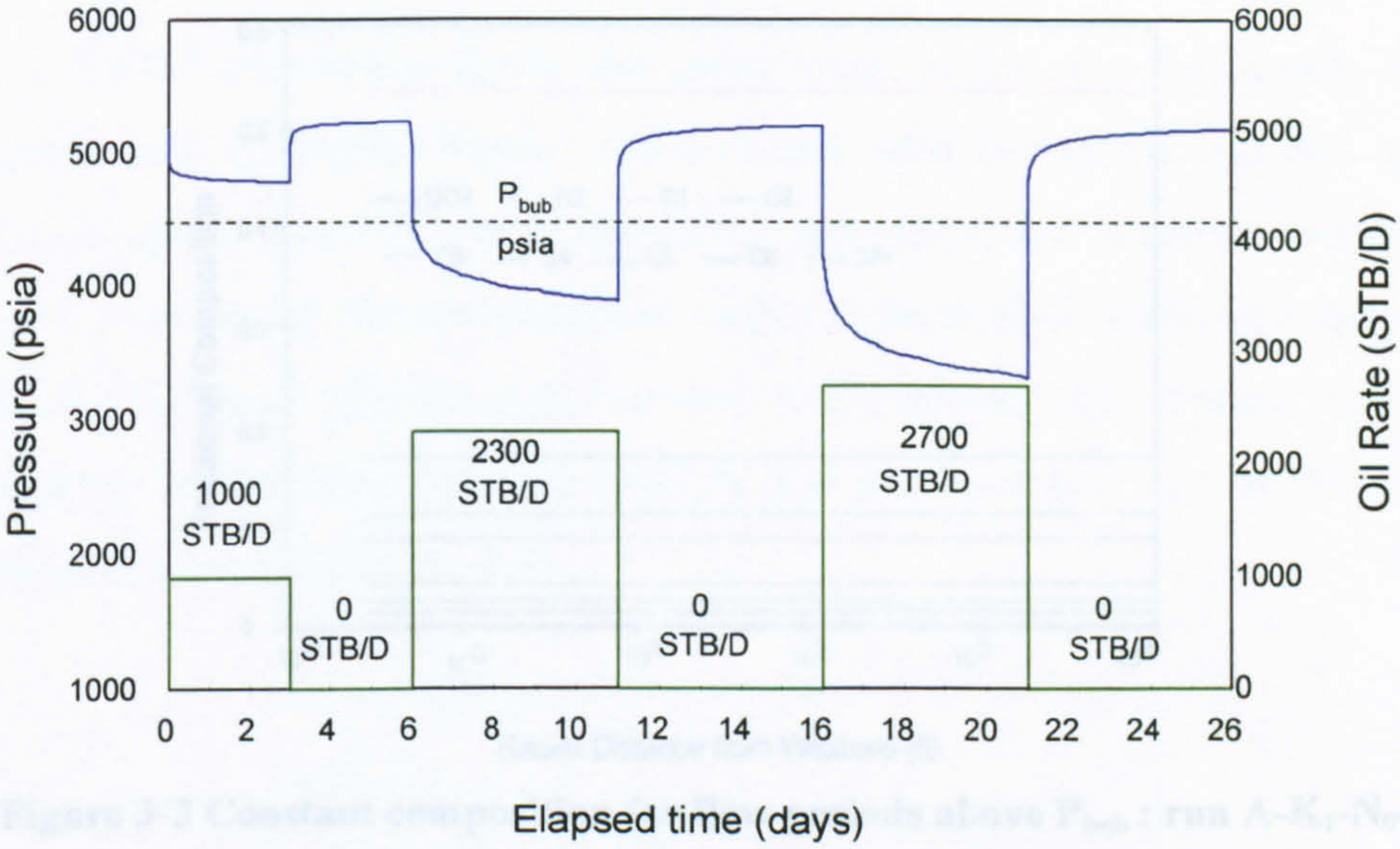

Figure 3-1 Pressure-rate history for simulation run A-K_1-N_0-D_0

3.1 Phase Behaviour and Dynamics

During a well test in a volatile oil reservoir, when the *BHP* is above bubble point, the saturation and composition are uniform throughout the reservoir for all *DD* and *BU* as shown by the simulated phase profiles in *Figure 3-2* and *Figure 3-3*. A slight increase in mobility occurs around the wellbore (*Figure 3-4*) corresponding a decrease in oil viscosity due to volumetric expansion (*Figure 3-5*).

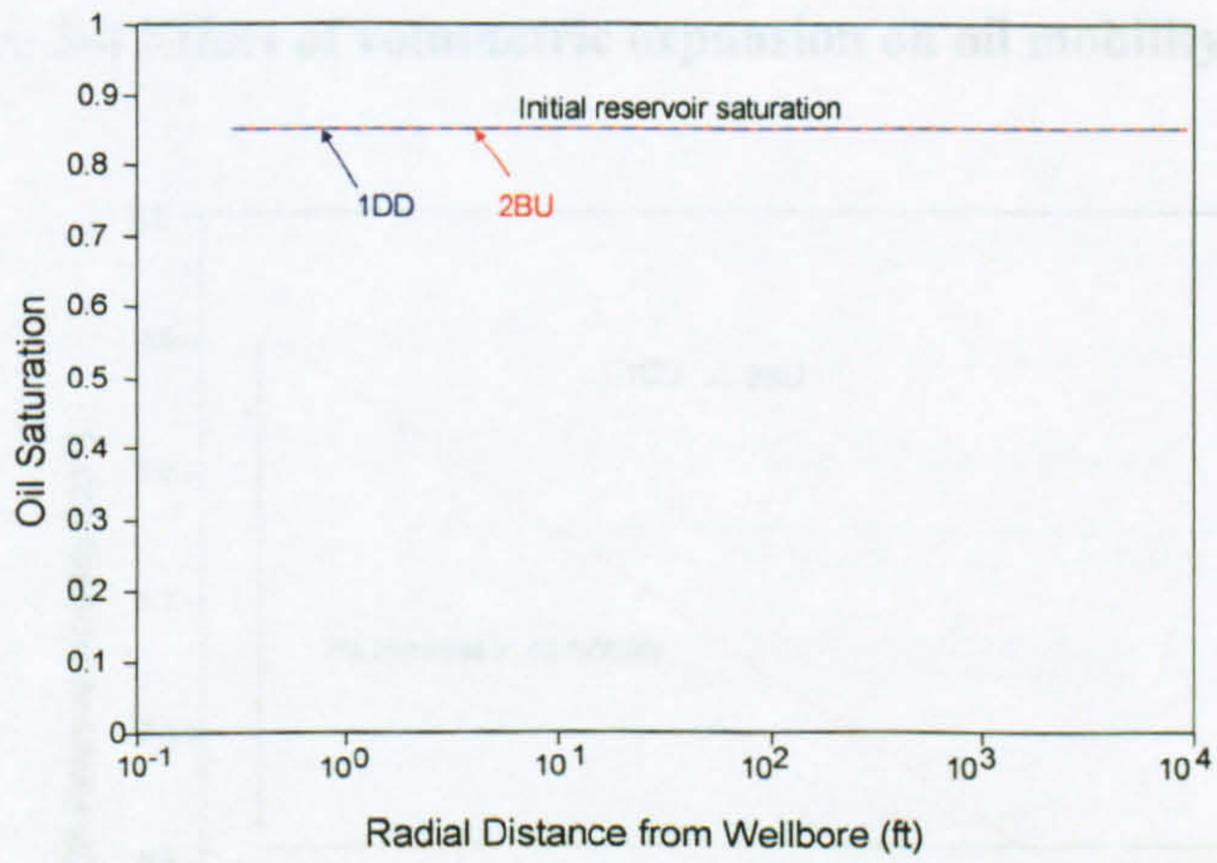

Figure 3-2 Constant saturation for flow periods above P_{bub} : run A-K_1-N_0-D_0

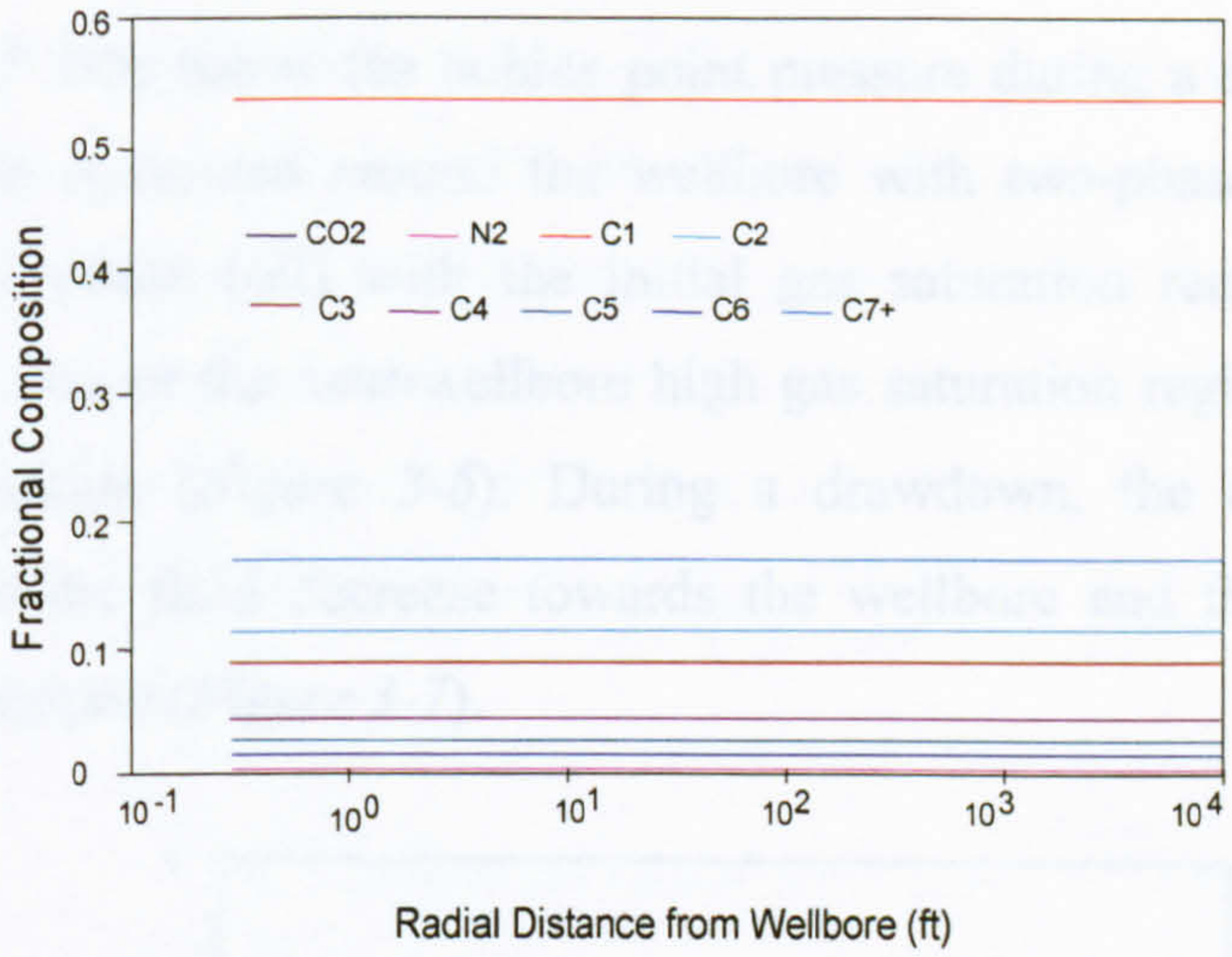

Figure 3-3 Constant composition for flow periods above P_{bub} : run A-K_1-N_0-D_0

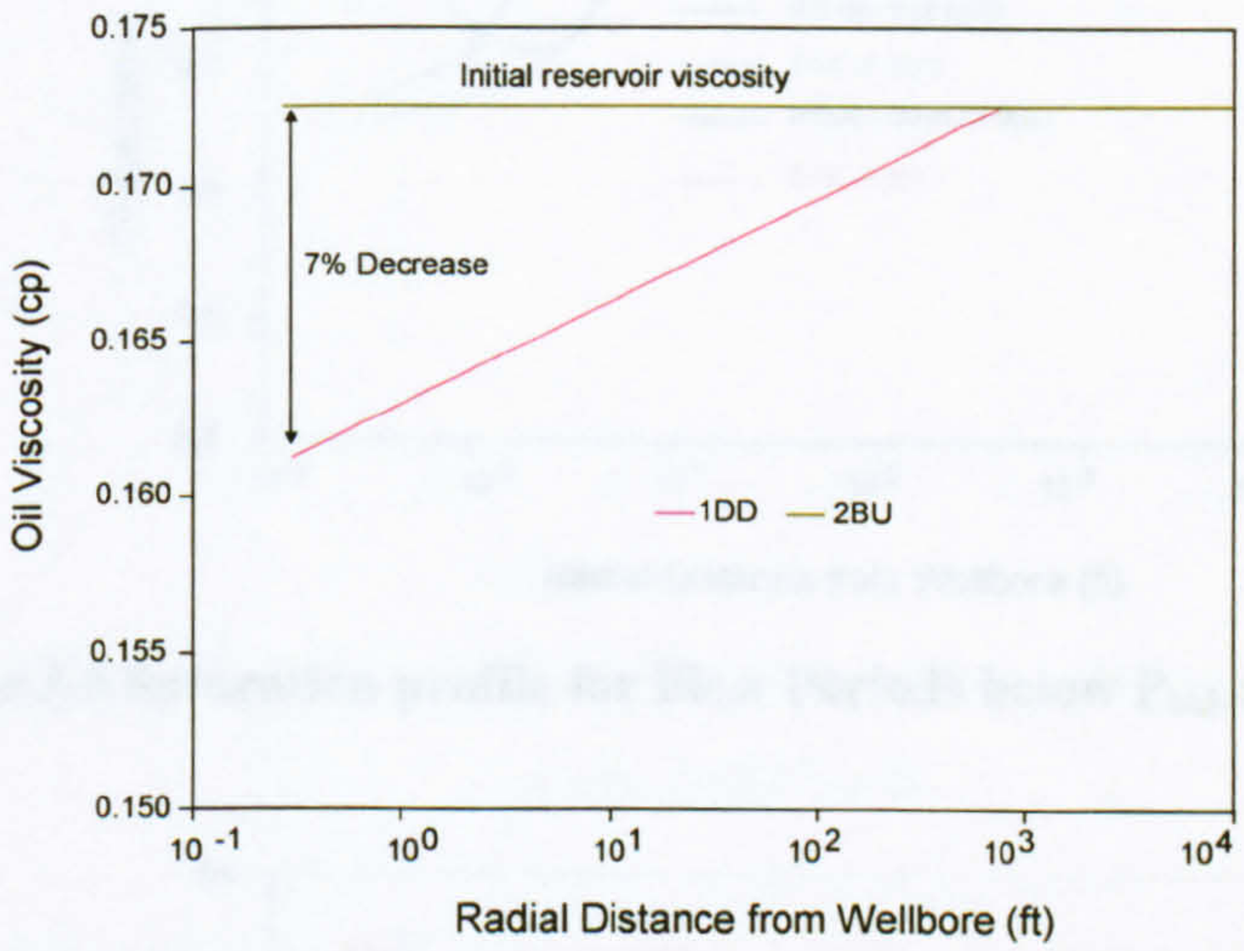

Figure 3-4 Effect of volumetric expansion on oil mobility: run A-K_1-N_0-D_0

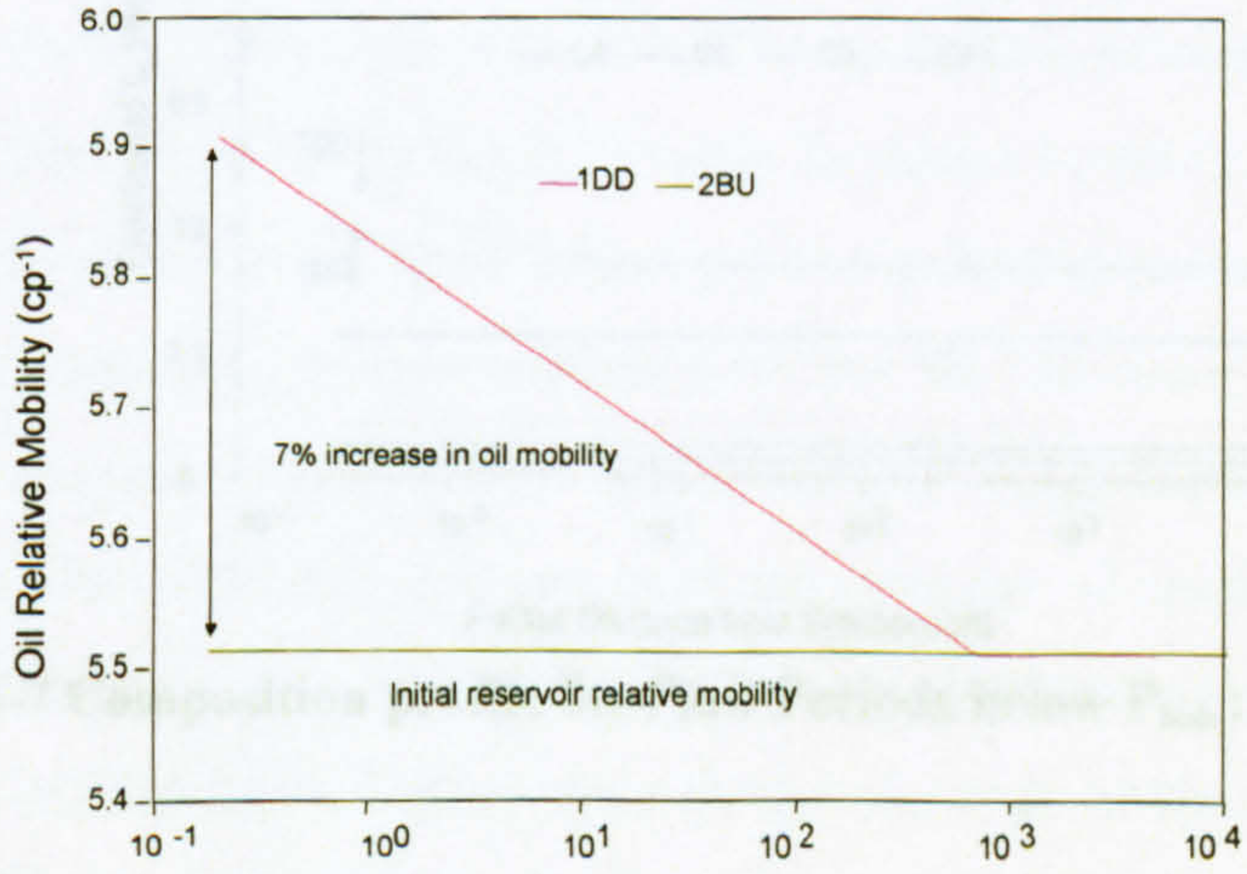

Figure 3-5 Effect of volumetric expansion on oil viscosity: run A-K_1-N_0-D_0

When the *BHP* falls below the bubble point pressure during a drawdown, a high gas saturation zone is created around the wellbore with two-phase (oil and gas) flow, whereas single phase (oil) with the initial gas saturation remains away from the wellbore. The size of the near-wellbore high gas saturation region increases with the drawdown duration (*Figure 3-6*). During a drawdown, the amount of light end components in the fluid decrease towards the wellbore and that of the heavy end components increase (*Figure 3-7*).

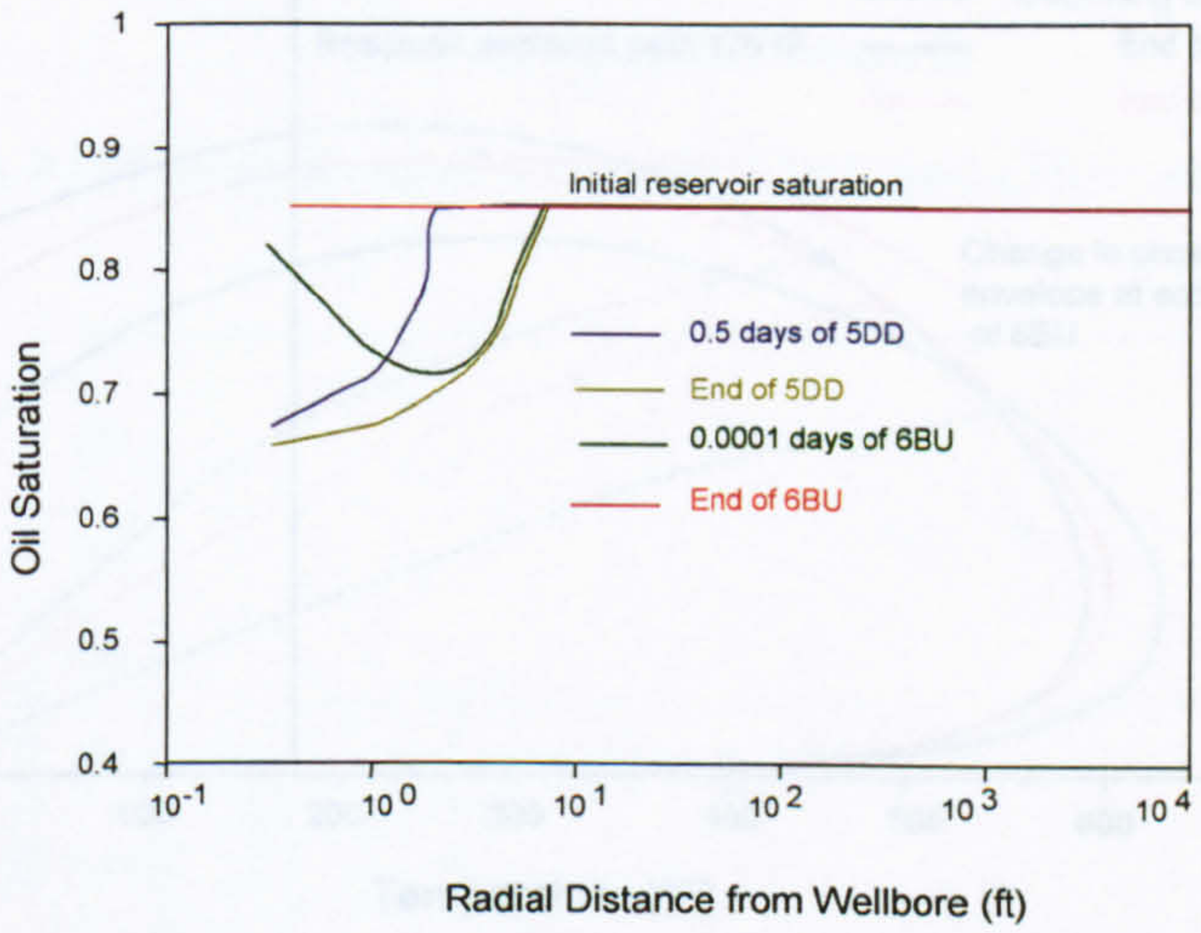

Figure 3-6 Saturation profile for Flow Periods below P_{bub} : run A-K_1-N_0-D_0

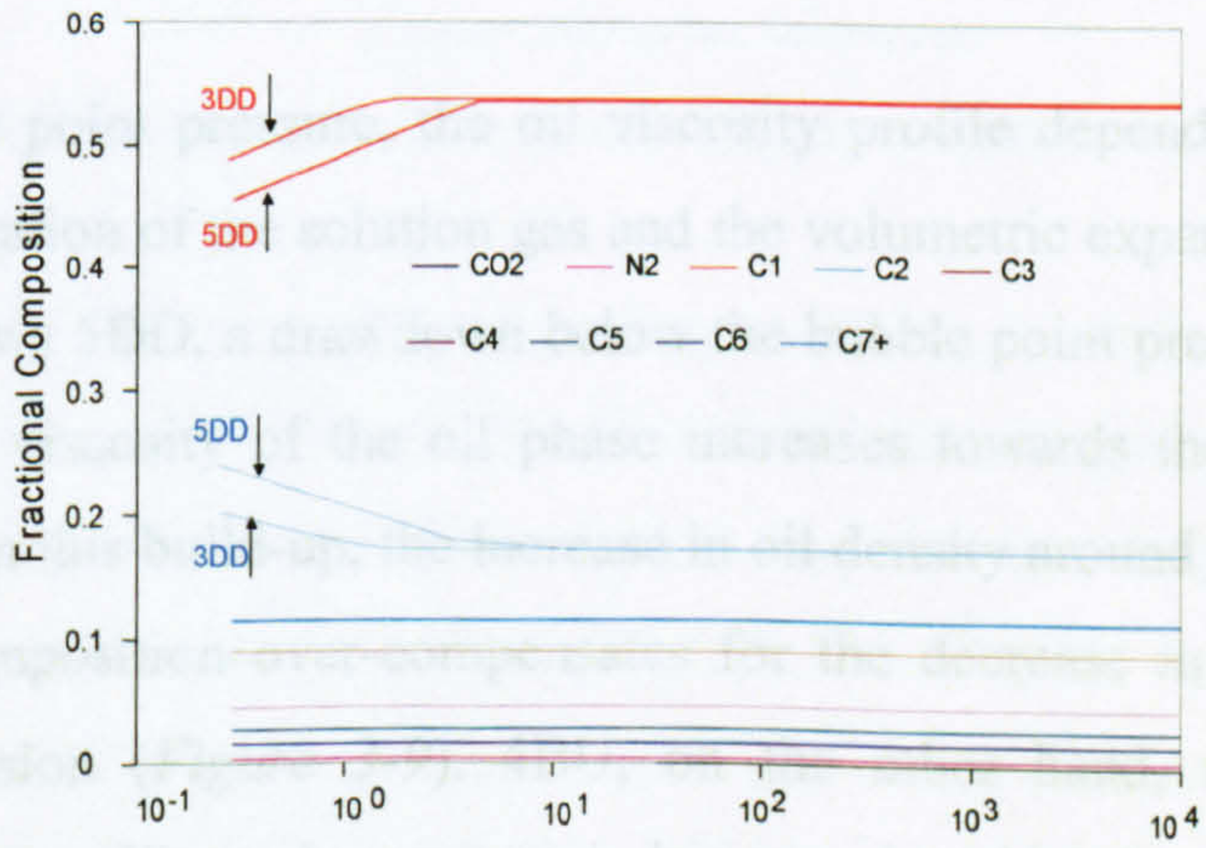

Figure 3-7 Composition profile for Flow Periods below P_{bub} : run A-K_1-N_0-D_0

During the subsequent build-up, the gas created around the wellbore during the preceding drawdown condenses into the oil and the saturation in the near-wellbore region returns to the initial gas saturation (*Figure 3-6*). The fluid composition in the near-wellbore region, however, does not return to the initial fluid composition, due to the loss of the light components (the pressure-temperature phase envelope of the fluid shifts downwards to the right as shown in *Figure 3-8*).

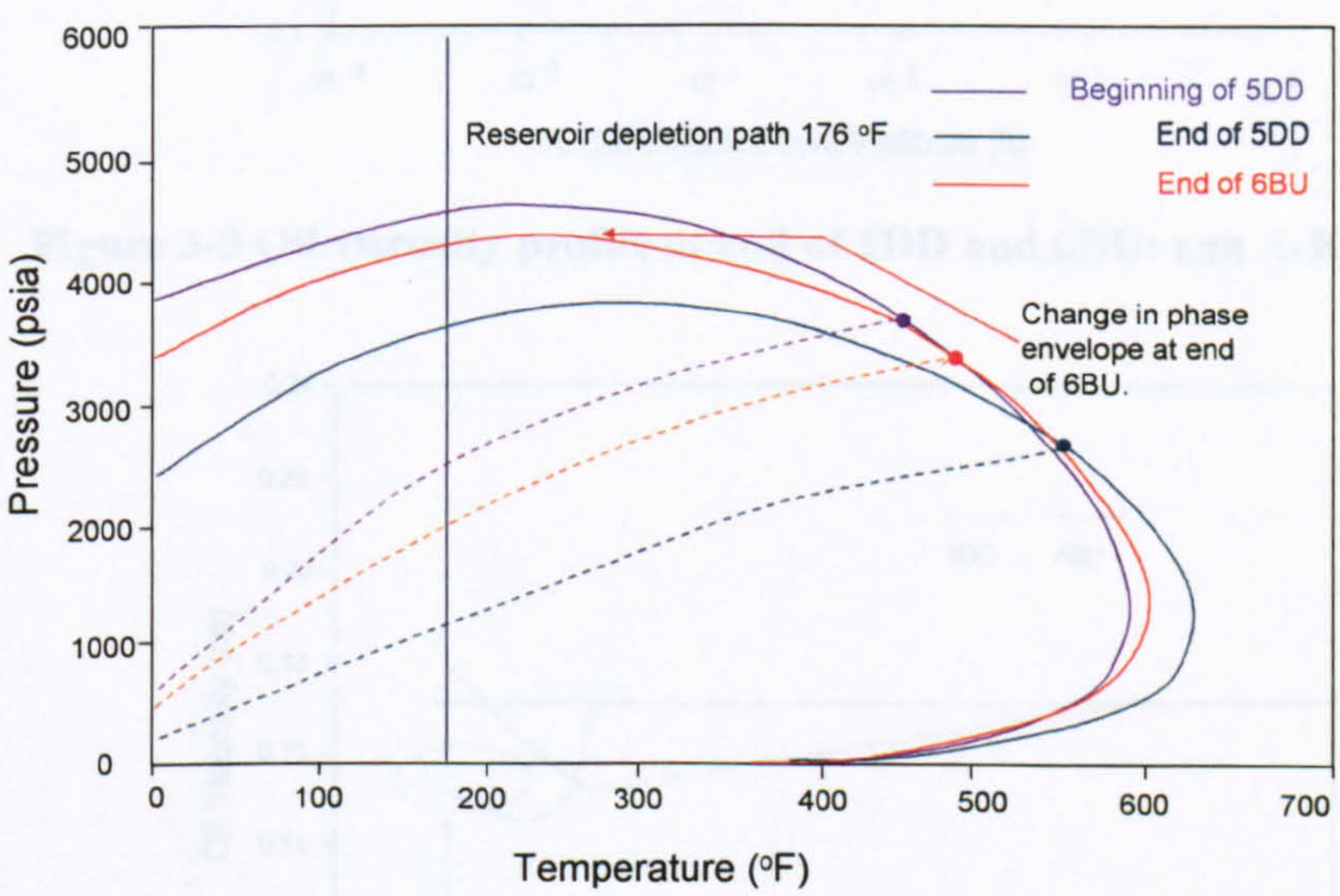

Figure 3-8 Change in phase in envelope due to loss of light end hydrocarbon: run A-K_1-N_0-D_0

Below the bubble point pressure, the oil viscosity profile depends on the combined effects of the liberation of the solution gas and the volumetric expansion of the oil. For 6BU (which follows 5DD, a drawdown below the bubble point pressure with a rate of 2700 Bbl/D), the viscosity of the oil phase increases towards the well in the near-wellbore region. In this build-up, the increase in oil density around the wellbore due to the change in composition over-compensates for the decrease in oil density due to volumetric expansion (*Figure 3-9*). 4BU, on the other hand, shows a lower oil viscosity near the wellbore because the decrease in viscosity due to volumetric expansion dominates the increase in oil viscosity due to the change in composition (*Figure 3-10*). 4BU follows 3DD, a drawdown below the bubble point pressure with a rate of 2300 Bbl/D.

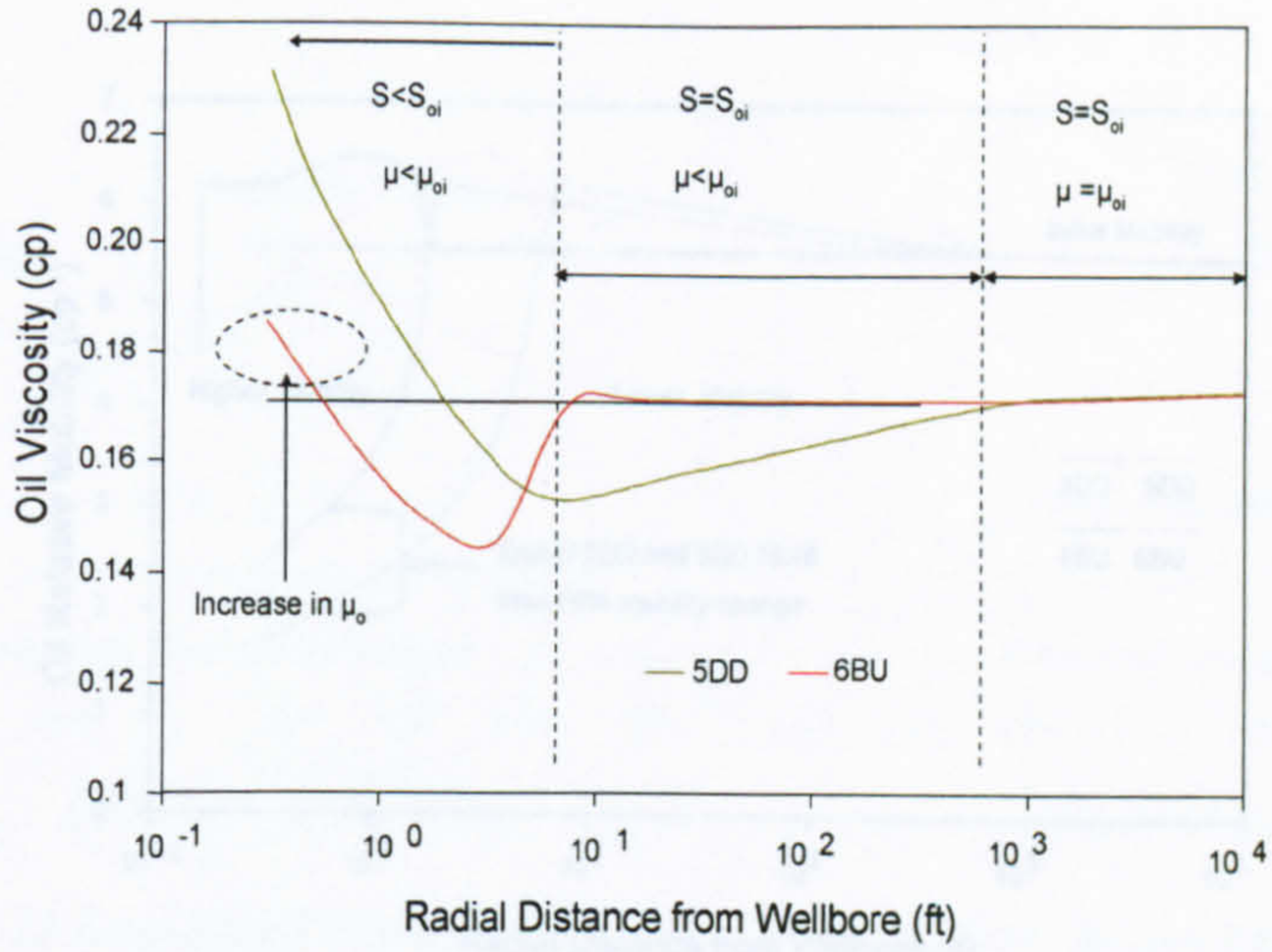

Figure 3-9 Oil viscosity profile at end of 5DD and 6BU: run A-K_1-N_0-D_0

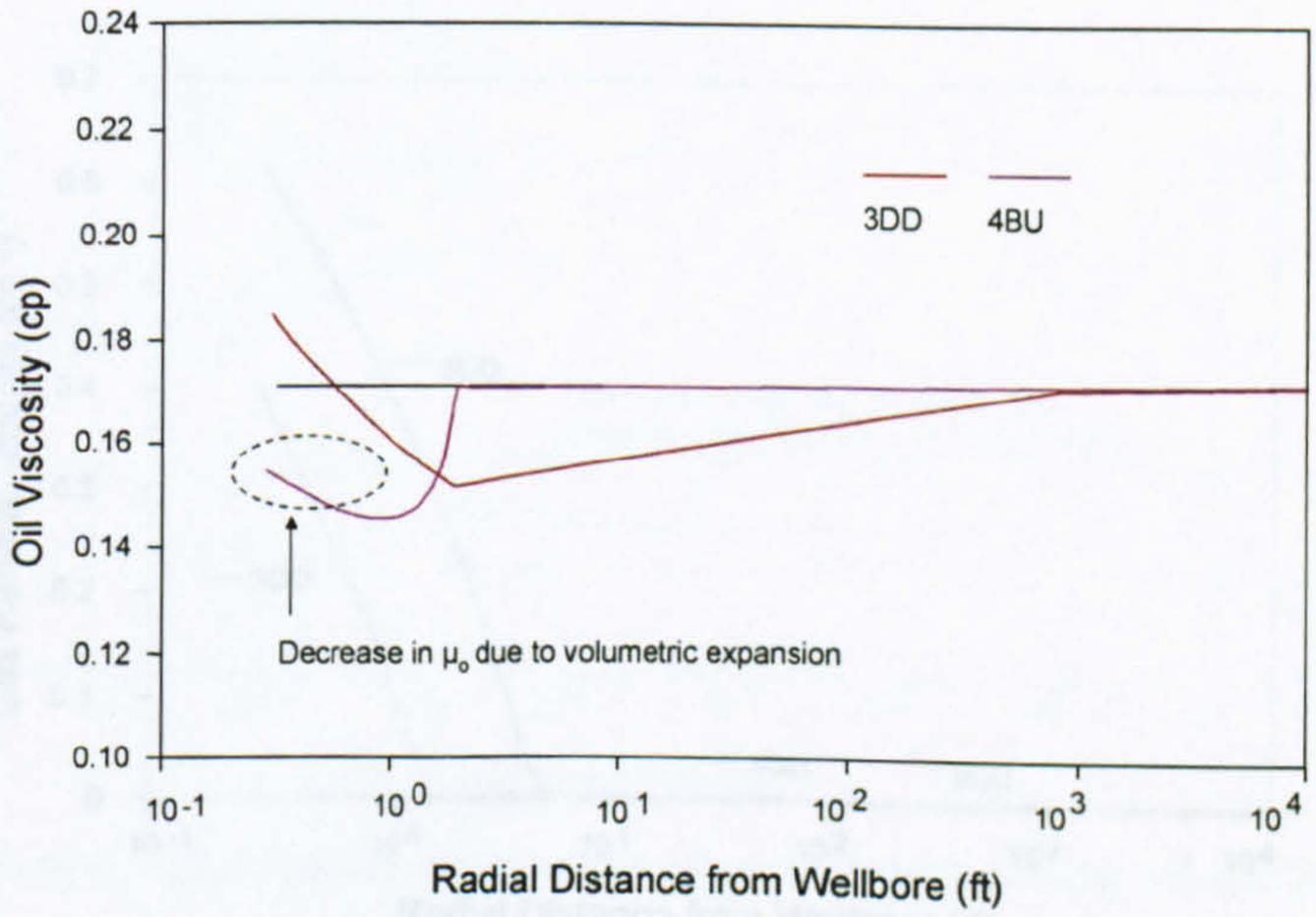

Figure 3-10 Oil viscosity profile at end of 3DD and 6BU: run A-K_1-N_0-D_0

The decrease in oil relative mobility around the wellbore, in all the drawdowns below the bubble point pressure, is due to the combination of an increase in gas saturation and an increase in oil viscosity. At the end of all the build-ups, the gas saturation in the near-wellbore region returns to its initial value. The oil relative mobility increases around the wellbore at the end of a build-up due to volumetric expansion of fluid. It decreases only when the flow rate of the oil phase is high enough to change the composition (*Figure 3-11*). Gas becomes mobile as soon as the reservoir pressure falls below the bubble point pressure. The mobility of the gas phase increases with time during a drawdown and returns to zero at the end of the subsequent build-up when gas re-dissolves into oil (*Figure 3-12*).

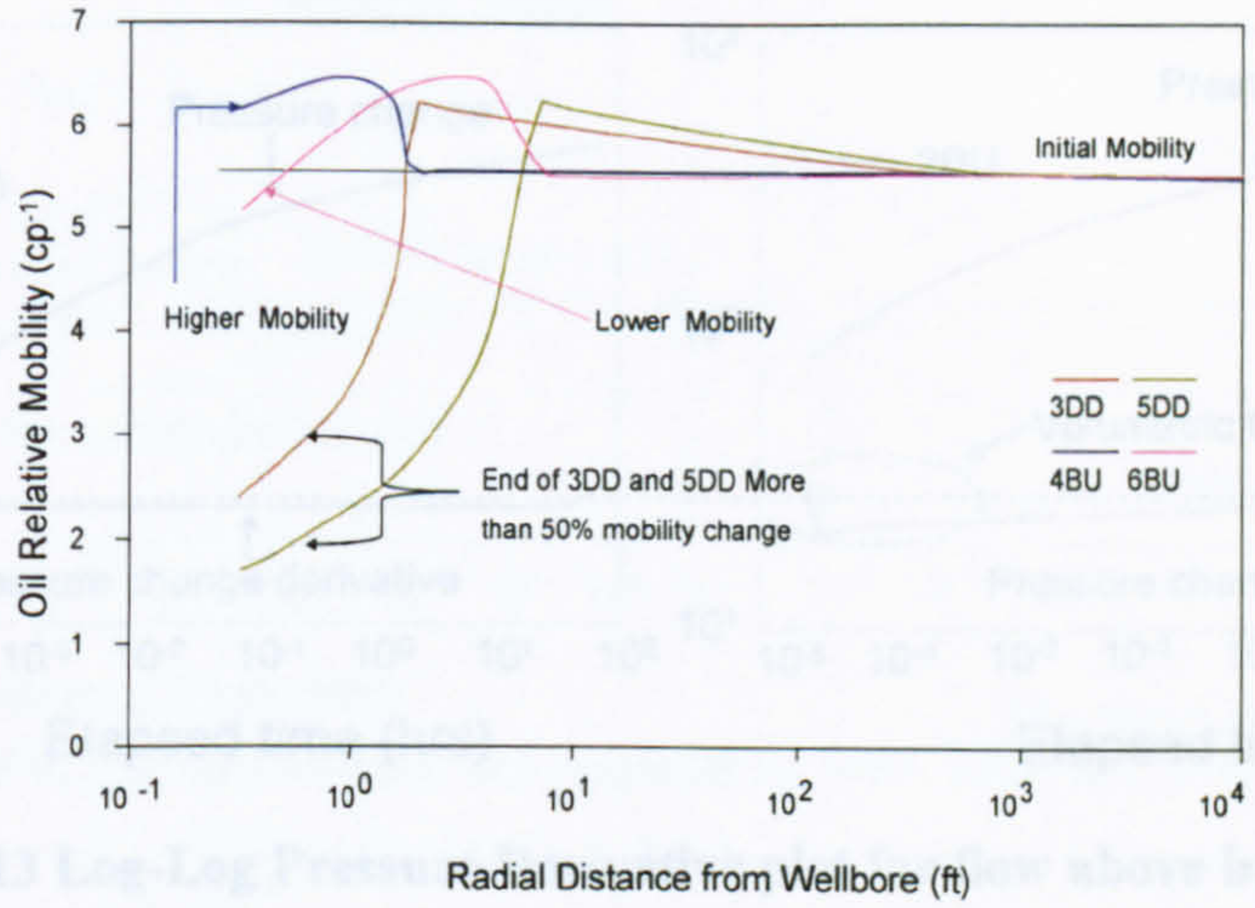

Figure 3-11 Oil Relative Mobility profile at end of 5DD and 6BU

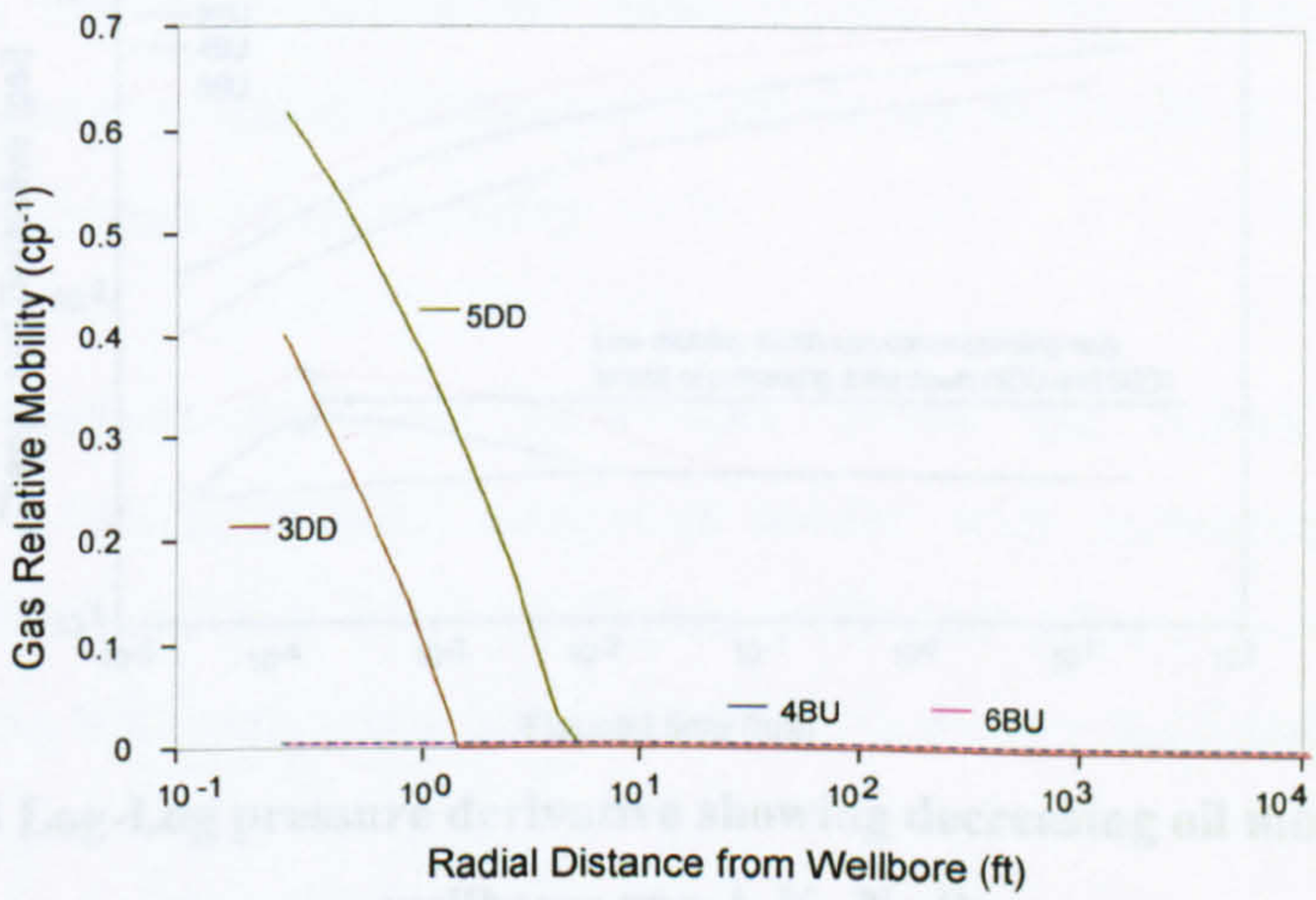

Figure 3-12 Gas relative mobility profile at end of flow periods

3.2 Well Test Behaviour of Volatile Oil Reservoirs

The 7% increase in the relative mobility of the volatile oil shown in *Figure 3-4*, when *BHP* is above the bubble point pressure, is not significant enough to be seen on the log-log pressure-derivative (1DD and 2BU in *Figure 3-13*). Therefore, the mobility of volatile oils above the bubble point pressure can be evaluated as for black oil.

Below the bubble point pressure, lower oil relative mobilities can be seen at the beginning of 4BU and 6BU (higher early time derivative stabilizations in *Figure 3-14*). They correspond to the lower mobilities at the end of 3DD and 5DD (higher late time derivative stabilizations in *Figure 3-15* and *Figure 3-16*, respectively).

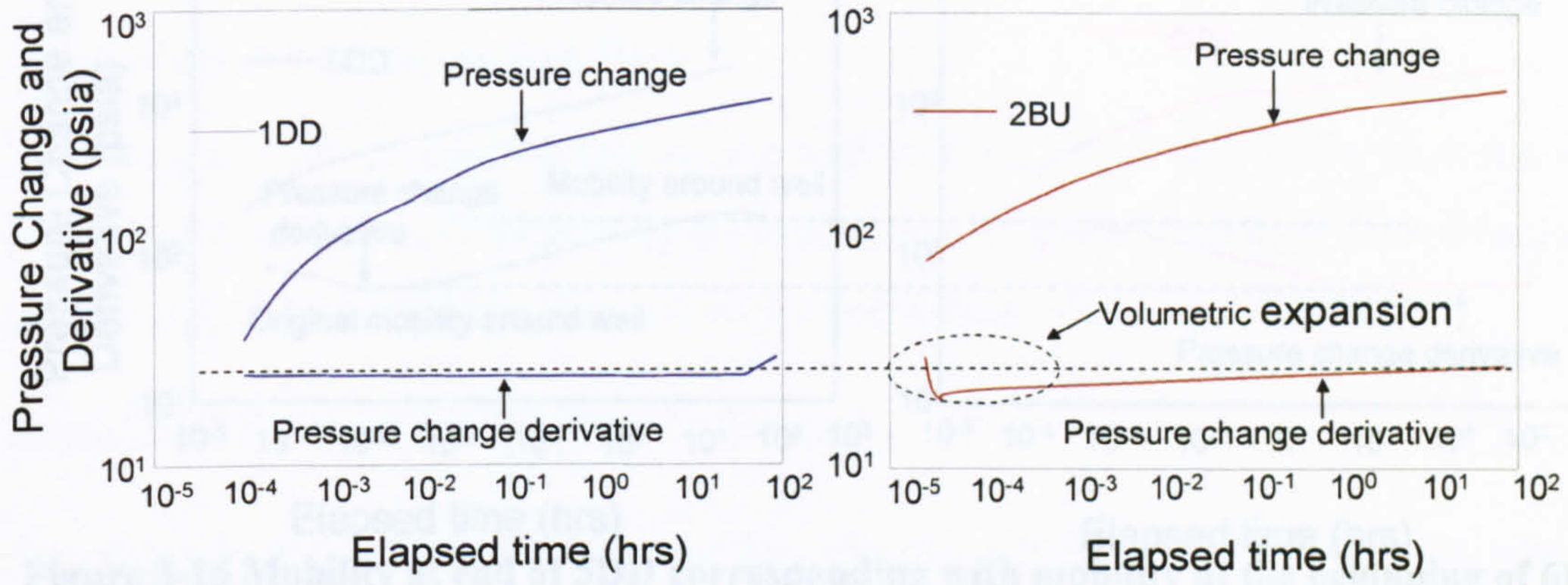

Figure 3-13 Log-Log Pressure Derivative plot for flow above bubble point: run A-K_1-N_0-D_0

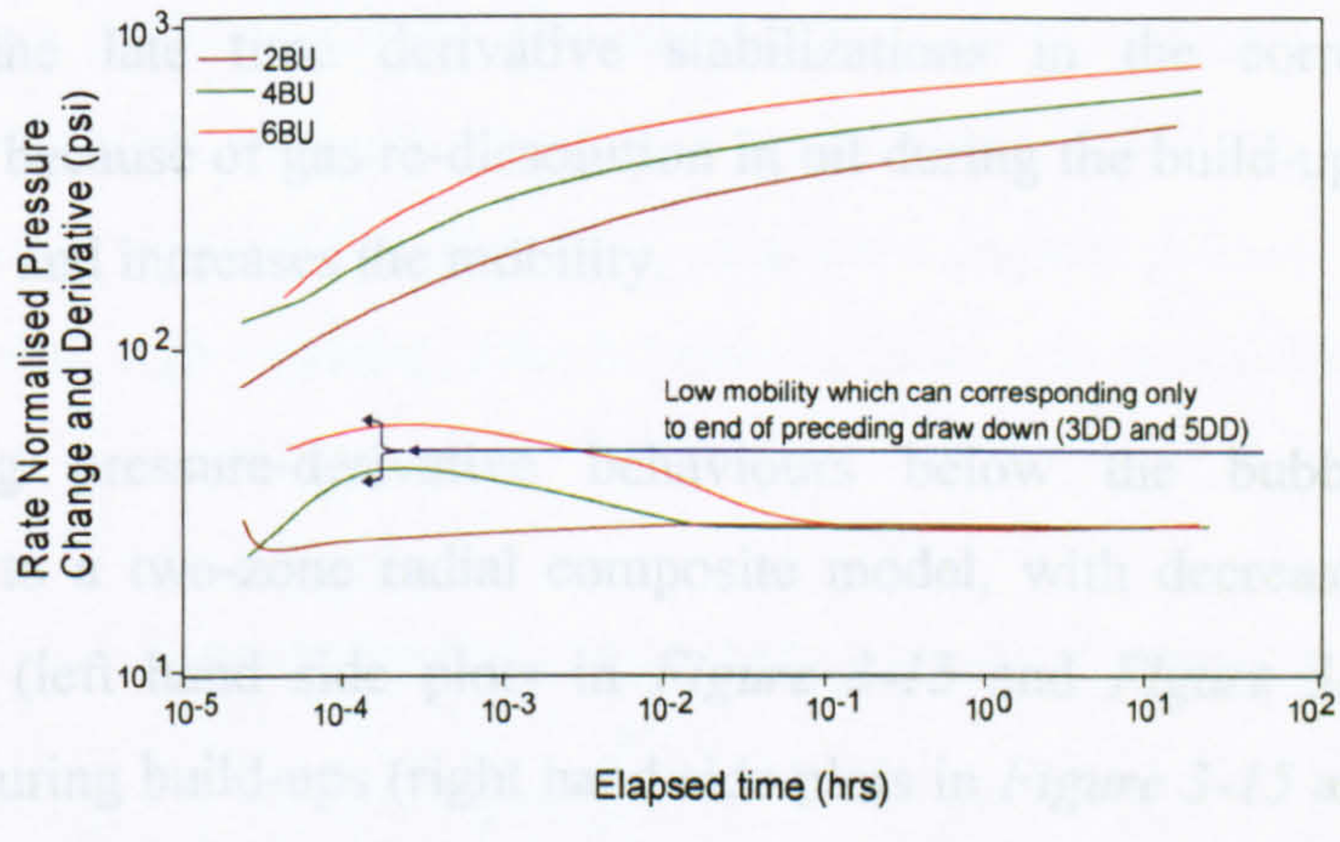

Figure 3-14 Log-Log pressure derivative showing decreasing oil mobility towards wellbore: run A-K_1-N_0-D_0

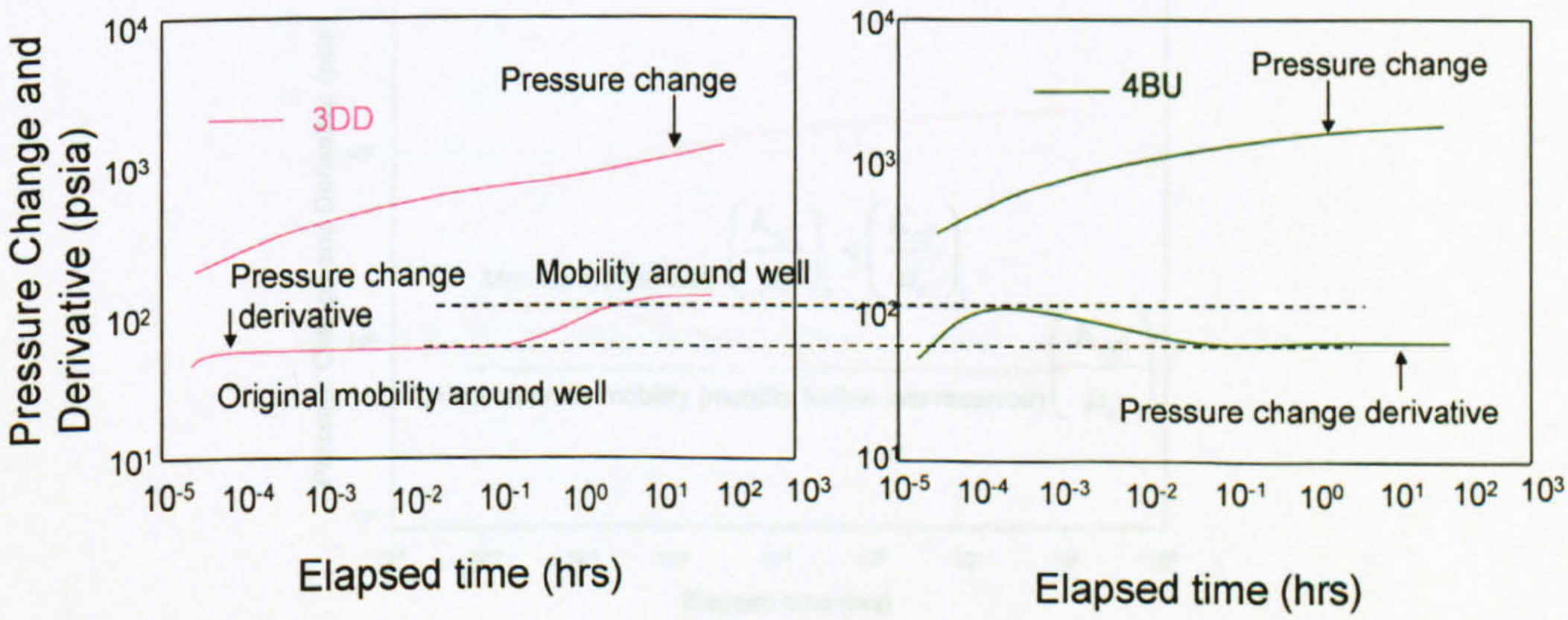

Figure 3-15 Mobility at end of 3DD corresponding with mobility at the beginning of 4BU run A-K_1-N_0-D_0

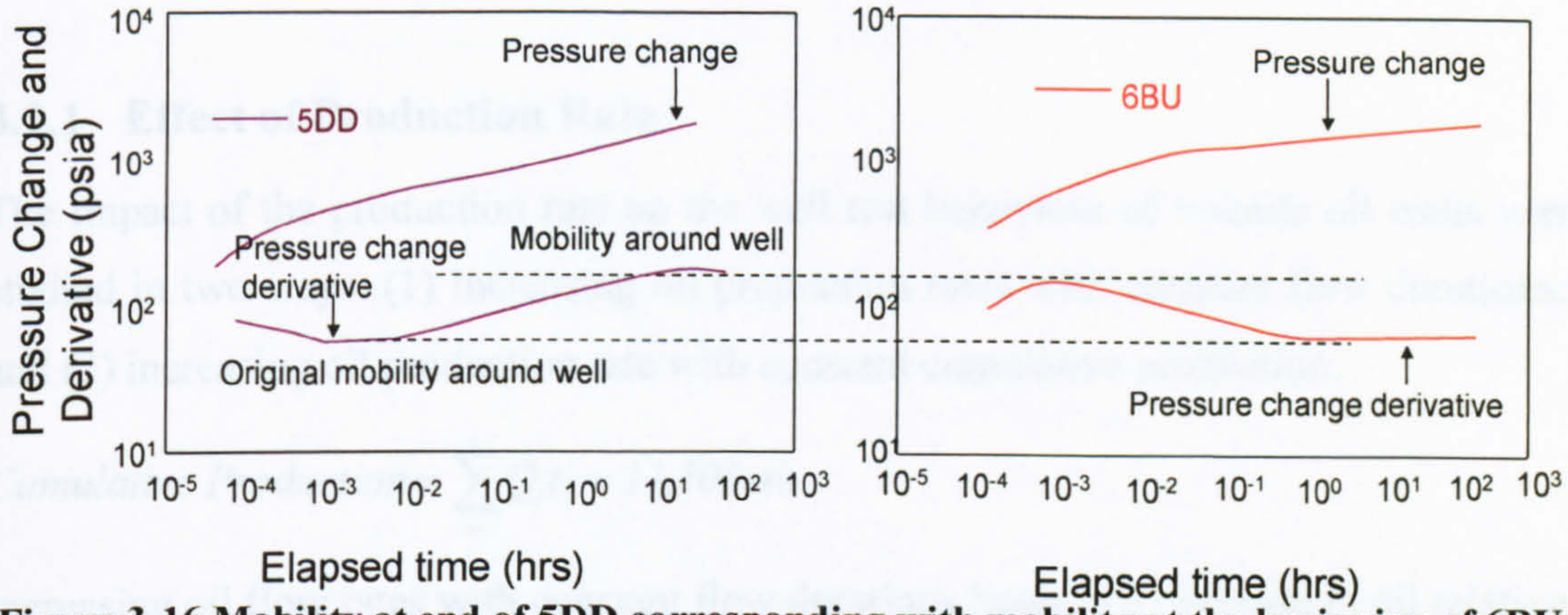

Figure 3-16 Mobility at end of 5DD corresponding with mobility at the beginning of 6BU run A-K_1-N_0-D_0

The early time derivative stabilizations during the build-ups are actually slightly lower than that the late time derivative stabilizations in the corresponding previous drawdowns because of gas re-dissolution in oil during the build-up, which reduces the oil viscosity and increases the mobility.

The log-log pressure-derivative behaviours below the bubble point therefore correspond to a two-zone radial composite model, with decreasing mobility during drawdowns (left hand side plots in *Figure 3-15* and *Figure 3-16*) and increasing mobilities during build-ups (right hand side plots in *Figure 3-15* and *Figure 3-16*, and *Figure 3-17*).

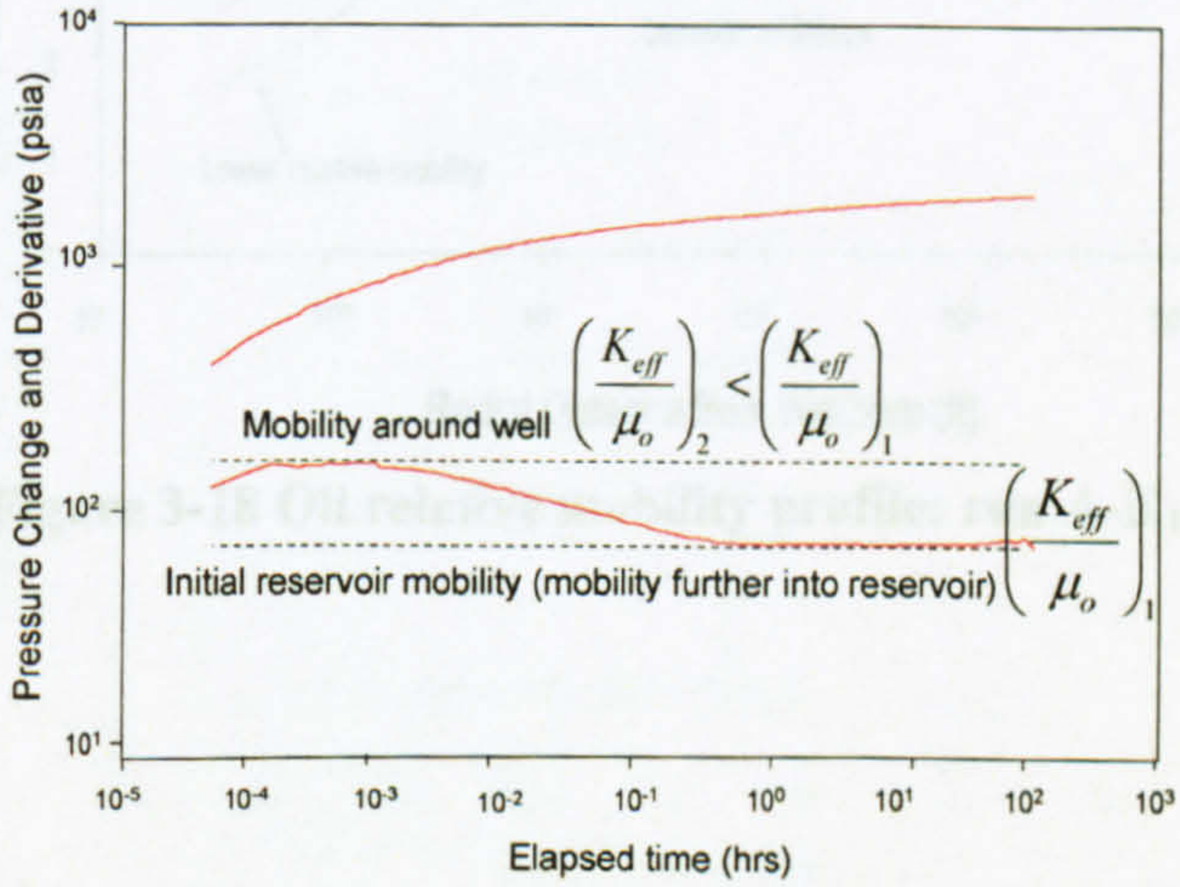

Figure 3-17 Two-zone composite behaviour of volatile oil reservoir below bubble point

3.2.1 Effect of Production Rate

The impact of the production rate on the well test behaviour of volatile oil wells was studied in two ways: (1) increasing oil production rates with constant flow durations; and (2) increasing oil production rate with constant cumulative production.

$$Cumulative\ Production = \sum_{n}^{i} Q_i t_i = 11{,}500 stb$$

Increasing oil flow rates with constant flow durations leads to a decrease in oil relative mobility (*Figure 3-18*). This is due to the increase in the size of the near-wellbore, high gas saturation region (*Figure 3-19*) and the increase in viscosity towards the well *(Figure 3-20*). This decrease in oil relative mobility can be clearly seen on the derivative plot of *Figure 3-21*. The same behaviour is obtained when increasing oil production rate with constant cumulative production (11,500 stb in *Figure 3-22*). The increase in the size of the high gas saturation region is due to the high energy associated with high velocity, which leads to more gas production than at lower oil rate.

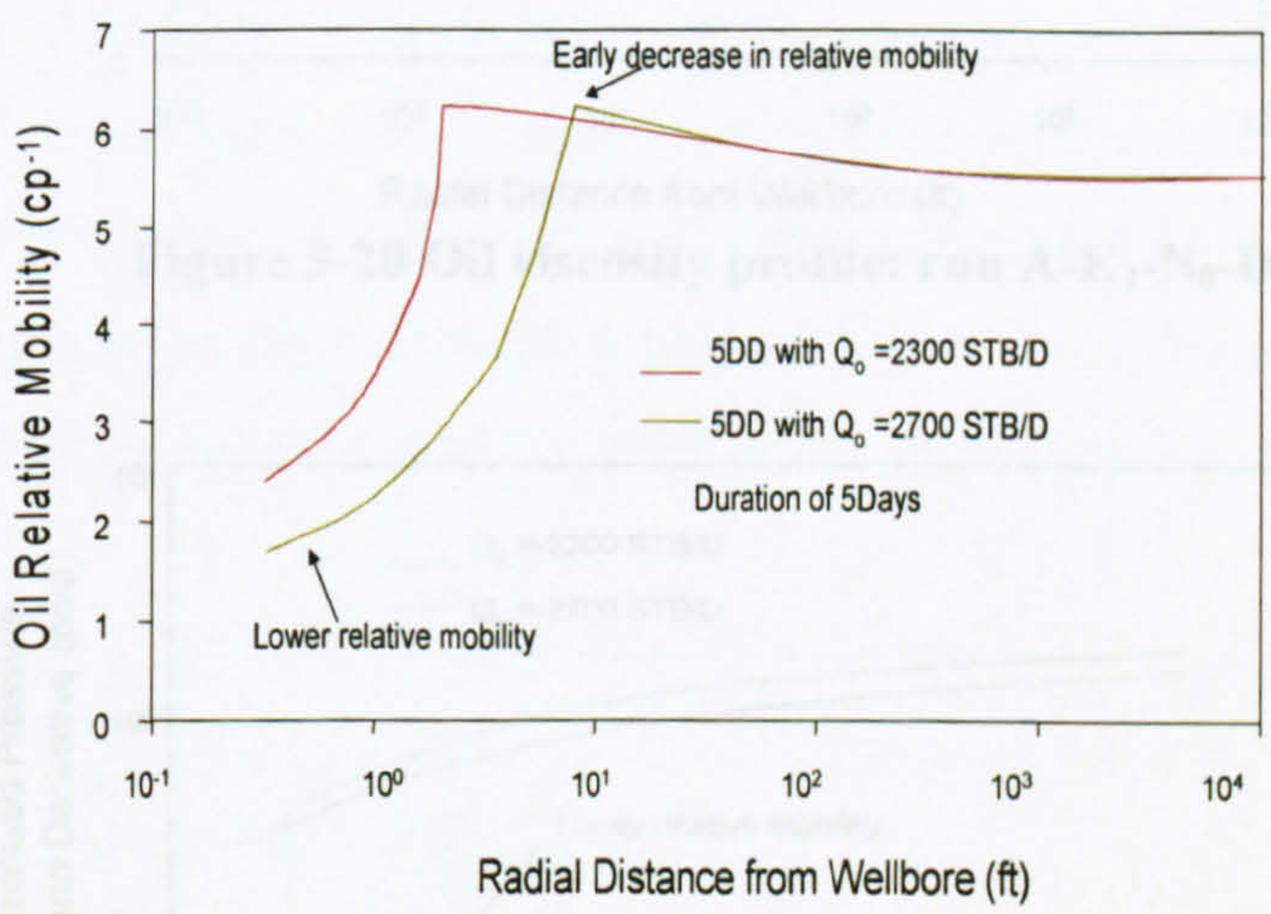

Figure 3-18 Oil relative mobility profile: run A-K_1-N_0-D_0

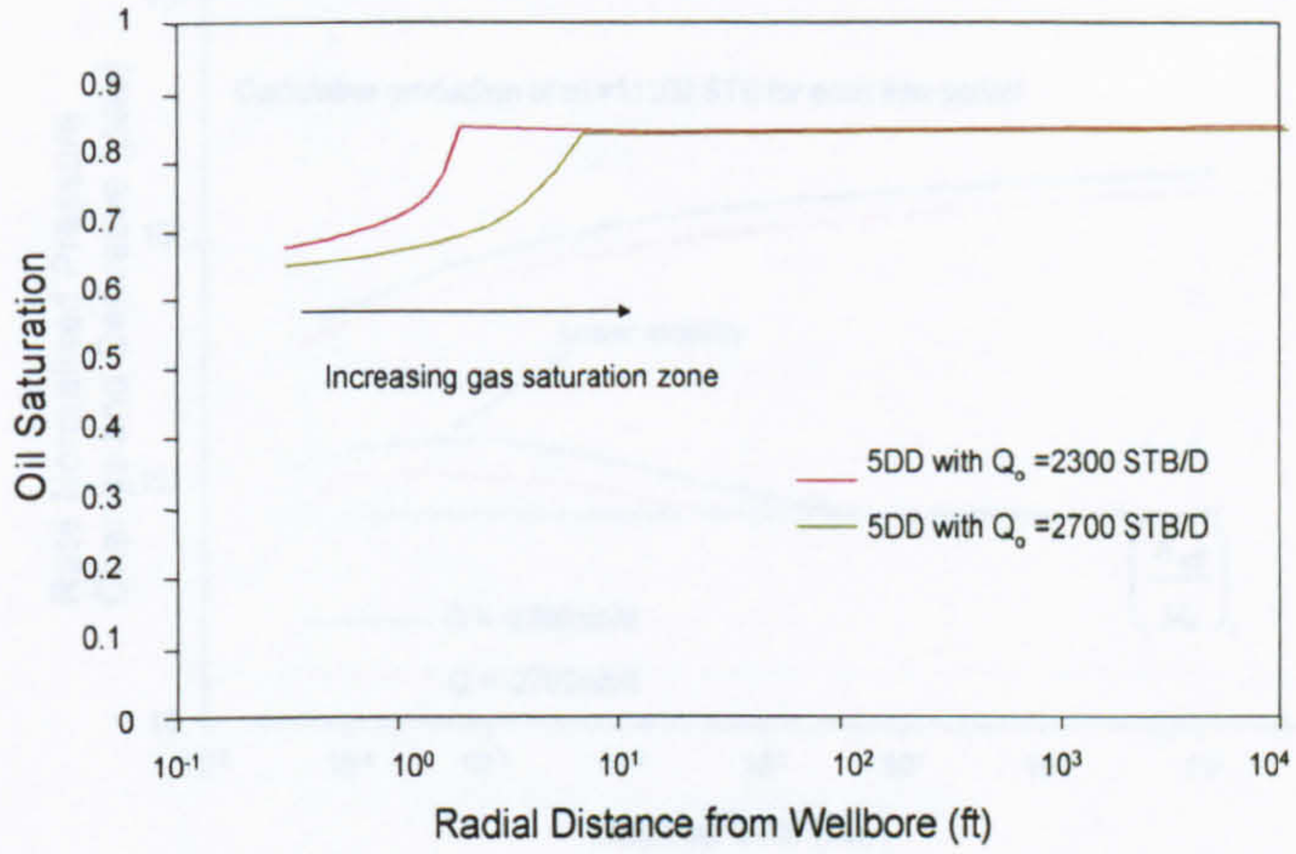

Figure 3-19 Oil saturation profile: run A-K_1-N_0-D_0

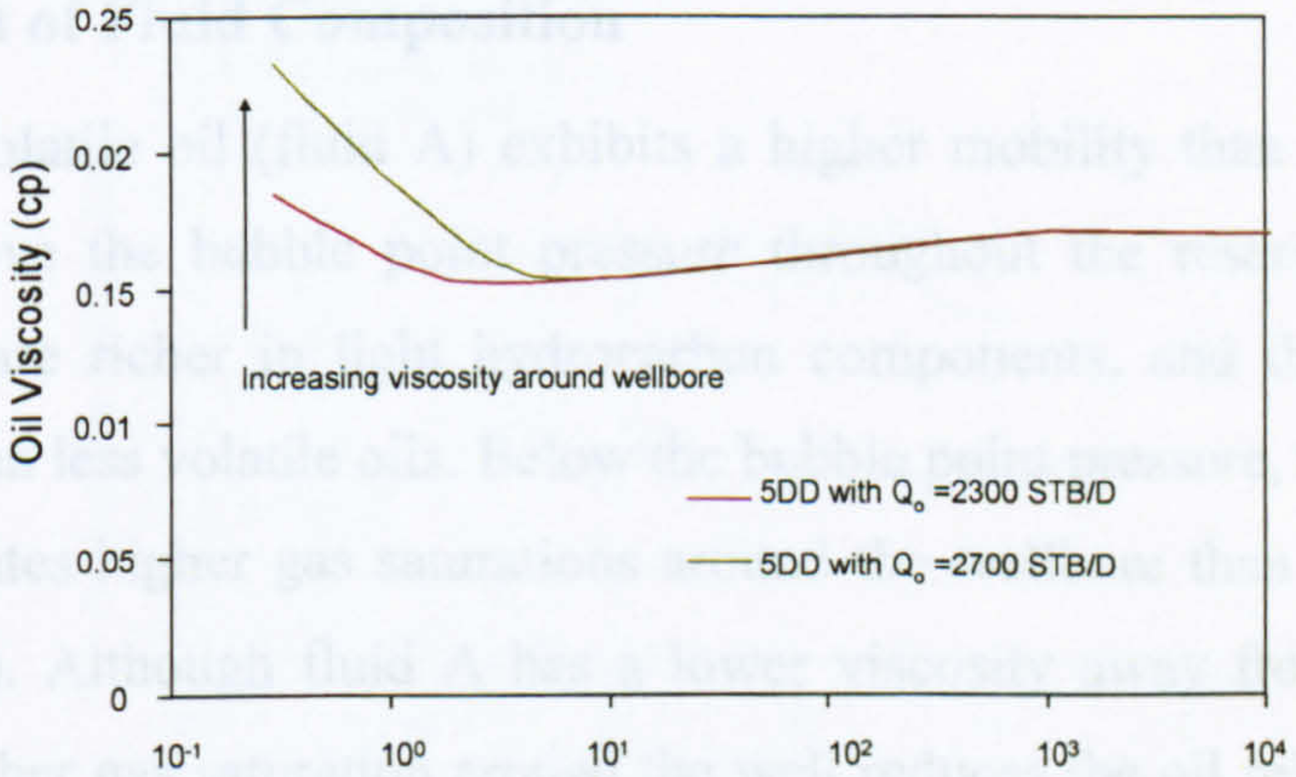

Figure 3-20 Oil viscosity profile: run A-K_1-N_0-D_0

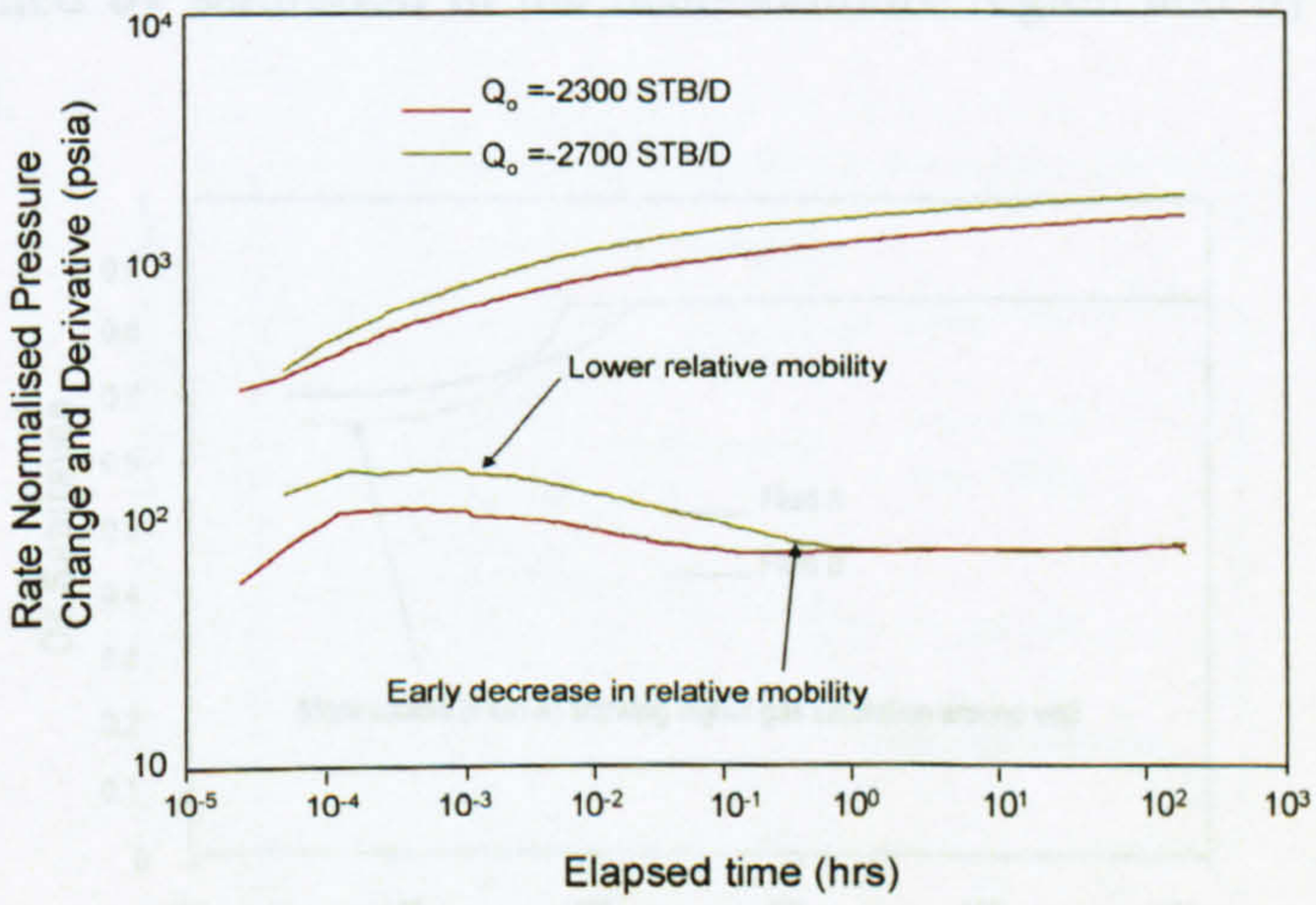

Figure 3-21 Log-Log derivative plot showing effect of production: run A-K_1-N_0-D_0

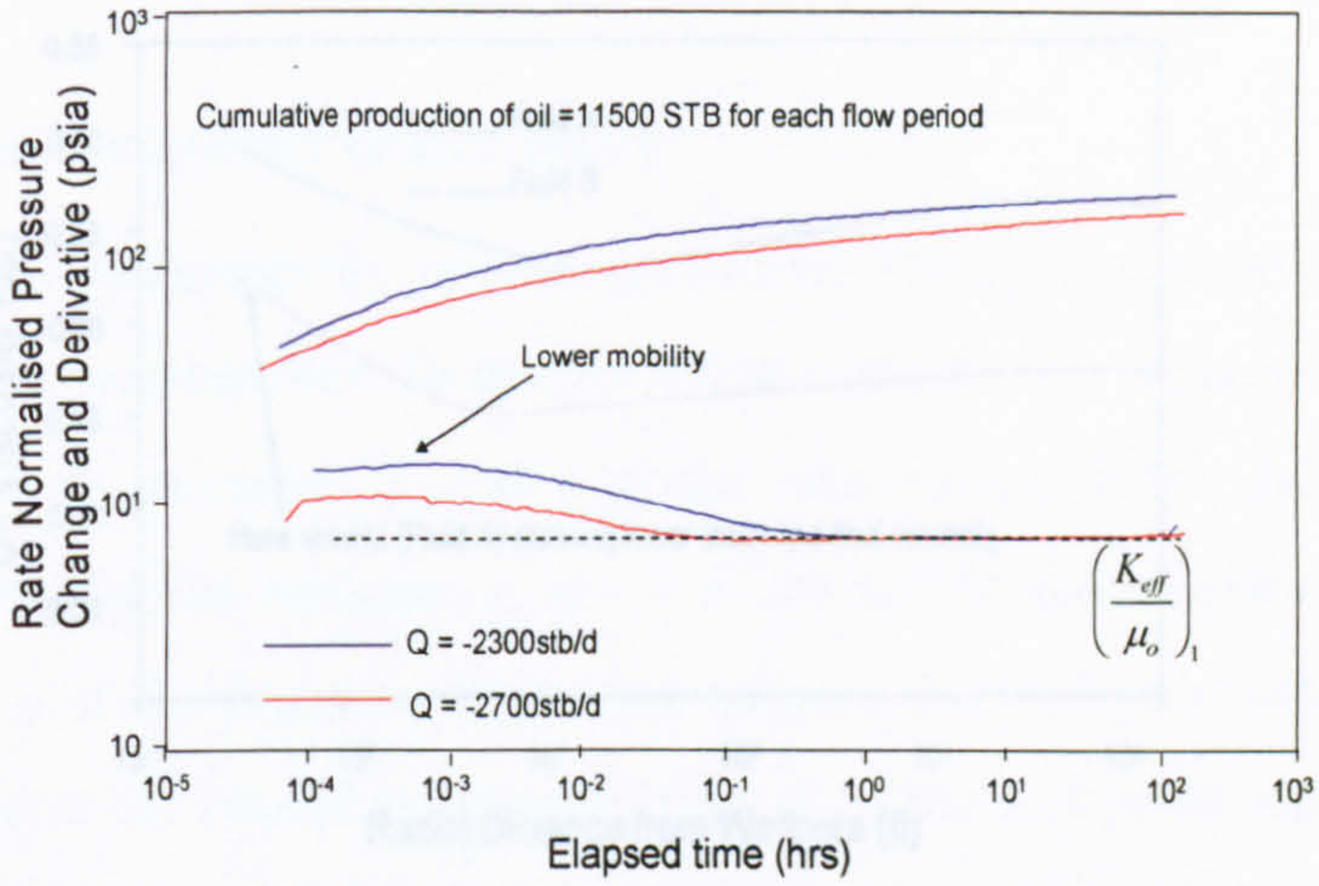

Figure 3-22 Log-Log derivative plot showing effect of production:

run A-K_1-N_0-$D_{0\text{const cumm}}$

3.2.2 Effect of Fluid Composition

The highly volatile oil (fluid A) exhibits a higher mobility than the less volatile oil (fluid B) above the bubble point pressure throughout the reservoir because highly volatile oils are richer in light hydrocarbon components, and therefore have lower viscosities than less volatile oils. Below the bubble point pressure, the more volatile oil (fluid A) creates higher gas saturations around the wellbore than the less volatile oil (*Figure 3-23*). Although fluid A has a lower viscosity away from the well (*Figure 3-24*), the higher gas saturation around the well reduces the oil relative mobility more than for the less volatile oil (fluid B) as shown in *Figure 3-25*. This behaviour can be seen on the log-log pressure derivative plot of *Figure 3-26*, which shows oil mobility being dominated by saturation in the near-wellbore region and by oil viscosity away from the well.

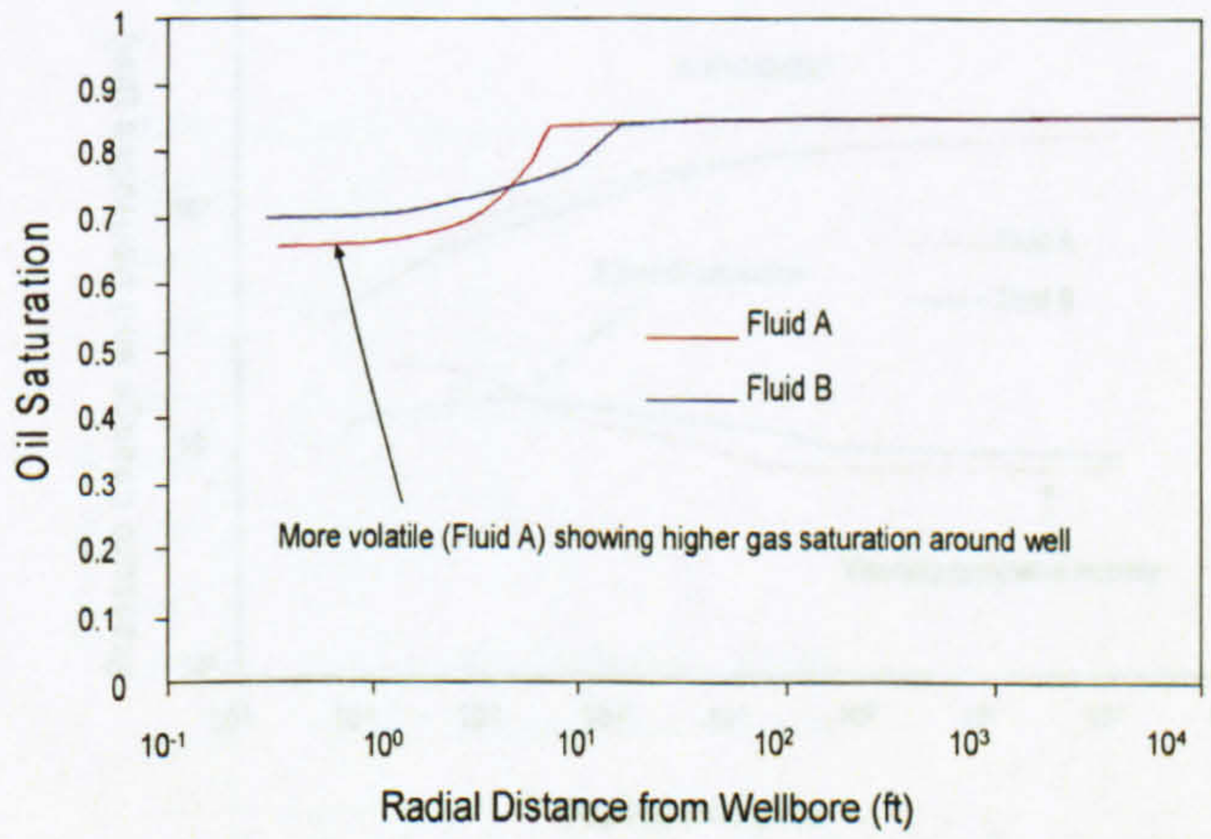

Figure 3-23 Oil saturation profile showing effect of fluid composition:

run A-K_1-N_0-D_0 and B-K_1-N_0-D_0

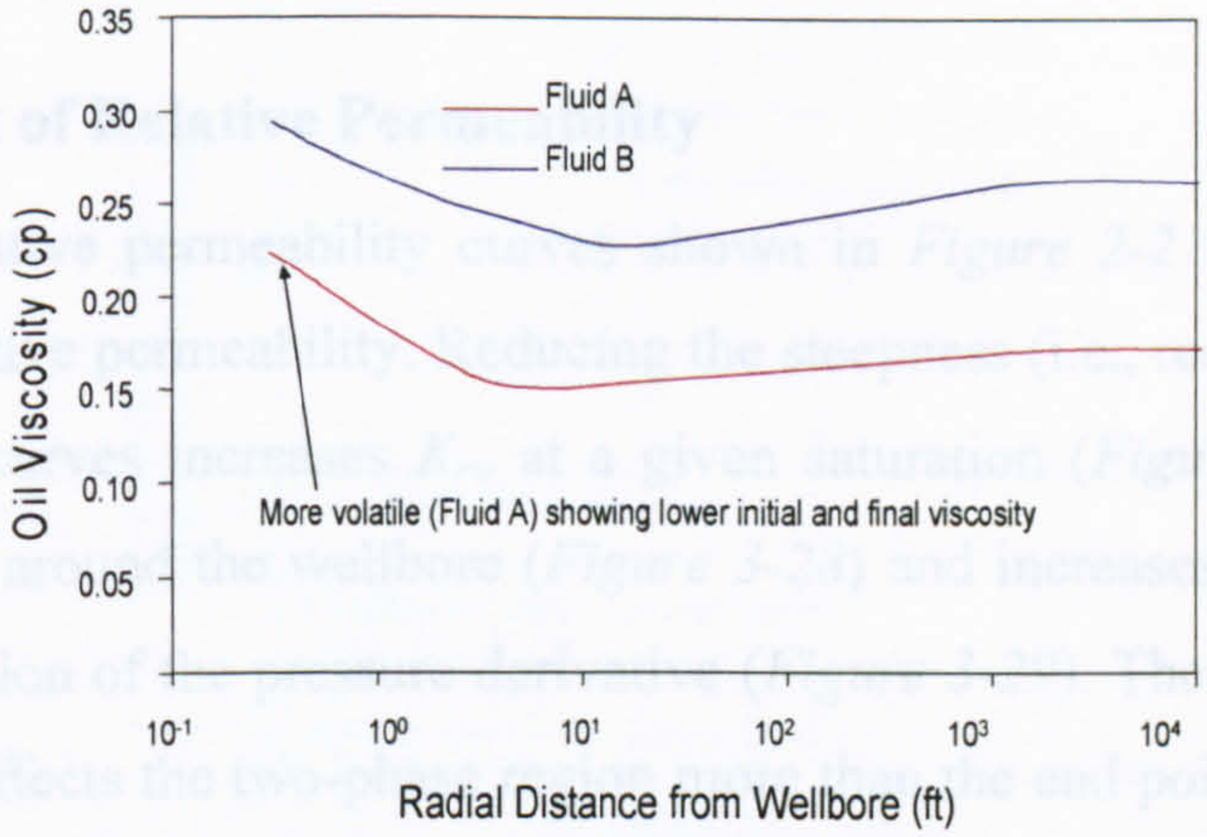

Figure 3-24 Oil viscosity profile showing effect of fluid composition: run A-K_1-N_0-D_0 and B-K_1-N_0-D_0

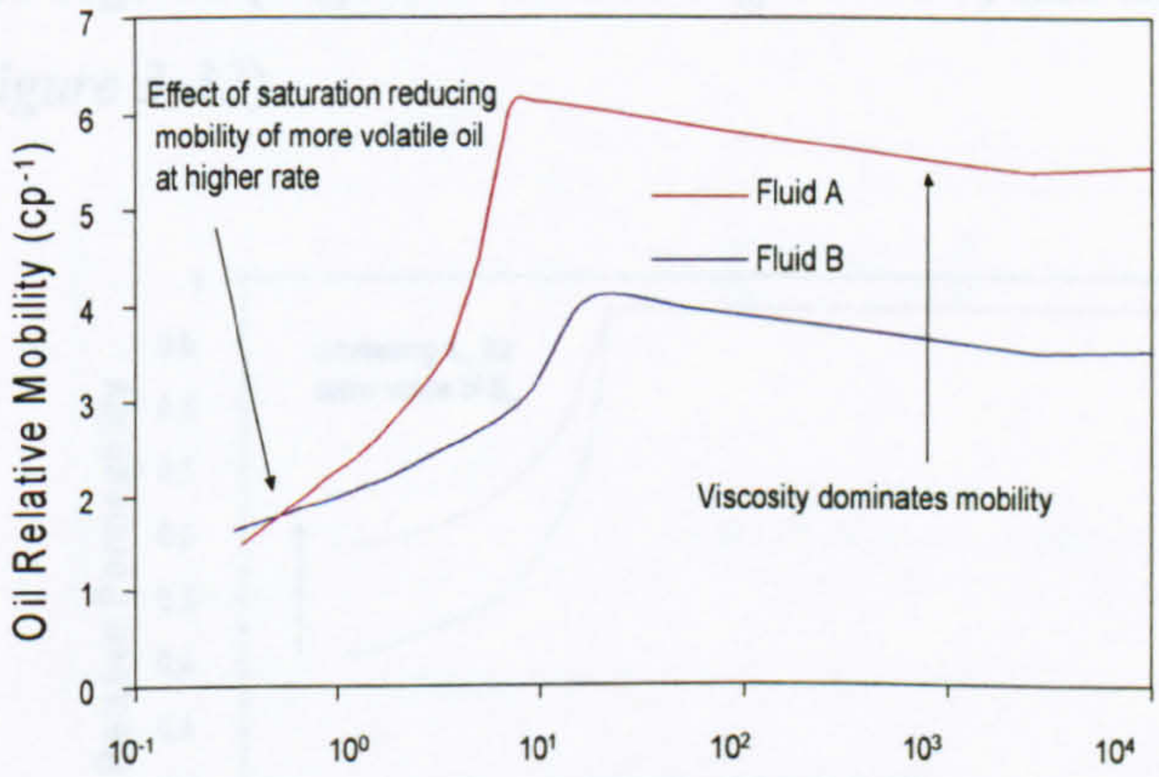

Figure 3-25 Oil relative mobility profile showing higher mobility for more volatile oil further from wellbore: run A-K_1-N_0-D_0 and B-K_1-N_0-D_0

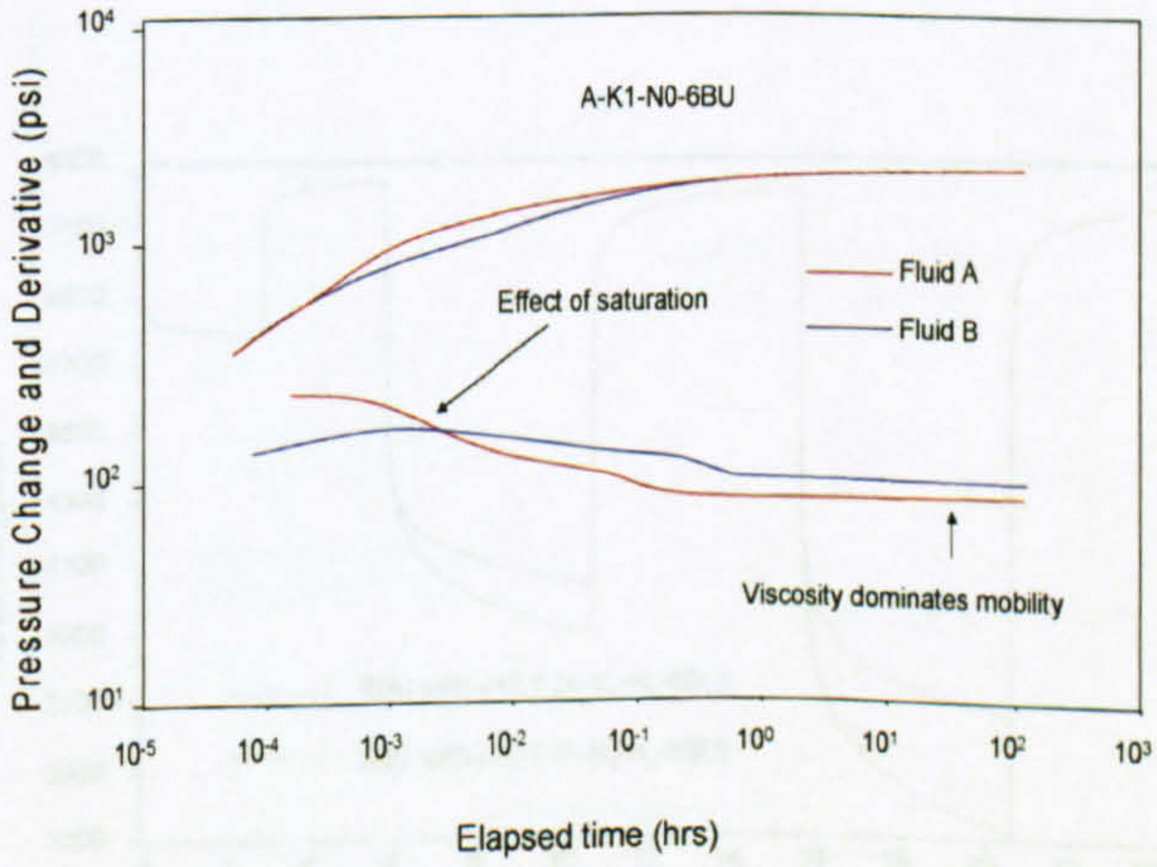

Figure 3-26 Log-log pressure derivative plot showing effect of fluid composition: run A-K_1-N_0-D_0 and B-K_1-N_0-D_0

3.2.3 Effect of Relative Permeability

The three relative permeability curves shown in *Figure 2-2* were used to study the effects of relative permeability. Reducing the steepness (i.e., reducing ε) of the relative permeability curves increases K_{ro} at a given saturation (*Figure 3-27*), decreases the pressure drop around the wellbore (*Figure 3-28*) and increases the oil mobility in the two-phase region of the pressure derivative (*Figure 3-29*). The reason is that a change in steepness affects the two-phase region more than the end point relative permeability values, as shown in *Figure 2-2*.

Reducing K_{romax} decreases K_{ro} throughout the entire reservoir in both the single phase and the two-phase regions (*Figure 3-30* and *Figure 3-31*) and increases the bottomhole pressure drop (*Figure 3-32*).

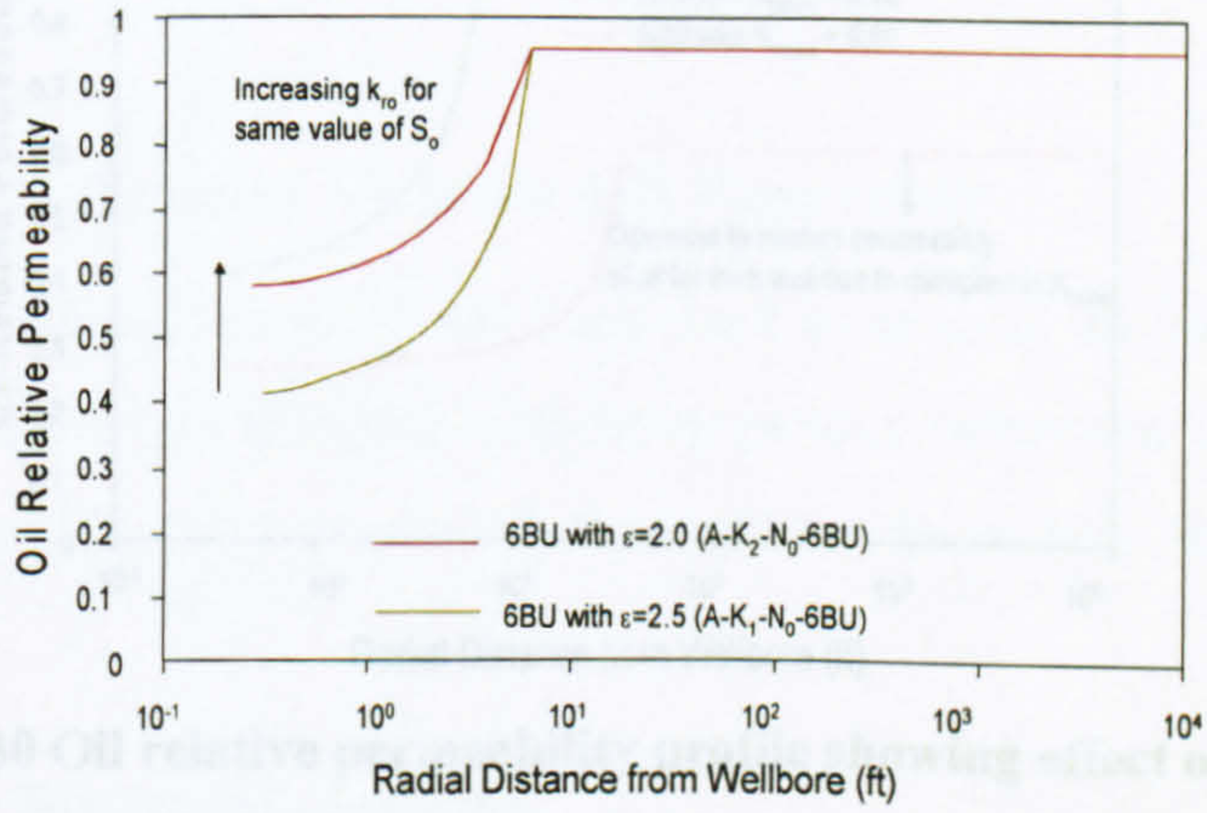

Figure 3-27 Oil relative permeability profile showing effect of ε: run A-K_1-N_0-D_0 and A-K_2-N_0-D_0

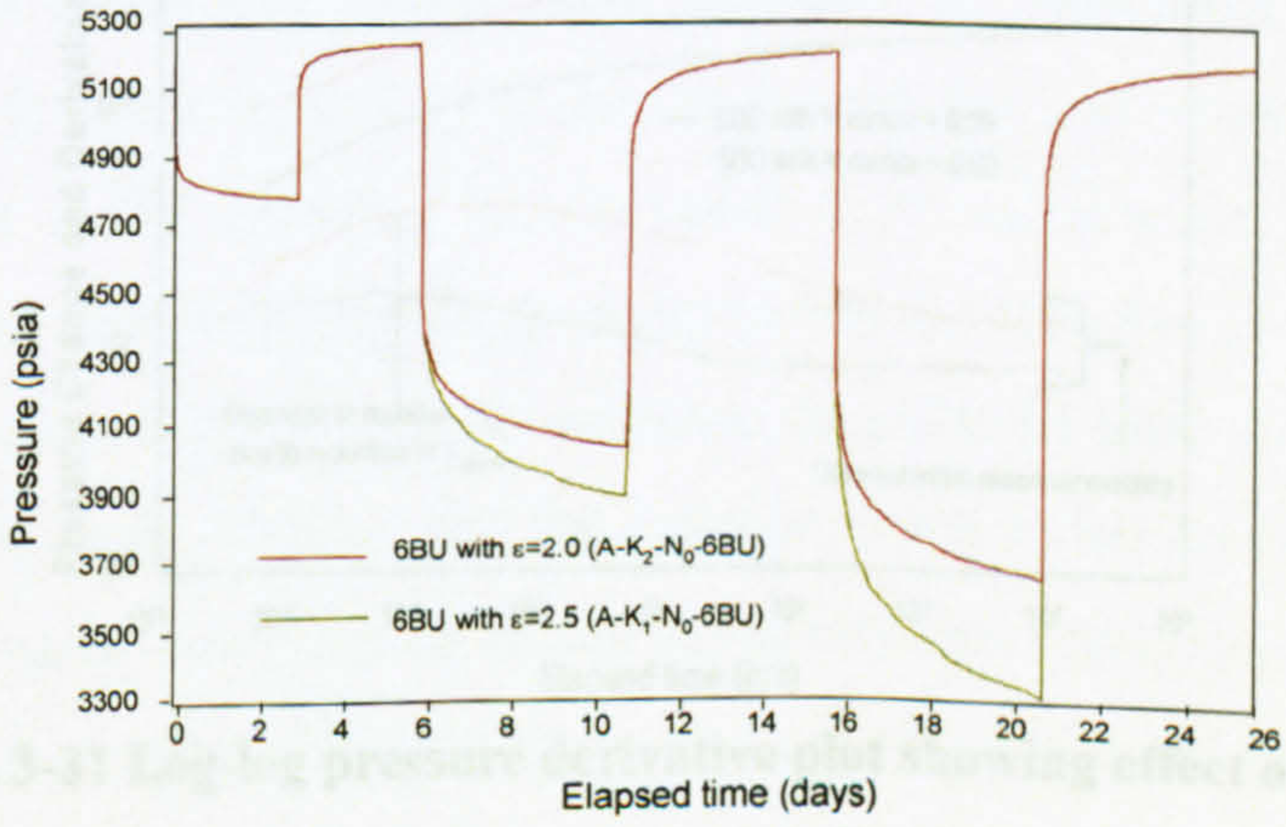

Figure 3-28 Pressure history for A-K_1-N_0-D_0 and A-K_2-N_0-D_0

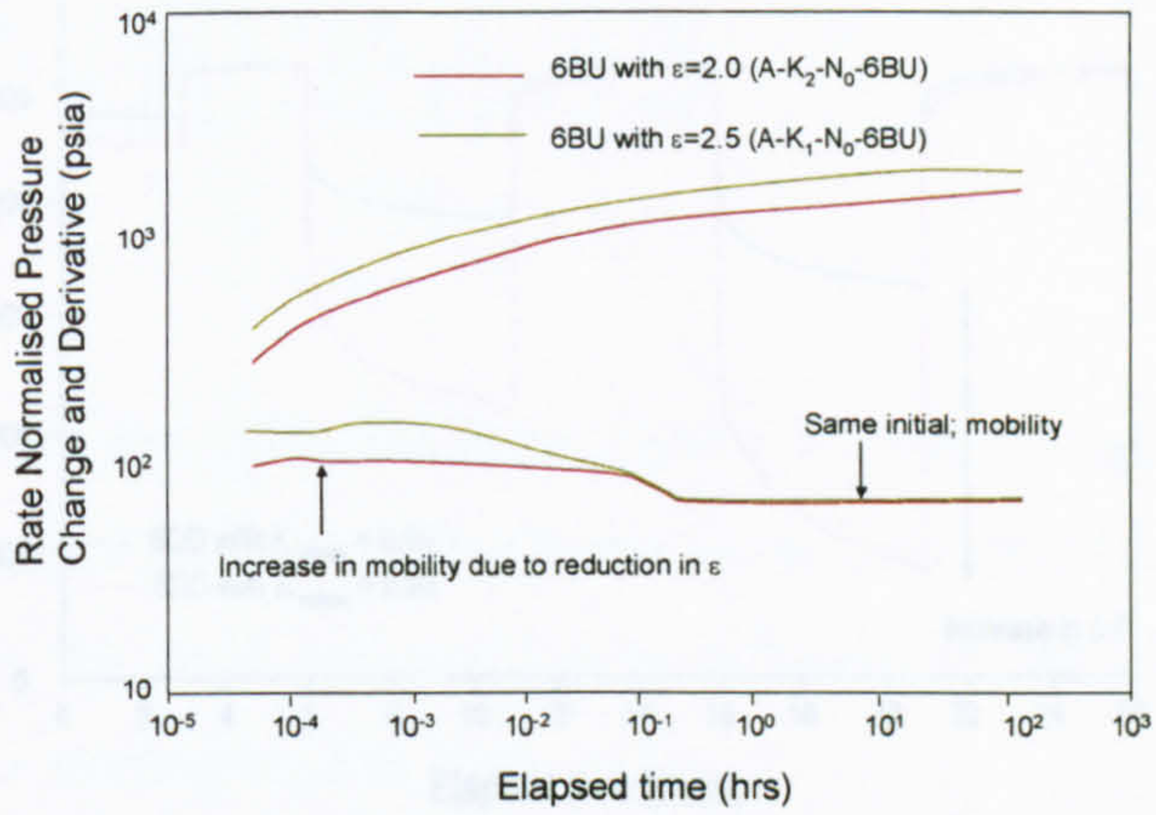

Figure 3-29 Log-log pressure derivative plot showing effect of ε: run A-K_1-N_0-D_0 and B-K_1-N_0-D_0

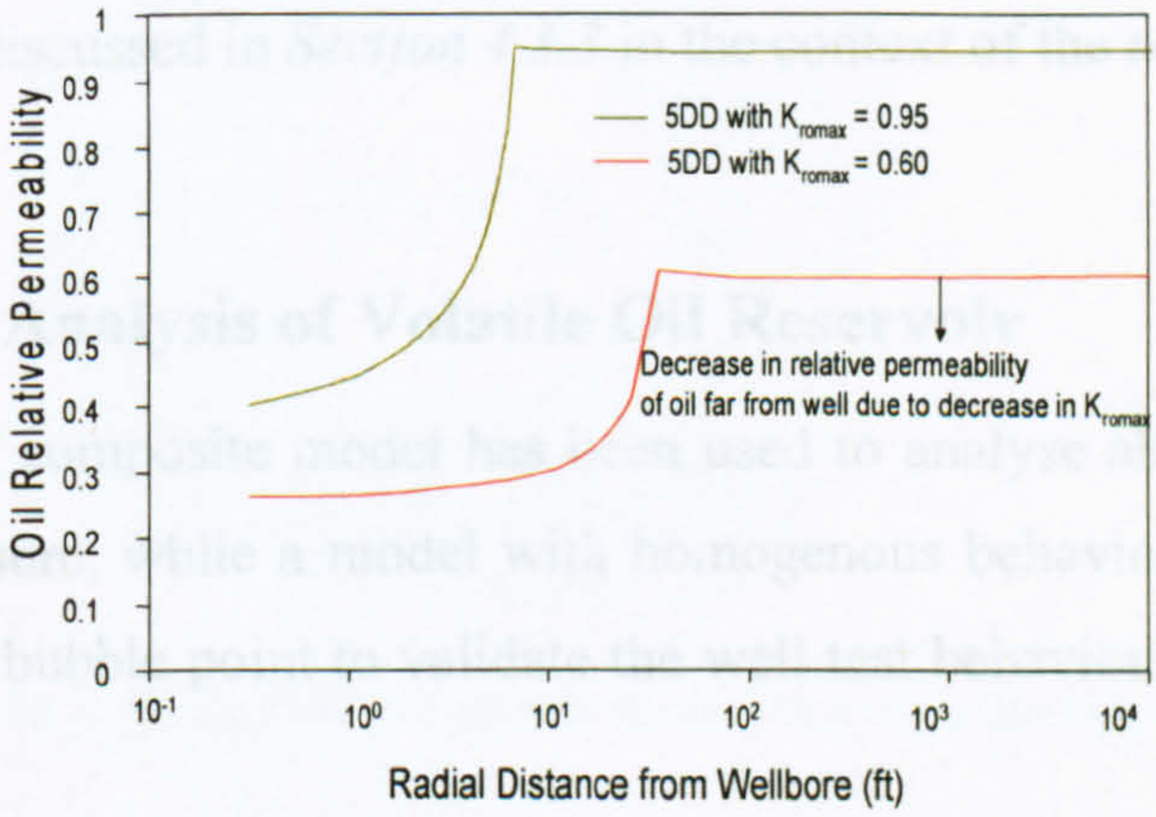

Figure 3-30 Oil relative permeability profile showing effect of K_{romax}: run A-K_1-N_0-D_0 and A-K_3-N_0-D_0

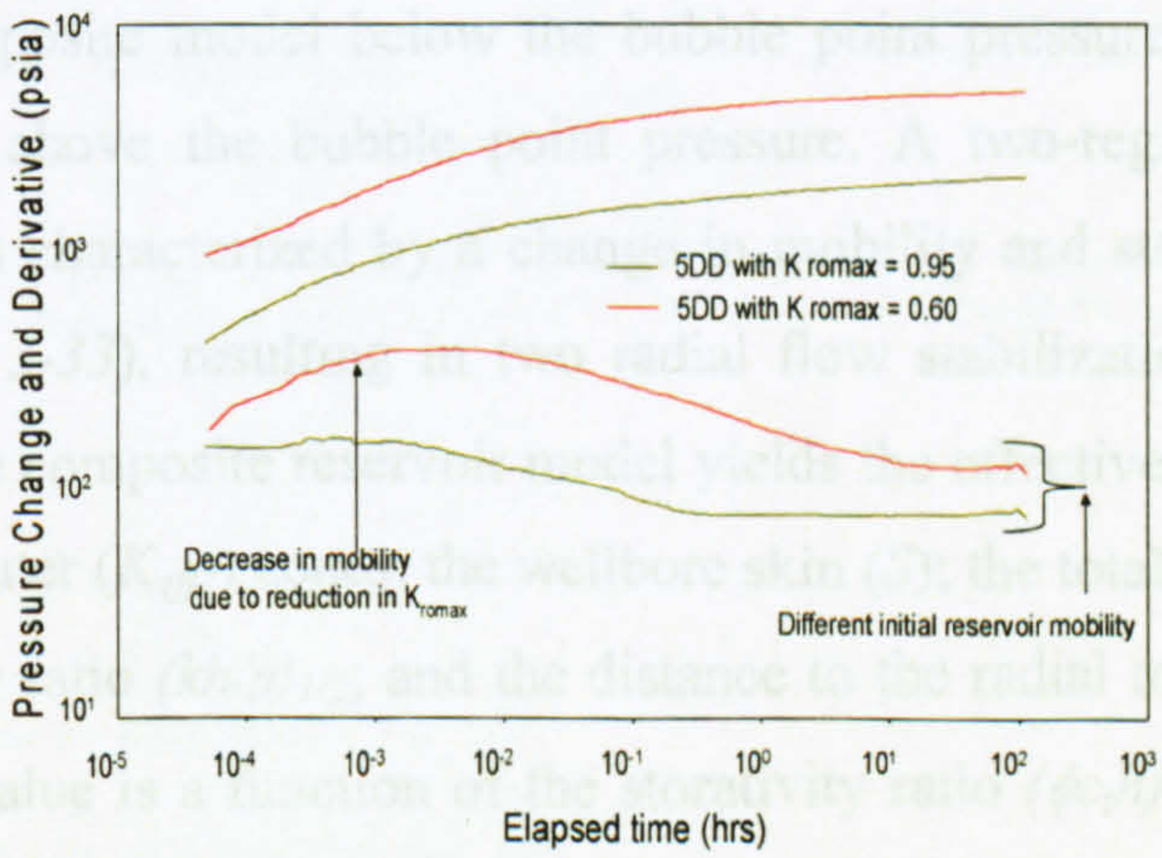

Figure 3-31 Log-log pressure derivative plot showing effect of K_{romax}: run A-K_1-N_0-D_0 and A-K_3-N_0-D_0

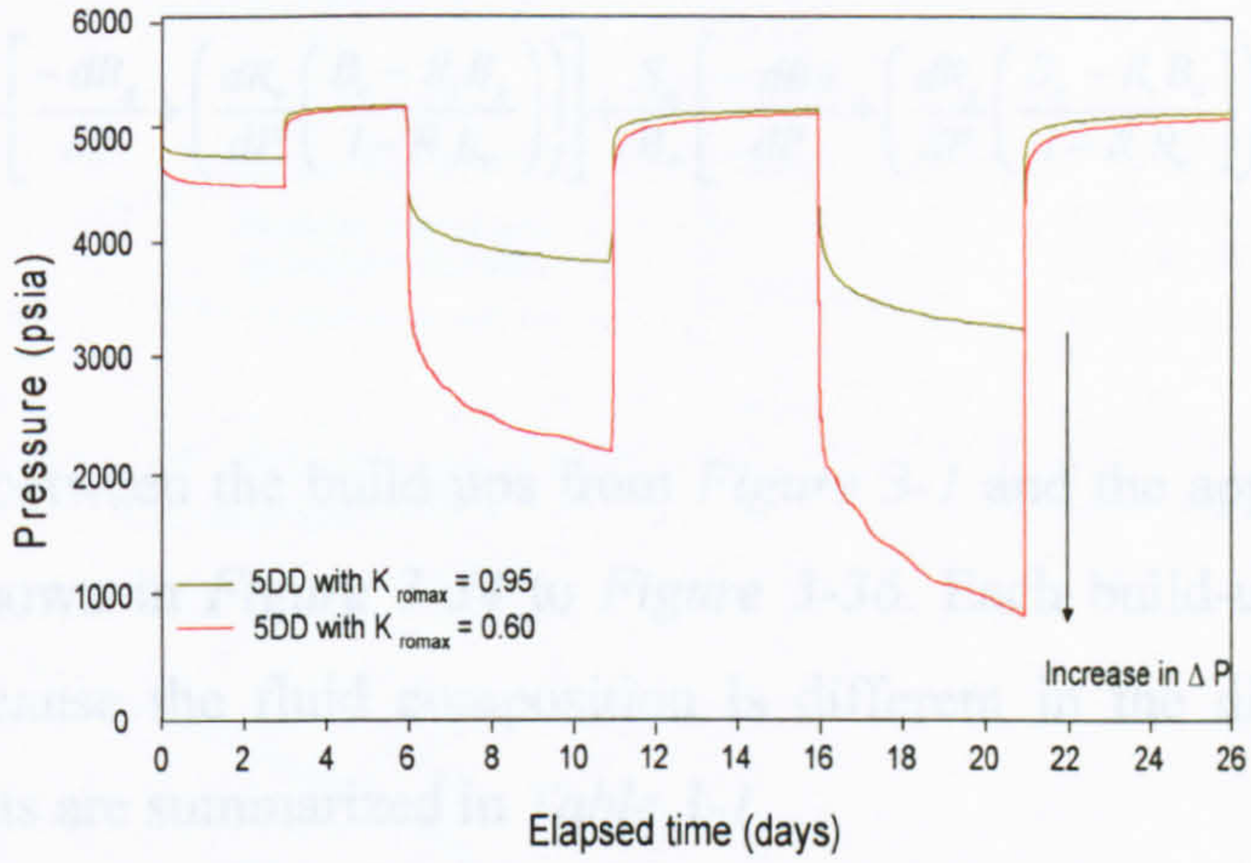

Figure 3-32 Pressure history for A-K_1-N_0-D_0 and A-K_3-N_0-D_0

3.2.4 Effect of Capillary Number and non-Darcy flow

These effects are discussed in *Section 4.3.3* in the context of the actual field data.

3.3 Well Test Analysis of Volatile Oil Reservoir

A two-zone radial composite model has been used to analyse all build-ups below the bubble point pressure, while a model with homogenous behaviour was used for flow periods above the bubble point to validate the well test behaviour discussed in *section 3.2*.

3.3.1 Composite Reservoir, 2 zones

The well test interpretation model for build-ups in a volatile oil reservoir is a two-region radial composite model below the bubble point pressure, and a homogenous behaviour model above the bubble point pressure. A two-region radial composite reservoir model is characterized by a change in mobility and storativity in the radial direction (*Figure 3-33*), resulting in two radial flow stabilization on the derivative. Analysis using the composite reservoir model yields the effective permeabilities of the inner (K_{eff1}) and outer (K_{eff2}) zones; the wellbore skin (S); the total skin (S_t) due to inner zone; the mobility ratio $(kh/\mu)_{1/2}$; and the distance to the radial mobility discontinuity, r_1. The actual r_1 value is a function of the storativity ratio $(\phi c_t h)_{1/2}$, which requires to calculate the total compressibility in the two-phase region around the wellbore (Ayan and Lee, 1986):

$$C_t = (1-S_w)\left\{\frac{S_g}{B_g}\left[\frac{-dB_g}{dP}+\left(\frac{dR_v}{dP}\left(\frac{B_o-R_sB_g}{1-R_sR_v}\right)\right)\right]+\frac{S_o}{B_o}\left[\frac{-dBo}{dP}+\left(\frac{dR_s}{dP}\left(\frac{B_g-R_vB_o}{1-R_sR_v}\right)\right)\right]\right\}+S_wC_w+C_f \quad (7)$$

The matches between the build-ups from *Figure 3-1* and the applicable interpretation models are shown in *Figure 3-34* to *Figure 3-36*. Each build-up had to be matched separately because the fluid composition is different in the different flow periods. Analysis results are summarized in *Table 3-1*.

Fluid parameters used for analysis of each of the flow periods are summarised in *Appendix C*.

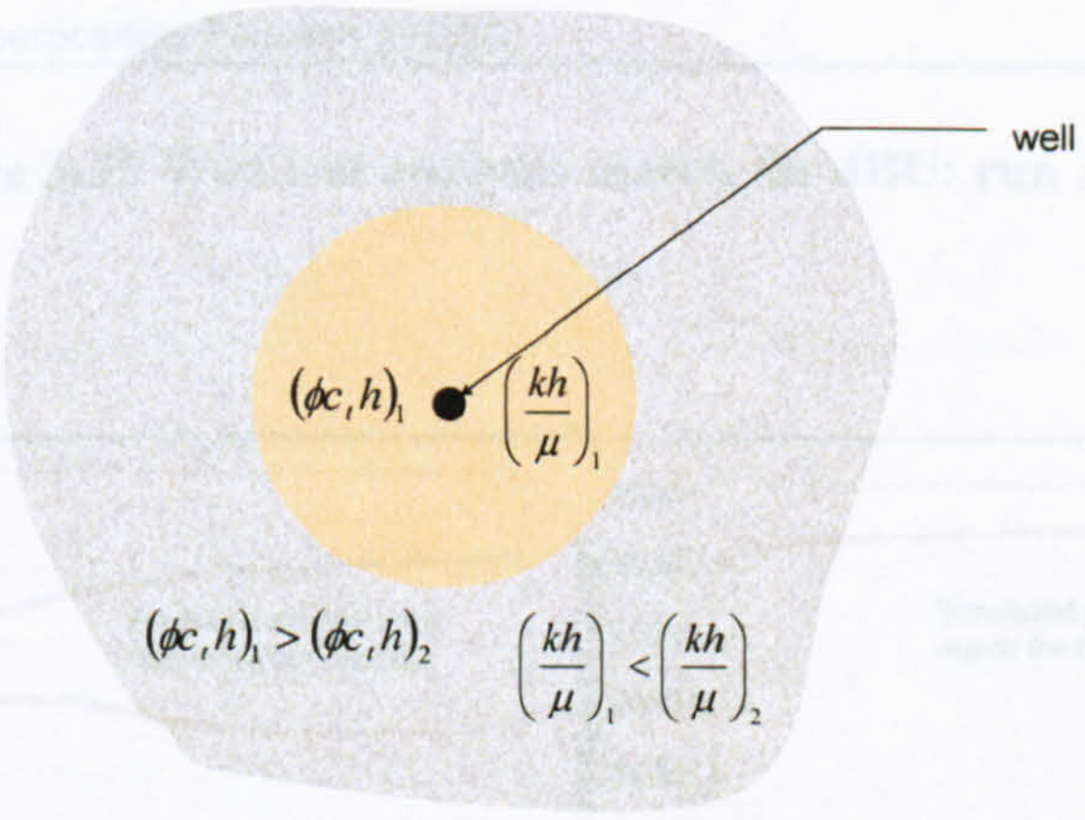

Figure 3-33 Radial composite model in a volatile oil reservoir

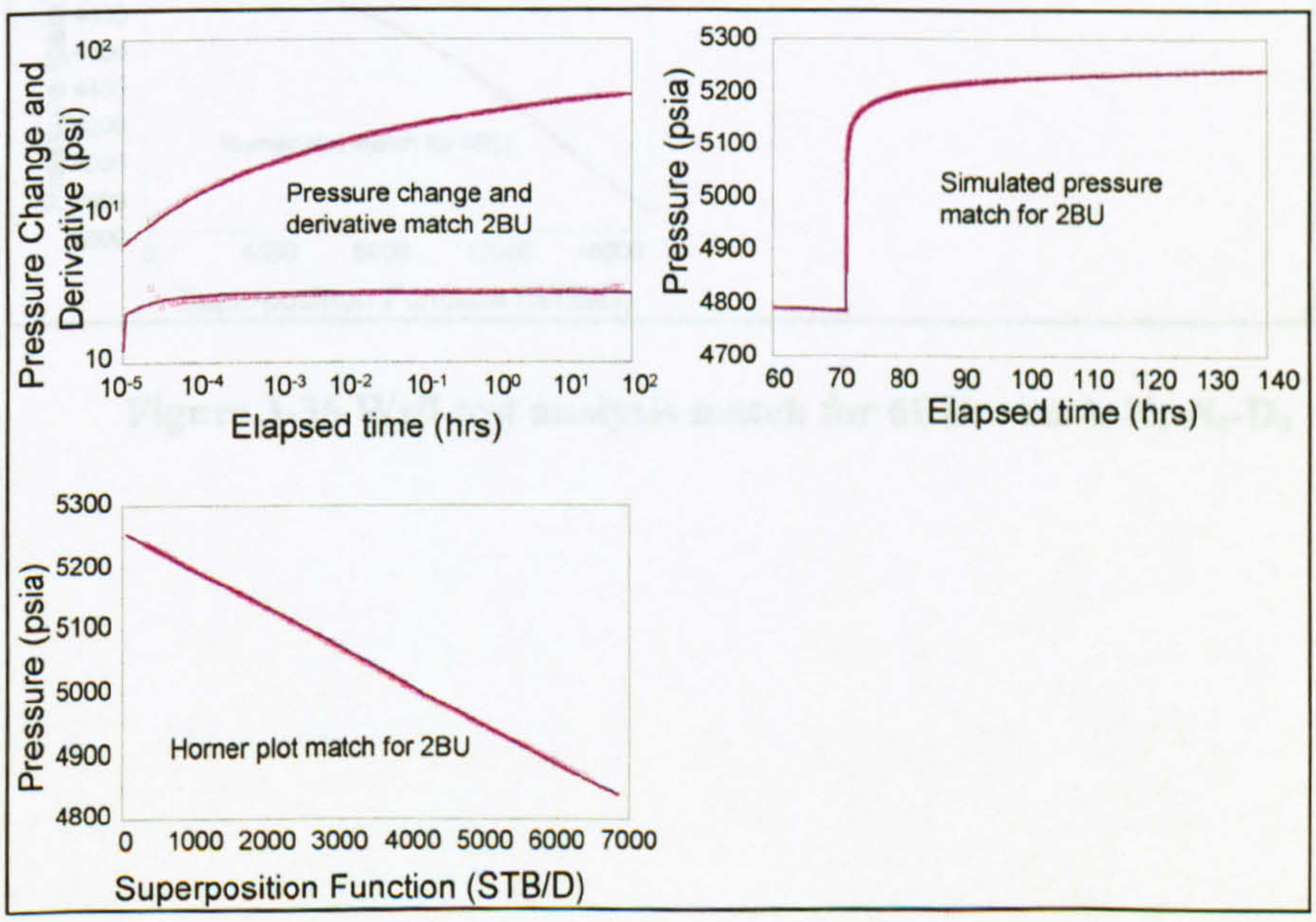

Figure 3-34 Well test analysis match for 2BU: run A-K_1-N_0-D_0

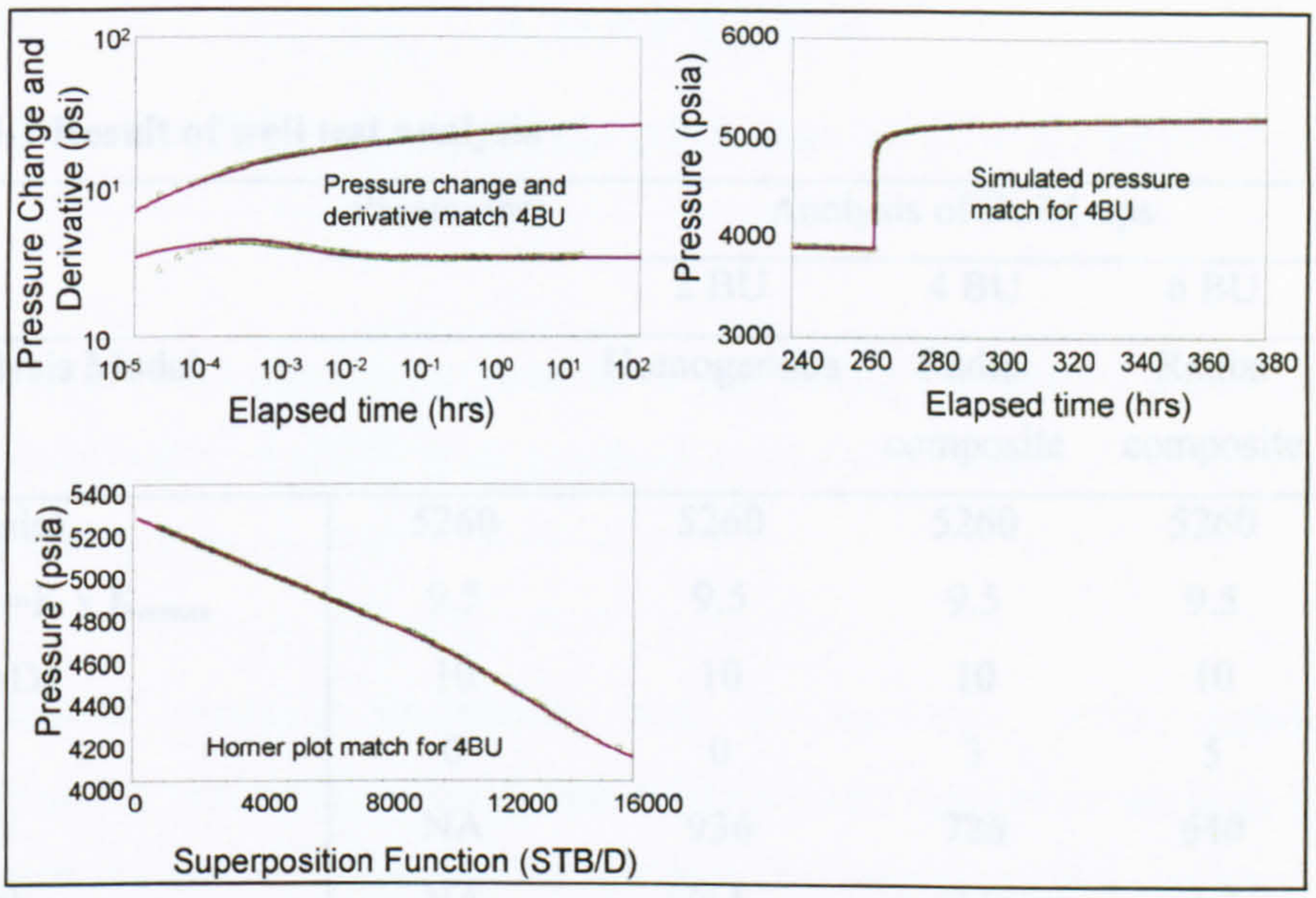

Figure 3-35 Well test analysis match for 4BU: run A-K_1-N_0-D_0

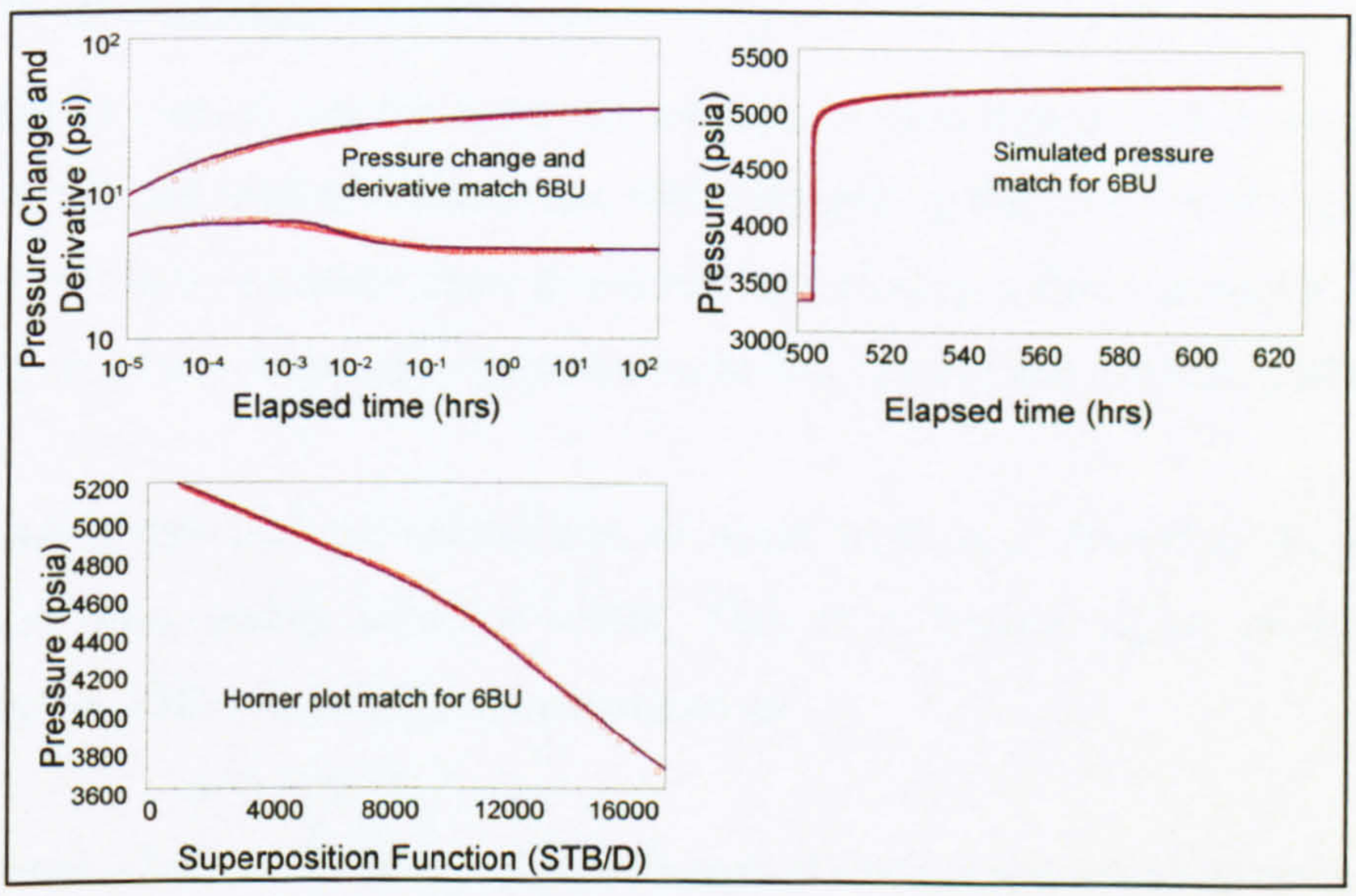

Figure 3-36 Well test analysis match for 6BU: run A-K_1-N_0-D_0

Table 3-1 Result of well test analysis

	Parameters	Analysis of Build-ups		
		2 BU	4 BU	6 BU
Analysis Model		Homogenous	Radial composite	Radial composite
P_i (psia)	5260	5260	5260	5260
$K_{oeff} = K \times K_{romax}$	9.5	9.5	9.5	9.5
K (mD)	10	10	10	10
$S_{(t)}$	0	0	3	5
r_i (ft)	NA	936	726	640
$(Øch)_{1/2}$ (from fluid analysis)	NA	NA	2.5	3.2
$(Kh/\mu)_{1/2}$	NA	NA	0.67	0.54

CHAPTER 4

Well Test Analysis of Volatile Oil Reservoirs

This chapter illustrates the application of the findings described above to the analysis of an actual well test (DST-Well-15) from a volatile oil reservoir in the Pur-Taz region of Western Siberia.

Conventional analysis techniques and deconvolution were supplemented by compositional simulation to verify the existence and the size of the high gas saturation region around the wellbore, and investigate the impact of the capillary number and non-Darcy flow.

4.1 Well Testing

Well test is carried out for reservoir evaluation, description and management. This involves flowing well at constant rate while measuring the pressure change (decline) as function of time –pressure draw down test and closing a flowing well to measure the pressure recovery (build-up) - pressure build-test (Zheng and Corbett, 2005).

Well testing involves perturbing one or more wells and observing the effect at the perturbed well and/or adjacent wells. This is a typical signal analysis problem (Gringarten, 1986). Symbolically described as:

$$I \rightarrow S \rightarrow O \qquad (4\text{-}1)$$

In this case a known input signal ***I*** (a change of rate) is applied to an unknown system ***S*** (the well and reservoir) resulting in an output signal ***O*** (the pressure response). The reservoir model that satisfies the known input and output becomes the solution. The evaluation becomes an inverse problem with a non-unique solution. This is not uncommon to most reservoir characterisation process. The non-uniqueness can be reduced by having more test data and checking consistency of result with other reservoir characterisation method such as geophysics, geology, petrophysics, etc.

The mathematical formulation describing the behaviour of the interpretation model is obtained by solving the diffusivity equation, which governs the flow of fluid in a porous medium.

4.1.1 Diffusivity Equation

The diffusivity equation governs variation in pressure in the reservoir with time. The diffusion is formulated from the following equations:

1, Darcy's law describing 1-dimensional radial flow fluid flow in porous media:

$$u = -\frac{k}{\mu}\frac{\partial p}{\partial r} \tag{4-2}$$

Darcy's law is valid within a time interval when the flow rate and other parameters are constant. It does not depend on the porosity of the medium, or the on the compressibility of either the fluids or the rock (Bourdarot, 1998).

2, Continuity equation (mass conservation equation) for 1-dimensional radial flow shown in (*4.3*).

$$-\frac{\partial(\rho u)}{\partial r} = \frac{\partial(\rho\phi)}{\partial t} \tag{4-3}$$

3, Equation of state which accounts for variation of fluid properties with pressure is shown in (*4.4*) and relationship which accounts for dependence of porosity on pressure is shown in (*4.5*).

$$c_o = \frac{1}{\rho}\frac{\partial p}{\partial p} \tag{4-4}$$

$$c_f = \frac{1}{\phi}\frac{\partial \phi}{\partial p} \tag{4-5}$$

The diffusivity equation for 1 dimensional radial flow is expressed in as:

$$\frac{1}{r}\frac{\partial}{\partial r}\left(r\frac{\partial p}{\partial r}\right) = \frac{\phi\mu c_t}{k}\frac{\partial p}{\partial t} \tag{4-6}$$

Conditions for validity of the Diffusivity equation can be summarised below:

- Darcy's law applies
- Small pressure gradients everywhere
- Negligible gravity forces

- Slightly compressible fluid
- k, ϕ and μ are constant (independent of pressure and location)
- Reservoir is homogenous and isotropic

The diffusivity does not apply directly to highly compressible fluid (gas) or rock (unconsolidated formation) hence the need to linearise the diffusivity equation by using pseudo-pressures (Gringarten, 2006a).

Solution of Diffusivity equation

The diffusivity equation can be solved for with three boundary conditions described as:

- Pressure at the beginning of test (initial condition)
- Inner boundary conditions (flow rate at well)
- Outer boundary conditions (pressure at the reservoir boundaries)

Different flow regime classifications are defined depending on $(\partial p/\partial t)$ in the diffusivity equation.

- $\frac{\partial p}{\partial t} = f(location, time)$: Transient flow
- $\frac{\partial p}{\partial t}$ = Constant :Pseudo- or semi-steady state (depletion in closed reservoirs)
- $\frac{\partial p}{\partial t} = 0$: Steady state (developed patterns with constant pressure boundaries)

The pressure variations at the well give an indication of the properties of the part of the reservoir involved in the compressible zone. At the beginning of the test the pressure drop reflects the reservoir properties in the vicinity of the well. Later on, the test reaches areas that are further away.

Transient flow:

During well testing, reservoirs behave as if infinite in extent until the compressible zone reaches the boundaries of the reservoir or comes under the influence of another well.

Pseudo steady-State flow:

When the compressible zone reaches a series of no-flow boundaries, the flow regime becomes *pseudo steady state*. This is the type of flow in a producing reservoir with no flow boundaries.

Steady-state flow:

Steady-state flow occurs when the compressible zone is affected by some constant pressure outer boundaries. This is the type of flow in the reservoir producing under gas-cap or water drive conditions when mobility of the water is high compared to that of the oil (Bourdarot, 1998).

The diffusivity equation can be solved using methods which include:

- Laplace Transform (Van Everdingen and Hurst, 1949). Numerical Laplace Transform Inversion using Stefhest Algorithm has improved capabilities to solve more complex reservoir models.
- Green's functions. Gringarten and Ramey (1973) used Green functions to solve unsteady state flow problem in reservoirs. Instantaneous Green and source functions were prepared. This can be used with the Newman's product method to generate solution for different reservoir flow problems.
- Other methods include Boltzmann transformation (for radial flow); Hankel transforms and Numerical (finite differences, finite elements) (Gringarten, 2006a).

The diffusivity equation is linear for slightly compressible fluid as $(\phi\mu c_t)/k$ is independent of pressure and time. The linearity of the diffusivity equation makes it possible for superposition of solutions in time (well producing/injecting at different starting times) and superposition of solutions in space (well producing/injecting at different locations). However, the same initial conditions must apply to individual and superposed solutions (Gringarten, 2006a).

Well test analysis often makes use of dimensionless variables. The importance of dimensionless variable is that they simplify the reservoir models by embodying the reservoir parameters (such as k), thereby reducing the total number of unknowns. They also have the advantage of providing model solution independent of any unit system.

Dimensionless pressure p_D is defined in (*4-7*) and (*4-8*) in oilfield and consistent units respectively.

$$p_D = \frac{kh}{141.2qB\mu}(p_i - p_{wf}) \tag{4-7}$$

$$p_D = \frac{2kh}{qB\mu}(p_i - p_{wf}) \tag{4-8}$$

Dimensionless time t_D is defined in (*4-9*) and (*4-10*) in oilfield and consistent units respectively.

$$t_D = \frac{0.000264kt}{\phi\mu c_t r_w^2} \tag{4-9}$$

$$t_D = \frac{kt}{\phi\mu c_t r_w^2} \tag{4-10}$$

Dimensionless time can be defined based upon reservoir area as shown in (*4-11*).

$$t_{DA} = \frac{0.000264kt}{\phi\mu c_t A} \tag{4-11}$$

Relationship between t_D and t_{DA} is shown:

$$t_D = t_{DA}\frac{A}{r_w^2} = t_{DA}\pi\frac{r_e^2}{r_w^2} \tag{4-12}$$

Dimensionless radius, r_D is defined as:

$$r_D = \frac{r}{r_w} \tag{4-13}$$

The concept of dimensionless variables can be used to solve the diffusivity equation. The dimensionless diffusivity equation is:

$$\frac{1}{r_D}\frac{\partial}{\partial r_D}\left(r_D\frac{\partial p_D}{\partial r_D}\right) = \frac{\partial p_D}{\partial t_D} \tag{4-14}$$

In the absence of wellbore storage and skin effects, the pressure transient due to infinite acting radial flow into a line source wellbore producing at constant flow rate is given by:

$$p_D = -\frac{1}{2}Ei\left(-\frac{r_D^2}{4t_D}\right) \tag{4-15}$$

Where Ei is the exponential integral function which is valid throughout the reservoir for $r_D \geq 1$, thus can be used for interference tests as well as drawdown and build-up test.

For r_D=1, the exponential integral solution can be approximated by:

$$p_{wD} = \frac{1}{2}\left(\ln t_D + 0.80907\right) + S \qquad \text{for } \frac{t_D}{r_D^2} > 10 \tag{4-16}$$

$$p_{wf} = p_i - 162.6\frac{qB\mu}{kh}\left(\log t + \log\frac{k}{\phi\mu_i r_w^2} + 0.8686S - 3.2274\right) \tag{4-17}$$

Where (S) is the dimensionless skin factor (Van Everdingen, 1953)

From (*4-17*), a plot of pressure drop against the logarithm of time should contain a straight line with slope given in by:

$$m(slope) = 162.6\frac{qB\mu}{kh} \tag{4-18}$$

The skin factor can hence be estimated from difference between p_i and the intercept of the straight line. This often done by substituting the time 1 hour in (*4-17*), and solving for S:

$$S = 1.151\left(\frac{p_i - p_{1hr}}{m} - \log\frac{k}{\phi\mu c_t r_w^2} + 3.2274\right) \tag{4-19}$$

Most of the information from well test comes from interpreting the pressure build-ups. Interpreting a drawdown test is limited by the flow rate fluctuations inherent to production. During build-up the shut-in pressure (p_{ws}) is expressed as:

$$p_{ws} = p_i - 162.6\frac{qB\mu}{kh}\left(\log\frac{(t_p + \Delta t)}{\Delta t} + \log\frac{k}{\phi\mu_i r_w^2} + 0.8686S - 3.2274\right) \tag{4-20}$$

(*4-20*) suggests that a semi-log plot of p_{ws} versus $(t_p+\Delta t)/\Delta t$ (Horner plot) yields a straight line with a slope m which is used in calculating k. The straight line extrapolates to p^* at infinite shut-in times. The value of p^* equal to the initial reservoir pressure p_i only in the case of an infinite reservoir, and can be used to calculate the average reservoir pressure in the case of a depleted well.

Another interpretation method different from semi-log analysis is the use of transient pressure data is log-log type curve analysis. Log-log type curve analysis matches data and an applicable interpretation model on a log-log graph to obtain the desired well and reservoir parameters. An interpretation model applicable to the data exhibits the same behaviour as the data, and since dimensionless pressure and time are linear functions of actual pressure and time by definition, the actual pressure drop on a log-log graph differs from the applicable dimensionless interpretation model by shifts along both the pressure and the time axes. Calculating the shifts, or "matching" the two curves, which is equivalent, gives estimates of the reservoir and well parameters that characterizes the model, such as mobility, skin effect, etc.

Several kinds of type curves have been published in literature. These include: Agarwal *et al.* (1970); Wattenbarger and Ramey (1970); McKinley (1971); Gringarten *et al* (1974); Earlougher and Kersch tyrpe curves (1974); Gringarten *et al.* (1979); Bourdet and Gringarten (1980).

Bourdet *et al.* (1983) presented a new set of type curves. They included the pressure derivative plot. The advantage of the derivative is that it magnifies the difference in shapes between the various flow regimes that can be present during a given flow period, thus enhancing the diagnostic capability of the interpreter.

Other type curves include: Duong (1987); Onur and Reynolds (1988); Blasingame *et al.* (1989); and Bourgeois *et al.* (1991).

4.1.2 Well Test Interpretation Process.

This involves model identification which is defined by flow regime. The log-log pressure derivative is a very common method of identifying flow regimes near wellbore, reservoir and boundaries. This process involves identifying flow regimes that could create various types of test data (Gringarten, 2006b).

Flow regimes include: near wellbore-early times (wellbore storage, skin, fractures, partial penetration, horizontal well); reservoir behaviour-middle times (homogenous and heterogeneous: 2 –porosity, 2-permeability and composite) and boundary effects-late times (infinite extent, specified rates, specified pressure and leaky boundary) (Gringarten, 2006b). Components of well test interpretation model are summarised in *Figure 4-1*.

Near Wellbore Effects	**Reservoir Behaviour**	**Boundary Effects**
Wellbore Storage	Homogeneous	Specified Rates
Skin	Heterogeneous	Specified Pressure
Fractures	2-Porosity	Leaky Boundary
Partial Penetration	2-Permebaility	
Horizontal Well	Composite	
Early Times	**Middle Times**	**Late Times**

Figure 4-1 Components of Well test interpretation model (Gringarten, 2006b)

The evaluation of well test parameters has evolved from straight line to deconvolution. The presence of different method has lead to integrated approach to analysis well test data. This method can be summarised as: straight line techniques; type curve matching and use of non-linear regression (Gringarten, 2006b). The various analysis techniques, their age and ranking with respect to power in identification and verification of interpretation model can be summarised in *Figure 4-2*.

Time	**Analysis Method**	**Identification**	**Verification**
50's	Straight Lines	Poor	None
70's	Pressure Type Curves	Fair (Limited)	Fair to Good
80's	Pressure Derivatives	Very Good	Very Good
00's	Deconvolution	Much Better	Same as Derivative
Next	?	>>>	>>>

Figure 4-2 Ranking of well test interpretation methods (Gringarten, 2006b).

The model verification involves matching simulated data with real data using log-log; Horner plot; simulated pressure history and use of common sense. Well test interpretation process can be summarised with flow diagram in *Figure 4-3*.

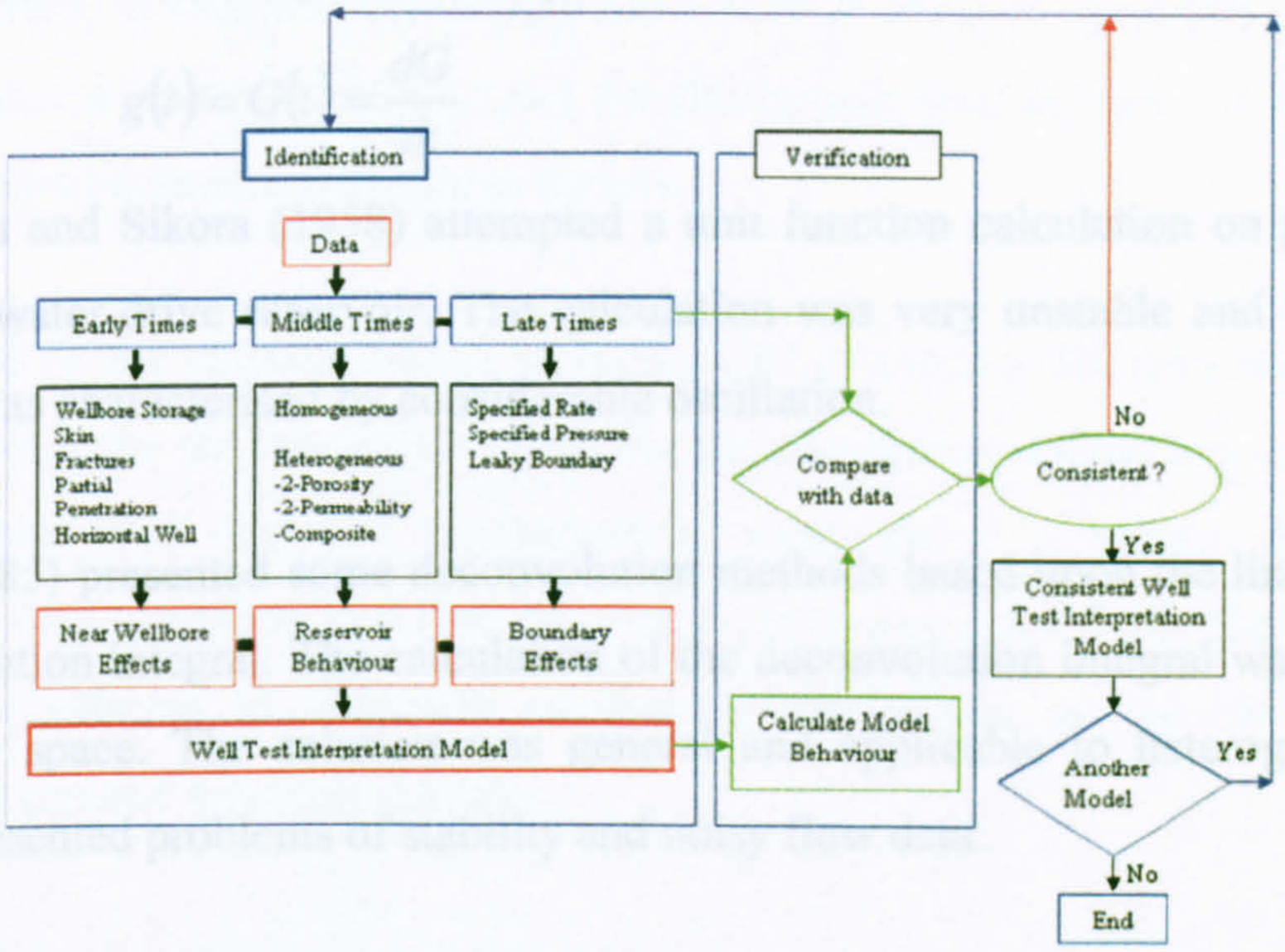

Figure 4-3 Well test Interpretation Model Identification Process (Gringarten, 2006b).

4.1.3 Deconvolution of Well Test Data

Deconvolution transforms variable rate pressure to constant rate initial draw down with duration equal the total duration of test and yields directly corresponding pressure derivative normalised to a unit rate (Gringarten, 2006b). The ability of deconvolution to analyses well test data at variable rate has made it important in analying large set of well test data ranging over long periods of time from permanent dowhole gauges (Von Schroeter *et al*., 2004). Such data contain information about the reservoir at distances from the well which can be several orders of magnitude larger than the radius of investigation from of single flow period (Von Schroeter *et al*., 2004).

The pressure drop signal observed in a well test with time varying flow rate satisfies the Duhamel's principle (*4-21*). This principle is valid if the inflow in the reservoir is governed by set of equations which are linear in pressure and production rate. In situations where nonlinearities play an important role, as for gas or multiphase flow, it can only be an approximation (Von Schroeter *et al*., 2004).

$$\Delta P(t) = \{Q * g\}(t) = \int_0^t Q(t')g(t-t')dt' \tag{4-21}$$

Where g denotes the impulse response, which is the ordinary time derivative of the rate-normalised wellbore pressure drop:

$$g(t) = \dot{G}(t) = \frac{dG}{dt} \tag{4-22}$$

Hutchinson and Sikora (1958) attempted a unit function calculation on pressure and rate for a water-drive reservoir. The calculation was very unstable and the resulting response was characterised by considerable oscillation.

Kucuk (1985) presented some deconvolution methods based upon the linearization of the convolution integral. The calculation of the deconvolution integral was carried out in Laplace space. The solution was general and applicable to heterogeneous. The method presented problems of stability and noisy flow data.

Thompson and Reynolds (1986) described the use of piecewise approximation for either pressure of flow rate in the evaluation of the convolved integral. The deconvolution integral was carried out in the real time which creates a general solution. The calculation is however complex and time consuming. The real time deconvolution described by the author involves a complicated recurrence relation which has severe numerical difficulties.

Roumboutsos and Stewart (1988) used piecewise linear approximations to transform rate and pressure measurements into Laplace space. The constant-rate pressure response was then obtained by inverting a quotient of Laplace transforms this was also characterised by instability.

Von Schroeter *et al.* (2004) presented a deconvolution algorithm based on the Total Least Square method, which provides stable results. The algorithm estimates both rates (called "adapted" rates herein) and normalised derivative by minimising an error measure, *E*, (*4-23*), which is a weighted combination of pressure match, rate match, and a penalty term based on the overall curvature of the graphed derivative and whose purpose is to enforce smoothness of the resulting deconvolved derivative.

$$E = \underbrace{\left\| P_i - P - y * g \right\|^2}_{\text{pressure match}} + \nu \underbrace{\left\| y - q^2 \right\|}_{\text{rate match}} + \lambda \underbrace{\left\| DZ - K \right\|^2}_{\text{curvature}} \qquad (4\text{-}23)$$

The expression is minimised over p_i, y and Z with P and q as input data. Matrix D and vector K are curvature operators. v is a weighting parameter for rate match, and λ is the regularization parameter (roughness factor).

The weight of the pressure match is normalized to one and the estimate depends on two weights, v for the rate match, and λ for the roughness penalty. v is usually set at a default value and only the regularisation parameter λ is varied. Regularisation introduces bias, however, and thus the user must choose a level of λ that imposes just enough smoothness to eliminate small-scale oscillations on the derivative while preserving genuine reservoir features.

The use of deconvolution requires selecting control parameters which yields different deconvolved derivatives. Hence the use of deconvolution required knowledge of conventional well test interpretation. Levitan *et al.* (2006a) examined the Total Least Square method on simulated data with different levels of noise Gringarten *et al.* (2003) and Gringarten (2005) applied the deconvolution algorithm on actual data from different fields. The methodology for well test analysis using deconvolution is summarised in *Figure 4-4*.

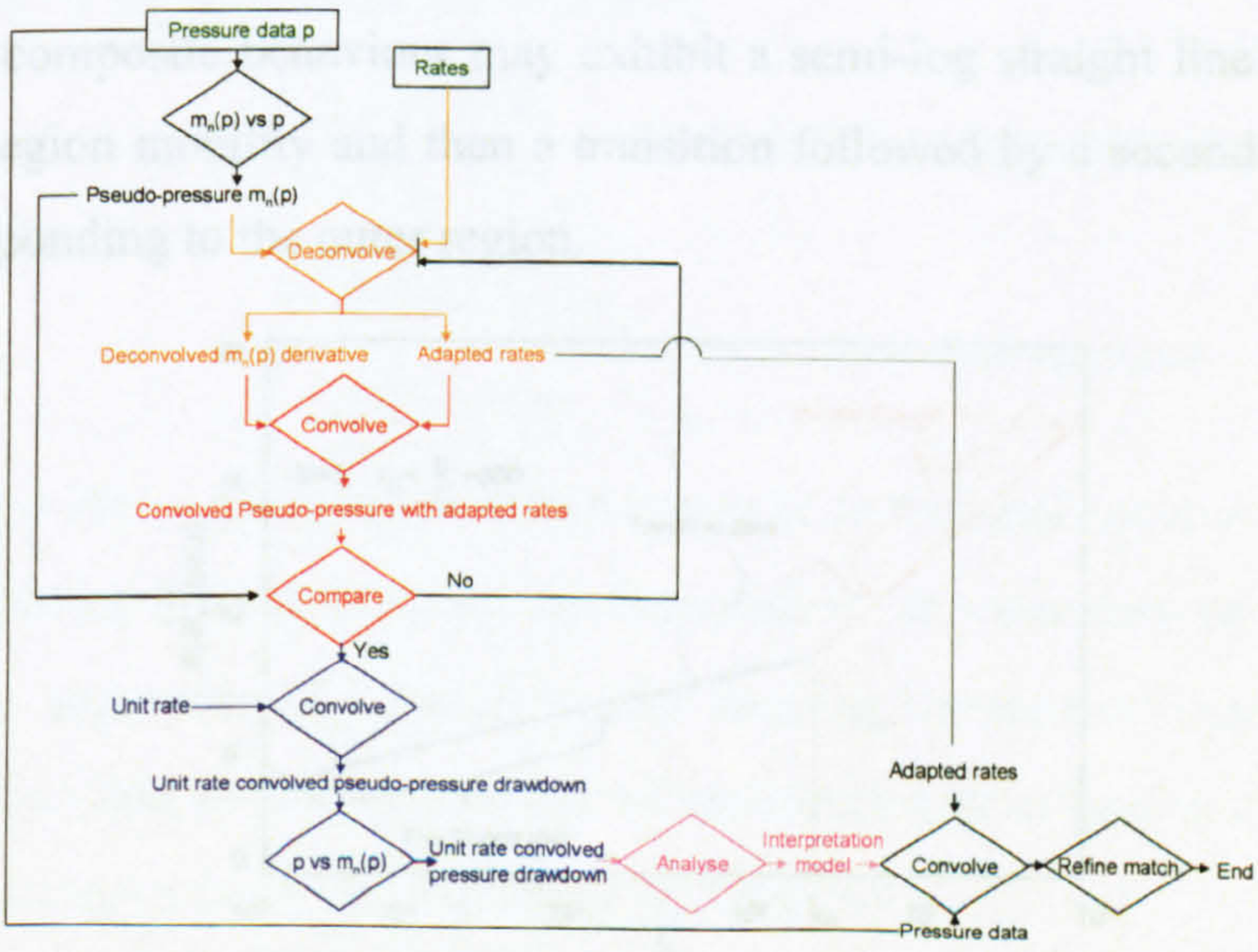

Figure 4-4 Well test analysis using deconvolution (Gringarten, 2006a)

4.1.4 Composite Behaviour in Well Testing

The basic reservoir dynamic behaviour reflects the number of porous media of different mobilities and storativities that participate in the flow process (Gringarten, 1984; Gringarten, 1986). Hence reservoir behaviour from well test can be broadly classified as either homogeneous (one mobility and storativity) or heterogeneous (more than one mobility and or storativity). Heterogeneous behaviour can be double porosity, double permeability or composite behaviours (Gringarten, 2006b).

Composite behaviour is characterised by one set of mobility and storativity around the well and different values away from the well. They are composed of concentric zones with discontinuity in one or more of: saturation, permeability, thickness or porosity.

Loucks and Guerrero (1961) solved the differential equation for continuity of mass in a two composite region to predict the pressure distribution in a composite a reservoir. They showed that the size of the inner zone can be determined from a Horner plot, and the size of inner zone can be estimated the time at which the second linear portion begins.

Odeh (1969) presented a graphical correlation (*Figure 4-5*) for estimating mobility of two concentric radial composite reservoir and radius of radial discontinuity. This correlation was developed from the observation that pressure data measured at a shut-in well in composite behaviour may exhibit a semi-log straight line corresponding to the inner region mobility and then a transition followed by a second semi log straight line corresponding to the outer region.

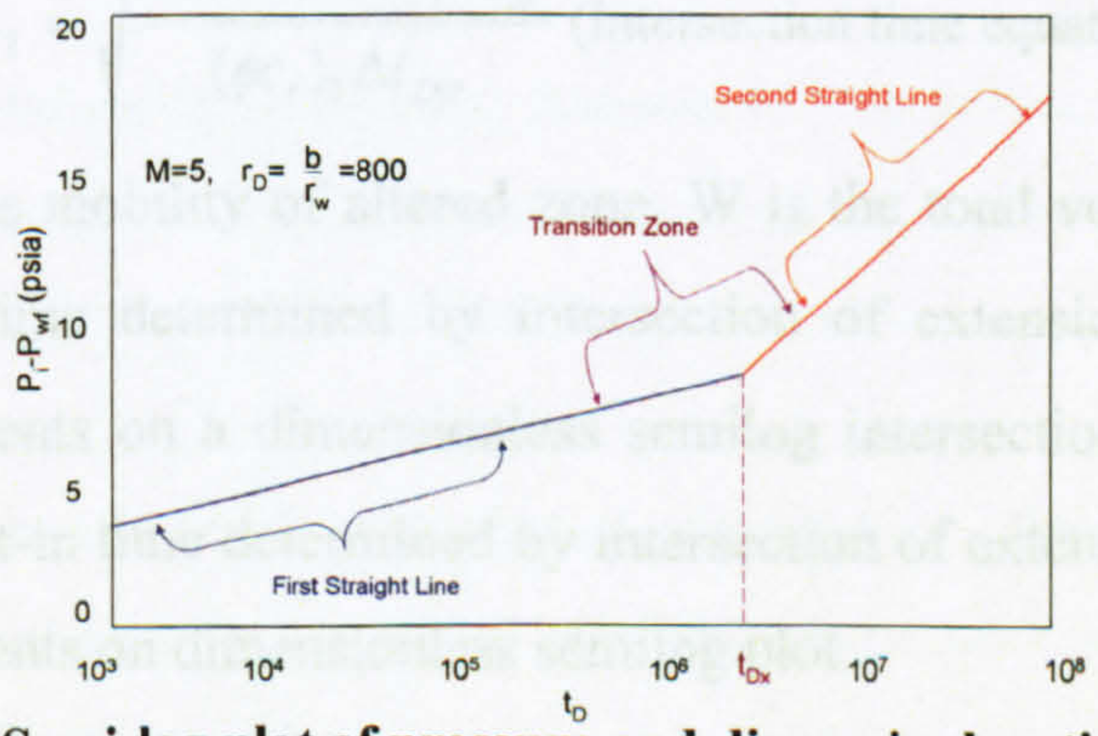

Figure 4-5 Semi-log plot of pressure and dimensionless time (Odeh, 1969)

Where *b* (*Figure 4-5*) is the radial distance to the discontinuity and hence (b/r_w) is dimensionless radial distance of discontinuity with the dimensionless intersection time (t_{Dx}). He further presented an equation relating a dimensionless radius discontinuity with dimensionless intersection time (t_{Dx})

$$r_D = \frac{b}{r_w} = \left(\frac{2.25 t_{Dx}}{M^{\frac{M}{(M-1)}}} \right)^{\frac{1}{2}} \tag{4-24}$$

For drawdown, t_{Dx} is given by:

$$t_{Dx} = \frac{6.32 \times 10^{-3} k_1 \Delta t_x}{\phi_1 \mu_1 c_1 r_w^2} \tag{4-25}$$

For Build-up, t_{Dx} is given by:

$$t_{Dx} = \frac{6.32 \times 10^{-3} k_1 \Delta t_{wsx}}{\phi_1 \mu_1 c_1 r_w^2} \tag{4-26}$$

Where t_x is the time, in days at which the intersection of the two straight lines occurs and t_{wsx} is the shut-in time, in days, at which the intersection of the two straight lines occurs.

Merrill *et al.* (1979) estimated the distance of fluid bank in composite behaviour due to a saturation discontinuity as a result of fluid injection around a well. They presented a trial-and-error method to estimate the properties of the first and second zones and equations for location of the first discontinuity for water flooding, r_{f1} using either (*4-27*) or (*4-28*) if sufficient data are available:

$$r_{f1} = \sqrt{\frac{5.6146 WB_w}{\pi h \phi (S_w - S_{wc})}} \text{ (Material balance equation)} \tag{4-27}$$

$$r_{f1} = \sqrt{\frac{0.0002637 \lambda_1 \Delta t_{fx}}{(\phi c_t)_1 \Delta t_{Dfx}}} \text{ (Intersection time equation)} \tag{4-28}$$

Where λ_1 (*4-29*) is mobility of altered zone, W is the total volume of injected fluid, and Δt_{fx} shut-in time determined by intersection of extension of first and second straight-line segments on a dimensionless semilog intersection time and Δt_{Dfx} is the dimensionless shut-in time determined by intersection of extension of first and second straight-line segments on dimensionless semilog plot.

Where λ_1 is defined as:

$$\lambda_1 = \frac{162.6qB_w}{m_1 h} \tag{4-29}$$

Olarewaju *et al.* (1991) presented family of type-curves generated from composite model that is most applicable to the analysis of well-test data from radially damaged and stimulated wells. The model was expressed in terms of a dimensionless wellbore pressure drop, p_D and t_D/R_{DI}^2. Where R_{DI} is dimensionless radius of inner zones (r_1/r_w) and t_D is dimensionless time defined by (*4-30*) and p_D defined by (*4-31*). Type curve matching with this model yields the inner region mobility from the pressure match:

$$t_D = \frac{0.0002637k_2 t}{\phi\mu c_t r_w^2} \tag{4-30}$$

$$p_D = \frac{k_2 h\Delta p}{141.2qB\mu} \tag{4-31}$$

From the match on type curve of, p_D vs t_D/R_D^2, k_2 and r_1 can be estimated.

Producing volatile oil below the bubble point creates a two-phase region in region around the wellbore region and single-phase oil in region far from wellbore which is two zone composite reservoir model due to discontinuity in saturation.

4.1.5 Phase Redistribution

Phase redistribution occurs in wells when there is multiphase flow and production rate is controlled at the surface. Wellbore phase redistribution though limited to early times behaviour, may dominate a well test for several hours (Ali *et al.*, 2005). The presence of wellbore phase redistribution can cause erroneous interpretation of well test data.

Stegemeire and Matthews (1958) using statistical study of a south Texas field, showed that the sizes of humps on log-log pressure derivative due to phase redistribution are greater in wells with low productive index, associated to low permeability and skin..

Pitzer *et al.* (1959) discussed how phase redistribution affects most surface shut-in build-up curves and how bottom-hole shut-in techniques can be used to eliminate phase redistribution.

Hassan and Kabir (1993) used and explained the mechanism of wellbore phase redistribution in vertical and deviated wellbores. They further showed that the magnitude of the anomalous pressure rise increases with increasing damaged skin, decreasing wellhead pressure, and increasing bubble rise velocity.

4.2 Interpretation of Well Test Data from DST-Well15

The pressure and rate histories of DST-Well-15 are shown in *Figure 4-6*. There is an initial drawdown of 41.8 days; a build-up of of 6.4 days (2BU); a drawdown of 26 hours at 3 different rates (4 to 6DD); a build-up of 2.7days (7BU); a drawdown of 26 hours at 7 different rates (8 to 15DD); and a final build-up of 6.2 days (16BU). The reservoir fluid was initially thought to be gas condensate, with gas as the dominant fluid and only the measured gas rate was made available. However, fluid analysis showed the reservoir fluid to be volatile oil (identified as sample B in *Table 2-1* and *Appendix A*). The oil rate had to be estimated from the measured gas rate and the GOR at known separator conditions (*Table 4-1*). The oil rate was validated with compositional simulation and deconvolution. The initial pressure of 4076 psia was obtained from the fluid analysis report (and confirmed by both conventional analysis and deconvolution).

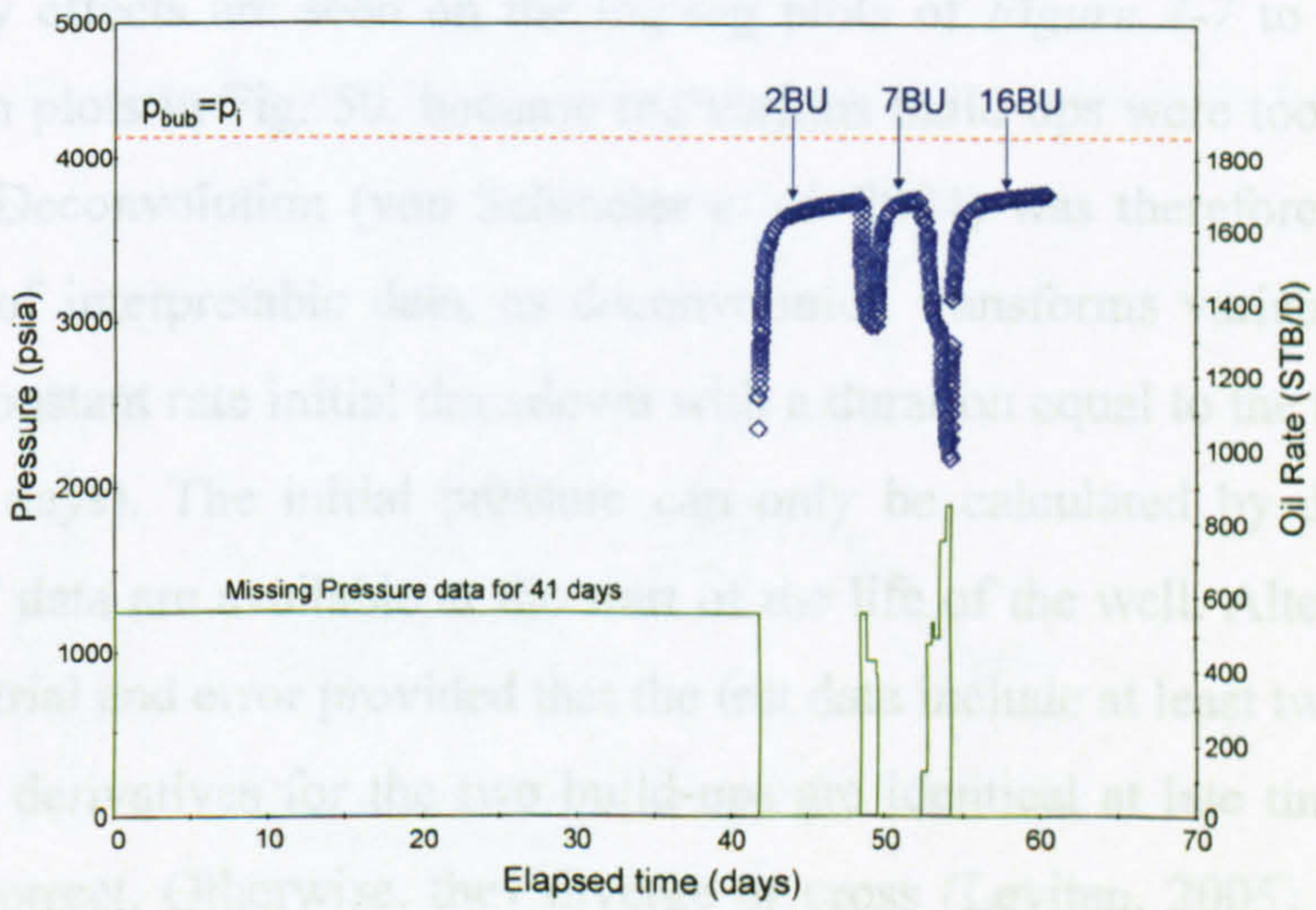

Figure 4-6 DST Pressure Rate History of DST-Well15

Table 4-1 Estimation of oil rate from measured gas rate and GOR

Flow Period	Recorded Gas Rate Mscf/D	Estimated Oil Rate Using measured GOR Stb/D
1DD	1000	560
2BU	0	0
3DD	0	0
4DD	1000	560
5DD	770	431
6DD	700	392
7BU	0	0
8DD	0	0
9DD	225	126
10 DD	860	482
11DD	960	538
12DD	890	498
13DD	1350	756
14DD	1525	854
15DD	1530	857
16BU	0	0

No boundary effects are seen on the log-log plots of *Figure 4-7* to *4-10*, or on the superposition plots in Fig. 50, because the various build-ups were too short (6.4 days maximum). Deconvolution (von Schroeter *et al.* 2004) was therefore used to extend the amount of interpretable data, as deconvolution transforms variable rate pressure data into a constant rate initial drawdown with a duration equal to the total duration of the test (38 days). The initial pressure can only be calculated by deconvolution if reliable DST data are available at the start of the life of the well. Alternatively, it can be found by trial and error provided that the test data include at least two build-ups: the deconvolved derivatives for the two build-ups are identical at late times if the initial pressure is correct. Otherwise, they diverge or cross (Levitan, 2005). This procedure confirmed the value of 4076 psia from the fluid analysis report.

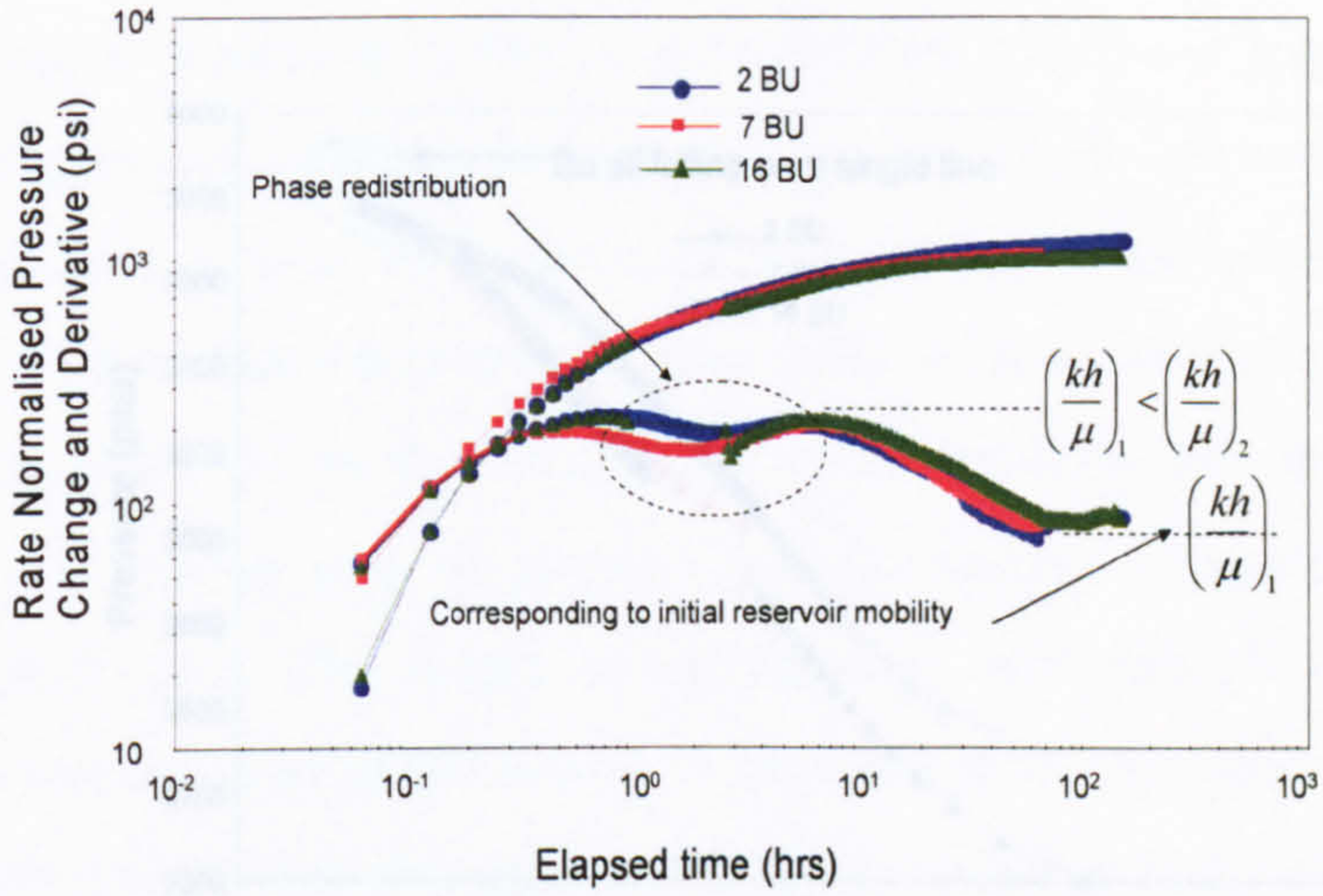

Figure 4-7 Combination of all Log-Log Pressure and Derivative Plots for Build-up

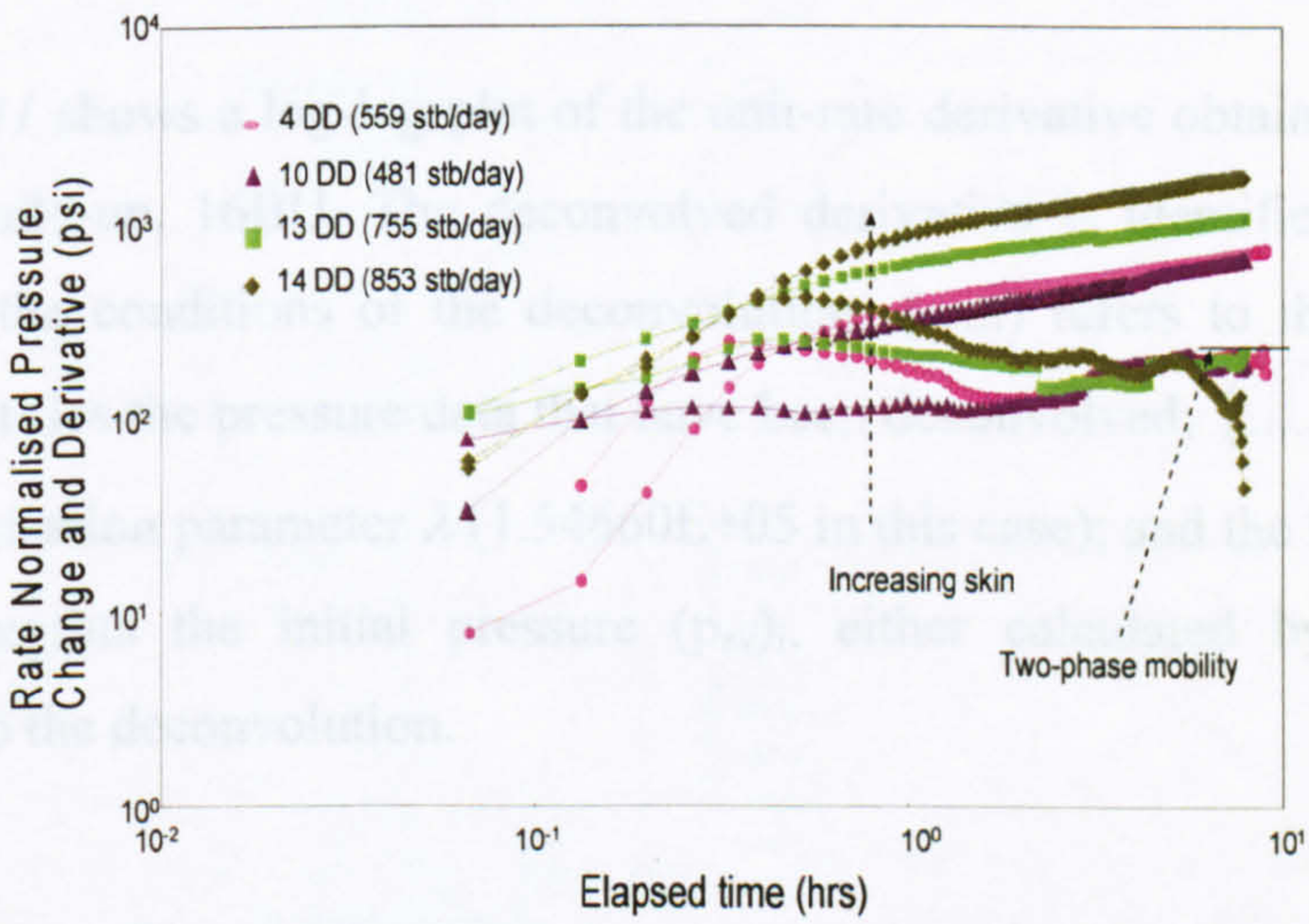

Figure 4-8 Combinations of Log-Log Pressure and Derivative Plots for Drawdowns

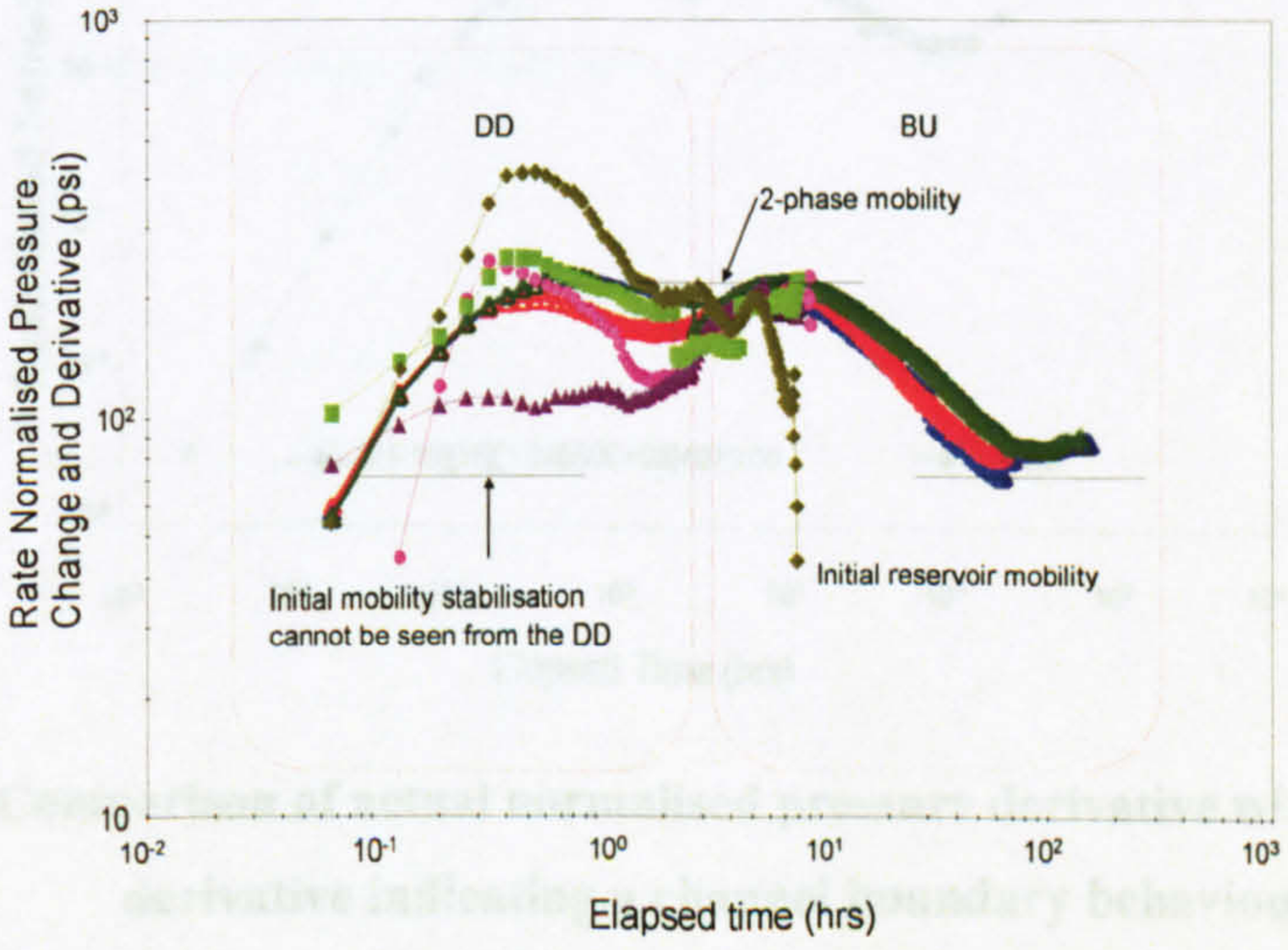

Figure 4-9 Combinations of log-log pressure and derivative plots for drawdowns and Build-ups

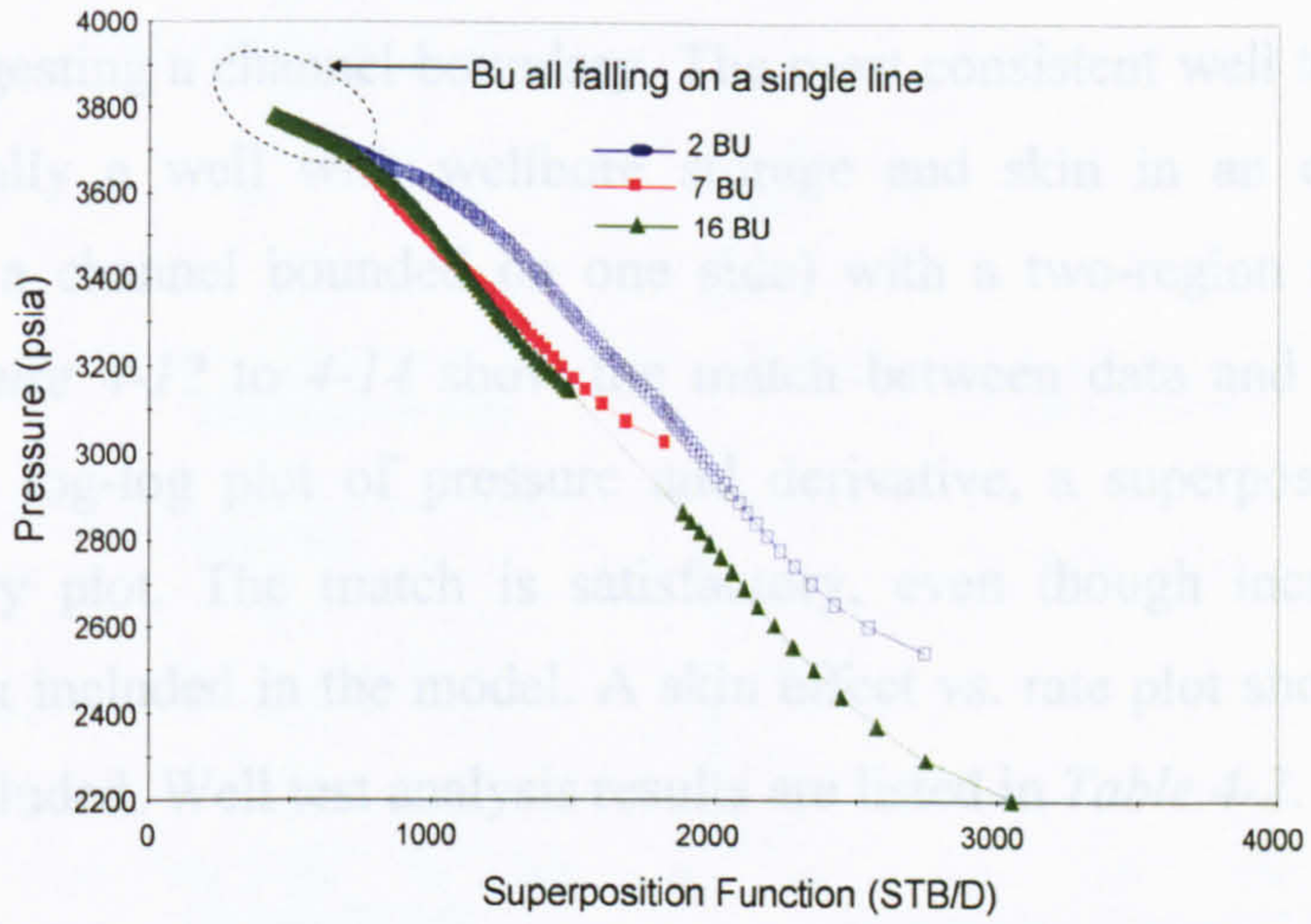

Figure 4-10 Superposition function plots showing reservoir as non-depleting

Figure 4-11 shows a log-log plot of the unit-rate derivative obtained by deconvolving the last build-up, 16BU. The deconvolved derivative is identified by a label which describes the conditions of the deconvolution: (.....) refers to the rate record used; [.....] identifies the pressure data that have been deconvolved; {.....} states the value of the regularisation parameter λ (1.54660E+05 in this case); and the last parameter in the label represents the initial pressure $(p_{av})_i$, either calculated by deconvolution or imposed to the deconvolution.

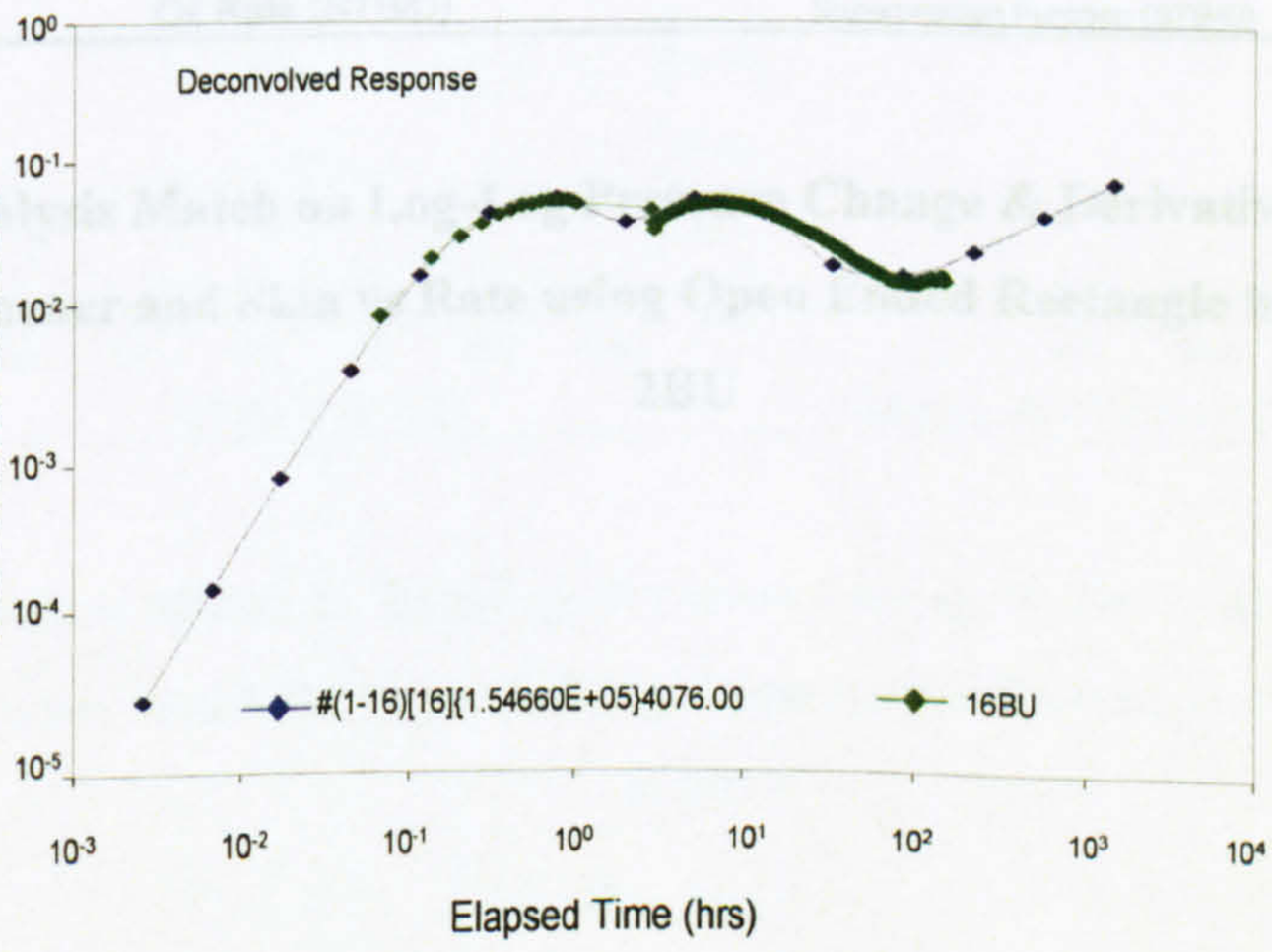

Figure 4-11 Comparison of actual normalised pressure derivative with best deconvolved derivative indicating a channel boundary behaviour.

The deconvolved derivative in *Figure 4-11* exhibits a half-unit log-log straight line at late times, suggesting a channel boundary. The most consistent well test interpretation model is actually a well with wellbore storage and skin in an open rectangular reservoir (i.e., a channel bounded on one side) with a two-region radial composite behaviour. *Figure 4-12* to *4-14* show the match between data and model, for each build-up, on a log-log plot of pressure and derivative, a superposition plot and a pressure history plot. The match is satisfactory, even though increasing wellbore storage was not included in the model. A skin effect vs. rate plot showing non-Darcy flow is also included. Well test analysis results are listed in *Table 4-2*.

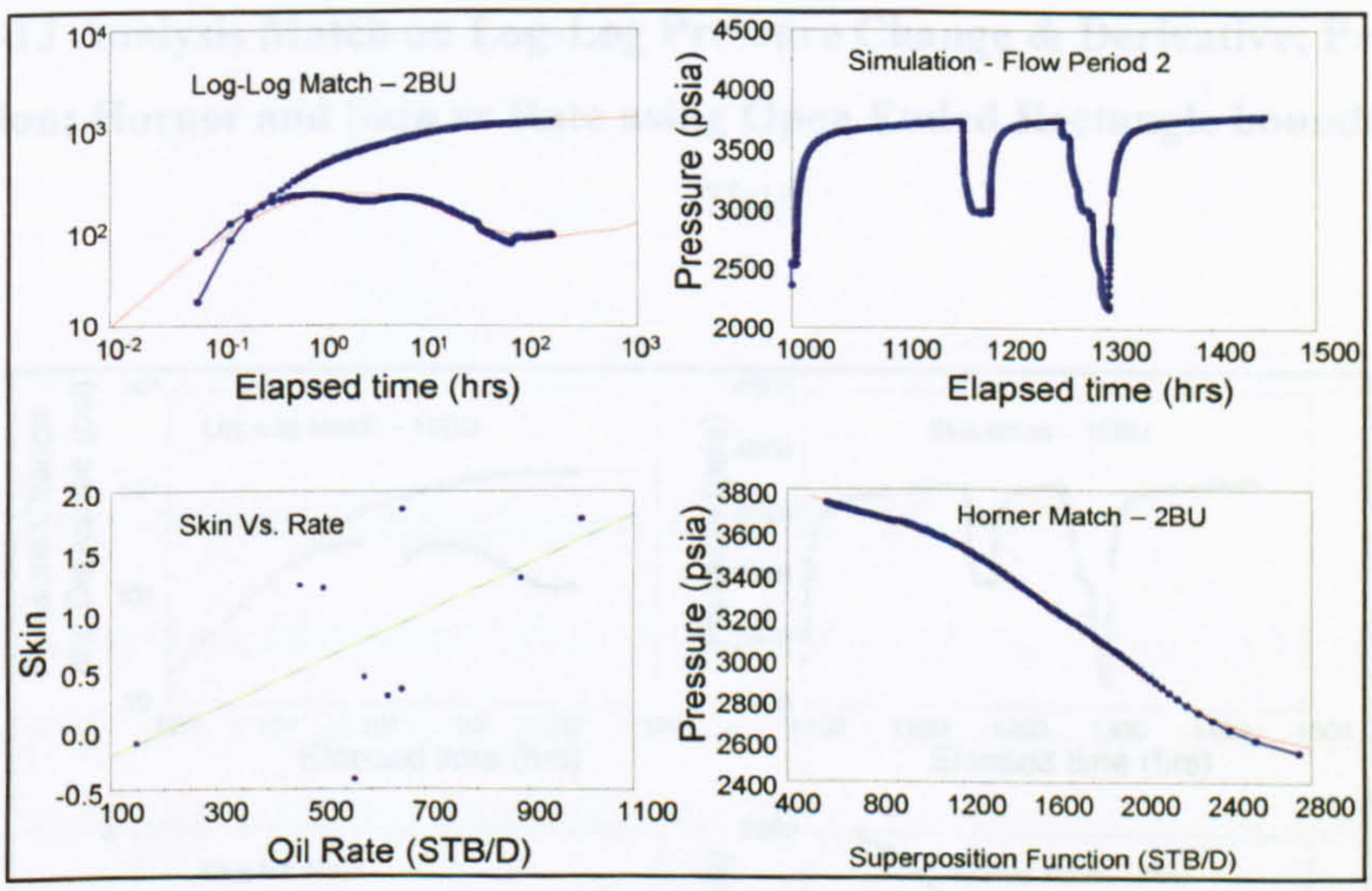

Figure 4-12Analysis Match on Log-Log Pressure Change & Derivative; Pressure History Simulation; Horner and Skin vs Rate using Open Ended Rectangle boundary condition-2BU

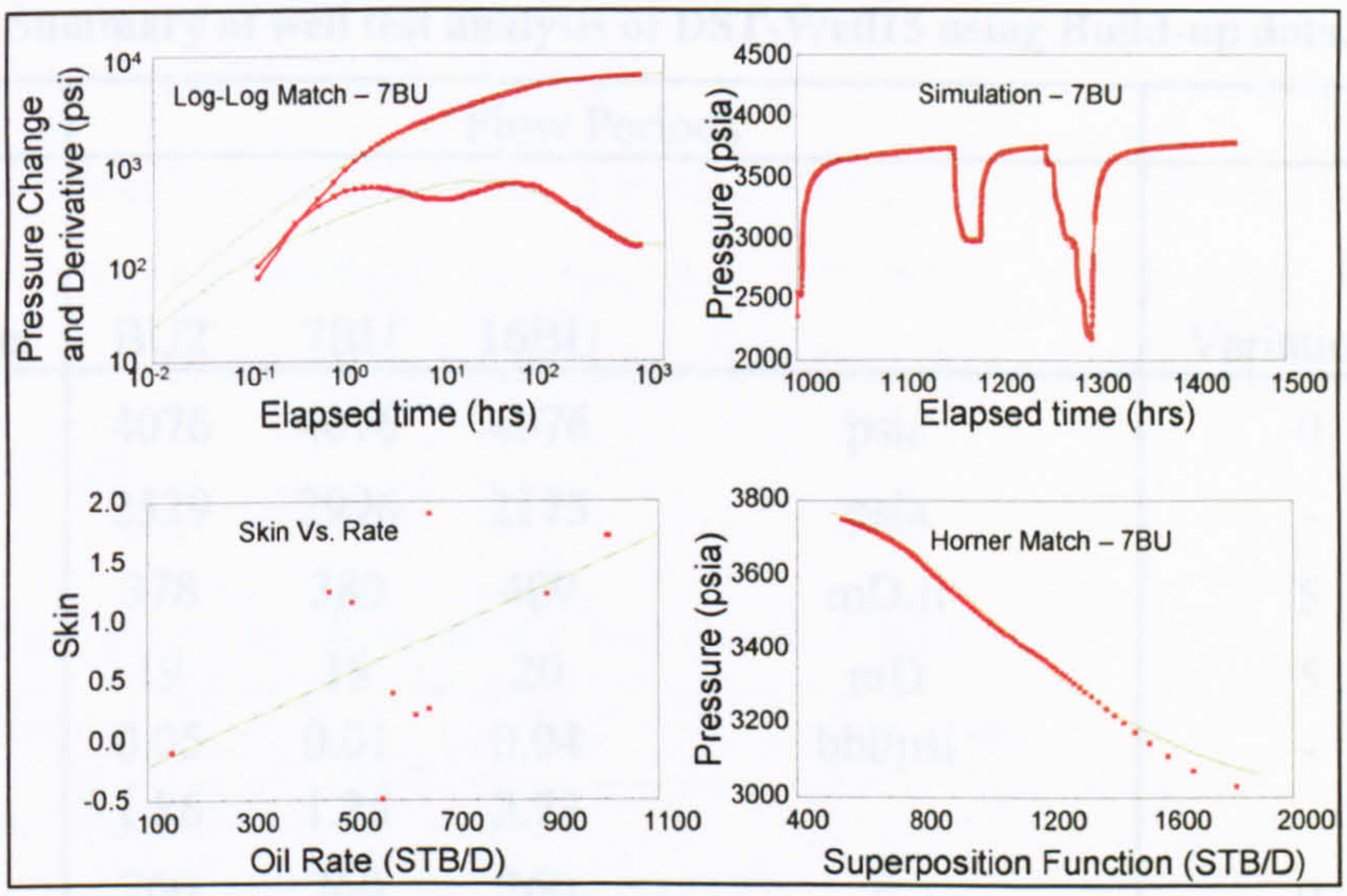

Figure 4-13 Analysis Match on Log-Log Pressure Change & Derivative; Pressure History Simulation; Horner and Skin vs Rate using Open Ended Rectangle boundary condition-7BU

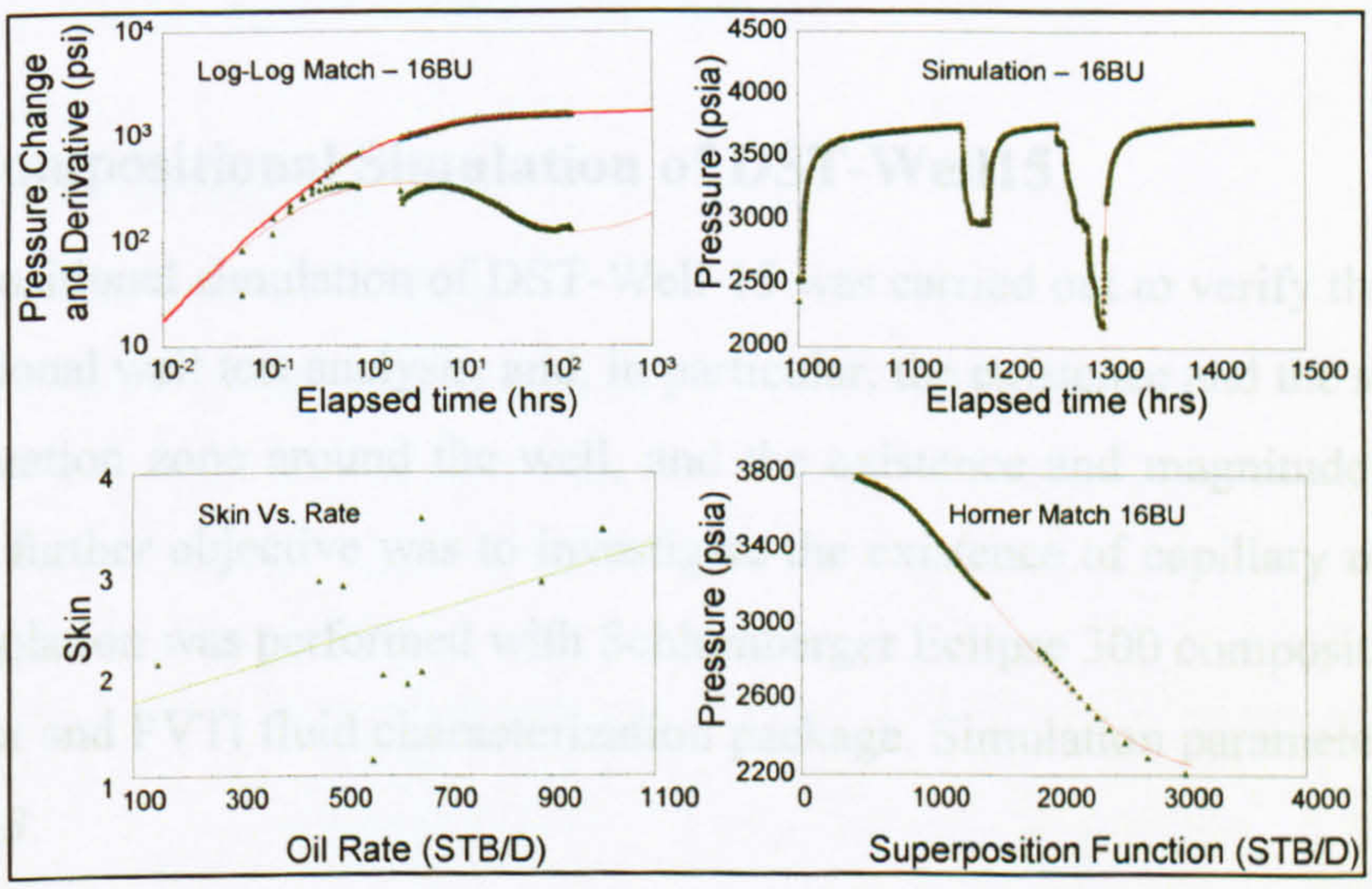

Figure 4-14 Analysis Match on Log-Log Pressure Change & Derivative; Pressure History Simulation; Horner and Skin vs Rate using Open Ended Rectangle boundary condition-16BU

Table 4-2 Summary of well test analysis of DST-Well15 using Build-up data.

	Flow Periods				
Parameter	BU2	7BU	16BU		Variation %
$(pav)_i$	4076	4076	4076	psia	0
p_{wf}	2529	2996	2175	psia	-
$kh_{(2)}$	378	380	409	mD.ft	5
$k_{2\ eff}$	19	19	20	mD	5
C	0.05	0.01	0.04	bbl/psi	-
S(t)	1.86	1.25	2.73		-
r_1	260	260	260	ft	0
$(\phi ch)_{1/2}$	2.13	1.6	2.58	From Fluid Analysis	-
$(kh/u)_{1/2}$	0.32	0.21	0.29		-
d_1	5164	5164	5164	ft	0
d_2	2711	2711	2711	ft	0
d_3	1190	1190	1190	ft	0

4.3 Compositional Simulation of DST-Well15

A compositional simulation of DST-Well-15 was carried out to verify the results of the conventional well test analysis, and, in particular, the existence and the size of the high gas saturation zone around the well, and the existence and magnitude of non-Darcy flow. A further objective was to investigate the existence of capillary number effects. The simulation was performed with Schlumberger Eclipse 300 compositional reservoir simulator and PVTi fluid characterization package. Simulation parameters are listed in *Table 4-3*.

4.3.1 Grid Model

A Cartesian grid (52 x 10 x 1) with local grid refinement was used. The simulation model has three sealing faults. Distances from the well to the faults were set at the values obtained in well test analysis (*Figure 4-15*).

4.3.2 Relative Permeability Model

Relative permeability curves were generated using Corey's model (*Figure 4-16*). Several relative permeability models and end point values were tested using compositional reservoir simulation to select the ones that provided a good match with all the build-ups.

Table 4-3 Parameters for simulation of well test DST-Well5

Parameter	Value
Wellbore Radius (ft)	0.31
Reservoir Thickness (ft)	20
Net to Gross Ratio	1
Top of Reservoir (ft)	10,000
Initial Reservoir Pressure at gauge Depth (psia)	4067
Gauge Depth (190 ft above top perforation) (ft)	9810
Average Radial Reservoir Permeability (mD)	19 mD
Kv/Kh Ratio	0.1
Reservoir Porosity (%)	20%
Initial water Saturation (S_{wi})	0.4
Bubble Point Pressure (psia)	4067
d_1 (ft)	5165
d_2 (ft)	2712
d_3 (ft)	1190

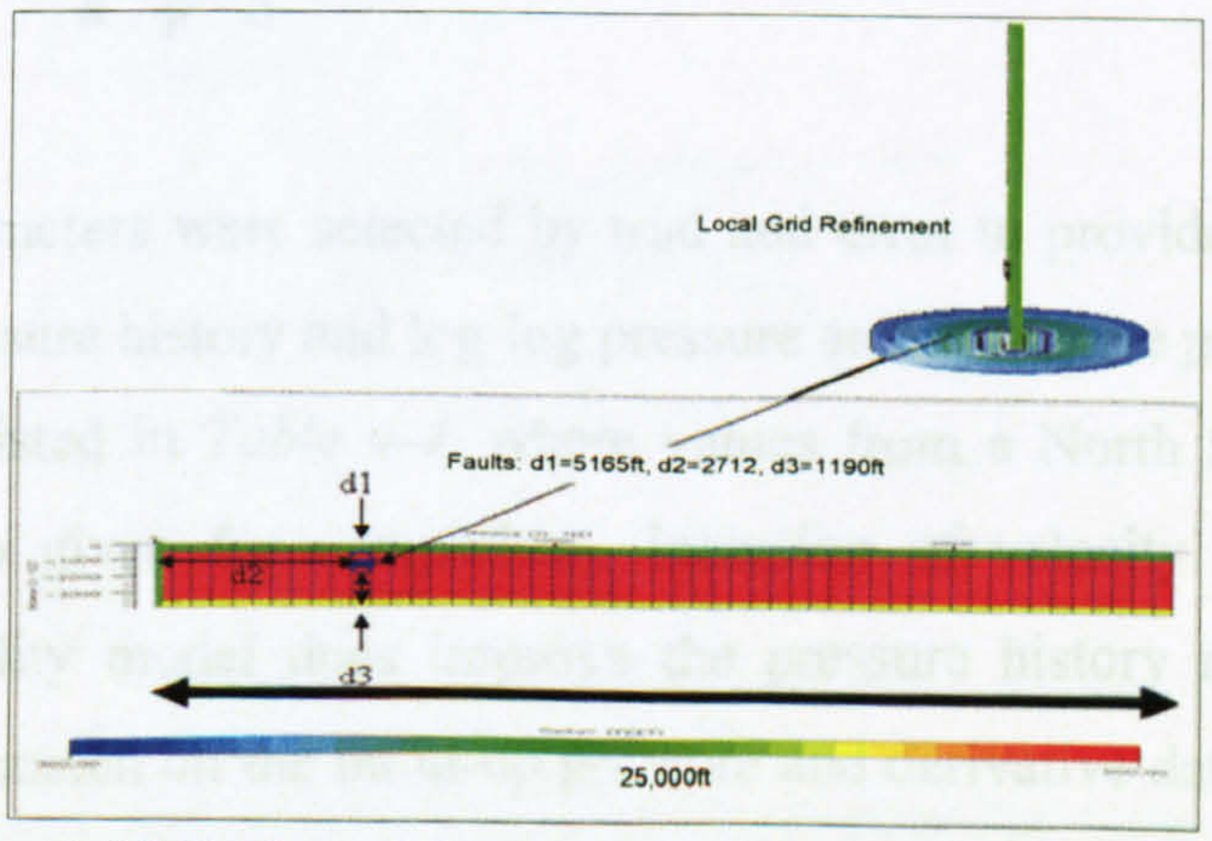

Figure 4-15 Grid model for simulation of well test DST-Well5

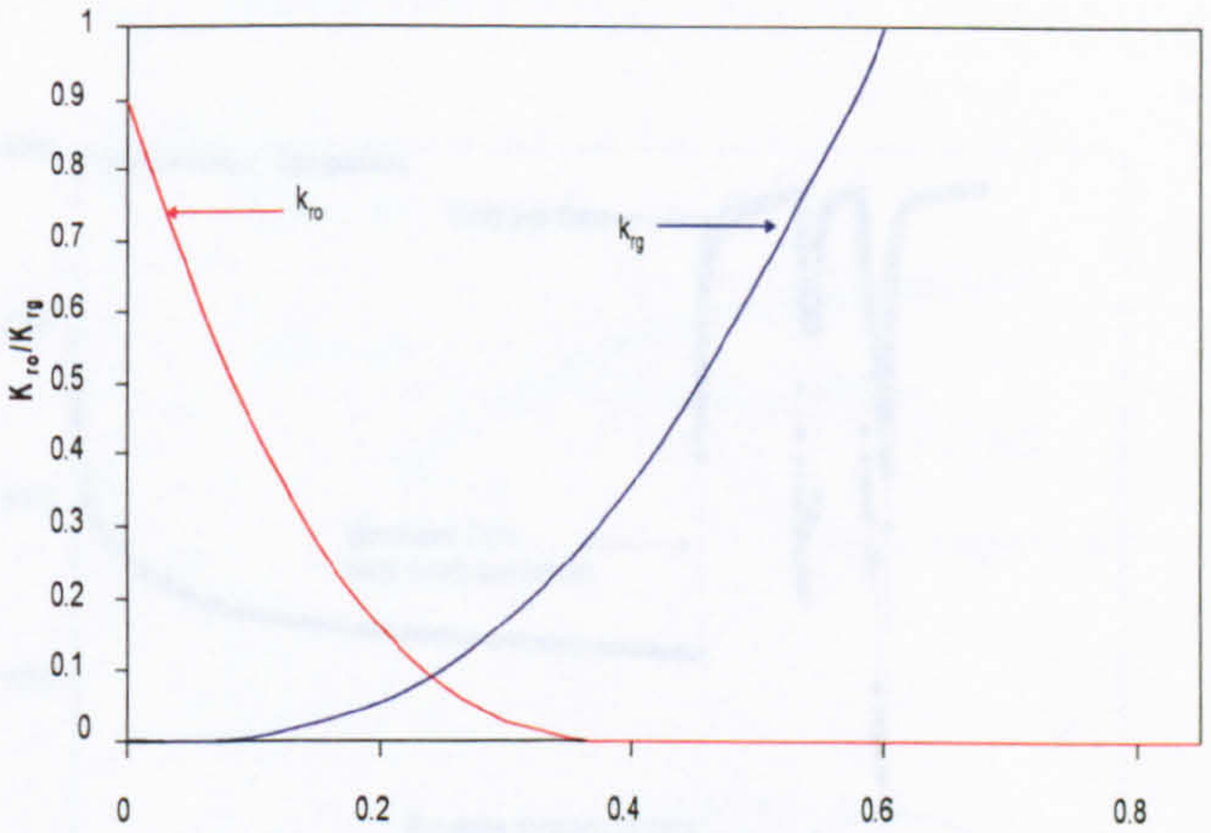

Figure 4-16 Relative permeability curve used for compositional simulation

4.3.3 Velocity Dependence of Relative Permeability

Figure 4-17 compares the depth-adjusted pressure from compositional simulation with the actual pressure history from DST-Well-15. While the build-ups do match, the drawdowns exhibit excessive pressure drops, with the simulated pressure in flow period 15DD even dropping to zero. This suggests that the capillary number, which reduces the pressure drop, affects the actual data. Both capillary number and non-Darcy flow (identified in the well test analysis) were therefore incorporated in the simulation.

The capillary number in Schlumberger Eclipse 300 compositional simulator is based on Henderson's eight parameter model (Henderson *et al.* 2000), whereas non-Darcy flow uses Geertsma's relationship (Geerstma 1974) to estimate the β parameters (4-32):

$$\beta \approx \frac{0.005}{k^{0.5}\phi^{5.5}S^{5.5}} \text{ cm}^{-1} \qquad (4\text{-}32)$$

Henderson's parameters were selected by trial and error to provide the best match on the simulated pressure history and log-log pressure and derivative plots (*Figure 4-17* to *4-21*). They are listed in *Table 4-4*, where values from a North Sea gas condensate reservoir are also given for comparison. Inclusion of velocity dependence in the relative permeability model does improve the pressure history match as shown in *Figure 4-18*. The match on the build-up pressure and derivative data in *Figure 4-19* to *4-21* is not perfect, possibly because of inaccuracies in the PVT properties.

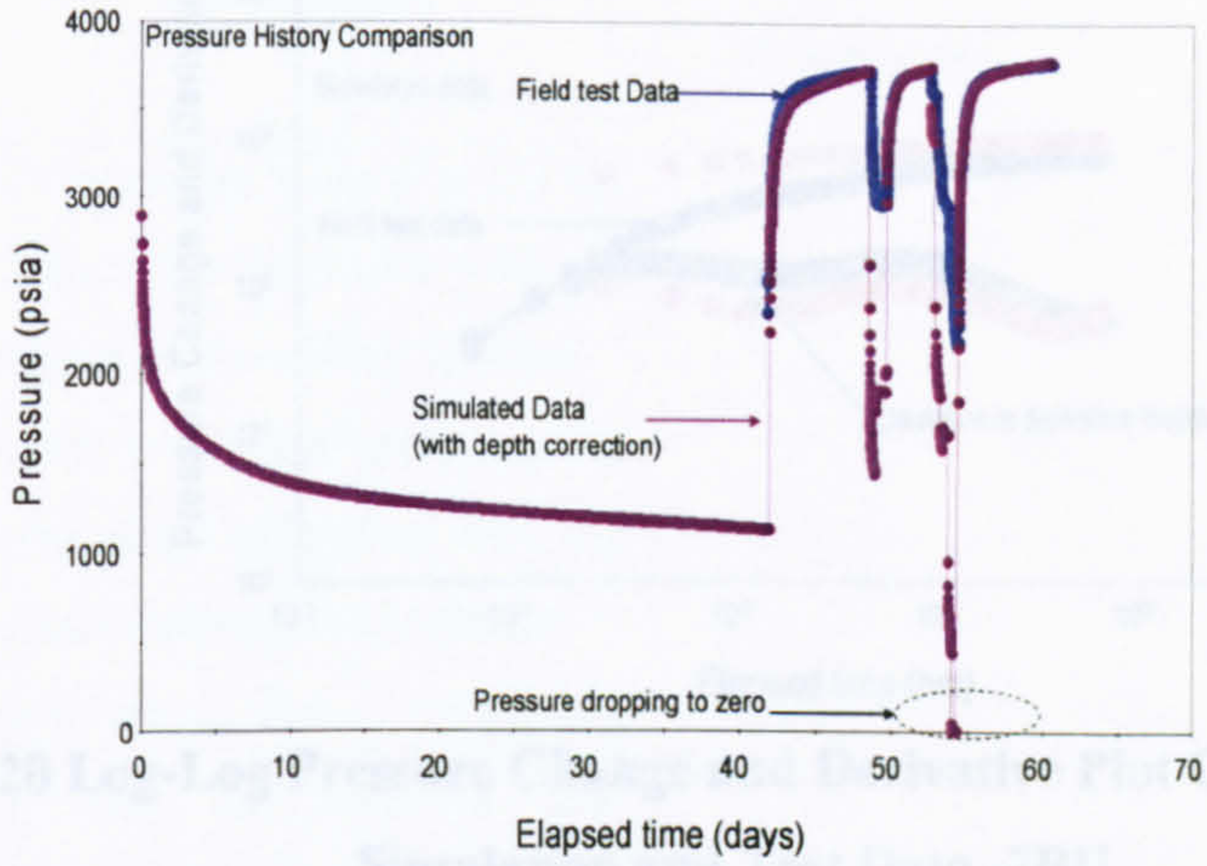

Figure 4-17 Comparison of simulated and actual pressure history with depth correction

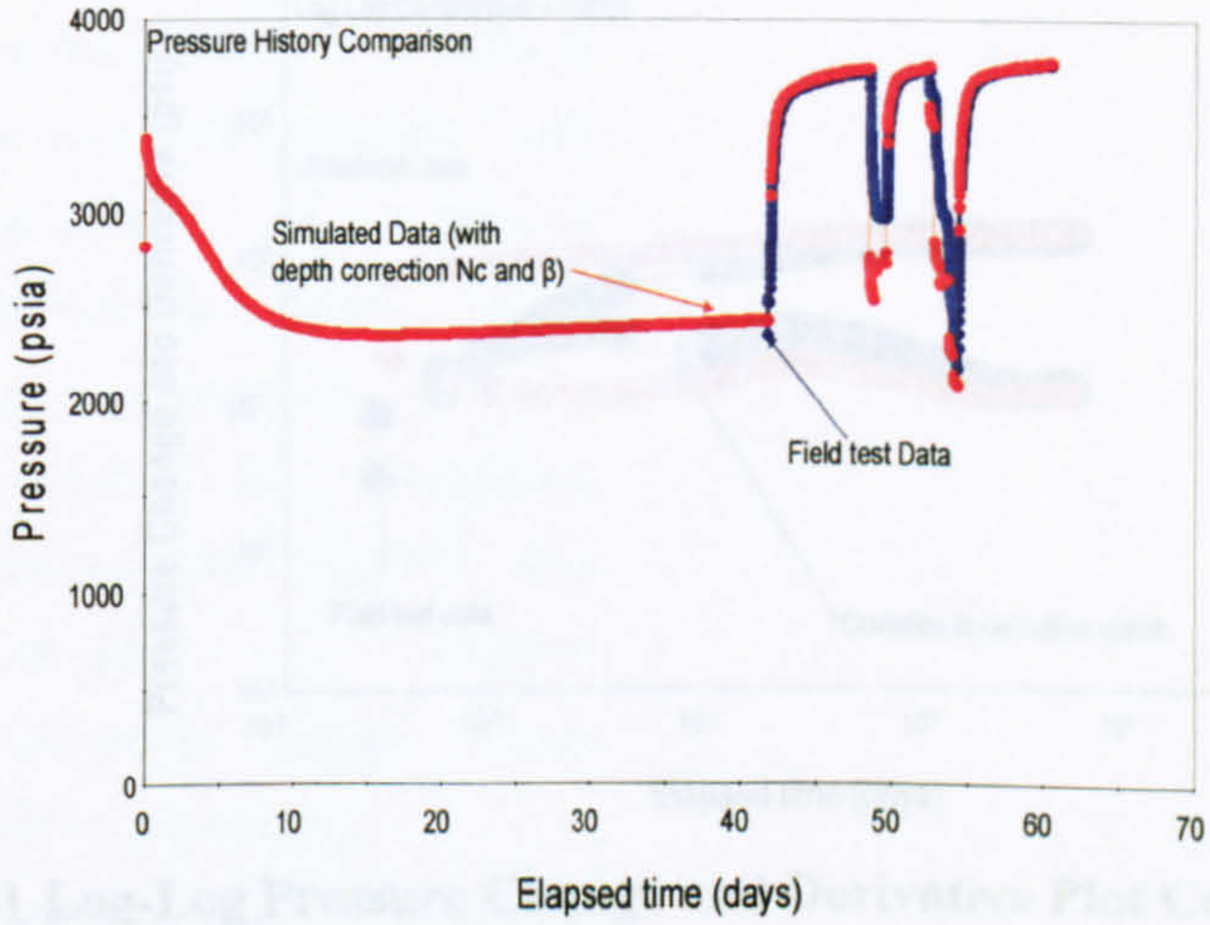

Figure 4-18 Comparison of simulated and actual pressure history with Nc and β

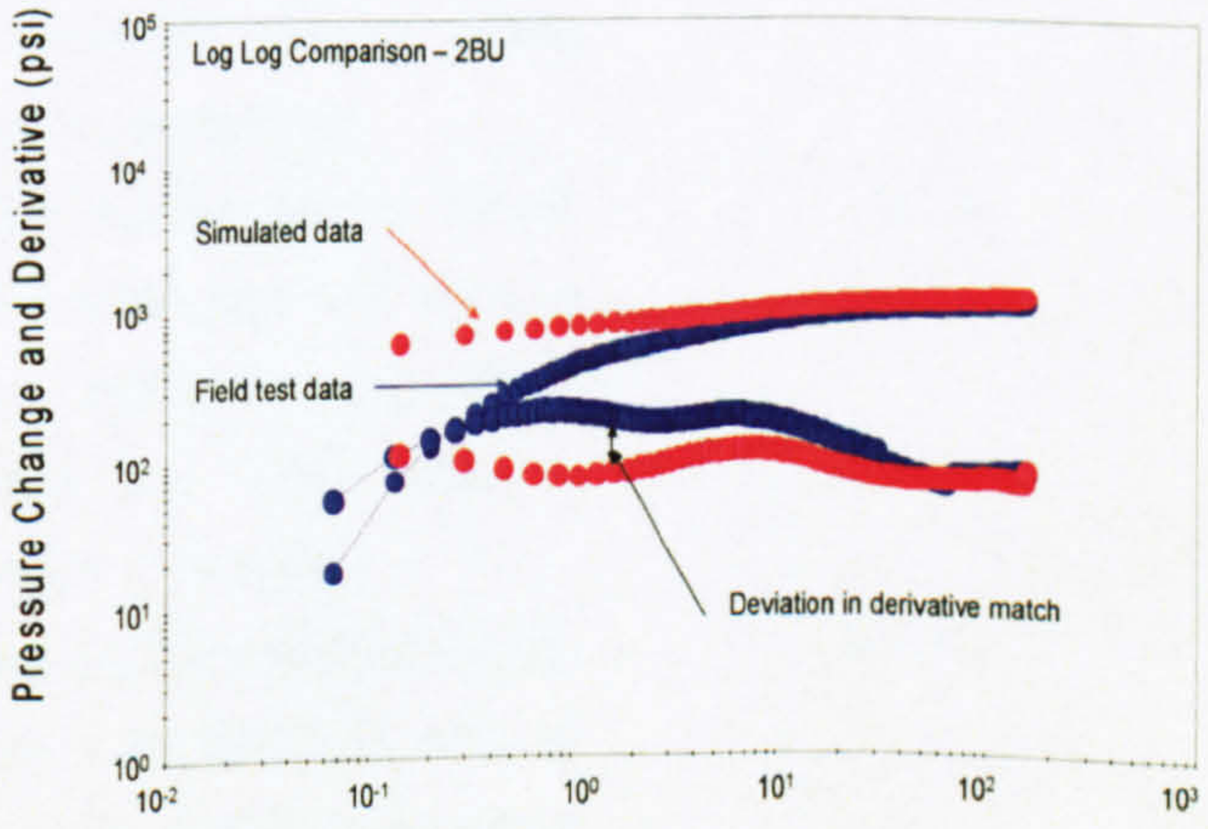

Figure 4-19 Log-Log Pressure Change and Derivative Plot Comparison between Simulation and Test Data -2BU

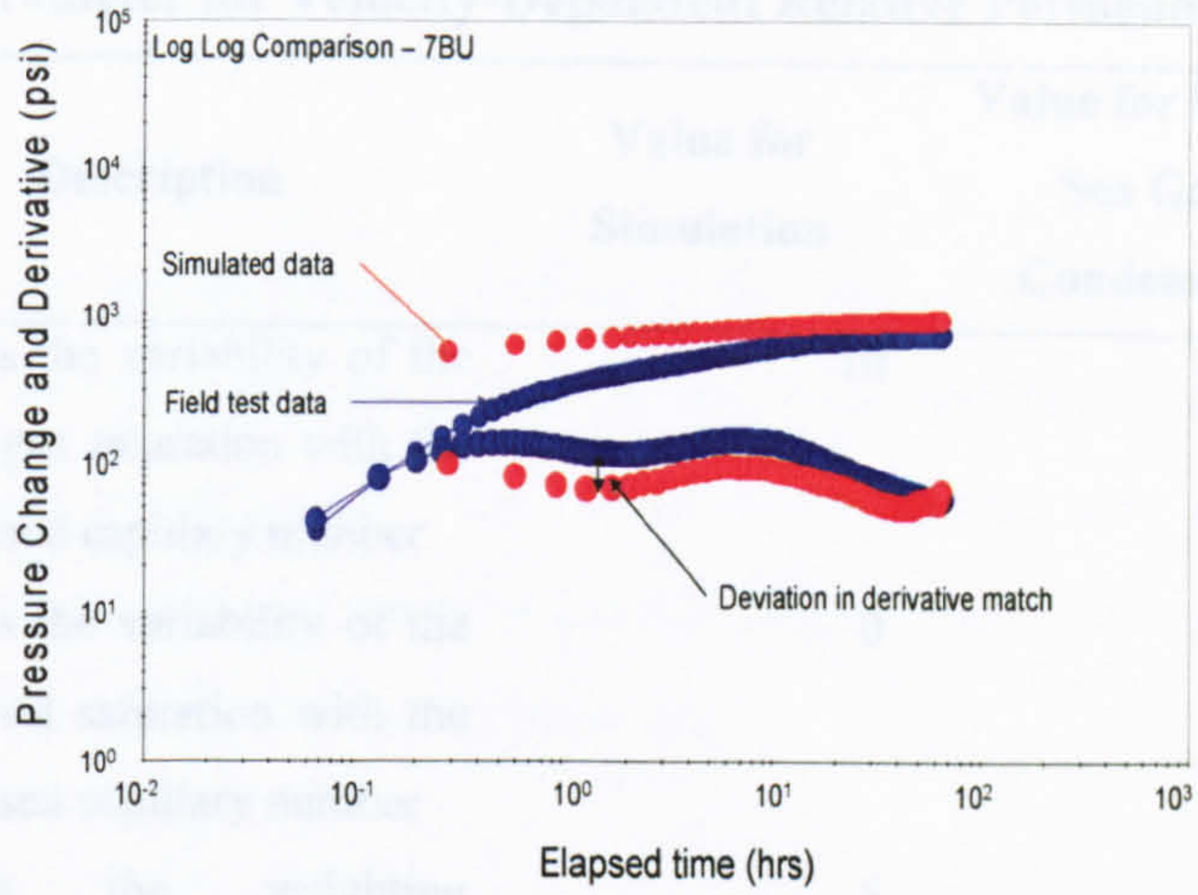

Figure 4-20 Log-Log Pressure Change and Derivative Plot Comparison between Simulation and Test Data -7BU

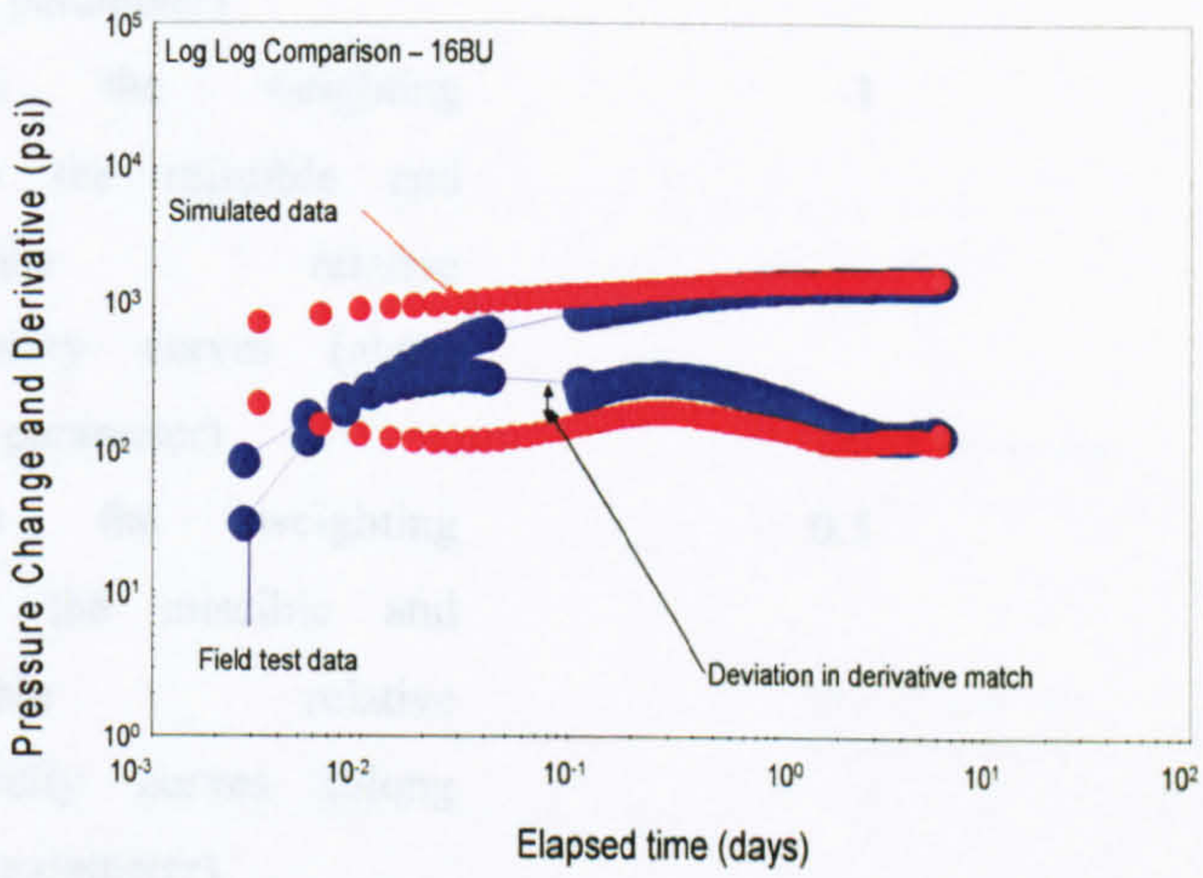

Figure 4-21 Log-Log Pressure Change and Derivative Plot Comparison between Simulation and Test Data -16BU

Table 4-4 Input Parameter for Velocity-Dependent Relative Permeability Model

Parameter	Description	Value for Simulation	Value for North Sea Gas Condensate
m_g	Controls the variability of the critical gas saturation with the normalised capillary number	10	23.89
m_o	Controls the variability of the critical oil saturation with the normalised capillary number	0	79.62
n_{1g}	Controls the weighting between the miscible and immiscible relative permeability curves (along with n_{2g} parameter)	5	6.23
n_{2g}	Controls the weighting between the miscible and immiscible relative permeability curves (along with n_{1g} parameter)	-1	0
n_{1o}	Controls the weighting between the miscible and immiscible relative permeability curves (along with n_{2o} parameter)	0.5	24.2
n_{2o}	controls the weighting between the miscible and immiscible relative permeability curves (along with n_{1o} parameter)	0	0
N_{cbo}	Base capillary number for oil. This is the threshold value of the capillary number above which the VDRP effect is thought to be active.	1.0E-06	1.0E-06
$N_{cbg.n}$	Base capillary number for gas. This is the threshold value of capillary number above which the VDRP effect is thought to be active	1.0E-011	1.0E-06

4.3.4 Phase Behaviour

Figure 4-22 shows the oil saturation profiles at the end of all the build-ups. Although the gas around the well has dissolved into the oil, a two-phase region still exists away from the well. This is because, with the initial reservoir pressure at the bubble point pressure and the long duration of the first drawdown, the build-ups are too short for the reservoir pressure to return to the initial pressure.

Figure 4-22 also displays the radius of the high gas saturation region estimated from well test analysis. It compares reasonably well with that from compositional simulation, although the simulation shows a continuous change in mobility rather than an abrupt one.

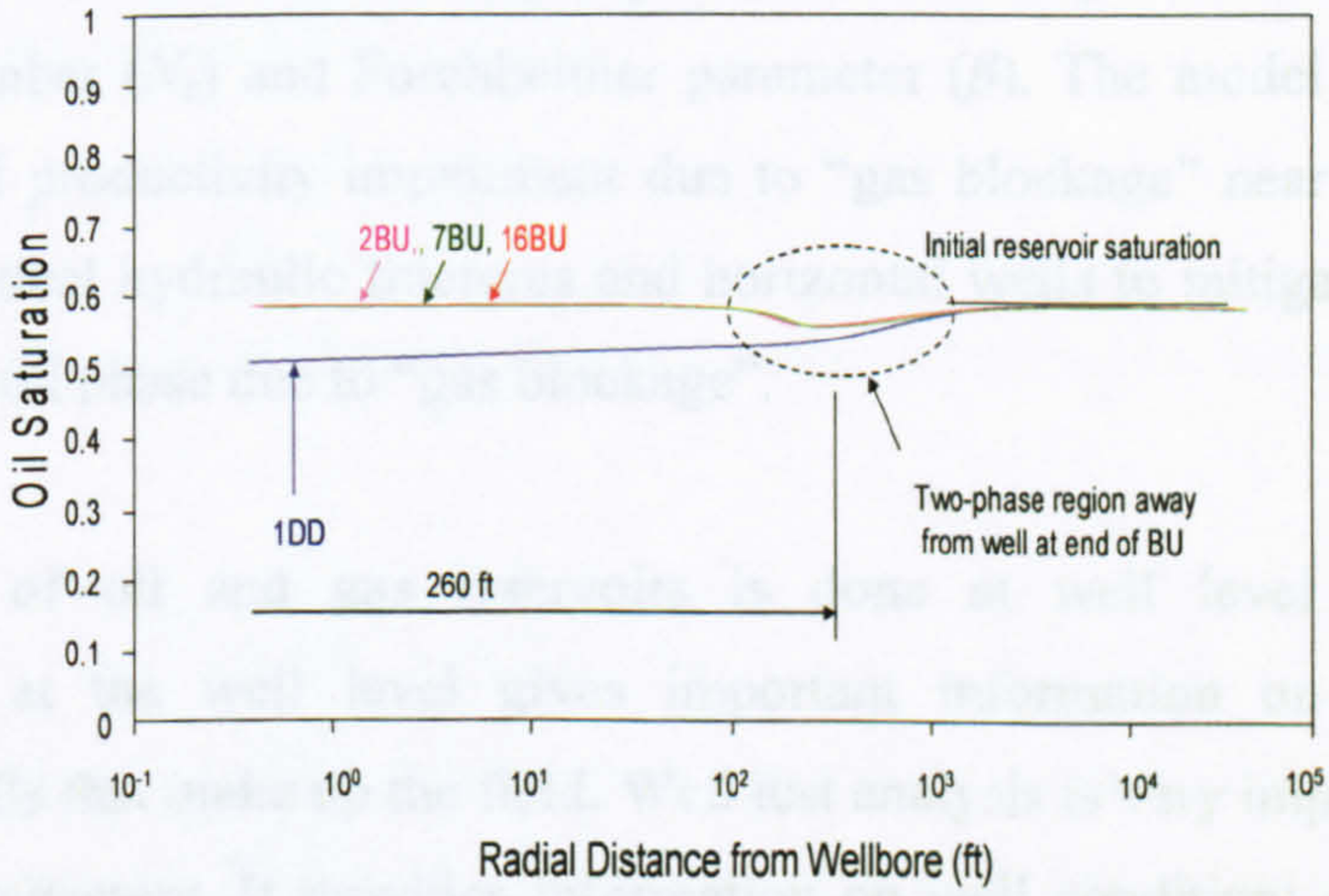

Figure 4-22 Saturation profile in the region around DST-Well15

Figure 4-23 summarises the process for well test analysis of volatile oil reservoirs.

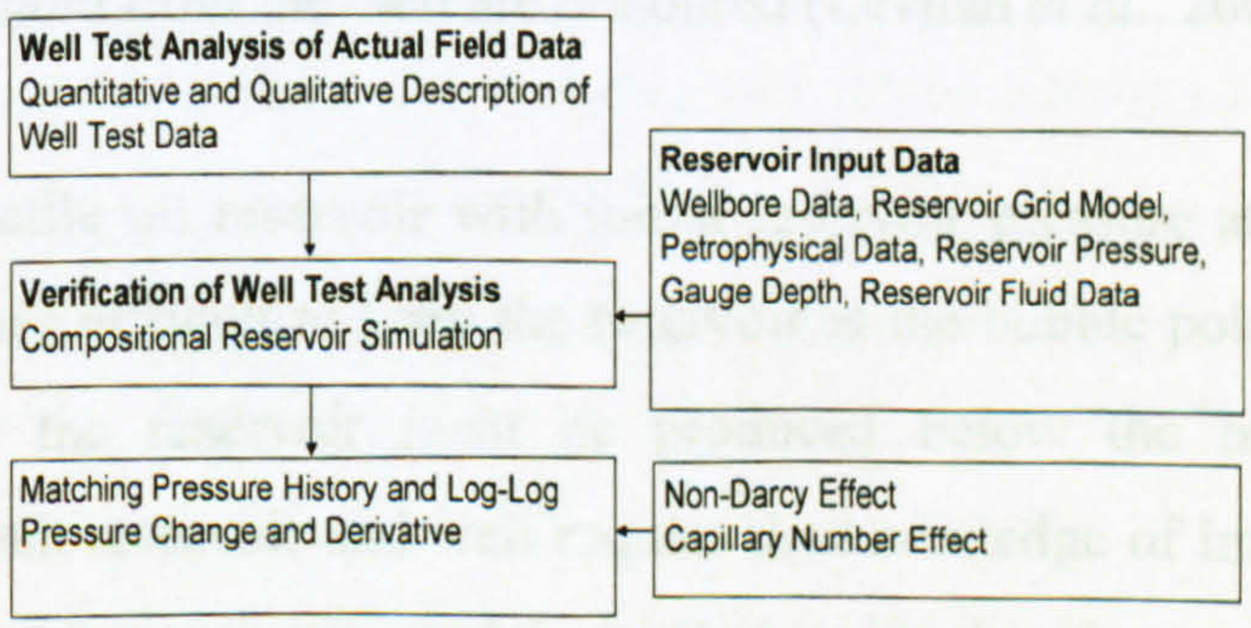

Figure 4-23 Methodology for well test analysis of volatile oil reservoirs

CHAPTER 5

Application of Well Testing for Well Deliverability Forecasting in Volatile Oil Reservoirs

This chapter presents the results of a study on the factors affecting well deliverability in volatile oil reservoirs producing at flowing bottomhole pressure below bubble point pressure and methods for mitigating well productivity decline due to "gas blockage" when volatile oil reservoirs are producing at flowing bottomhole pressure below bubble point pressure.

For this purpose, actual well producing at flowing bottomhole pressure below bubble point pressure was modelled using a one-dimensional single well compositional reservoir simulation, with velocity-dependent relative permeabilities functions of Capillary Number (N_c) and Forchheimer parameter (β). The model was then used to investigate oil productivity impairment due to "gas blockage" near the wellbore and the use of vertical hydraulic fractures and horizontal wells to mitigate the impairment to flow of the oil phase due to "gas blockage".

Management of oil and gas reservoirs is done at well level and field scale. Management at the well level gives important information on deliverability of individual wells that make up the field. Well test analysis is very important in reservoir and well management. It provides information on well condition; dynamic reservoir behaviour and reservoir boundaries. In well test analysis, the goal is to develop a simple reservoir model that honours all relevant static and dynamic data acquired during reservoir appraisal. The model is be tuned to ensure that all the pressure transient data acquired from the well are honoured (Levitan *et al.*, 2006b).

In a saturated volatile oil reservoir with initial reservoir pressure at the bubble point pressure, it becomes difficult to keep the reservoir at the bubble point pressure during production hence the reservoir must be produced below the bubble point. The management of such reservoir and well require the knowledge of impairment that can arise due to high gas saturation around the wells (gas blockage).

Woods (1955) presented a case history of reservoir performance of a highly volatile type oil reservoir. Increasing trend in *API* and *GOR* was recorded in two years of producing the reservoir with well characteristics becoming similar to that of a gas producing well rather than oil. As the reservoir pressure declined, the proportion of light volatile hydrocarbons recovered increased and correspondingly, the liquid phase remaining in the reservoir became richer in heavy hydrocarbons.

Another objective of well test analysis, apart from reservoir characterisation, is the prediction of well deliverability for production optimisation. One method of defining well deliverability is using productivity index (*PI*) which is the ratio of the flow rate by the drawdown pressure drop, expressed from the average reservoir pressure (p_{av}).

This gives an estimation of the reservoir capacity to deliver fluid to the wellbore and expressed mathematically as:

$$PI = \frac{q}{(p_{av} - p_{wf})} \tag{5-1}$$

Ideal productivity which is for well of zero skin is defined by Matthews and Russell (1967):

$$PI_{(s=0)} = \frac{q}{(p_{av} - p_{wf}) - \Delta p_{skin}} \tag{5-2}$$

During infinite acting, average reservoir pressure is approximately equal to initial reservoir pressure, so PI can be defined in terms of reservoir parameters for single-phase at steady state condition:

$$PI = \frac{kh}{162.6B\mu\left(\log\Delta t + \log\frac{k}{\phi\mu c_t r_w^2} - 3.23 + 0.87S\right)} \tag{5-3}$$

During pseudo steady state flow, PI is constant and can be expressed as

$$PI = \frac{kh}{162.6B\mu\left(\log\frac{A}{r_w^2} - \log(C_A) + 0.351 + 0.87S\right)} \tag{5-4}$$

An inflow performance relationship (*IPR*) enables estimation of well production rate when a given back pressure is exerted on the wellhead. Since the early days of testing wells, most efforts have concentrated on the formulation of simple equations expressing the relationship between volumetric flow rate and bottomhole flowing pressure over the practical range of production conditions (Golan and Whitson, 1994). When there is evolution of free gas inflow performance of oil phase is reduced. Vogel (1968) established an empirical relationship to estimate *IPR* for solution-gas drive wells.

IPR curves were generated for different reservoirs that have similar shapes, but depend in a given reservoir on the degree of depletion.

Inflow performance relationship has been extended to: damaged wells producing by solution-gas drive (Standing, 1970); solution-gas drive horizontal wells (Bendakhlia and Aziz, 1989); damaged or improved solution-gas drive wells (Klins and Majcher, 1992); perforated wells producing from solution gas drive reservoir (Sukamo and Tobing, 1995). Due to the dependence of *IPR* on depletion, they can not be used for transient production.

Fetkovich (1973) demonstrated that gas wells and oil wells behave very similarly, and therefore should be tested and analysed for well performance using the same basic flow equations. A rate-pressure relationship was developed on empirical observations for isochronal testing of oil wells, but the validity of his approach was not discussed.

In volatile oil and condensate reservoirs with flowing bottomhole pressure below the saturation pressure, it becomes difficult to define *PI* in terms of reservoir parameters due to: multiphase flow; capillary number dependence of relative permeabilities and recovery of liquid hydrocarbon from gas phase during separation process. Compositional reservoir simulation remains the best way to describe transient *PI* of volatile oil and gas condensate reservoirs below saturation pressure. Bozorgzadeh and Gringarten (2005), showed using single-phase and two-phase pseudo-pressures, that gas relative permeability at near-wellbore saturation and at the initial liquid saturation,

and the absolute permeability, are the most important parameters for predicting well productivity in gas condensate reservoirs.

In estimating oil recoveries from reservoirs containing highly volatile oils, it is important to include condensate that may be recovered from the gas produced from the reservoir. Cook *et al.* (1951) suggested that recoverable hydrocarbon liquids can be estimated from possible recovery from processing gas in a natural-gasoline plant or field separators. He described estimating the volume of recoverable hydrocarbon liquid by summing the volume of stock-tank and volume of condensate recovered from produced gas.

In this work a 2-D single well compositional well model with a 4 stage separator was used to study factors affecting *PI* of a well producing volatile at flowing bottomhole pressure below the bubble point pressure.

5.1 Improving recovery from volatile oil reservoirs

5.1.1 Hydraulic Fractures

Hydraulic fracturing is a common approach for improving productivity of oil and gas producing from damaged wells or wells producing from low-permeability reservoirs. Hydraulic fracturing involves pumping high pressure fluid into the formation to exceed the rock strength and open a fracture into the rock. The vertical fracture created is filled with propping agents to prevent the fracture from closing.

Fractures can generally be defined as infinite or finite conductivity. Gringarten *et al.* (1974) developed the analytical solutions for fractured wells for the uniform flux and the infinite conductivities fractures. Gringarten *et al.* (1974) showed by numerical simulation that, in infinite conductivity fractures, the flux distribution changes after the early response, and reaches a stabilized profile along the fracture length. When the pressure gradient along a given fracture is significant, the finite conductivity fracture model must be used. Cinco-ley and Samaniego (1981a) presented a pressure type curve with dimensionless pressure P_D as a function of dimensionless time t_{DxF} for varying values of dimensionless fractured conductivity defined as :

$$k_{fD}w_{fD} = \frac{k_f w_f}{kx_f} \tag{5-5}$$

They also presented a graph of dimensionless effective wellbore radius r_{we}/x_f versus dimensionless fracture conductivity and indicated that the infinite conductivity assumption is valid when the dimensionless fracture conductivity $K_{fD}w_{fD}$ greater than 300. For a fractured well, the following criteria are often used to estimate the effectiveness of a fracture treatment (Joshi, 1991): $K_{fD}w_{fD}$ <10 ineffective treatment; 10< $K_{fD}w_{fD}$ <50 effective treatment and $K_{fD}w_{fD}$ >50 very effective treatment.

Well test analysis can be used to describe fracture properties. Lee and Salter (1989) used post-fracture pressure transient analysis techniques for evaluation of fracture properties. They validated their result by production matching and suggested that future cumulative production for most of the studied wells in the reservoir could be further increased by improvement in the fracture conductivity.

Valkó and Economides (1998) introduced an optimisation technique using the fracture length and fracture conductivity to calculate an optimal dimensionless fracture conductivity at which productivity is maximised.

The performance of fractured wells can be impaired by the condition of the proppants fracture permeability which is greatly affected by the packing of the proppants. The permeability, normal to the fracture face and extending to the reservoir can also be impaired, leading to reduction in the performance of fracture. This type of damage is called fracture-face damage. Cinco-Ley and Samaniego (1981b) introduced the concept of fracture face skin. They provided an expression of the fracture face skin effect that is added to the dimensionless pressure for the finite conductivity fracture performance:

$$S_{fs} = \frac{\pi b_s}{2x_f}\left(\frac{k}{k_s} - 1\right) \tag{5-6}$$

where b_s is the penetration of damage and k_s is the damaged permeability.

Wang *et al.* (2000) extended (5-6) to estimate the skin effect due to condensate blockage in hydraulically fractured wells:

$$S_{fs} = \frac{\pi b_s}{2x_f}\left(\frac{1}{k_{rg}} - 1\right) \tag{5-7}$$

In this case, b_s and k_{rg} are the radius and the gas relative permeability of the two phase region, respectively.

Hashemi and Gringarten (2005) showed that performance improvement in gas condensate reservoirs with hydraulic fractures depends on facture length and fracture conductivity. Baig *et al.* (2005) investigated productivity of fractured and non-fractured wells in a lean/intermediate low permeability gas condensate reservoir. Their assessment showed that the length of the fracture controls the productivity of the gas condensate reservoirs. They showed further a long fracture yielding a high productivity improvement, despite low dimensionless fracture conductivity.

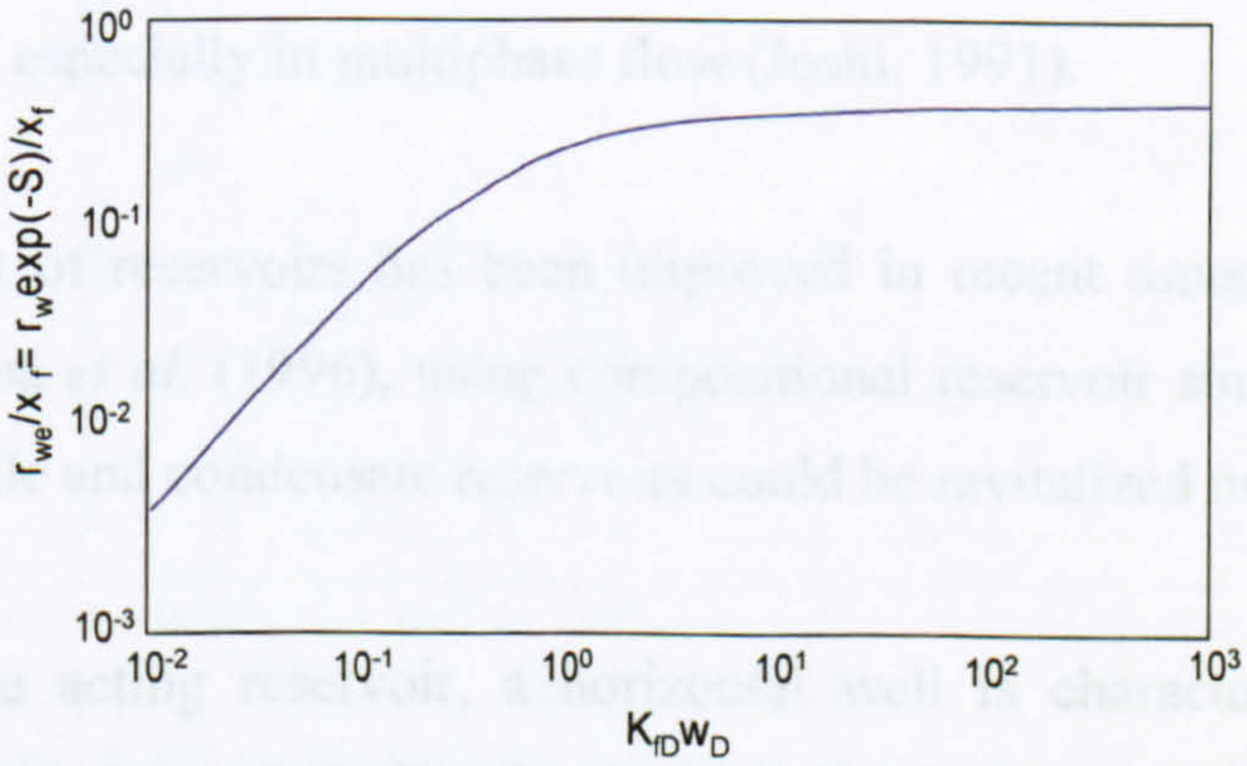

Figure 5-1 Relationship between fractured conductivity and wellbore radius for a finite conductivity fracture (Cinco-Ley and Samaniego, 1981a)

5.1.2 Horizontal Wells

The major purpose of a horizontal well is to enhance reservoir contact and thereby enhance well productivity. In general, a horizontal well is drilled parallel to the reservoir bedding plane (Joshi, 1991). One major disadvantage of horizontal wells is their cost. Typically, they cost about 1.4 to 3 times more than a vertical well, depending upon drilling method, completion technique and drilling experience in the given location (Joshi, 1991).

Horizontal wells have been used in several applications, some of which include: in reservoirs with water and gas coning problem to minimize coning problems and enhance oil production (Cooper and Troncoso, 1986, Stramp, 1980); in high permeability gas reservoirs, with high near-wellbore gas velocity in vertical wells, horizontal wells can be used to reduce near wellbore velocity hence reducing turbulence and improving deliverability (Celier, 1989); in naturally fractured reservoirs to drain reservoirs effectively by intersecting fractures with horizontal wells (Sheikholeslami et al., 1990, Yost II et al., 1988); in low permeability gas reservoirs, to improve drainage area per well and reduce the number of wells that are required to drain the reservoir (Joshi, 1991); in thermal *EOR* projects to enhance productivity by providing a large reservoir contact area (Cline and Basham, 2002, Luo and Baker, 2006, McKay *et al.*, 2003).

Rarely are horizontal wells truly horizontal; rather they wander up and down in the vertical plane. In low rates wells, well shape can have significant impact on well productivity, especially in multiphase flow (Joshi, 1991).

Development of reservoirs has been improved in recent times by drilling horizontal wells. Villalba *et al.* (1996), using compositional reservoir simulation, showed that a mature volatile and condensate reservoirs could be revitalized using horizontal wells.

In an infinite acting reservoir, a horizontal well is characterised by three typical regimes (*Figure 5-2* to *5-5*). The first is the radial flow regime in the vertical plane; the second is a linear flow regime which occurs when the upper and lower reservoir limits are reached and finally horizontal radial flow regime which flow lines converge from all reservoir directions towards the well.

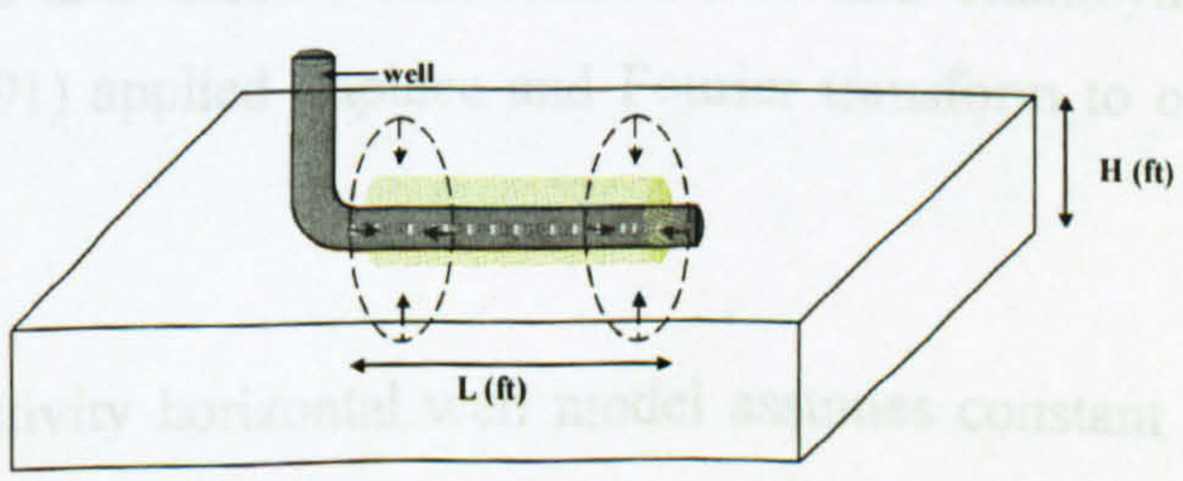

Figure 5-2 Vertical radial flow geometry in a horizontal well

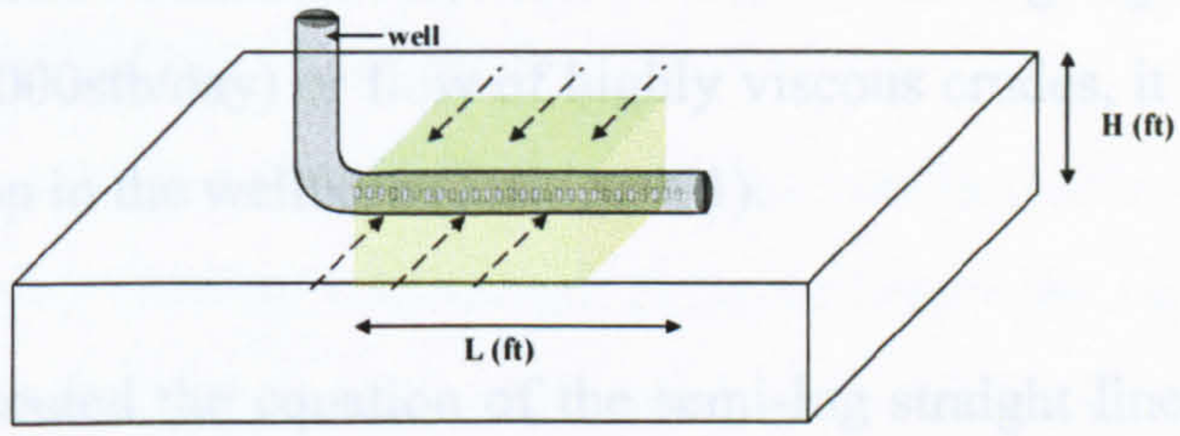

Figure 5-3 Linear flow geometry in a horizontal well

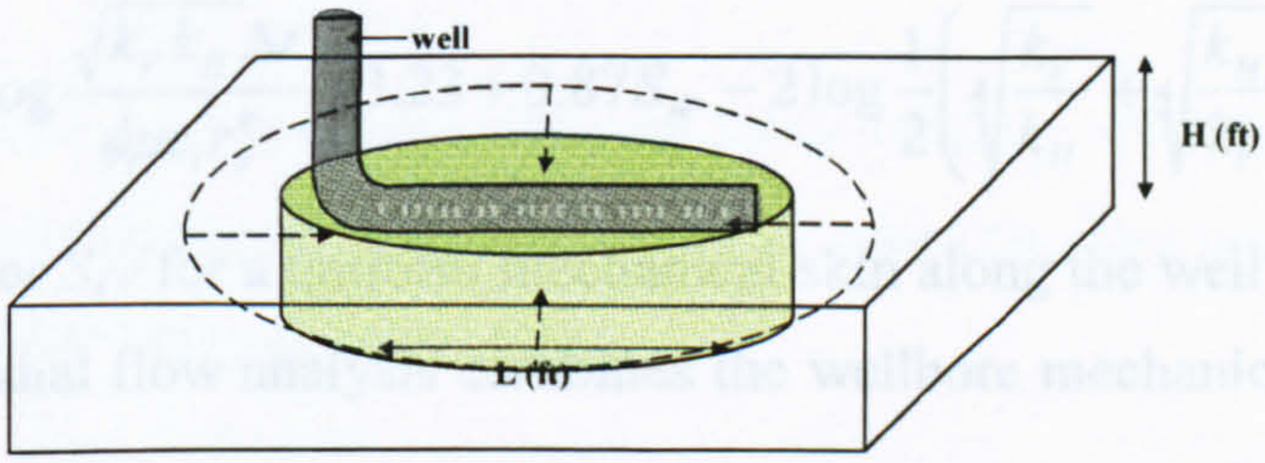

Figure 5-4 Horizontal radial flow geometry in a horizontal well

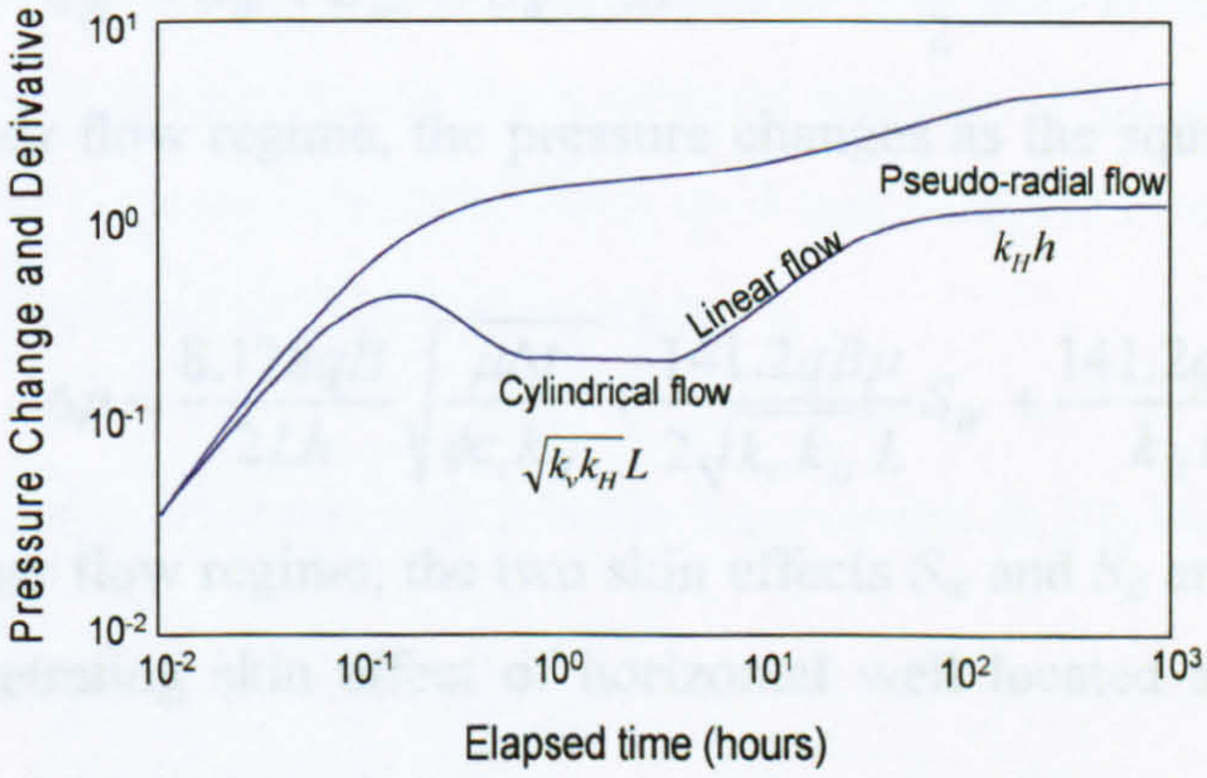

Figure 5-5 Log-log plot for different flow regimes in a horizontal well

Analytical well test solution for uniform flux and infinite conductivity horizontal well was derived by: Clonts and Ramey (1986); Davlau *et al.* (1988); Rosa and Carvalho (1989) using source and Green's functions. Goode and Thambynayagm (1987) and Kuchuck *et al.* (1991) applied Laplace and Fourier transform to obtain an analytical solution.

The infinite conductivity horizontal well model assumes constant pressure along the wellbore. In general, pressure drop along the well length is very small and can be ignored.

However, under certain circumstances, such as those involving high flow rates of light oil (greater than 10,000stb/day) or flow of highly viscous crudes, it is possible to have a larger pressure drop in the wellbore (Joshi, 1991).

Kuchuk (1995) presented the equation of the semi-log straight line for vertical radial flow regime equation:

$$\Delta p = \frac{162.6qB\mu}{2\sqrt{k_V k_H}L}\left[\log\frac{\sqrt{k_V k_H}\Delta t}{\phi\mu c_t r_w^e} - 3.23 + 0.87S_W - 2\log\frac{1}{2}\left(\sqrt[4]{\frac{k_V}{k_H}} + \sqrt[4]{\frac{k_H}{k_V}}\right)\right] \quad (5\text{-}8)$$

The total skin factor S_{TV} for a uniform mechanical skin along the well length measured from early time radial flow analysis combines the wellbore mechanical skin factor S_W and S_{ani}:

$$S_{TV} = S_W + S_{ani} = S_W - \ln\frac{\left(\sqrt[4]{k_V/k_H} + \sqrt[4]{k_H/k_V}\right)}{2} \quad (5\text{-}9)$$

During the linear flow regime, the pressure changes as the square root of the elapsed time:

$$\Delta p = \frac{8.128qB}{2Lh}\sqrt{\frac{\mu\Delta t}{\phi c_t k_H}} + \frac{141.2qB\mu}{2\sqrt{k_V k_H}L}S_W + \frac{141.2qB\mu}{k_H h}S_z \quad (5\text{-}10)$$

During the linear flow regime, the two skin effects S_w and S_Z are additive, where S_Z is the partial penetrating skin effect of horizontal well located at Z_W in the formation thickness:

$$S_z = -1.151\sqrt{\frac{k_H}{k_V}}\frac{h}{L}\log\left[\frac{\pi r_w}{h}\left(1+\sqrt{\frac{k_V}{k_H}}\right)\sin\left(\frac{\pi z_w}{h}\right)\right] \quad (5\text{-}11)$$

Using the well half-length as the reference for semi-log analysis of horizontal radial flow, Kuchuk *et al.* (1995) define the pseudo-radial flow from the reservoir as:

$$\Delta p = 162.6\frac{qB\mu}{k_H h}\left[\log\frac{k_H\Delta t}{\phi\mu c_t L^2} - 2.53\right] + \frac{141.2qB\mu}{2\sqrt{k_V k_H}L}S_W + \frac{141.2qB\mu}{k_H h}S_{zT} \quad (5\text{-}11)$$

Where S_{zT} is given by:

$$S_{zT} = S_z - 0.5\frac{k_H}{k_V}\frac{h^2}{L^2}\left(\frac{1}{3} - \frac{z_w}{h} + \frac{z_w^2}{h^2}\right) \quad (5\text{-}12)$$

5.2 Well Test Analysis of Well-3

Well-3 is located in a highly faulted sandstone reservoir in North Africa (*Figure 5-6*). A production test with flowing bottomhole pressure below the bubble point pressure was carried out. Depth corrected pressure rate history of Well-3 is shown in *Figure 5-7*. Depth correction was necessary because the pressure gauge was placed above the top perforation.

The Log-log pressure derivative plot with respect to build-up 170 (*Figure 5-8*) shows a composite behaviour due to mobility discontinuity when flowing bottomhole pressure falls below the bubble pressure of the fluid.

A well test analysis match was obtained with wellbore storage and skin in an open rectangular reservoir (i.e., a channel bounded on one side) with a two-region radial composite behaviour (*Figure 5-9*). The reservoir boundary condition is consistent with the structural fault map obtained from seismic analysis (*Figure 5-10*). Initial reservoir pressure of 5197 psia was obtained from well test analysis is which is consistent with the value obtained from the fluid analysis report.

Petrophysical and fluid properties of Well-3 are shown in *Appendix F*.

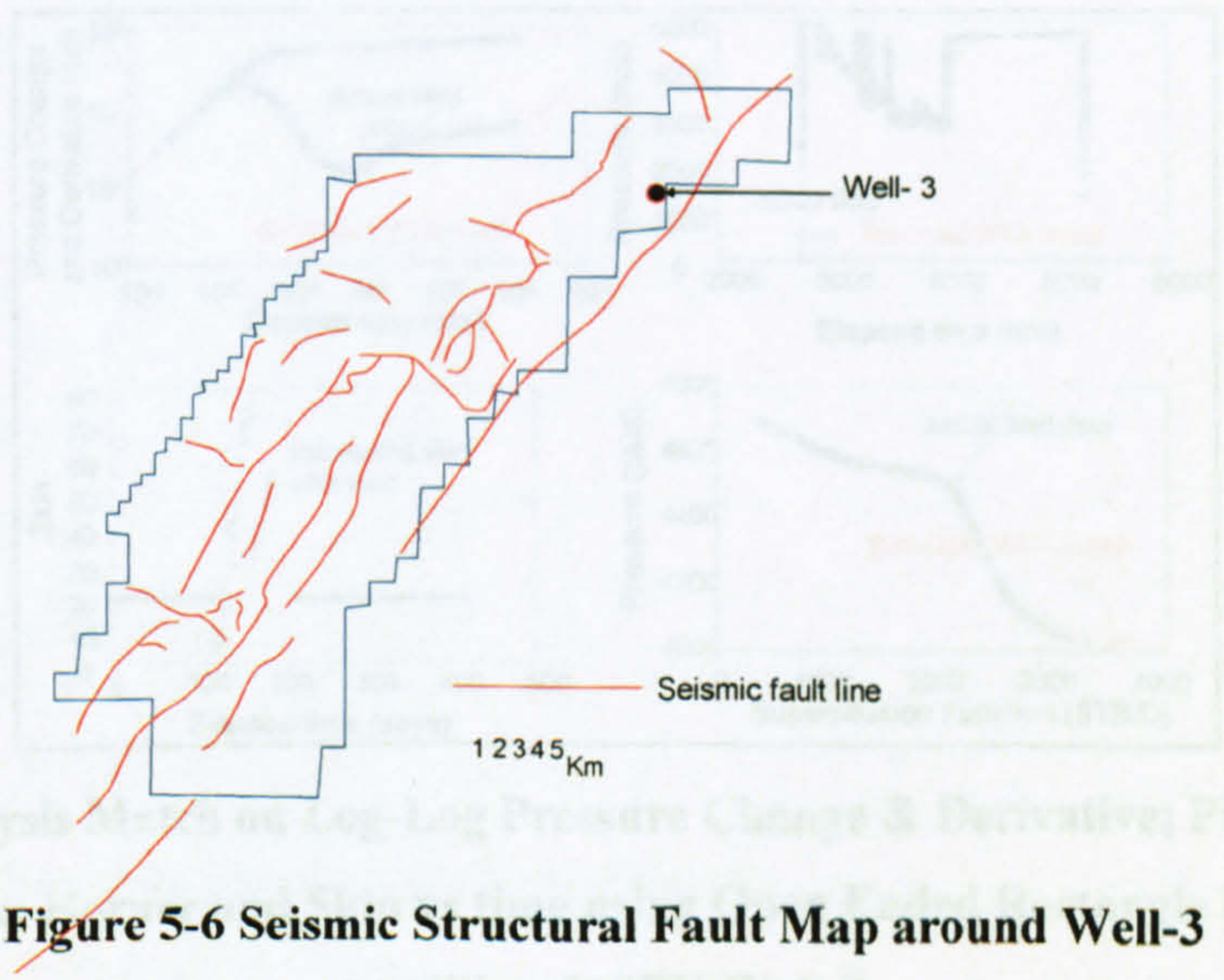

Figure 5-6 Seismic Structural Fault Map around Well-3

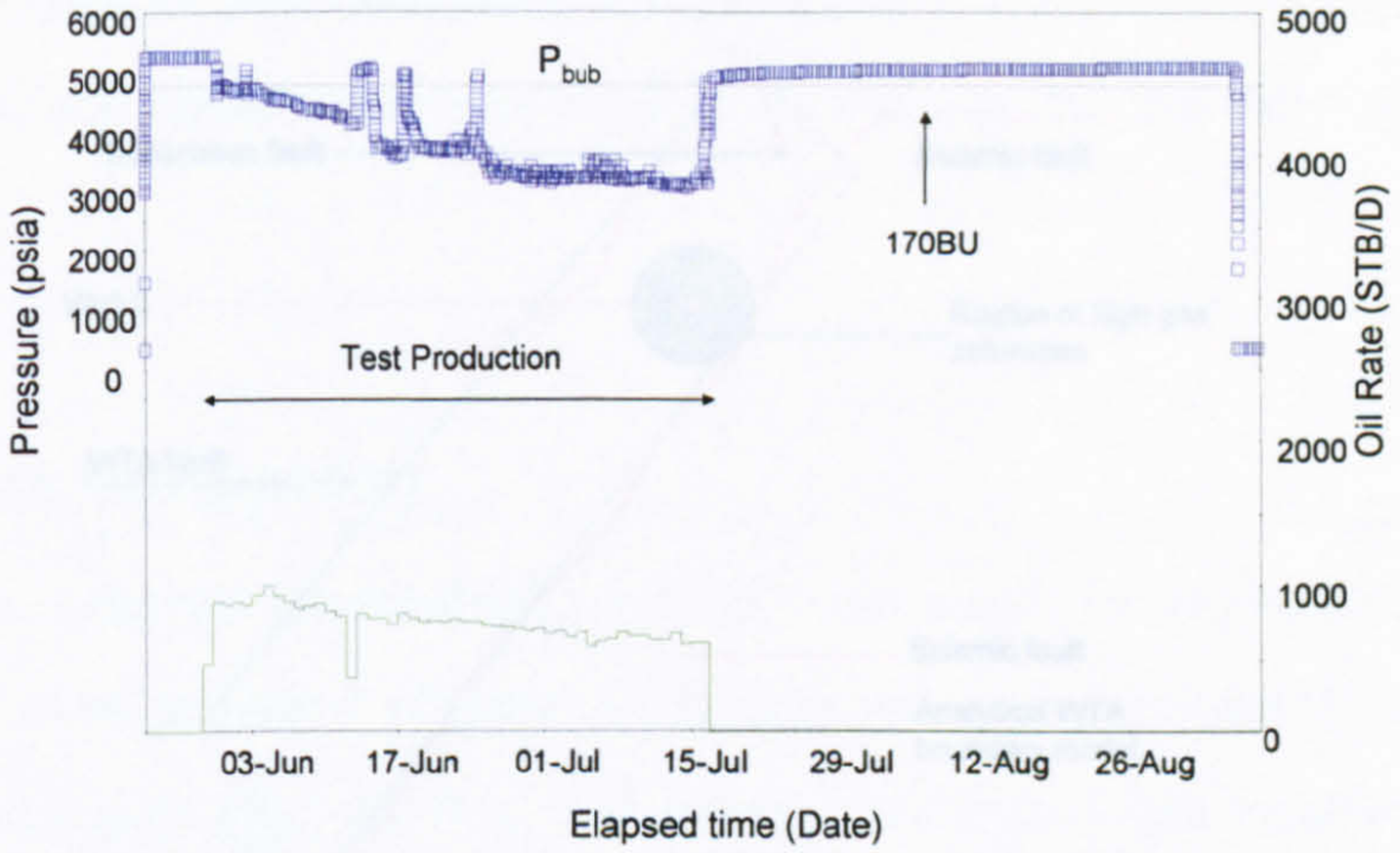

Figure 5-7 Pressure Rate History of Well-3

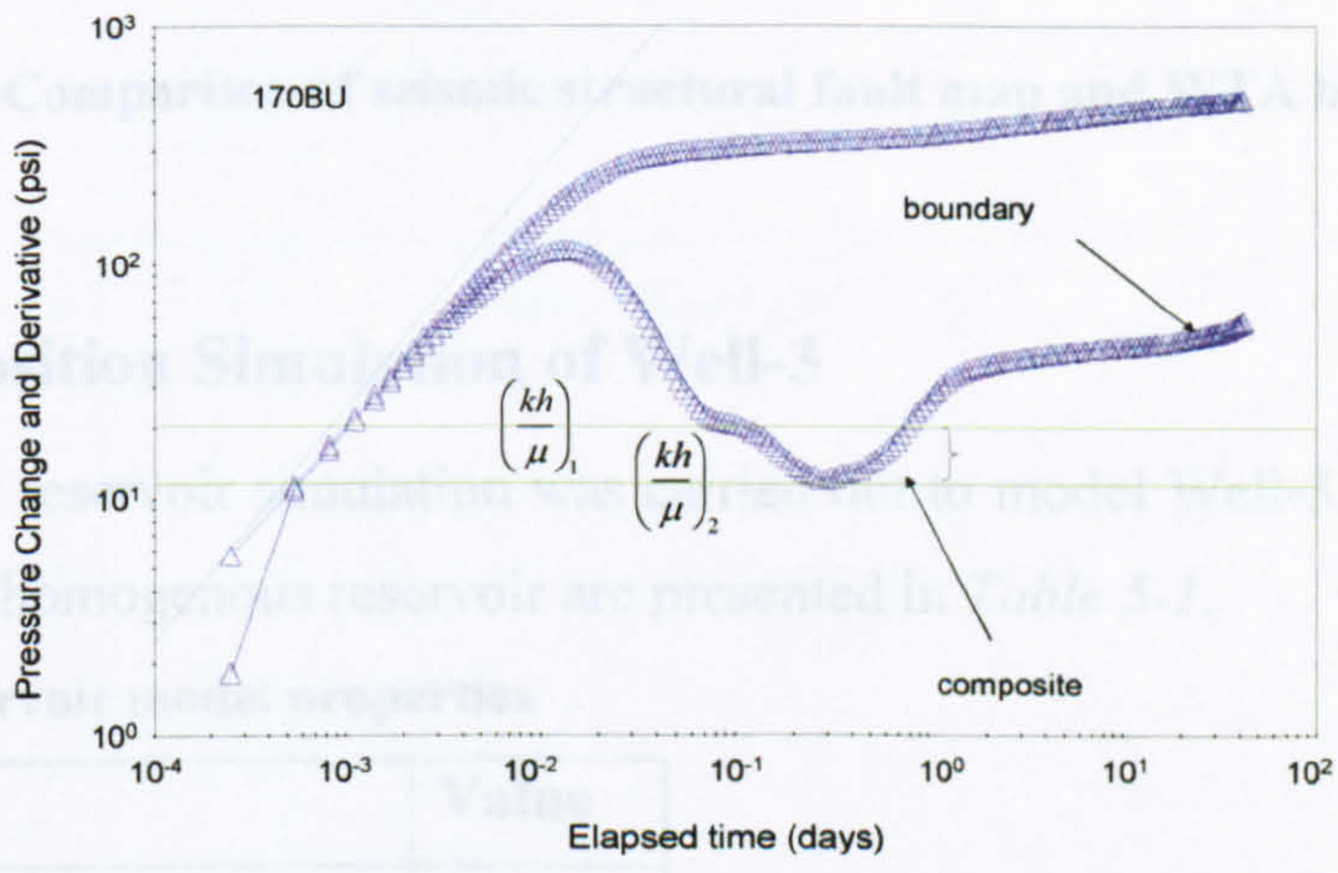

Figure 5-8 Log-Log Diagnostic - Flow Period 170- Well-3

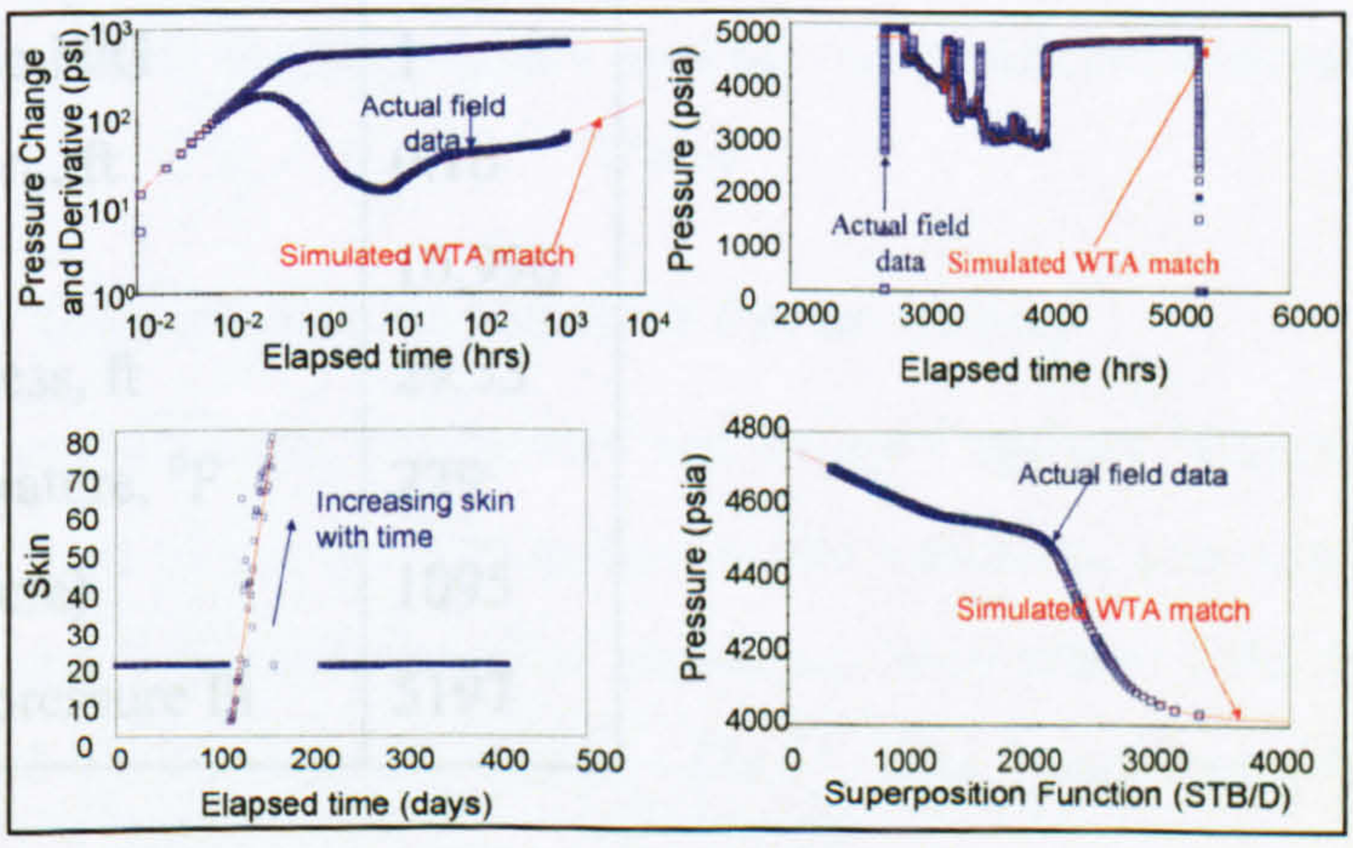

Figure 5-9 Analysis Match on Log-Log Pressure Change & Derivative; Pressure History Simulation; Horner and Skin vs time using Open Ended Rectangle boundary condition:170BU-Well-3

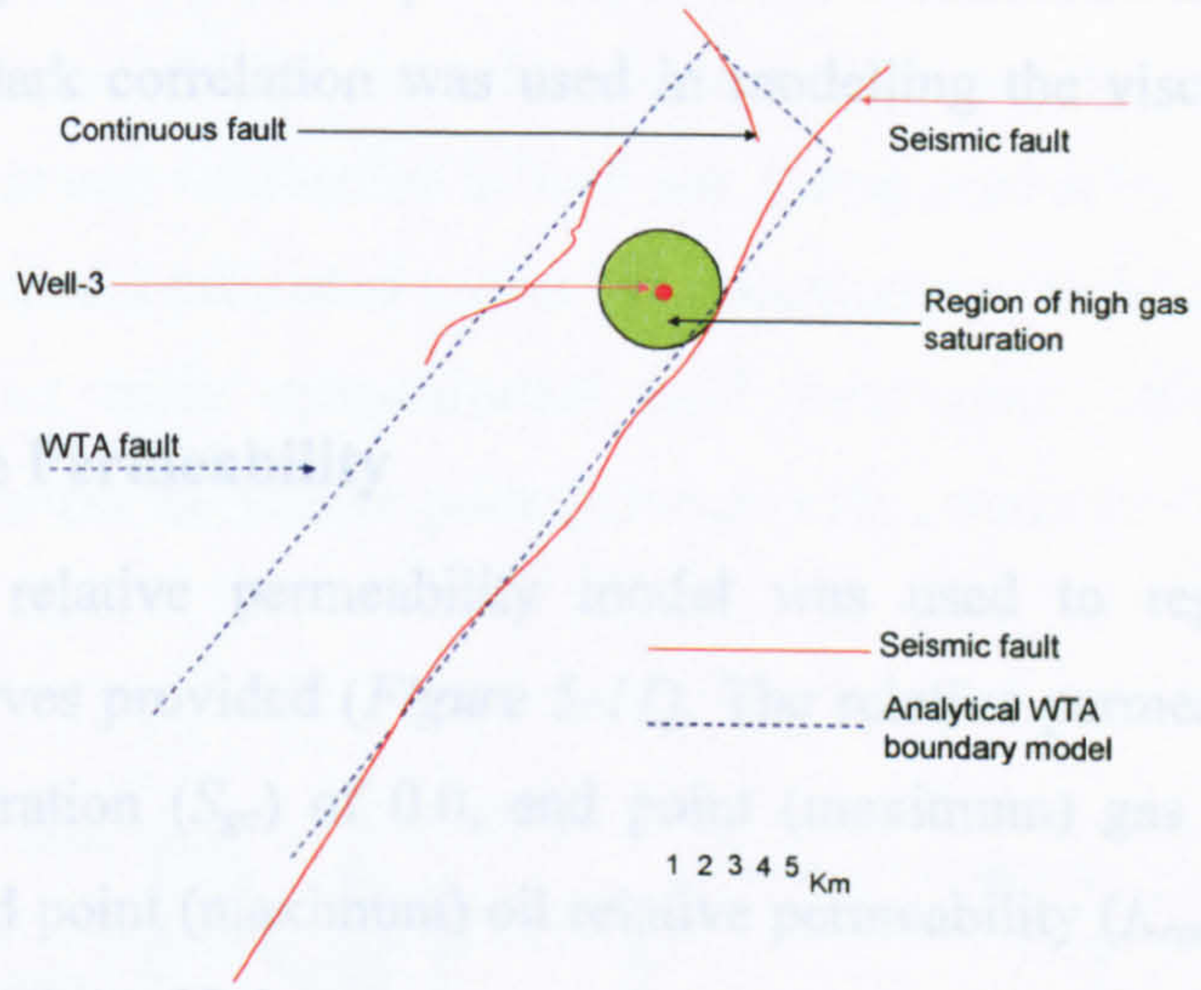

Figure 5-10 Comparison of seismic structural fault map and WTA boundary model

5.3 Composition Simulation of Well-3

Compositional reservoir simulation was carried out to model Well-3. Properties of the single-layered homogenous reservoir are presented in *Table 5-1*.

Table 5-1 Reservoir model properties

Parameter	Value
Porosity Ø, %	13
Absolute permeability k, mD	44
Net to-Gross ratio N/G	1
Wellbore radius r_w, ft	0.16
Top depth, ft	10,996
Reservoir thickness, ft	29.53
Reservoir temperature, ^oF	229
Drainage area (acre)	1095
Initial reservoir pressure Pi	5197

5.3.1 Fluid Characterisation and modelling.

The Modified Peng-Robinson EOS with 3 parameters was used for modelling *PVT* properties of the reservoir fluids. Regression was performed on the molecular weight (*MW*) of heavy components; critical pressure (P_c); critical temperature (T_c) of the

pseudo-components; and binary interaction coefficient between light and heavy components. *Appendix F-5* compares observed and simulated fluid experiments. The Lorentz-Bray-Clark correlation was used in modelling the viscosity of fluid sample from Well-3.

5.3.2 Relative Permeability

A Corey type relative permeability model was used to regenerate the relative permeability curves provided (*Figure 5-11*). The relative permeability curve (K_1) has critical gas saturation (S_{gc}) of 0.0, end point (maximum) gas relative permeability (K_{rgmax}) of 1, end point (maximum) oil relative permeability (K_{romax}) of 1, and connate water saturation (S_{wc}) of 0.4.

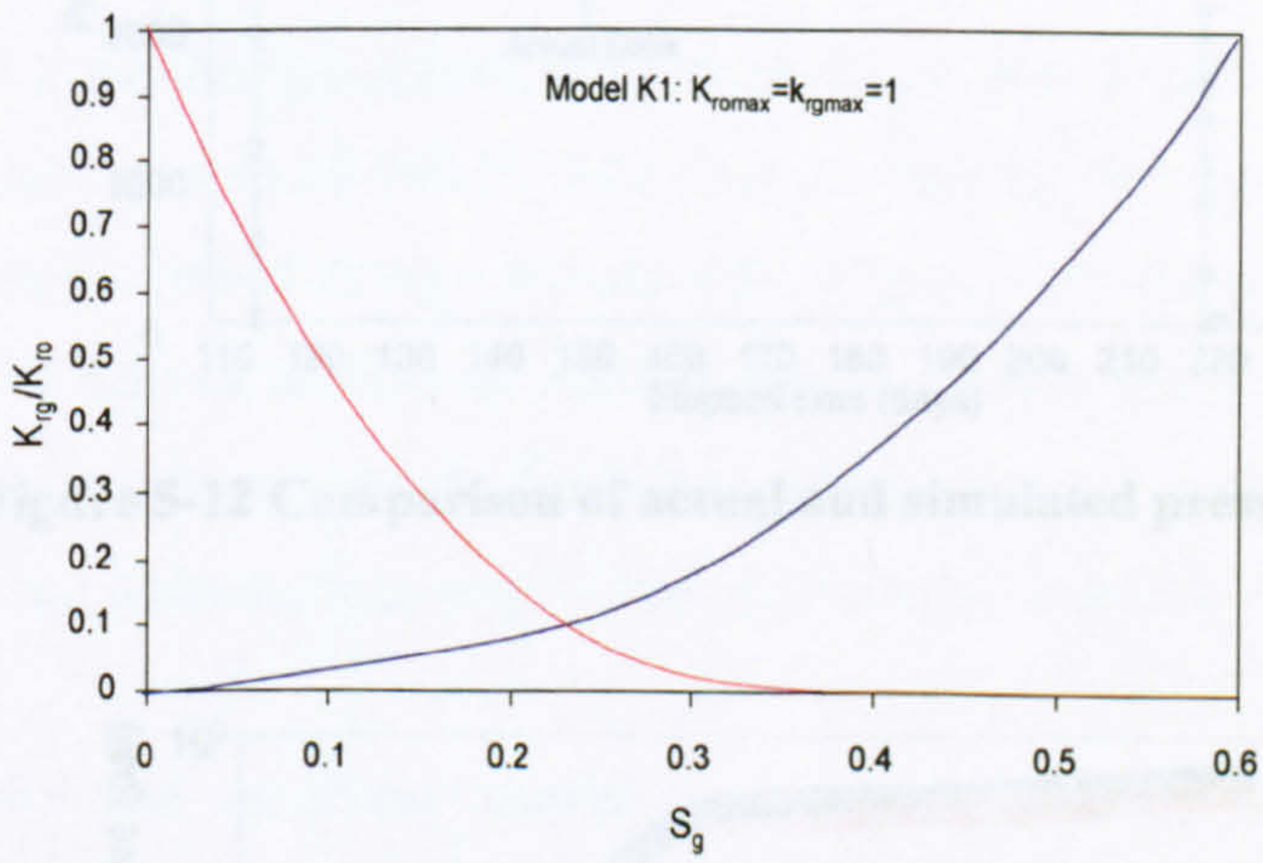

Figure 5-11 Relative permeability model used for compositional reservoir simulation of Well-3

5.3.3 Velocity Dependence of Relative Permeability

Iteratively, Henderson's eight parameters that define Capillary Number (Henderson *et al.* 2000) were varied to get the best match on the simulated pressure history; log-log pressure change and derivative match if simulation with actual field data from Well-3 (*Figure 5-12* and *5-13*), whereas the non-Darcy flow parameter (β) was estimated using Geertsma's relationship (Geerstma 1974). The parameters are listed and compared with values from a North Sea gas condensate in *Appendix F-6*.

There are 46 flow periods recorded during the main flow test, with a mean deviation of 13% in recorded rate which is less than the minimum accuracy of most flow meters. Hence the analysis and verification of well test during production becomes impossible. *Figure 5-14* compares estimated radius of discontinuous mobility (r_1) from well test analysis with that from compositional well simulation, which also shows high shrinkage in oil below the bubble point pressure with saturation discontinuity at bubble point pressure.

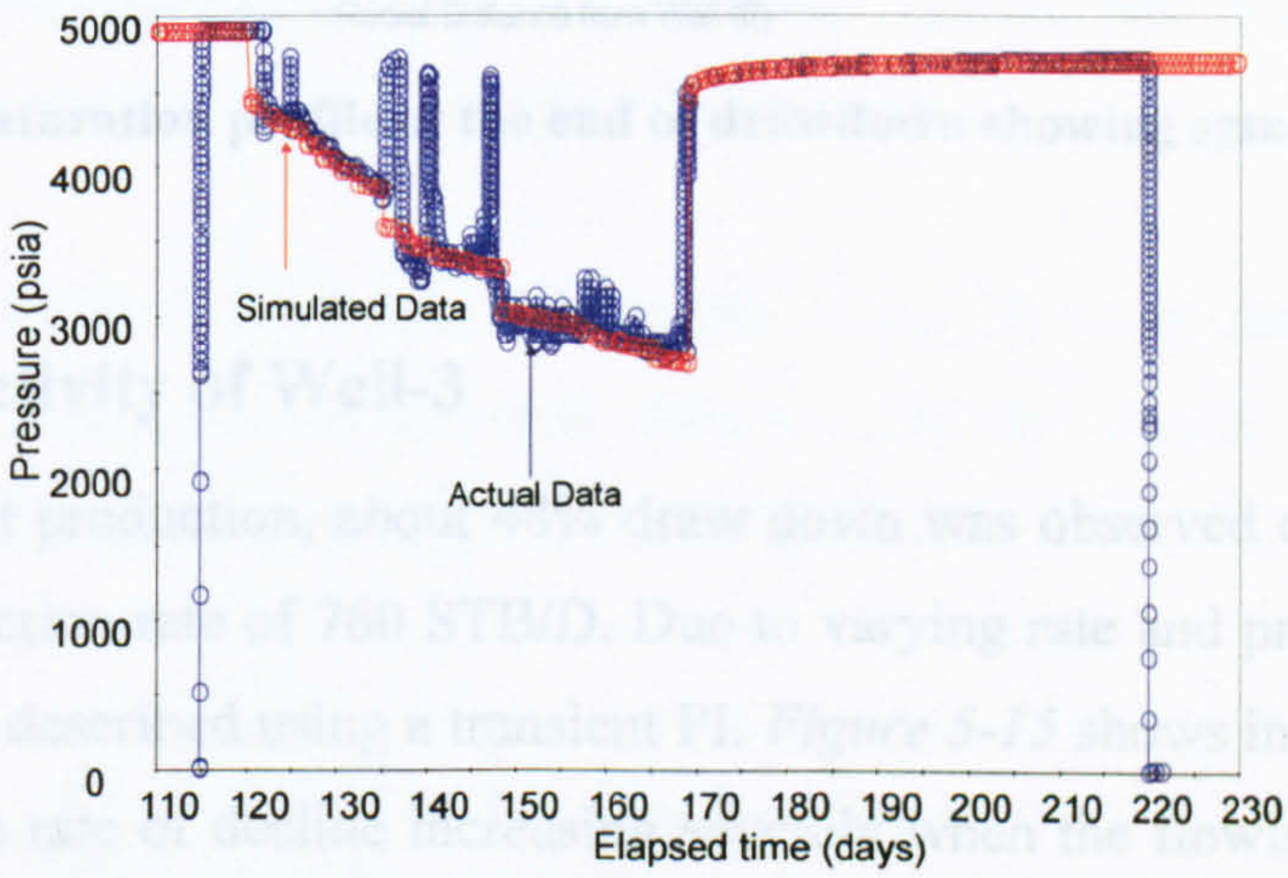

Figure 5-12 Comparison of actual and simulated pressure history

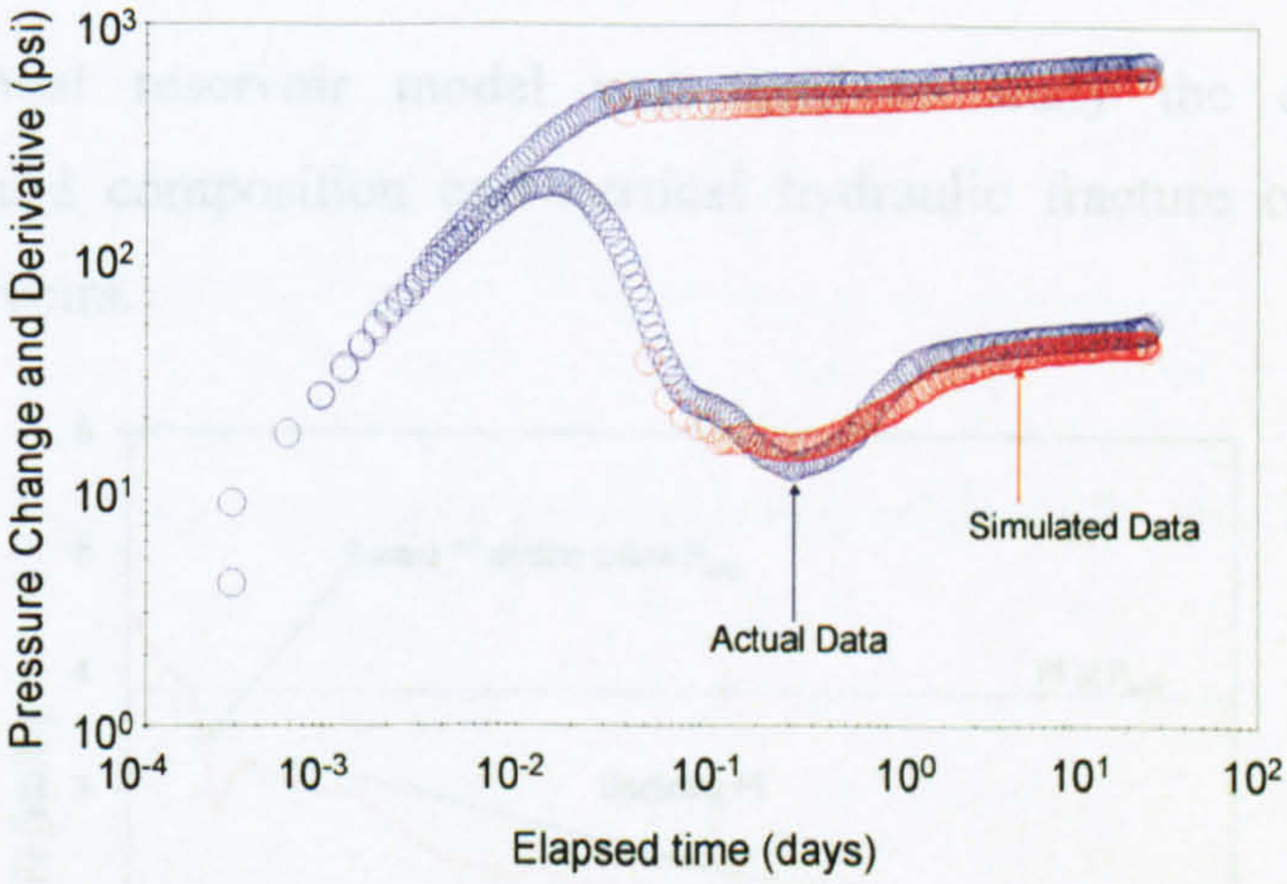

Figure 5-13 Comparison of actual and simulated log-log pressure derivative plot for flow period 170.

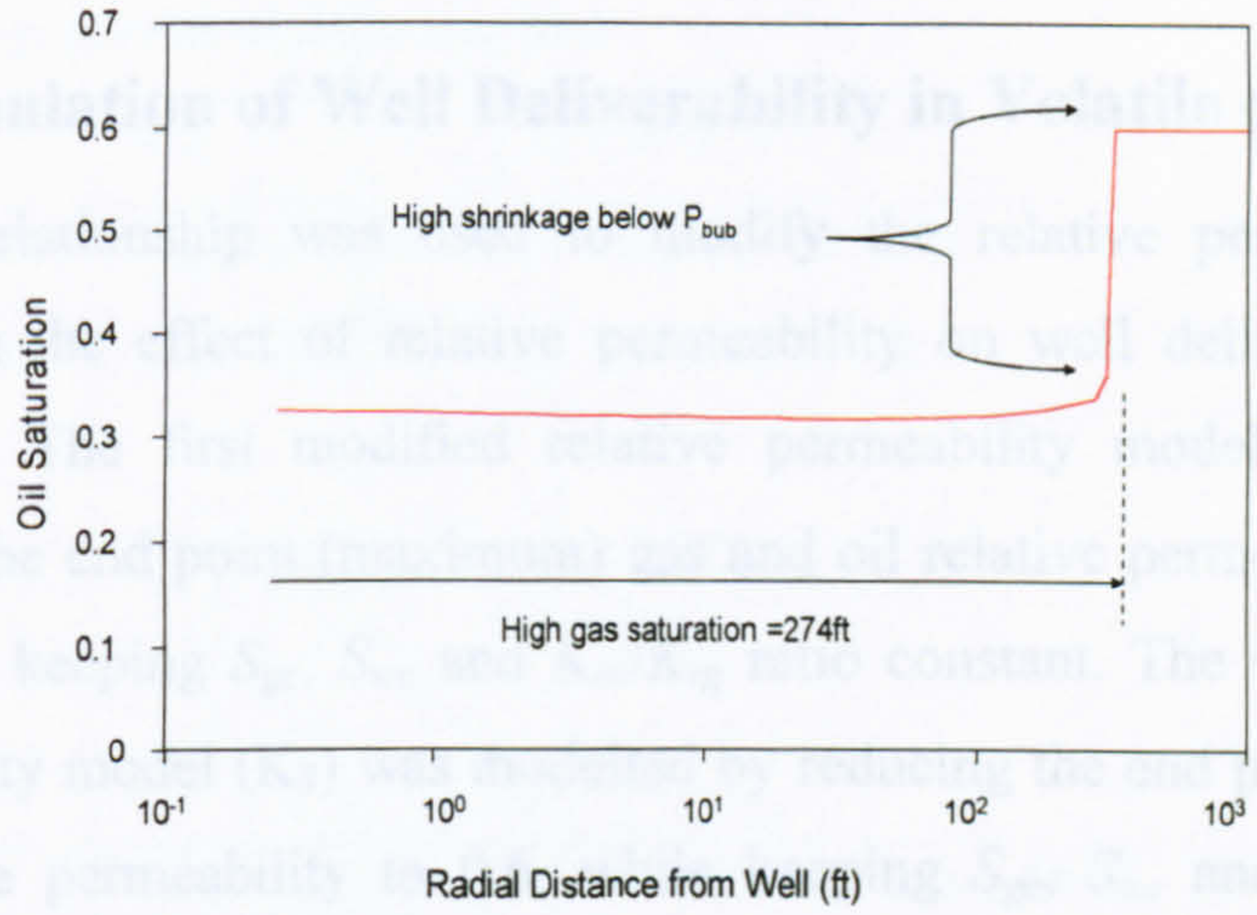

Figure 5-14 Saturation profile at the end of drawdown showing saturation discontinuity

5.4 Productivity of Well-3

During the test production, about 48% draw down was observed during 50 days with average production rate of 760 STB/D. Due to varying rate and pressure, productivity of Well-3 was described using a transient PI. *Figure 5-15* shows initial gradual decline in *PI*, with the rate of decline increasing severely when the flowing *BHP* falls below the bubble point pressure due to formation of high gas saturation around the wellbore hereby reducing ultimate recovery of the oil from the reservoir.

The compositional reservoir model was used to study the effect of relative permeability, fluid composition and vertical hydraulic fracture on productivity of volatile oil reservoirs.

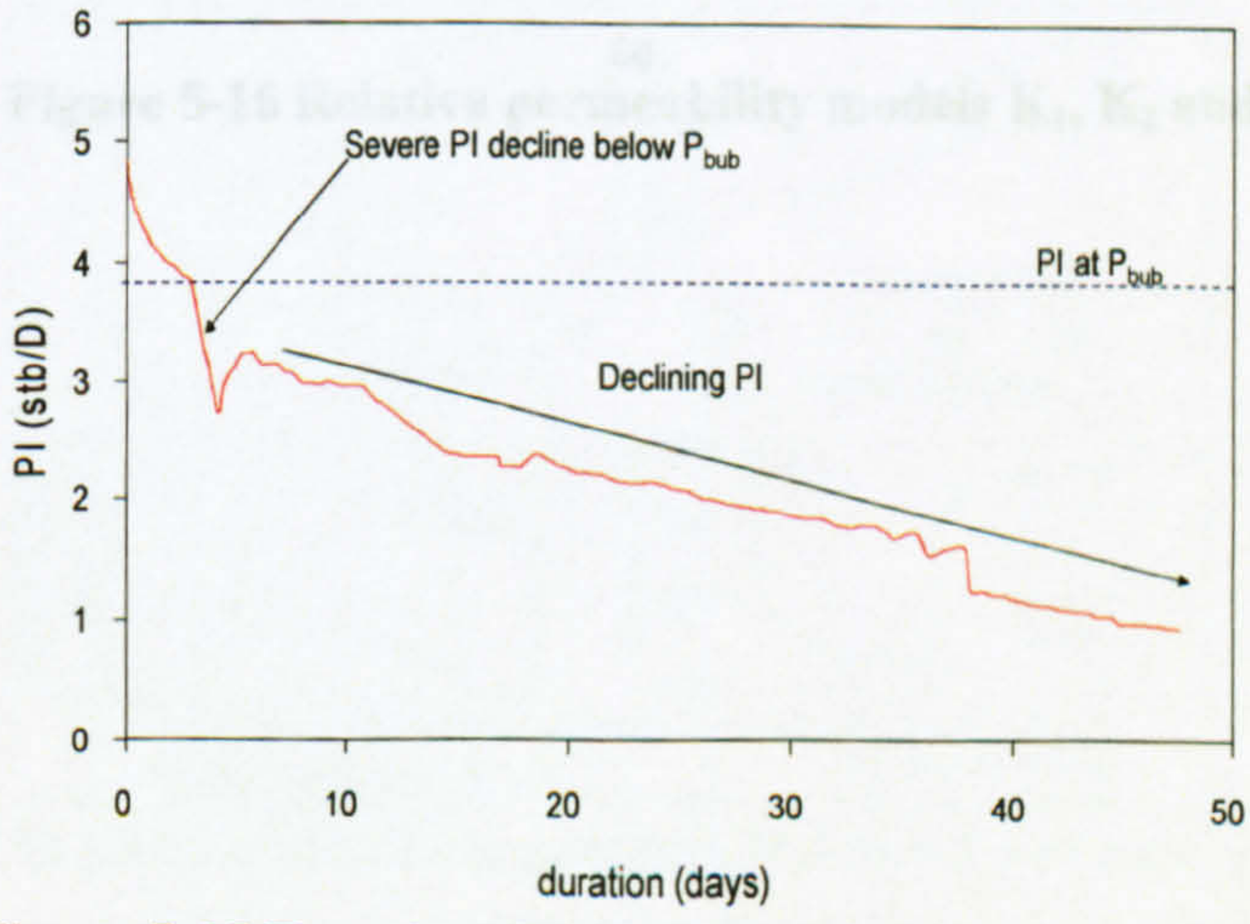

Figure 5-15 Transient PI of Well-3 during test production

5.5 Simulation of Well Deliverability in Volatile oil Reservoirs

Corey's relationship was used to modify the relative permeability model K_1 to investigate the effect of relative permeability on well deliverability in volatile oil reservoirs. The first modified relative permeability model (K_2) was modeled by reducing the end point (maximum) gas and oil relative permeability curves from 1 to 0.8, while keeping S_{gc}, S_{wc} and K_{ro}/K_{rg} ratio constant. The second modified relative permeability model (K_3) was modelled by reducing the end point (maximum) gas and oil relative permeability to 0.6, while keeping S_{gc}, S_{wc} and K_{ro}/K_{rg} ratio constant. *Figure 5-16* compares the relative permeability models.

Two other volatile oil fluid models (Sample A and B) were used to investigate the effect of fluid composition on well deliverability in volatile oil reservoirs. The properties of these fluid samples are listed in *Table 5-2*.

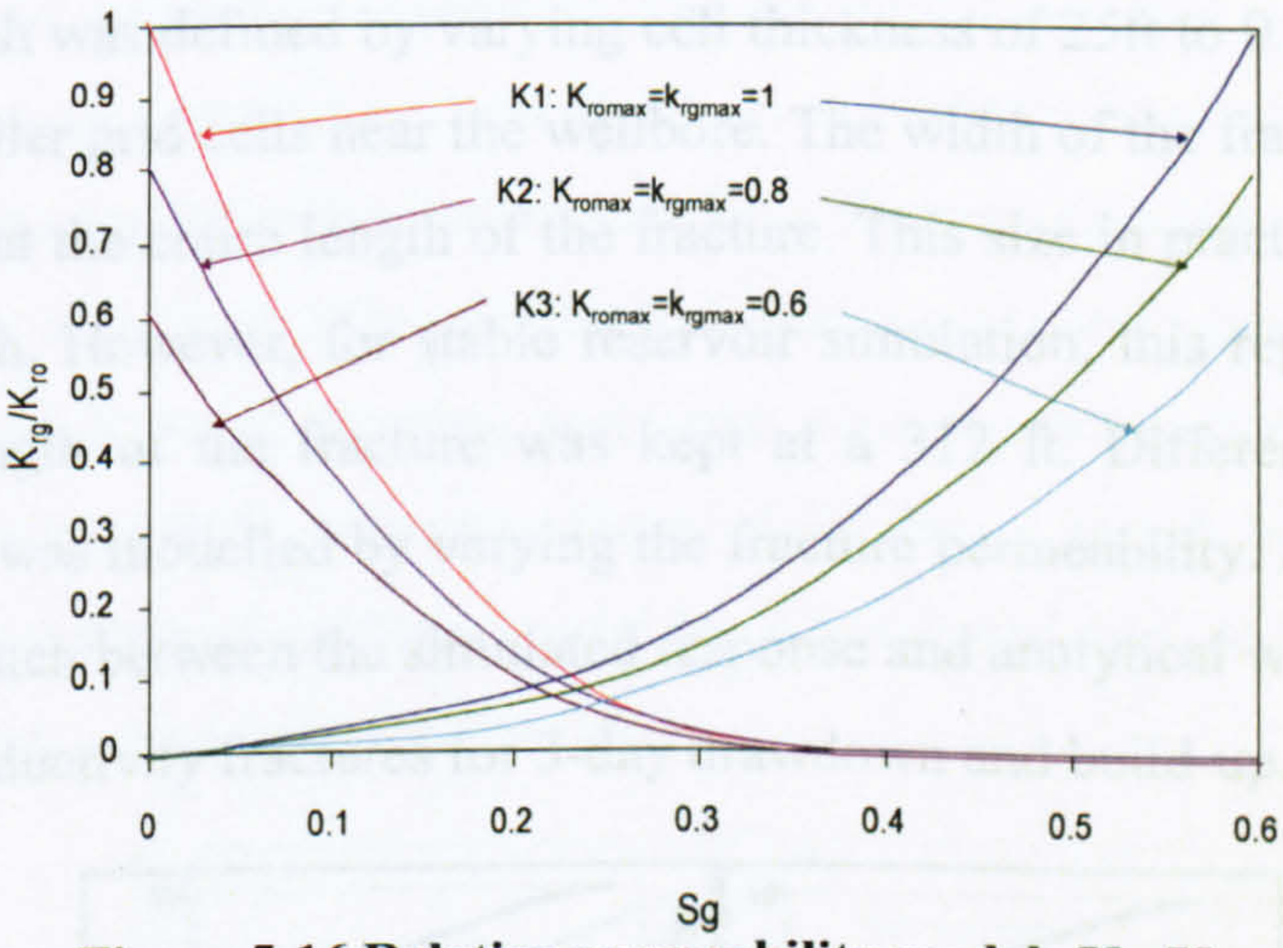

Figure 5-16 Relative permeability models K_1, K_2 and K_3

Table 5-2 Properties of fluid samples

Fluid	W3	Fluid A	Fluid B
Fluid type	Highly Volatile	Highly Volatile	Moderately Volatile
P_{bub} (psia)	4995 at 229°F	4475 at 176°F	4076 at 189°F
R_s (scf/bbl)	3,794 at 229°F	3,377 at 176°F	1,786 at 189°F
$Pi-P_{bub}$ (psia)	201	201	201
Source	*North Africa*	*Coats and Smart 1982*	*Western Siberia*

5.6 Vertical Hydraulic Fracture Model

A totally penetrating vertical fracture was modelled to investigate the effect of fractures on well deliverability in volatile oil reservoirs. The fracture was positioned at the centre; symmetrical with respect to the well axis and parallel to the x direction. The fracture length was defined by varying cell thickness of 25ft to 0.1ft in the x direction, with the smaller grid cells near the wellbore. The width of the fracture is 1 cm (0.0328 ft) throughout the entire length of the fracture. This size in practical sense is wide for fracture width. However, for stable reservoir simulation, this represents a reasonable size. The length of the fracture was kept at a 312 ft. Different values of fracture conductivity was modelled by varying the fracture permeability. *Figure 5-17* and *5-18* shows the match between the simulated response and analytical well test model for low and high conductivity fractures for 3-day drawdown and build-up.

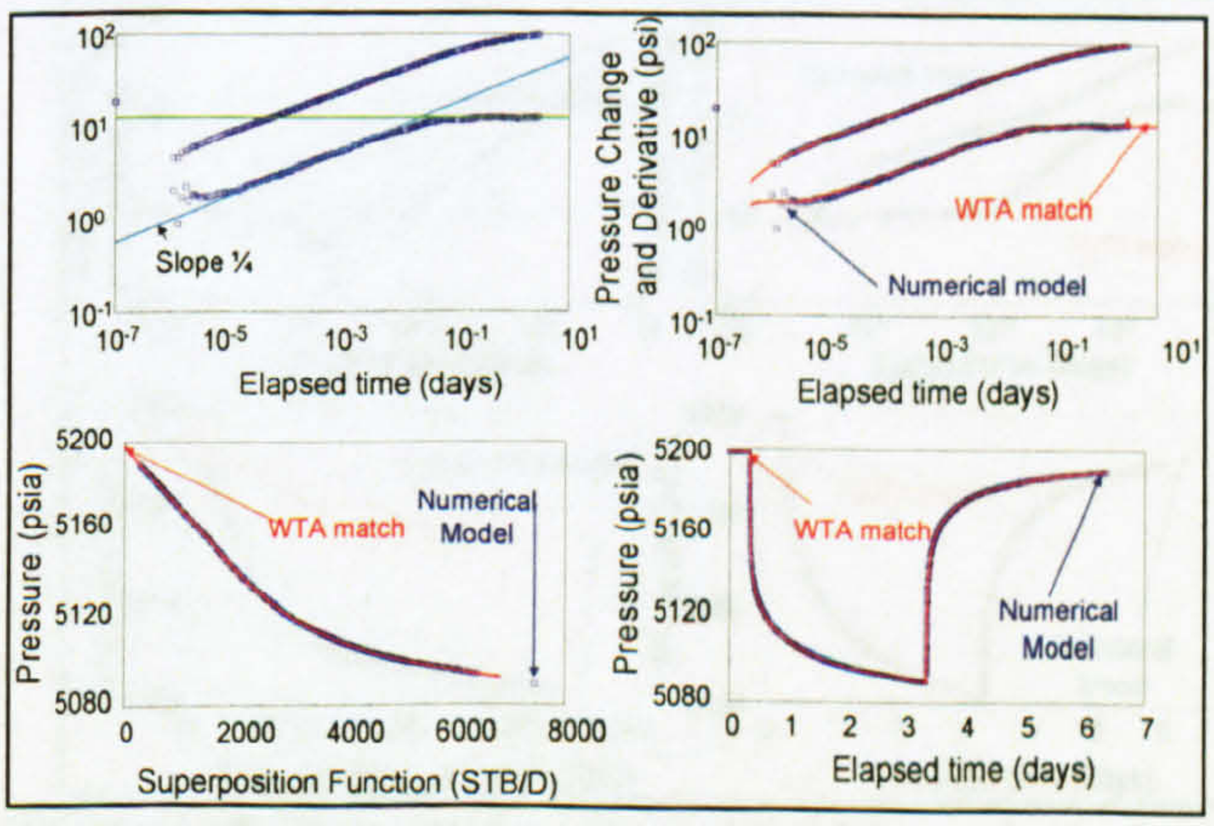

Figure 5-17 Validation of low conductivity fractured well numerical model with analytical solution

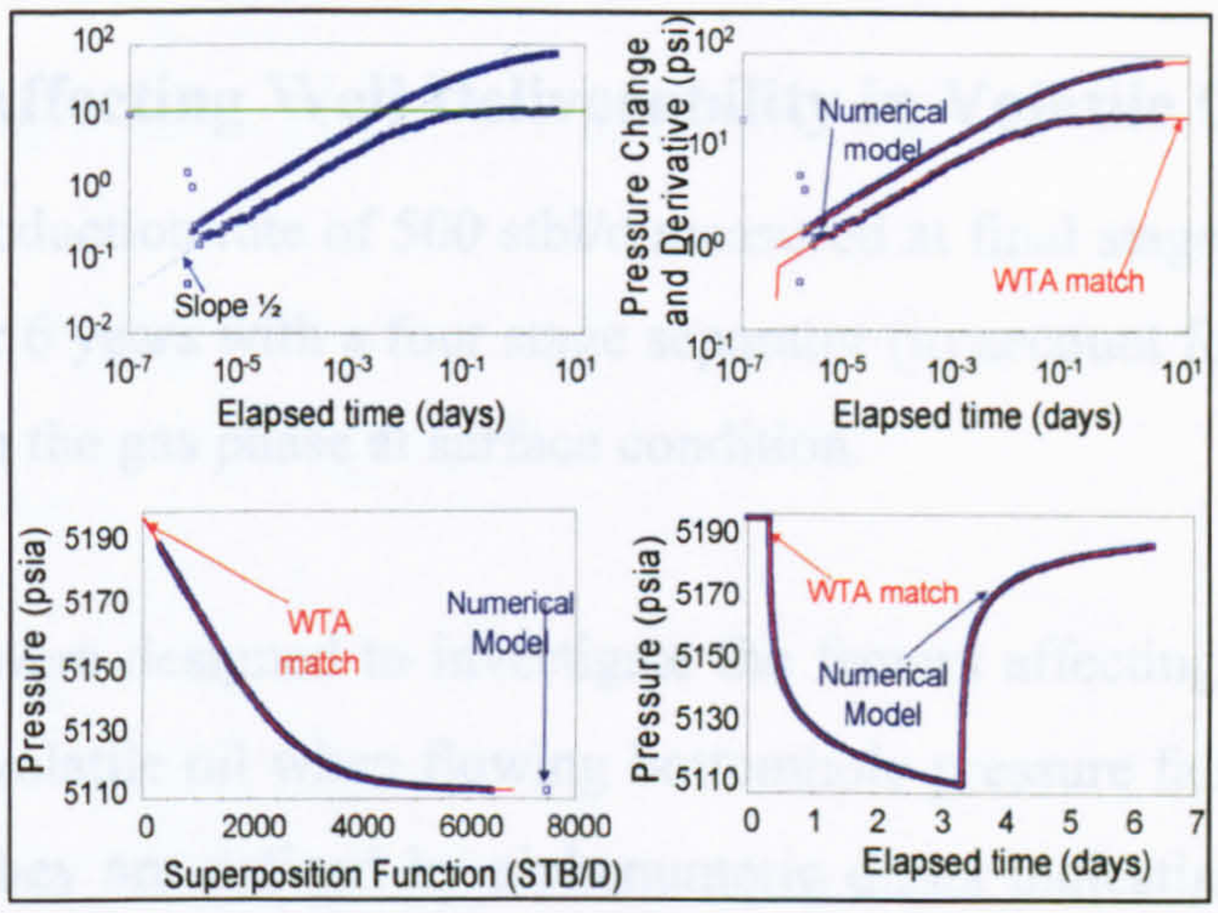

Figure 5-18 Validation of high conductivity fractured well numerical model with analytical solution

5.7 Horizontal Well Modelling

A single horizontal well was modelled to investigate the effect of horizontal well on deliverability of volatile oil reservoirs. The horizontal well was positioned at the centre of the reservoir and parallel to the x direction and perforated over its entire length, with grid size increasing logarithmically away from the well to allow accurate modelling of near-wellbore behaviour. The wellbore diameter of 0.16ft was used throughout the entire length of the well. Varying horizontal well length was modelled while keeping all reservoir dimensions constant. *Figure 5-19* shows match between the simulated response and analytical well test model for a horizontal well of length of 1400ft for a duration of 3-day drawdown and build-up.

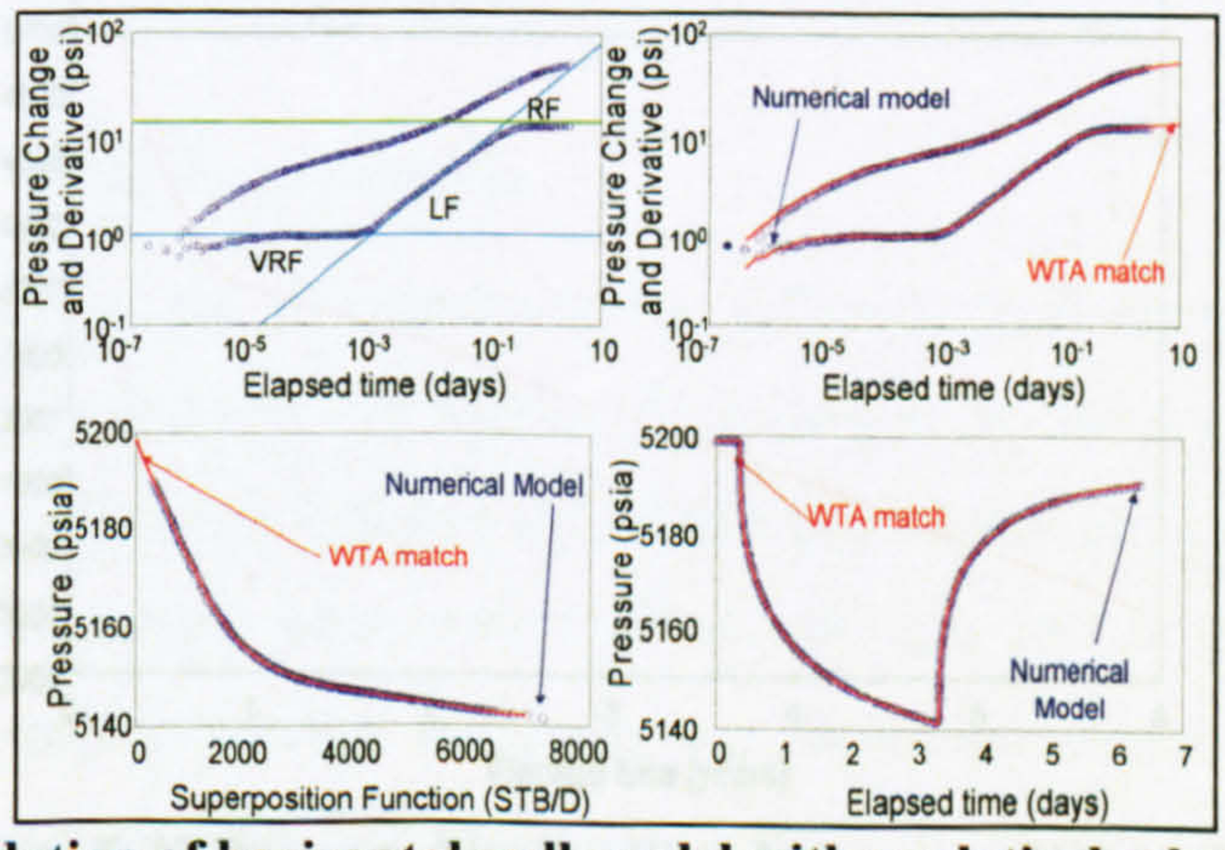

Figure 5-19 Validation of horizontal well model with analytical solution for horizontal well of length 1400ft

5.8 Factors Affecting Well Deliverability in Volatile Oil Reservoirs

A constant oil production rate of 500 stbl/d measured at final stage separator condition was simulated for 6 years with a four stage separator (to account for recovery of liquid hydrocarbon from the gas phase at surface condition.

Simulation runs were designed to investigate the factors affecting the productivity of wells producing volatile oil when flowing bottomhole pressure falls below the bubble point pressure. They are defined by alphanumeric digits indicating the fluid samples (W3, A or B where W3 represent Well-3); the relative permeability models (K_1, K_2, or K_3); vertical well condition ($Frac_i$ where i represent fracture conductivity, and i=0 represent unstimulated vertical well); horizontal well ($Horz_i$ where i represent well length in ft).

5.8.1 Effect of Relative Permeability

Figure 5-20 shows simulated pressure and rate history for unstimulated vertical well model with relative permeability model K_1. Pressure drop increases due to decrease in end point of K_{ro} for constant K_{ro}/K_{rg} ratio (*Figure 5-21*), subsequently causing a decrease in PI through out the simulated production duration (*Figure 5-22*). The deliverability of volatile oil wells above and below bubble point pressure therefore depends on absolute value of K_{romax} and not K_{ro}/K_{rg} ratio.

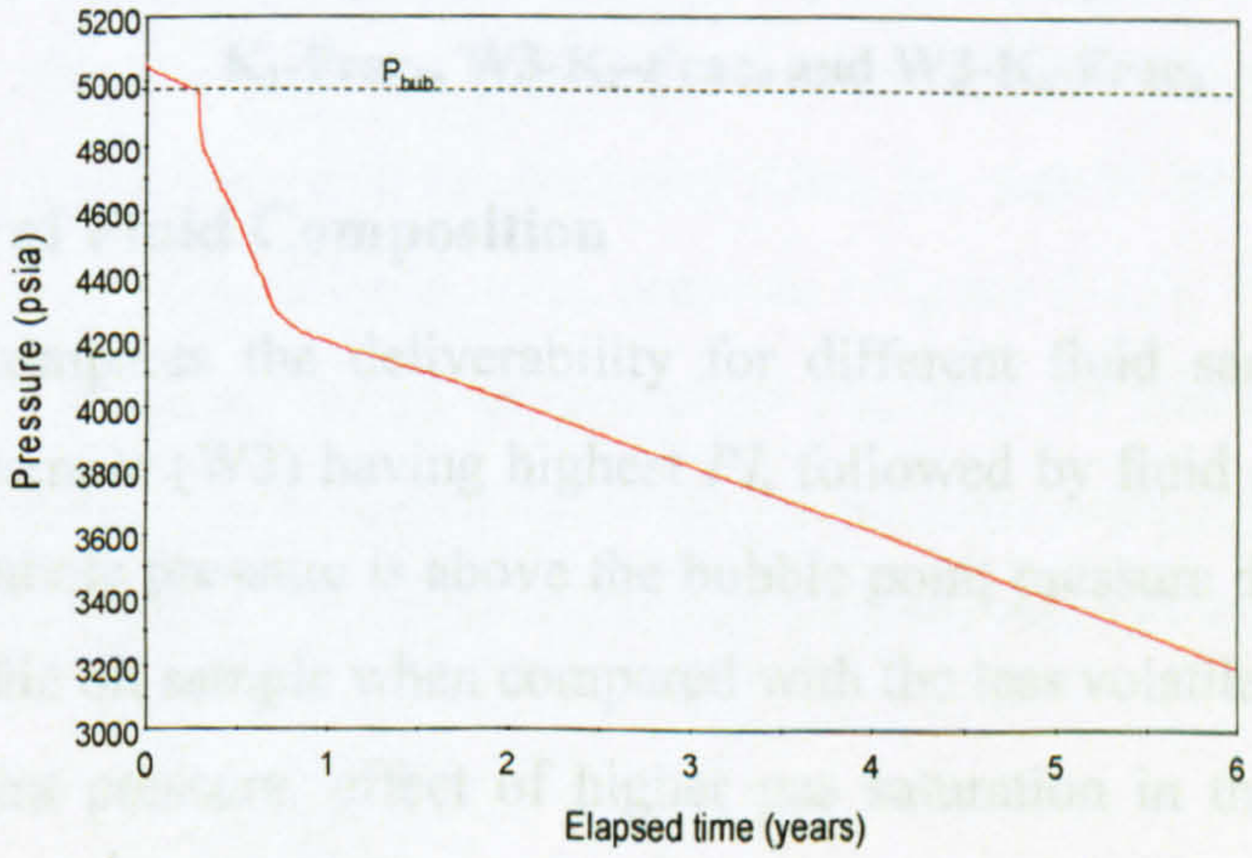

Figure 5-20 Pressure history. Simulation run: W3-K_1-$Frac_0$

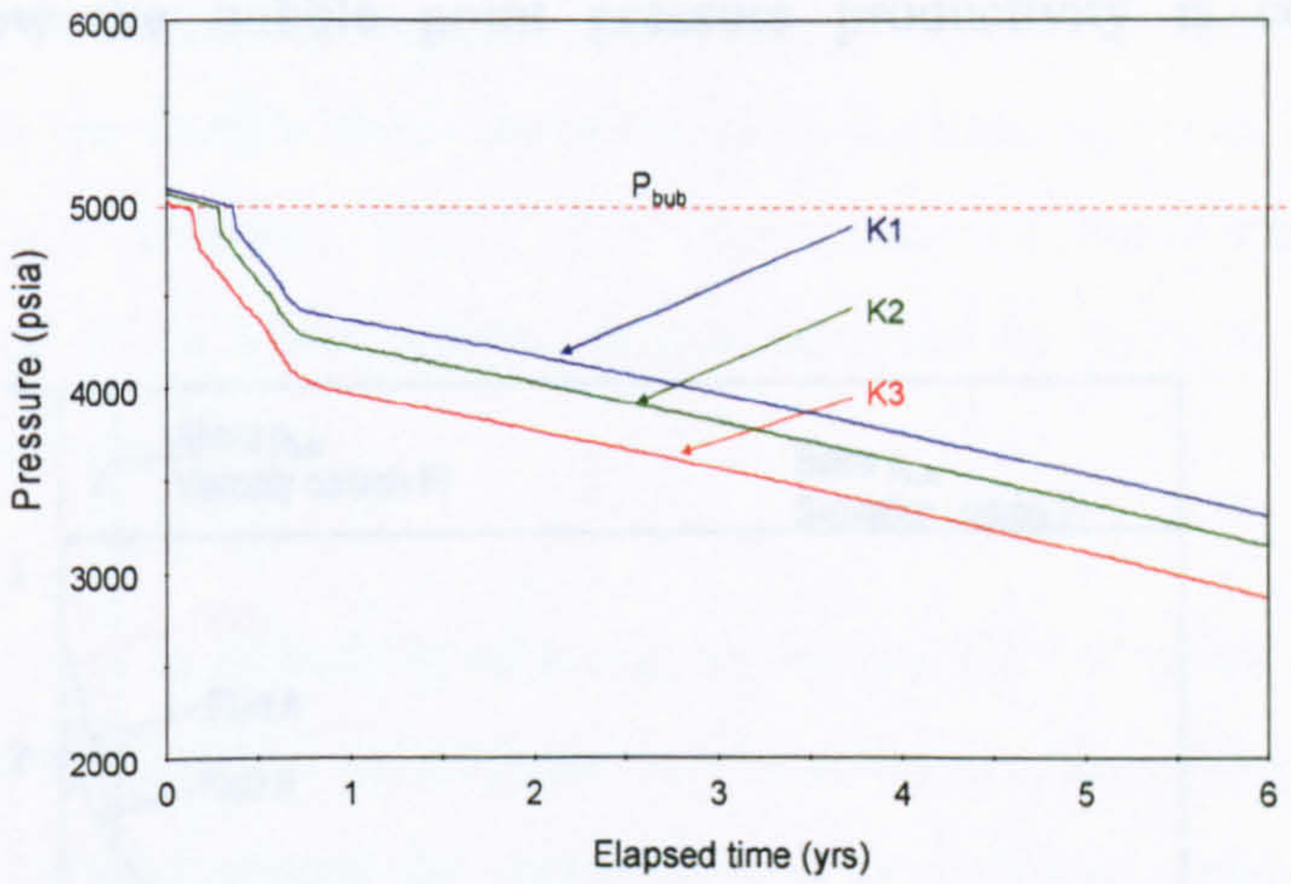

Figure 5-21 Effect of reducing endpoint relative permeability on pressure history. Simulation run: W3-K_1-$Frac_0$, W3-K_2-$Frac_0$ and W3-K_3-$Frac_0$

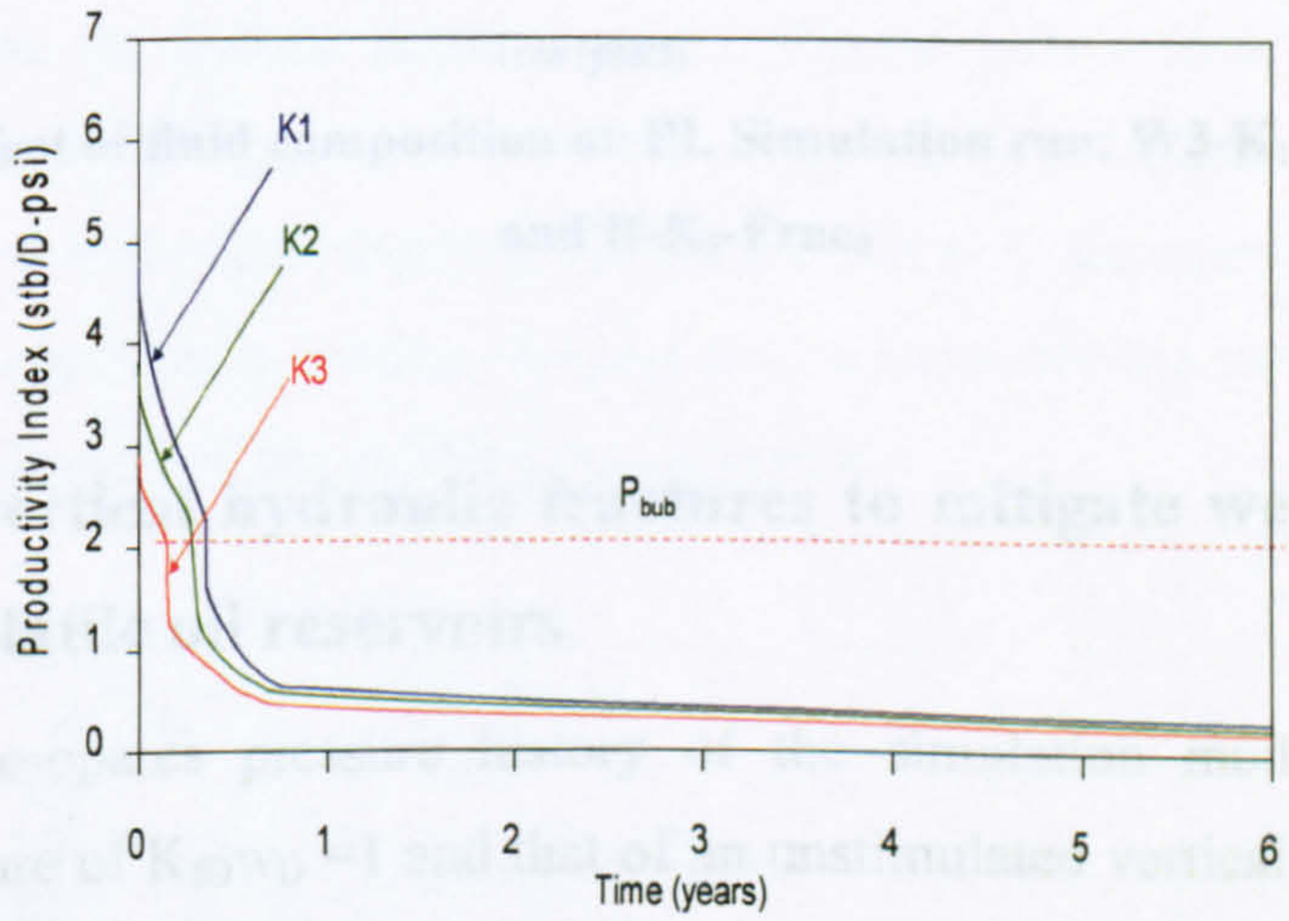

Figure 5-22 Effect of reducing endpoint relative permeability on PI. Simulation run: W3-K_1-$Frac_0$, W3-K_2-$Frac_0$ and W3-K_3-$Frac_0$

5.8.2 Effect of Fluid Composition

Figure 5-23 compares the deliverability for different fluid samples with the most volatile fluid sample (W3) having highest *PI*, followed by fluid A, then fluid B when flowing bottomhole pressure is above the bubble point pressure due to lower viscosity of highly volatile oil sample when compared with the less volatile oil. However, below the bubble point pressure, effect of higher gas saturation in the high volatility oils causes a relatively larger reduction in the productivity than in the less volatile oil.

Above the bubble point pressure, productivity of volatile oil is controlled by viscosity. However, below the bubble point pressure productivity is controlled by fluid saturation.

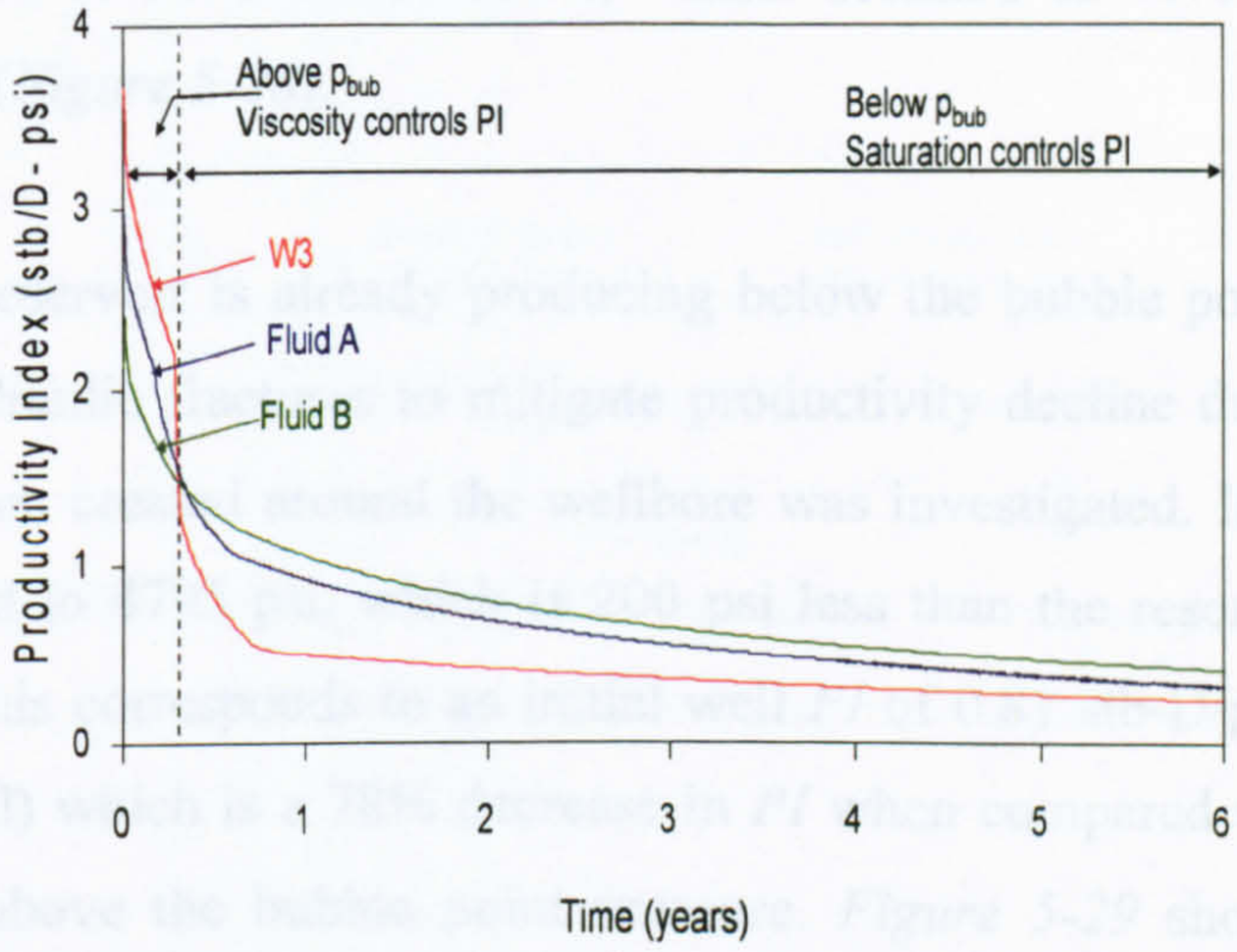

Figure 5-23 Effect of fluid composition on PI. Simulation run: W3-K_1-$Frac_0$, A-K_1-$Frac_0$ and B-K_1-$Frac_0$

5.9 Using vertical hydraulic fractures to mitigate well deliverability decline in volatile oil reservoirs

Figure 5-24 compares pressure history of the simulation model with a vertical hydraulic fracture of $K_{fD}w_D$ =1 and that of an unstimulated vertical well. Reduction in pressure drop around the wellbore due to hydraulic fracture, subsequently causes delay in the time when the flowing bottomhole pressure falls below the bubble point pressure, hence improving well productivity when the well is initially producing above then subsequently below bubble point pressure (*Figure 5-25*). *Figure 5-26* compares *PI* forecast for different values of modelled $K_{fwD}w_D$. *PI* increases with increasing $K_{fwD}w_D$ until value of 50 where increase in $K_{fwD}w_D$ does not lead to significant increase in *PI*, this value defines the optimum $K_{fwD}w_D$ value to improve productivity of the well.

Simulation result shows about 200% initial improvement in *PI* for $K_{fwD}w_D$ =1 (when compared with unstimulated vertical well), with delay in flowing bottomhole pressure dropping below the bubble point pressure, then declines to about 35% at the end of 6 years production (*Figure 5-27*). For optimum $K_{fwD}w_D$, which is 50, initial improvement of *PI* is about 400%, which declined to 40% at the end of 6 years production (*Figure 5-28*).

When the reservoir is already producing below the bubble point pressure, the use of vertical hydraulic fractures to mitigate productivity decline due to the effect of high gas saturation created around the wellbore was investigated. Initial reservoir pressure was reduced to 4795 psi, which is 200 psi less than the reservoir fluid bubble point pressure. This corresponds to an initial well *PI* of 0.81 stb-D/psi (for an unstimulated vertical well) which is a 78% decrease in *PI* when compared with the model initially producing above the bubble point pressure. *Figure 5-29* shows about 570% initial improvement in *PI* for $K_{wD}w_D$ =50 (when compared with unstimulated vertical well) which continuously declines to about 40% at the end of 6 years production.

Hydraulic fractures can be used to mitigate productivity decline even when reservoir is already producing below the bubble point pressure.

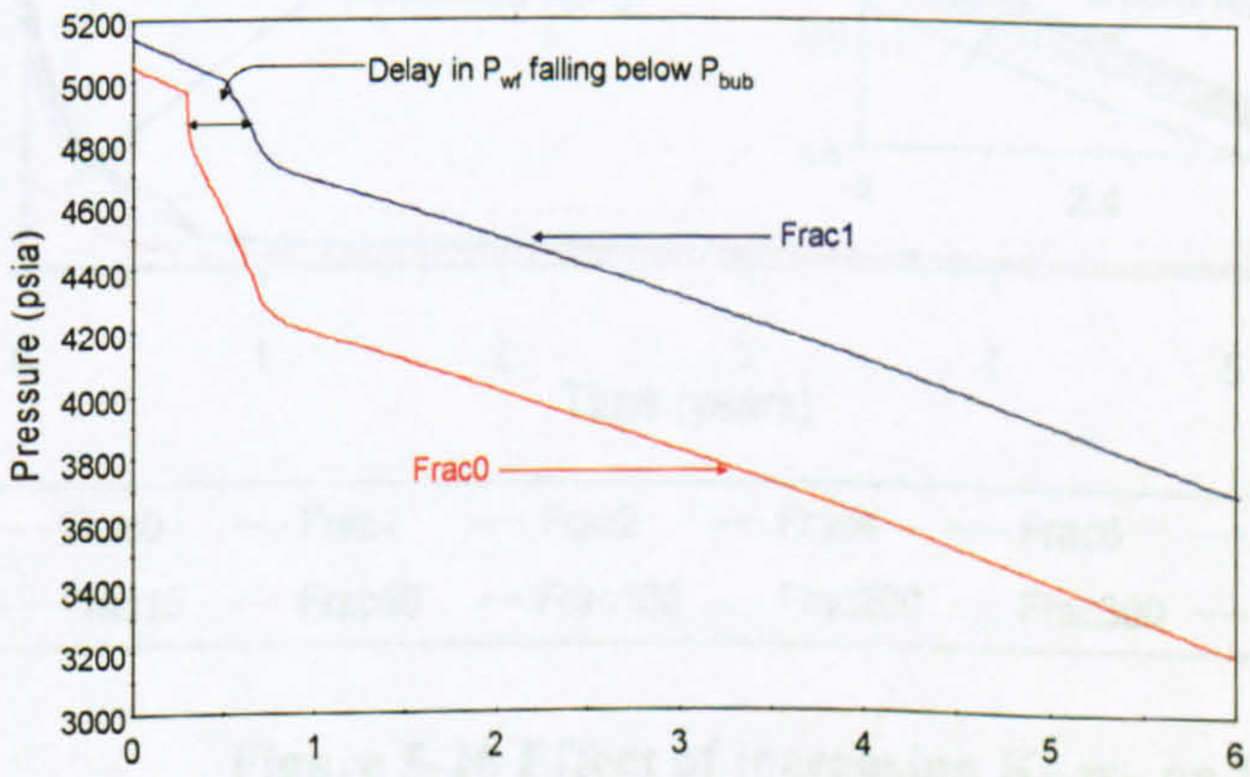

Figure 5-24 Effect of hydraulic fracture on pressure history. Simulation run: W3-K_1-$Frac_0$ and W3-K_1-$Frac_1$

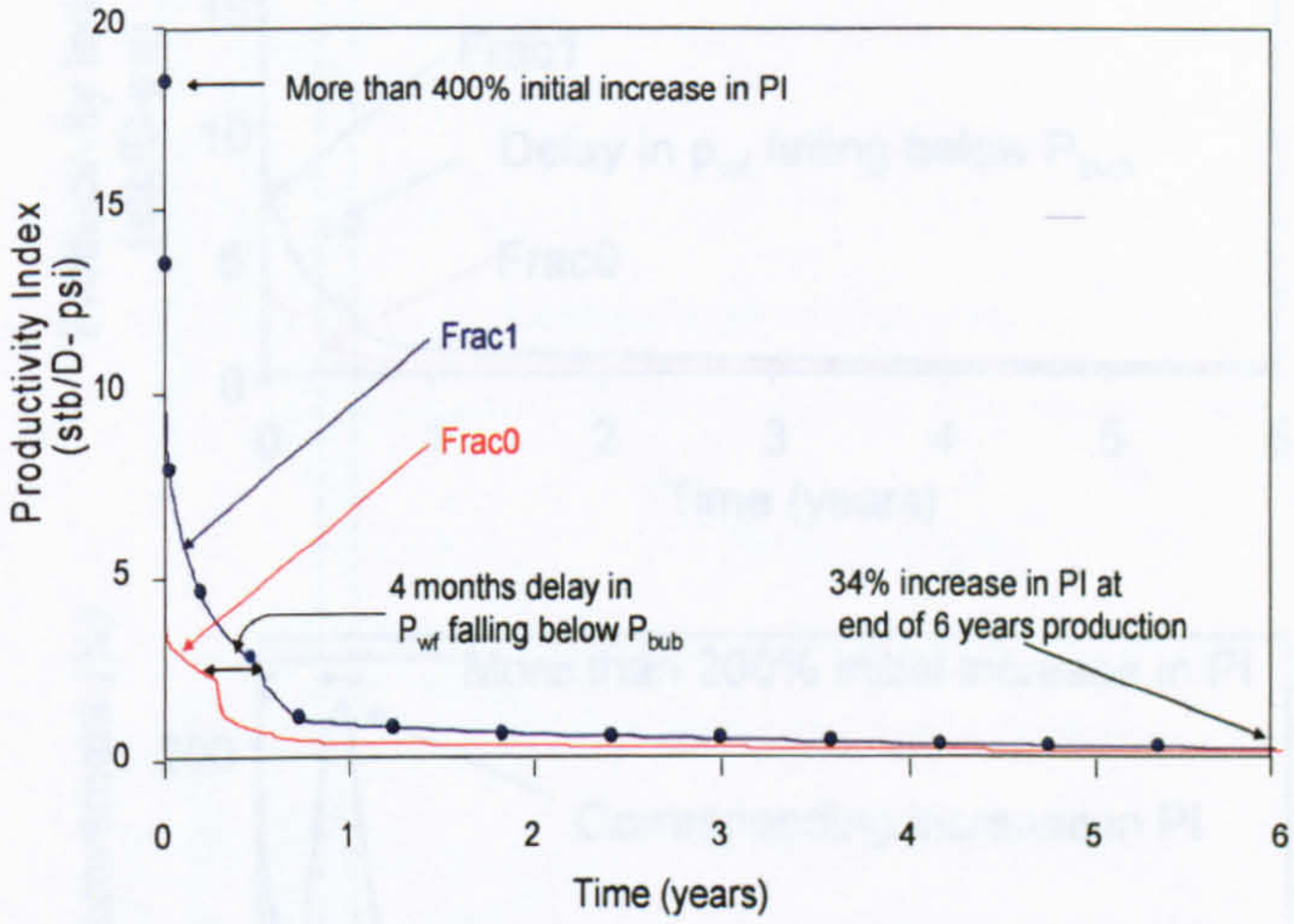

Figure 5-25 Improving productivity of volatile oil with vertical hydraulic fracture.

Simulation run: W3-K_1-Frac$_0$ and W3-K_1-Frac$_1$

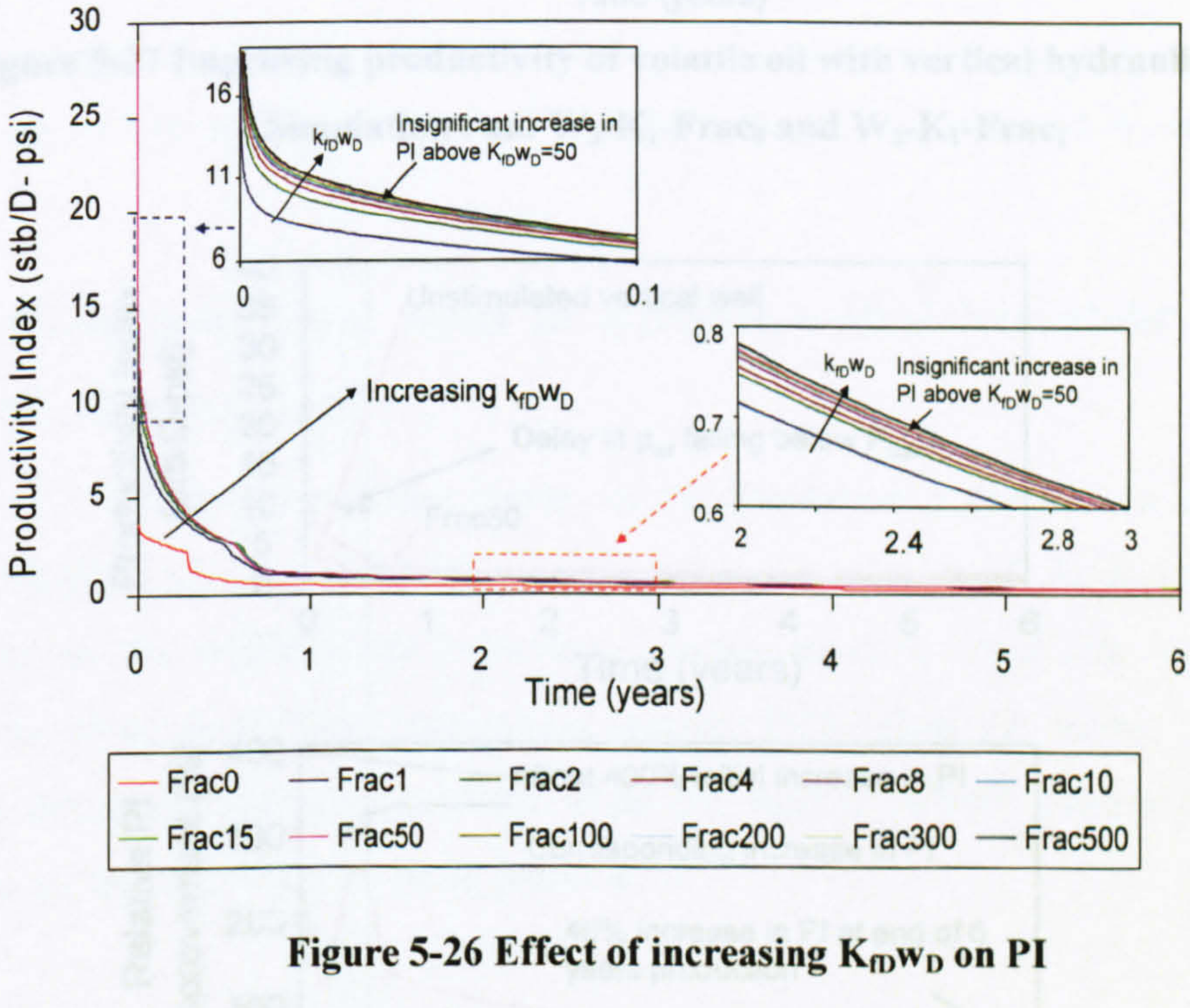

Figure 5-26 Effect of increasing $K_{fD}w_D$ on PI

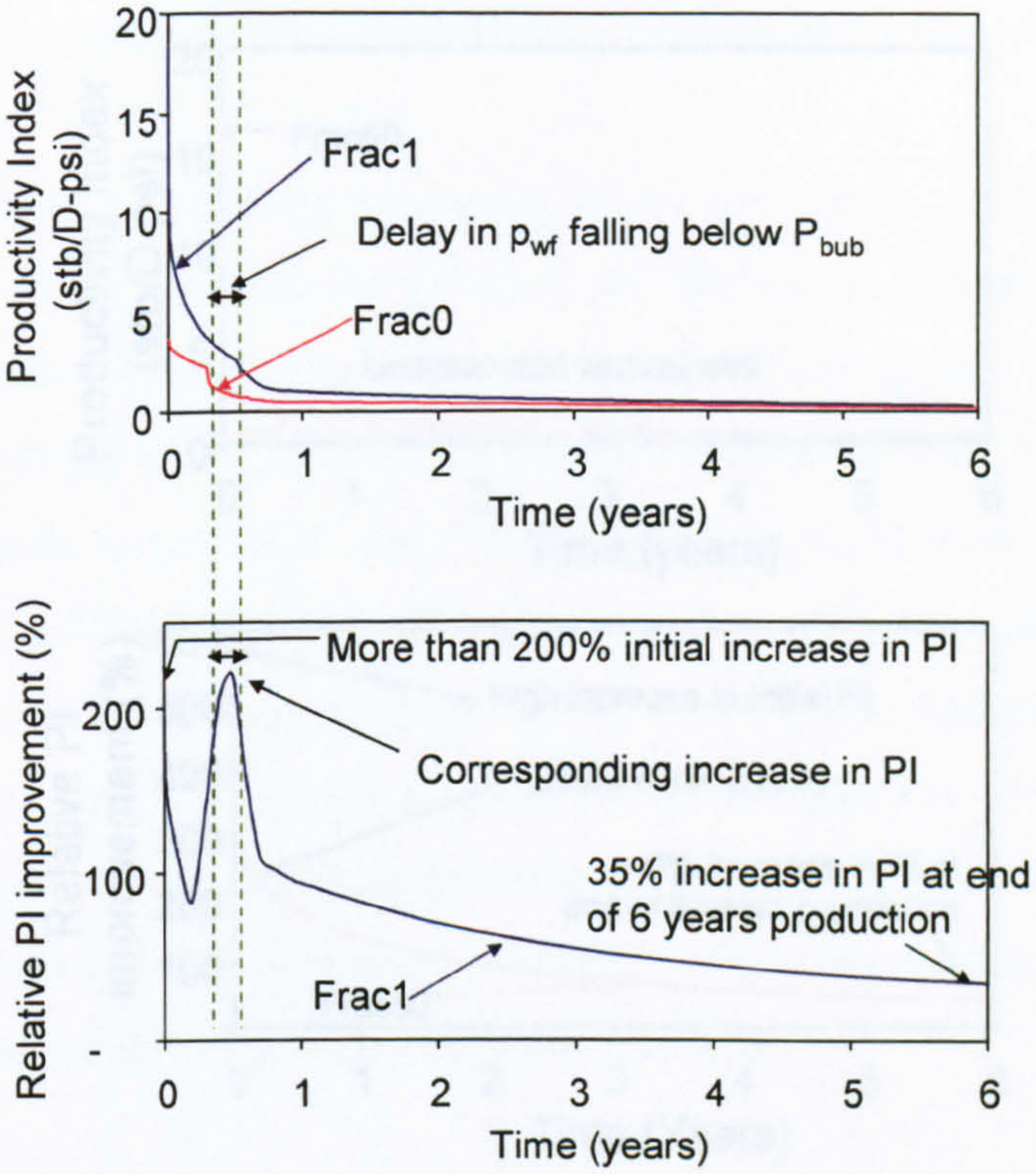

Figure 5-27 Improving productivity of volatile oil with vertical hydraulic fracture. Simulation run: W_3-K_1-$Frac_0$ and W_3-K_1-$Frac_1$

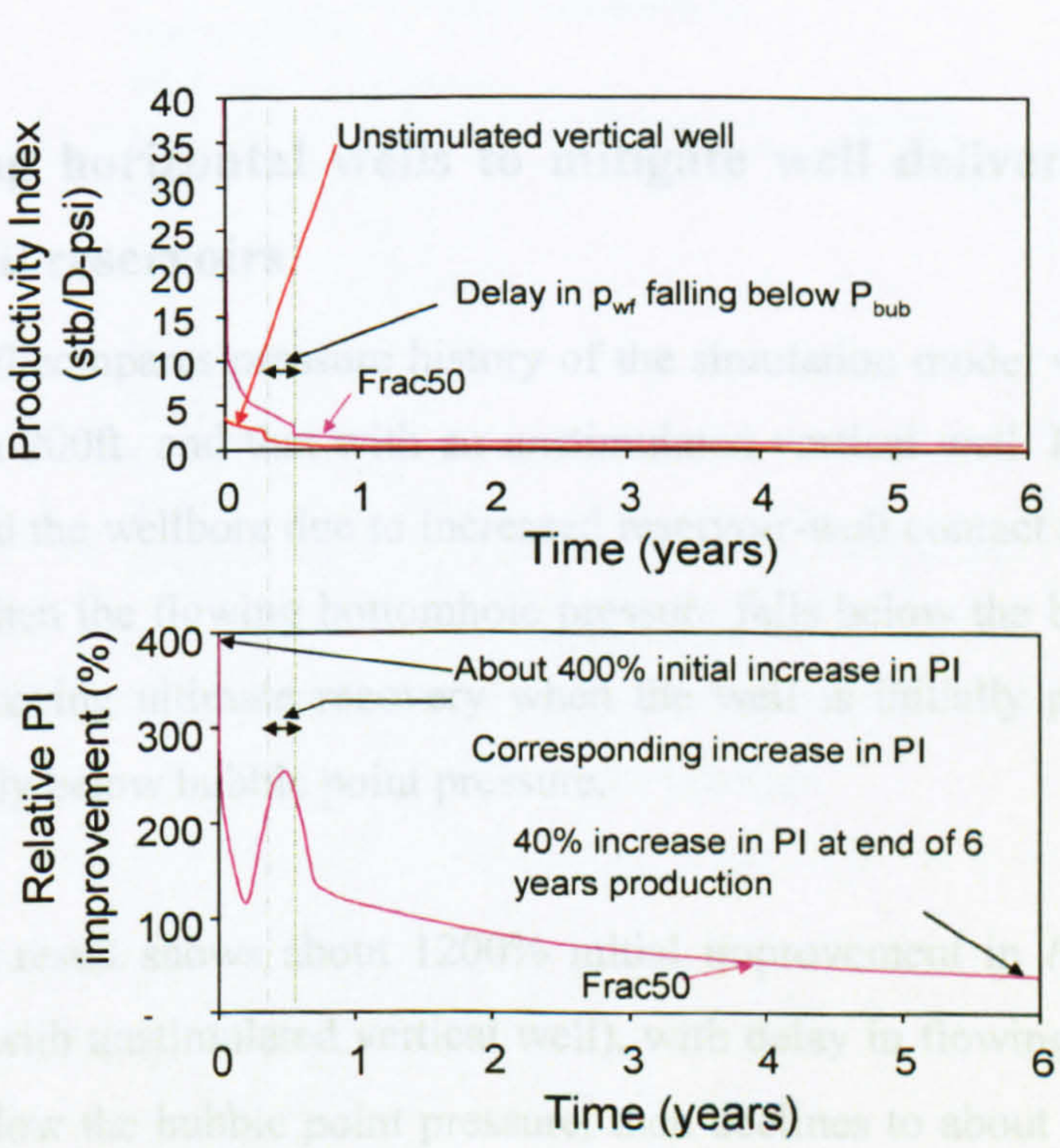

Figure 5-28 Optimum PI improvement using vertical hydraulic fracture. Simulation run: W_3-K_1-$Frac_0$ and W_3-K_1-$Frac_{50}$

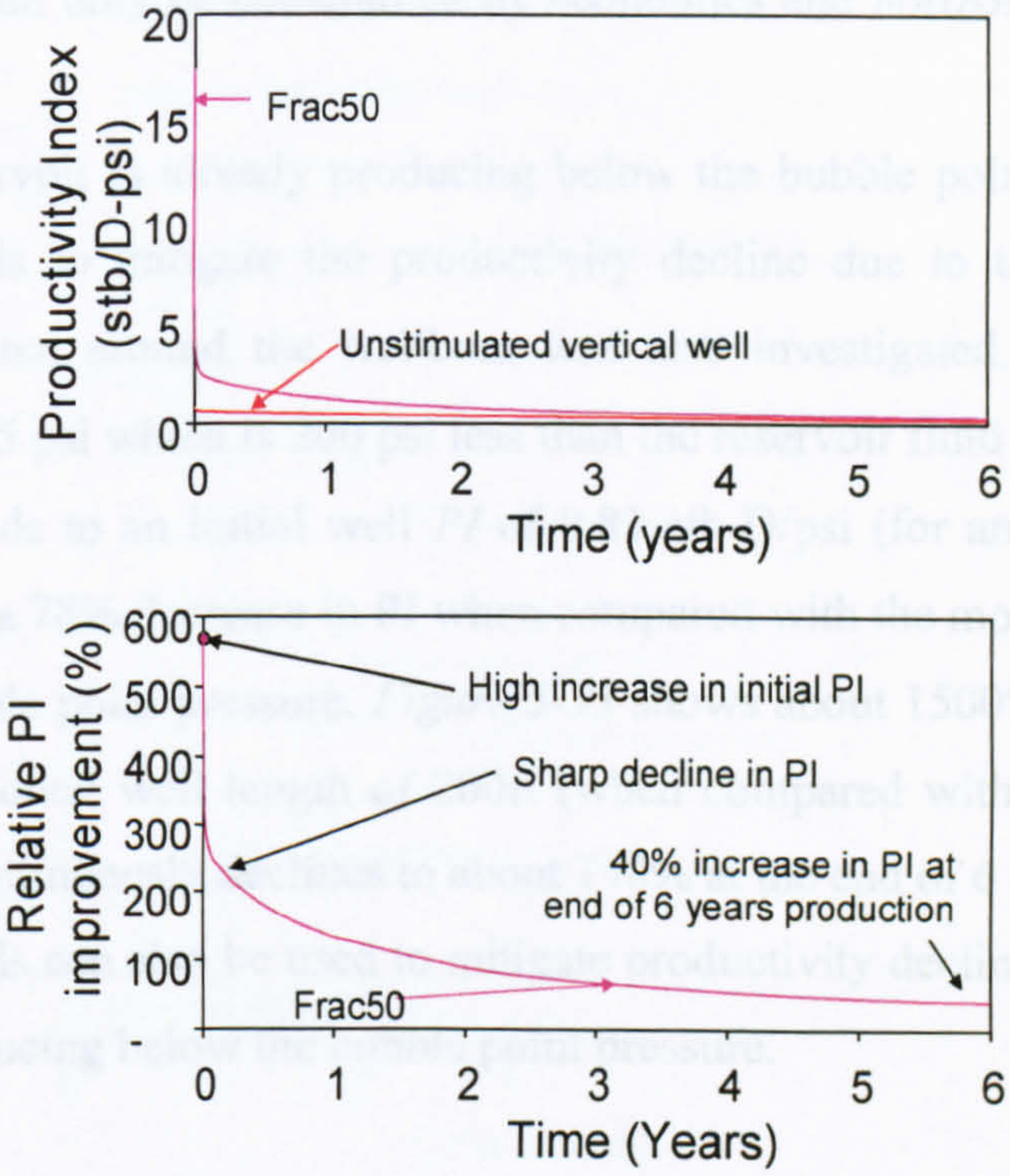

Figure 5-29 Improving productivity with hydraulic fracture for well already producing below bubble point pressure. Simulation run: W_3-K_1-$Frac_0$ and W_3-K_1-$Frac_{50}$

5.10 Using horizontal wells to mitigate well deliverability decline in volatile oil reservoirs

Figure 5-30 compares pressure history of the simulation model with a horizontal well with length 200ft and that with an unstimulated vertical well. Reduction in pressure drop around the wellbore due to increased reservoir-well contact area causes a delay in the time when the flowing bottomhole pressure falls below the bubble point pressure, hence improving ultimate recovery when the well is initially producing above then subsequently below bubble point pressure.

Simulation result shows about 1200% initial improvement in *PI* for L=200ft (when compared with unstimulated vertical well), with delay in flowing bottomhole pressure droping below the bubble point pressure, then declines to about 128% at the end of 6 years production (*Figure 5-31*).

Figure 5-32 compares *PI* improvement forecast for different values of modelled horizontal well length: 200ft, 3281ft (1km) and 6561ft (2km). The *PI* increases with

increasing horizontal well length. The optimum horizontal well length for productivity enhancement can only be constrained by economics and horizontal well tubing intake limits.

When the reservoir is already producing below the bubble point pressure, the use of horizontal wells to mitigate the productivity decline due to the effect of high gas saturation created around the wellbore was also investigated. Initial reservoir was reduced to 4795 psi which is 200 psi less than the reservoir fluid bubble point pressure. This corresponds to an initial well *PI* of 0.81 stb-D/psi (for an unstimulated vertical well) which is a 78% decrease in PI when compared with the model initially producing above the bubble point pressure. *Figure 5-33* shows about 1500% initial improvement in *PI* for horizontal well length of 200ft (when compared with unstimulated vertical well) which continuously declines to about 148% at the end of 6 years production. Horizontal wells can also be used to mitigate productivity decline even when reservoir is already producing below the bubble point pressure.

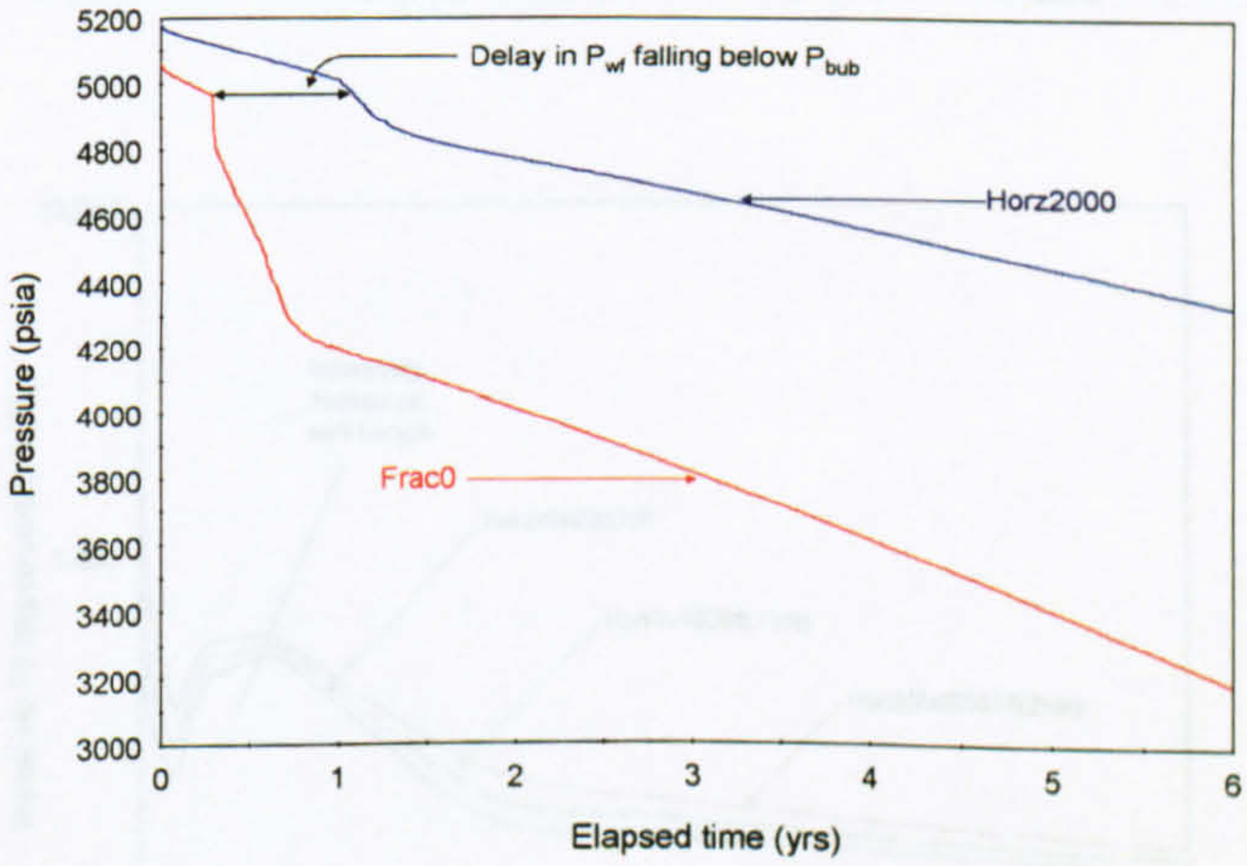

Figure 5-30 Effect of horizontal well on pressure history. Simulation run: W_3-K_1-$Frac_0$ and W_3-K_1-$Horz_{2000}$

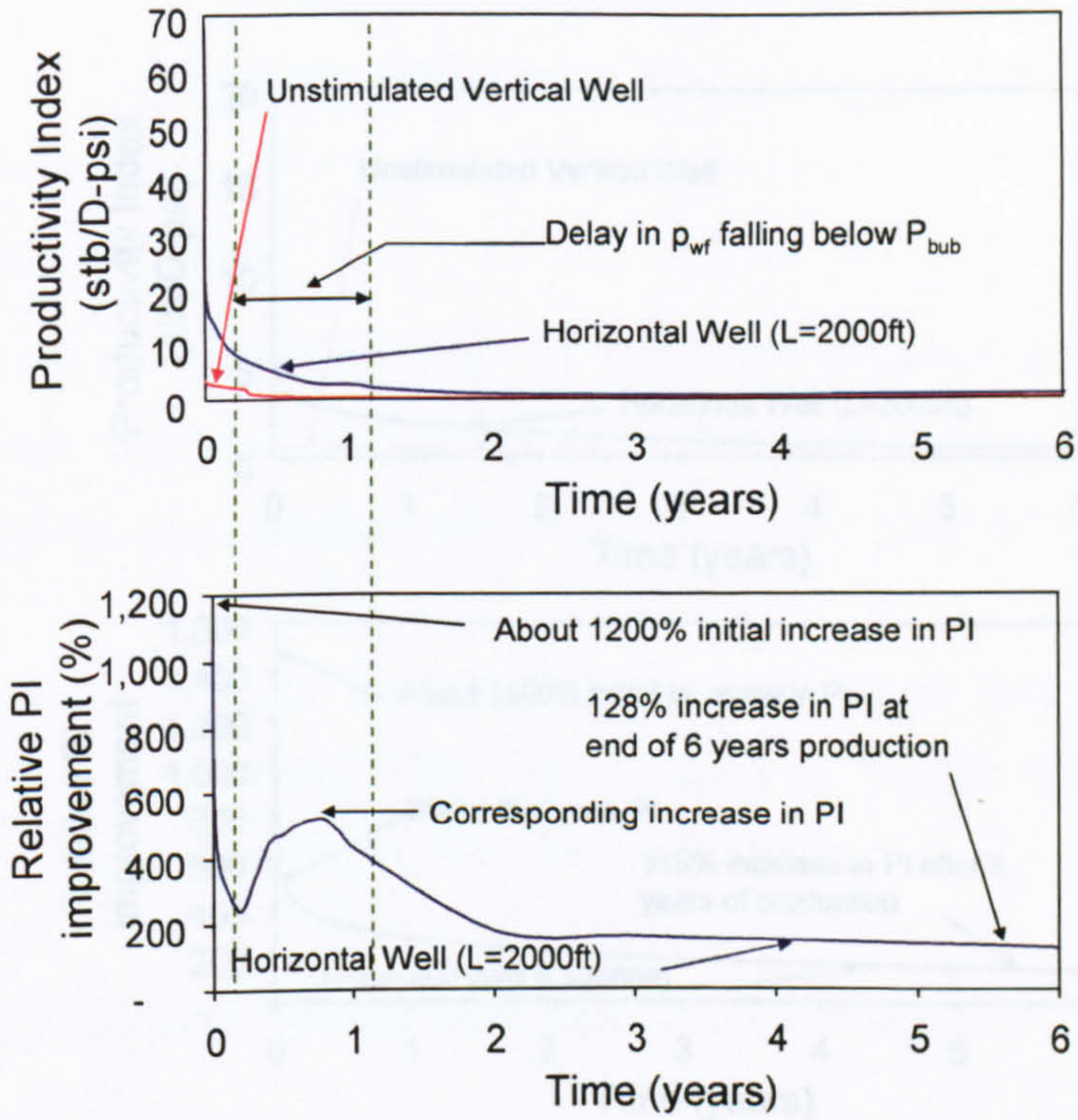

Figure 5-31 Improving productivity of volatile oil with a horizontal well. Simulation run: W_3-K_1-$Frac_0$ and W_3-K_1-$Horz_{2000}$

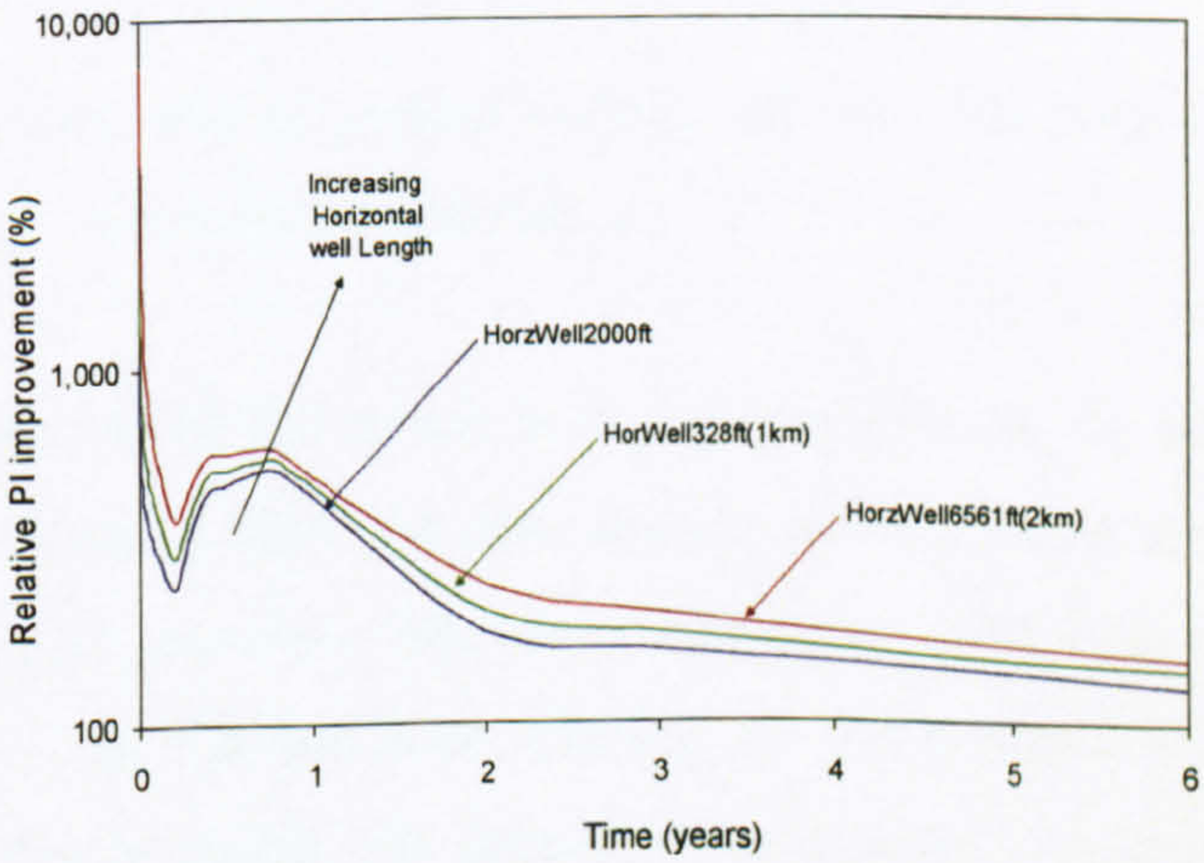

Figure 5-32 Effect of increasing horizontal well length on PI

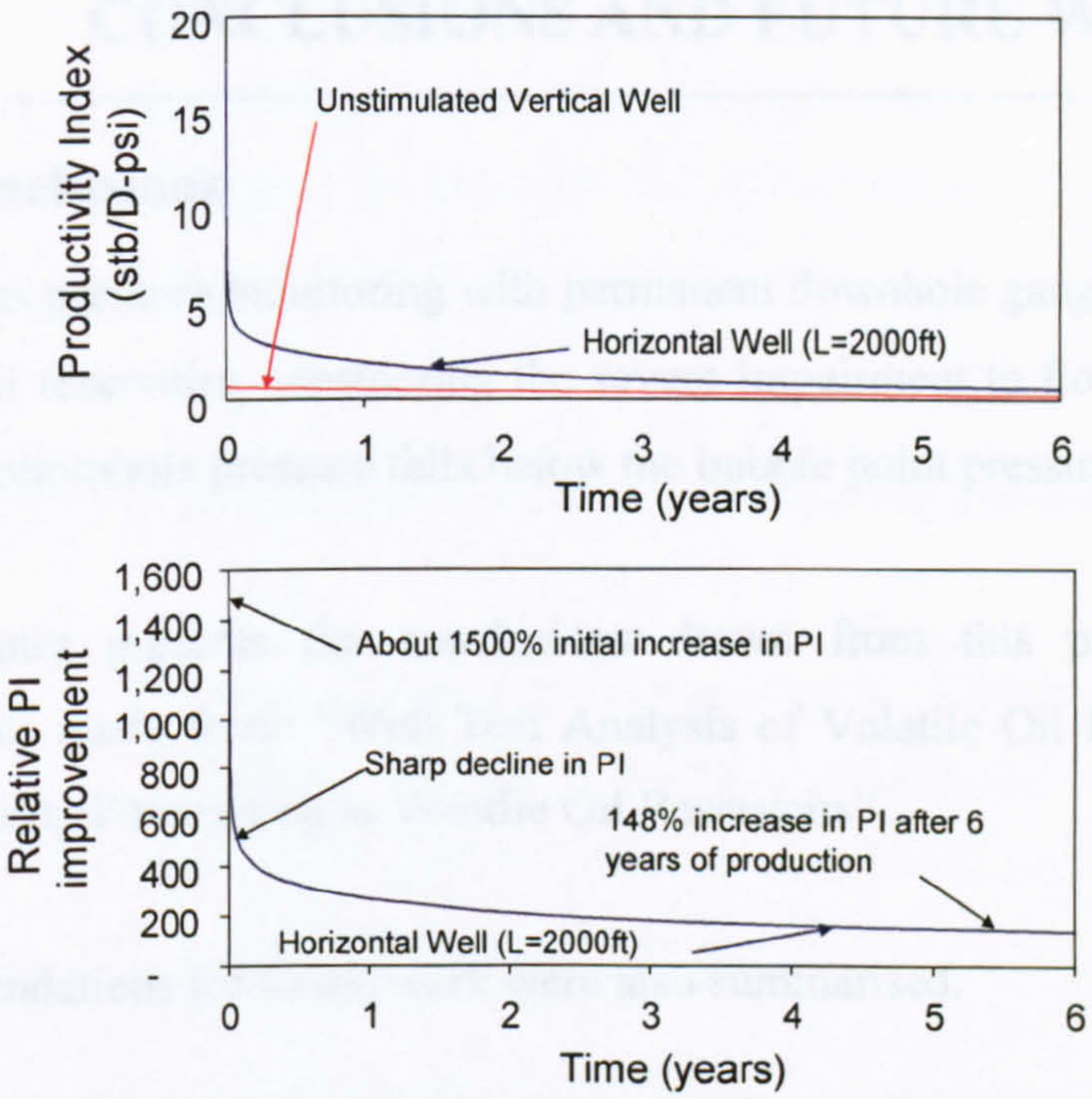

Figure 5-33 Improving productivity with horizontal well for well already producing below bubble point pressure. Simulation run: W_3-K_1-$Frac_0$ and W_3-K_1-$Horz_{2000}$

CHAPTER 6

CONCLUSIONS AND FUTURE WORK

6.1 Conclusions

Continuous pressure monitoring with permanent downhole gauges is very important in volatile oil reservoirs, considering the severe impairment to flow which may occur if flowing bottomhole pressure falls below the bubble point pressure.

This chapter presents the conclusions drawn from this project. It consists of conclusions made from: "Well Test Analysis of Volatile Oil Reservoirs" and "Well Deliverability Forecasting in Volatile Oil Reservoirs".

Recommendations for future work were also summarised.

6.1.1 Well Test Analysis of Volatile Oil Reservoirs

The objective of "Well Test Analysis of Volatile Oil Reservoirs" was to identify typical well test behaviours in volatile oil reservoirs below the bubble point pressure.

Currently, the only way to predict volatile oil well test behaviour for a specific well and reservoir is via numerical simulation.

It was found that, when the bottomhole pressure falls below the bubble point pressure during a drawdown, a high gas saturation zone is created around the wellbore with two-phase (oil and gas) flow, whereas single phase (oil) with the initial gas saturation remains away from the wellbore. During the subsequent build-up, the gas created around the wellbore during the preceding drawdown condenses into the oil and the saturation in the near-wellbore region returns to the initial gas saturation.

The impairment to flow due to the high gas saturation zone around the wellbore when the bottomhole pressure is below the bubble point pressure can be seen as a mobility contrast in well test analysis. The log-log pressure-derivative behaviours below the bubble point therefore correspond to a two-zone radial composite model, with decreasing mobility during drawdowns and increasing mobilities during build-ups. The

log-log pressure derivative plot of the build-up reflects the oil mobility distribution in the reservoir at the end of the preceding drawdown.

High volatility oils have higher mobilities than less volatile oils above the bubble point pressure. However, higher gas saturation below bubble point pressure causes relatively larger mobility reductions for the more volatile oils.

6.1.2 Well Deliverability Forecasting in Volatile Oil Reservoirs

The objective of "Well Deliverability Forecasting in Volatile Oil Reservoirs" was to identify factors affecting well deliverability in volatile oil reservoirs producing at flowing bottomhole pressure below bubble point pressure, and methods of mitigating well productivity decline due "gas blockage".

End point relative permeability of the oil phase and fluid composition are the most important factors affecting well productivity of volatile oil reservoirs producing below bubble point pressure.

Highly volatile oil reservoirs have higher productivity indices than low volatility oil reservoirs when producing above the fluid bubble point pressure. However, the effect of high gas saturation below bubble point pressure causes a relatively larger reduction in the productivity index of the highly volatile oil reservoirs than the less volatile oil reservoirs.

Vertical hydraulic fractures and horizontal wells can be used to improve well productivity in volatile oil reservoirs, even when reservoir is already producing below the bubble point pressure.

Vertical hydraulic fractures and horizontal wells should be implemented early in the wells life to delay the time when the flowing bottomhole pressure drops below the bubble point pressure, which consequently leads to improved recovery.

The optimum choice between hydraulically fractured vertical wells and horizontal well can only be made from economic analysis.

6.2 Recommendation for Future Work

Determining the principal integral pseudo-pressure transformation that will linearise the diffusivity equation for volatile oil reservoir producing below bubble point pressure.

Carrying out laboratory experiments to estimate the correct values of parameters which defines the capillary number (N_c) and non-Darcy (β) effect in volatile oil reservoirs.

Designing multi-rate well tests below the bubble point pressure in volatile oil reservoirs in order to study the contribution of non-Darcy (β) and N_c effects to the total skin during two-phase flow.

Including wellbore dynamics into productivity forecasts. Since optimum deliverability of a well is constrained by the capacity of the well tubing to deliver produced reservoir fluid to the surface.

Carrying out analysis on more well test data from volatile oil reservoirs.

Investigate the behaviour of the *GOR* and whether it can be used to history match the relative permeability end points.

Attempt to generalise the findings regarding well performance with a view to providing a simple method to predict productivity as a function of well, reservoir and fluid type.

Investigate whether the findings for volatile oils apply also to heavier oils in this case.

REFERENCES

Agarwal, R.G., Al-Hussainy, R., and Ramey, H.J.J.: "An investigation of Wellbore Storage and Skin Effect in Unsteady Liquid Flow. I: Analytical Treatment", Trans. AIME 249, 1970, pp. 279-290.

Ahmed, T.: "Hydrocarbon Phase Behavior", Contributions in Petroleum Geology & Engineering, Gulf Publishing Company, 1989.

Al-Hussainy, R., Ramey Jr., H. J., and Crawford, P. B.: "The Flow of Real Gas Through Porous Media," *Journal of Petroleum Technology* (May 1966), pp.637-642.

Ali, A.M., Falcone, G., Hewitt, G.F., and Gringarten, A.C.: "Experimental Investigation of Wellbore Phase Redistribution Effects on Pressure-Transient Data", paper SPE 96587 presented at the SPE Annual Technical Conference and Exhibition held in Dallas, Texas, Oct. 9 – 12, 2005.

Al-Kahlifa, A.J.A., Aziz, K., and Horne, R.N.: "A New Approach to Multiphase Well Test Analysis", paper SPE 16743 presented at the 62nd Annual Technical Conference and Exhibition held in Dallas, Texas, Sept. 27-30, 1987.

Archer, J.S. and Wall, C.G.: "Petroleum Engineering Principles and Practice", Kluwer Academic Publishers Group, Dordrecht / Boston, 1999.

Ayan, C. and Lee, W.J.: "Effects of Multiphase Flow on interpretation of Buildup Tests", *Society of Petroleum Engineers Formation Evaluation*, (June 1988), pp. 459-466.

Baig, T., Droegemueller, U., and Gringarten, A.C.: "Productivity Assessment of Fractured and Non-Fractured Wells in a Lean/Intermediate Low Permeability Gas Condensate Reservoir", paper SPE 93136 presented at the 14th Europec Biennial Conference held in Madrid, Spain, June 13-16, 2005.

Bardon, C. and Longeron, D.G.: "Influence of Very Low Interfacial Tensions on Relative Permeability", *Society of Petroleum Engineers Journal* (Oct. 1980), pp. 391-401.

Bendakhlia, H. and Aziz, K.: "Inflow Performance Relationships for Solution-Gas Drive Horizontal Wells", paper SPE 19823 presented at the 64th Annual Technical Conference and Exhibition of the Society of Petroleum Engineers held in San Antonio, Texas, Oct. 8-11, 1989.

Blasingame, T.A., Johnston, J.L., and Lee, W.J.: "Type-Curve Analysis Using the Pressure Integral Method", SPE 18799, paper presented at the SPE California Regional Meeting held in Bakersfield, California, Apr. 5-7, 1989, pp. 525-543.

Blom, S.M.P. and Hagoort, J.: "How to Include Capillary Number in Gas Condensate Relative Permeability Functions", paper SPE 49628 presented at the SPE Annual Technical Conference and Exhibition held in New Orleans, Louisiana, Sept. 27-30, 1998.

Blom, S.M.P., Hagoort, J., and Soetekouw, D.P.N.: "Relative Permeability at Near-Critical Conditions", *Society of Petroleum Engineers Journal* (June 2000), pp. 172-181.

Bourdarot, G.: "Well Testing: Interpretation Methods", Technip and Institut francais du petrole, 1998.

Bourdet, D. and Gringarten, A.C.: "Determination of Fissure Volume and Block Size in Fractured Reservoirs by Type-curve Analysis". paper SPE 9293 presented at the 55th Annual Fall Technical Conference of SPE-AIME held in Dallas, Texas, Sept. 21-24, 1980.

Bourdet, D., Whittle, T.M., Douglas, A.A., and Pirard, Y.M.: "A New Set of Type Curves Simplifies Well Test Analysis", Gulf publishing Co., Houston, World Oil, May, 1983, Vol. 5, pp. 95-106.

Bourgeois, M.J. and Horne, R.N: "Well Test Model Recognition with Laplace Space", *Society of Petroleum Engineers Formation Evaluation* (March 1993), pp. 17-25.

Bozorgzadeh, M. and Gringarten, A.C.: "Application of Build-Up Transient Pressure Analysis to Well Deliverability Forecasting in Gas Condensate Reservoirs Using Single-Phase and Two-Phase Pseudo-Pressures", paper SPE 94018 presented at the 14th Europec Biennial Conference held in Madrid, Spain, June 13-16, 2005.

Celier, C.M.: "Zuidwal: A Gas Field Development with horizontal Wells", SPE 19826 paper presented at the 64th Annual Technical Conference and Exhibition of the Society of Petroleum Engineers held in San Antonio, Texas, Oct. 8-11, 1989.

Cinco-Ley, H. and Samaniego, F.V.: "Transient Pressure Analysis for Fractured Wells", *Journal of Petroleum Technology* (September 1981), pp. 1749-1766.

Cinco-Ley, H. and Samaniego, V.F.: "Transient pressure analysis: finite conductivity fracture case versus damaged fracture case", paper SPE 10179 presented at the 56th Annual fall Meeting of SPE-AIME held in San Antonio, Texas, Oct. 5-7, 1981.

Cline, V.J. and Basham, M.: "Improving Project Performance in a Heavy Oil Horizontal Well Project in the San Joaquin Valley, California", SPE 78981, paper presented at SPE International Thermal Operations and Heavy Oil Symposium and International Horizontal Well Technology Conference held at Calgary, Alberta, Canada, Nov. 4, 2002.

Clonts, M.D. and Ramey Jr, H.J.: "Pressure Transient Analysis for Wells with Horizontal Drainholes", paper SPE 15116 presented at the 56th SPE California Regional Meeting held in Oakland California, April. 2-4, 1986.

Coats, K.H. and Smart, G.T.: "Application of Regression-Based EOS PVT Program to Laboratory Data", Society of *Petroleum Engineers Reservoir Engineering* (May 1986), pp. 277-299.

Cobenas, R.H. and Crotti, M.A.: "Volatile Oil. Determination of Reservoir Fluid Composition from a Non-Representative Fluid Sample", paper SPE 54005 presented at the 1999 SPE Latin American and Caribbean Petroleum Engineering Conference held at Caracas, Venezuela, Apr. 21-23, 1999.

Cook, A.B., Spencer, G.B., and Bobrowski, F.P.: "Special Considerations in Predicting Reservoir Performance of Highly Volatile Type Oil Reservoirs", Trans. AIME 192, 1951, pp. 37-46.

Cooper, R.E. and Troncoso, J.C.: "An Overview of Horizontal Well Completion Technology", paper SPE 17582, presented at the SPE International meeting of Petroleum Engineers held in Tianjin China, Nov. 1-4, 1988.

Davlau, F., Mouronval, G., Bourdarot, G., and Curutchet, P.: "Pressure analysis for horizontal wells", *Society of Petroleum Engineers formation Evaluation* (December 1988), pp.716-724.

Duong, A.H.: "A New set of Type Curves for Well-test Interpretation with the Pressure/Pressure-Derivative Ratio", *Society of Petroleum Engineers Formation Evaluation* (June 1989), pp. 264-272.

Earlougher Jr, R.C. and Kersch, K.M.: "Analysis of Short-Time Transient Test Data by Type-Curve Matching", *Journal of Petroleum Technology* (July 1974), pp. 793-800.

Evinger, H.H. and Muskat, M.: "Calculation of theoretical productivity Factor", Trans. AIME 146, 1942, pp. 126-139.

Fetkovich, M.J.: "The Isochronal testing of oil wells", paper SPE 4529 presented at the 48th Annual fall Meeting of SPE-AIME held at Las Vegas, Nev., Sept. 30-Oct. 3, 1973.

Fulcher, R.A.Jr., Ertekin, T., and Stahl, C.D.: "Effect of Capillary Number and Its Constituents on Two-Phase Relative Permeability Curves", *Journal of Petroleum Technology* (Feb. 1985), pp. 249-260.

Geertsma, J.: "Estimating the Coefficient of Inertial Resistance in Fluid Flow Through Porous Media", *Journal of Petroleum Technology* (Oct. 1974), pp. 445-450.

Golan, M. and Whitson, C.: "Well Performance", Kluwer Academic Publishers, 1994.

Gondouin, M., Iffly, R. and Husson, J.: "An Attempt to Predict the Time Dependence of Well deliverability in Gas-Condensate Fields," Society of Petroleum Engineers Journal (June 1967), pp. 112-124.

Goode, P.A. and Thambynayagam, R.K.M.: "Pressure drawdown and buildup analysis of horizontal wells in anisotropic media", *Society of Petroleum Engineers Formation Evaluation* (December 1987), pp. 683-687.

Gringarten A. C., Daungkaew S., Hashemi S. and Bozorgzadeh, M: "Well Test Analysis in Gas Condensate Reservoirs: Theory and Practice," paper SPE 100993, presented at the 2006 SPE Russian Oil and Gas Technical Conference and Exhibition, Moscow, Russia, 3–6 October 2006.

Gringarten, A.C. and Ramey, H.J.Jr.: "The Use of Source and Green's Functions in Solving Unsteady-Flow Problems in Reservoirs", *Society of Petroleum Engineers Journal* (October 1973), pp. 285-296.

Gringarten, A.C., Bourdet, D.P., Landel, P.A., and Kniazeff, V.J.: "A Comparison between Different Skin and Wellbore Storage Type-Curves for Early-Time Transient Analysis", paper SPE 8025 paper presented at the 54th Annual Fall Technical Conference of SPE-AIME held in Las Vegas, Nevada, Sept. 23-26 1979.

Gringarten, A.C., Ramey Jr, H.J., and Raghavan, R.: "Unsteady-state pressure distributions created by a well with a single infinite-conductivity vertical fracture", *Society of Petroleum Engineers Journal* (August, 1974), pp. 347-360.

Gringarten, A.C., Von Schroeter, T., Rolfsvaag, T., and Bruner, J.: "Use of Downhole Permanent Pressure Gauge Data to Diagnose Production Problems in a North Sea Horizontal Well", paper SPE 84470 presented at the SPE Annual Technical Conference and Exhibition, held in Denver, Colorado, Oct. 5-8, 2003.

Gringarten, A.C.: "Analysis of an Extended Well Test to Assess Connectivity Between Adjacent Compartments in a North Sea reservoir", paper SPE 93988 presented at the SPE Europec/EAGE Annual Conference held in Madrid, Spain, June 13-16, 2005.

Gringarten, A.C.: "Computer-Aided Well Test Analysis", paper SPE 14099 presented at the SPE International Meeting of Petroleum Engineering, held in Beijing, China, March, 17-20, 1986.

Gringarten, A.C.: "Flow in Porous Media", Msc Petroleum Engineering Course Notes, Imperial College London, 2006a.

Gringarten, A.C.: "From Straight Lines to Deconvolution: The Evolution of the State of the Art in Well Test Analysis", paper SPE 102079 presented at the SPE Annual Technical Conference and Exhibition held in San Antonio, Texas, Sept. 24-27, 2006b.

Gringarten, A.C.: "Interpretation of Tests in Fissured and Multilayered Reservoirs with Double-Porosity Behavior: Theory and Practice", *Journal of Petroleum Technology* (April, 1984), pp. 549-564.

Hasan, A.R. and Kabir, C.S.: "A Mechanistic Approach to Understanding Wellbore Phase Redistribution", paper SPE 26483 presented at the 68th Annual Technical Conference and Exhibition of the Society of Petroleum Engineers held in Houston, Texas, Oct. 3-6, 1993.

Hashemi, A. and Gringarten, A.C.: "Comparison of Well Productivity between Vertical, Horizontal and Hydraulically Fractured Wells in Gas-Condensate Reservoirs", SPE 94178, paper presented at the 14th Europec Biennial Conference held in Madrid, Spain, June 13-16, 2005.

Henderson, G.D., Danesh, A., Tehrani, D.H., Al-Kharusi,B.: "Generating Reliable Gas Condensate Relative Permeability Data Used to Develop a Correlation with Capillary Number," *Journal of Petroleum Science and Engineering* 25 (2000), pp. 79-91.

Hutchinson, T.S. and Sikora, V.J.: "A Generalized Water-Drive Analysis", Petroleum Transactions AIME (March 1959), pp. 169-178.

Jacoby, R.H. and Berry, V.J.Jr.: "A Method for Predicting Depletion Performance of a Reservoir Producing Volatile Crude Oil", (1957), pp. 27-33.

Joshi, S.D.: "Horizontal Well Technology", Joshi Technologies International, PennWell Publishing Company, Tulsa, Oklahoma, 1991.

Khan, S.A.: "Development of Viscosity Correlation for Crude Oils", Society of Petroleum Engineers Journal (Aug 1987).

Klins, M.A. and Majcher, M.W.: "Inflow performance relationships for damaged or improved wells producing under solution-gas drive", *Journal of Petroleum Technology* (December 1992), pp. 1357-1363.

Kniazeff, V.J. and Naville, S.A.: "Two-Phase Flow of Volatile Hydrocarbons", *Society of Petroleum Engineers Journal* (March 1965), pp. 37.

Kuchuk, F.J., Goode, P.A., Wilkinson, D.J., and Thambynayagam, R.K.M.: "Pressure transient behavior of horizontal wells with and without gas cap or aquifer", *Society of Petroleum Engineers formation Evaluation* (March, 1991), pp. 86-94.

Kuchuk, F.J.: "Well testing and interpretation for horizontal wells", *Journal of Petroleum Technology* (January1995), pp. 36-41.

Kucuk, F. and Ayestaran, L.: "Analysis of Simultaneously Measured Pressure and Sandface Flow Rate in Transient Well Testing", *Journal of Petroleum Technology* (February 1985), pp. 323-334.

Lee, B.O. and Salter, G.B.: "Evaluation of Hydraulic Fracturing Applications in Central Australia", paper SPE 19491 presented at the SPE Asia Pacific Conference held in Sydney, Australia, Sept. 13-15, 1989.

Levitan, M. M.: "Practical Application of Pressure/Rate Deconvolution to Analysis of Real Well Tests," Society of Petroleum Engineers Reservoir Evaluation & Engineering (April 2005) pp. 113-121.

Levitan, M.M., Ward, M.J., Boutaud de la Combe, J.L., and Wilson, M.R.: "The Use of Well Testing for Evaluation of Connected Reservoir Volume", paper SPE 102483 presented at the SPE Annual Technical Conference and Exhibition held in San Antonio, Texas, Sept. 24-27, 2006.

Loucks, T.L. and Guerrero, E.T.: "Pressure drop in a composite reservoir", Society of Petroleum Engineers Journal (September 1961), 170-176.

Luo, S. and Baker, A.: "Optimizing Horizontal-Well Steam-Stimulation Strategy for Heavy-Oil Development", SPE 104520, paper presented at the SPE Eastern Regional Meeting held at Canton, Ohio, USA, Oct. 11-13, 2006.

Martin, J.C.: "Simplified Equations of Flow in gas Drive reservoirs and the Theoretical Foundation of Multiphase Pressure Buildup Analyses", Trans., AIME 216 (March 1959) pp. 321-323.

Matthews, C.S. and Russell, D.G.: "Pressure Buildup and Flow Tests in Wells", Society of Petroleum Engineers Monograph, Dallas, Texas, 1967.

McCain, W.D.J.: "Properties of Petroleum Fluids", Penwell Books, Penwell Publishing Co, 1990.

McKay, C., Jones, J., and Pomerene, J.: "Successful Horizontal Producers in Midway-Sunset Thermal Operations", paper SPE 83479 presented at the SPE Western Regional/AAPG Pacific Section Joint Meeting held at Long Beach, California, May 19-24, 2003.

McKinley, R.M.: "Wellbore Transmissibility from After Flow-Dominated Pressure Buidup Data", *Journal of Petroleum Technology* (July 1971), pp. 863-872.

Merrill Jr, L.S., Kazemi, H., and Gogarty, W.B.: "Pressure Falloff analysis in Reservoirs with Fluid Banks", *Journal of Petroleum Technology* (July, 1974), pp. 809-818.

Moses, P.L.: "Engineering Application of Phase Behavior of Crude Oil and Condensate System", *Journal of Petroleum Technology* (July 1986), pp. 715-723.

Muskat, M. and Meres, M.W.: "The flow of heterogeneous fluids through porous media", Journal of Applied Physics 7 (Jul. 1963), pp. 346-363.

Odeh, A.S.: "Flow Test Analysis for a Well with Radial Discontinuity", *Journal of Petroleum Technology* (February 1969), pp. 207-210.

Olarewaju, J.S., Lee, W.J., and Lancaster, D.E.: "Type-and Decline-Curve Analysis with Composite Models", *Society of Petroleum Engineers Formation Evaluation* (March 1991), pp. 79-85.

Onur, M. and Reynolds, A.C.: "A New Approach for Constructing Derivative Type Curves for Well Test Analysis", *Society of Petroleum Engineers Formation Evaluation* (March 1988), pp. 197-206.

Ostos, A. and Maini, B.: "Capillary Number in Heavy Oil Solution Gas Drive and Its Relationship with Gas-Oil Relative Permeability Curves", paper SPE 89430 presented at the 2004 SPE/DOE 14th Symposium on Improved Oil recovery held in Tulsa, Oklahoma, U.S.A, Apr. 17-21 2004.

Palasthy, G., Papp, I., Lakos, B., and Tromboczky, S.: "How To Enhance the Recovery of Intermediate Components of an Extremely Volatile Oil", paper SPE 59010 presentation at the SPE International Petroleum Conference and Exhibition held in Villahermosa, Mexico, Feb. 1-3, 2000.

Perrine, R.L.: "Analysis of pressure Build up curves", API, Dallas, Drill & Prod. Prac, Jan. 1956, pp. 482-509.

Pitzer, S.C., Rice, J.D., and Thomas, C.E.: "A Comparison of Theoretical Build-up Curves with Field Curves Obtained from Bottom-hole Shut-in Tests", *Journal of Petroleum Technology* (August 1959), pp. 49-52.

Prats, M., Hazebroe, P., and Strickler, W.R.: "Effect of Vertical Fractures on Reservoir Behavior-Compressible-Fluid Case", *Society of Petroleum Engineers Journal* (June, 1962), pp. 87-94.

Raghavan, R.: "Well test Analysis: Wells Producing by Solution Gas-Drive", Society of Petroleum Engineers Journal (1976) 196-208; Trans., AIME.

Rosa, A.J. and Carvalho, R.S.: "A Mathematical Model for Pressure Evaluation in an Infinite-Conductivity Horizontal Well", *Society of Petroleum Engineers formation Evaluation* (December 1989), pp. 559-566.

Roumboutsos, A. and Stewart, G.: "A Direct Deconvolution or Convolution Algorithm for Well Test Analysis", paper SPE 18157 presented at the 63rd Annual Technical Conference and Exhibition held in Houston Texas, Oct. 2-5, 1988.

Rowlinson, J.S. and Widom, B.: "Molecular Theory of Capillarity", Courier Dover Publications, Inc, 1982.

Serra, K.V., Peres, A.M.M., and Reynolds, A.C.: "Well test Analysis for Solution-gas-Drive Reservoirs: Part 2 –Buildup Analysis", *Society of Petroleum Engineers Formation Evaluation*, June, 1990a.

Serra, K.V., Peres, A.M.M., and Reynolds, A.C.: "Well test Analysis for Solution-gas-Drive Reservoirs: Part3 - A unified treatment of the Pressure-Squared Method", *Society of Petroleum Engineers Formation Evaluation*, June, 1990b.

Sheikholeslami, B.A., Schlottman, B.W., Siedel, F.A., and Button, D.M.: "Drilling and production aspects of horizontal wells in the Austin Chalk", *Journal of Petroleum Technology*, (July 1990), pp. 773-779.

Standing, M.B.: "Inflow performance relationships for damaged wells producing by solution-gas drive", *Journal of Petroleum Technology* (November, 1970), pp. 1399-1400.

Stegemeier, G.L. and Matthews, C.S.: "A Study of Anomalous Pressure Build-up Behavior", Petroleum Transactions AIME (January 1958), 44-50.

Stramp, R.L.: "The use of Horizontal Drainholes in the Empire Abo Unit", paper SPE 9221 presented at the 55th Annual Technical Conference and Exhibition of the Society of Petroleum Engineers held in Dallas Texas, Sept. 21-24, 1980.

Sukamo, P. and Tobing, E.L.: "Inflow performance relationship for perforated wells producing from solution gas drive reservoir", paper SPE 29312 presented at the Asia pacific Oil & Gas Conference and Exhibition, Kualalumpur, Mar. 20-22, 1995.

Talabi, O., Pooladi-Darvish, M., and Okazawa, T.: "Effect of Rate and Viscosity on Gas Mobility during Solution-Gas Drive in Heavy Oils", paper SPE 84032 presented at the SPE Annual Technical Conference and Exhibition held Denver, Colorado, USA, Oct. 5-8 2003.

Thiebot, B.M. and Sakhthikumar, S.S.: "Cycling Fractured Reservoirs Containing Volatile Oil- Laboratory Investigation of the Performance of Lean Gas or Nitrogen Injection", paper SPE 21427 presented at the SPE Middle East Oil Show held in Bahrain, Nov. 16-19, 1991.

Thompson, L. and Reynolds, A.: "Analysis of Variable-Rate Well-Test Pressure Data using Duhamels Principle", *Society of Petroleum Engineers Formation Evaluation*, (October 1986), pp. 453-469.

Valko, P.P. and Economides, M.J.: "Heavy crude production from shallow formations: Long horizontal wells versus horizontal fractures", paper SPE 50421 presented at the International Conference on Horizontal Well Technology held in Calgary, Alberta, Canada, Nov. 1-4, 1998.

Van Evardingen, A.F. and Hurst, W.: "The Application of the Laplace Transformation to Flow Problems in Reservoirs", Petroleum Transactions AIME (December 1949), pp. 305- 324.

Van Evardingen, A.F.: "The Skin Effect and Its Influence on the Productive Capacity of a Well", Transactions AIME (1953), pp. 171- 176.

Villalba, M., Perez, P., Marcano, C., Rojas, G., Rodriguez, H., and Almeida, J.: "Revitalization of Matured Volatile Oil and Gas Condensate Oil Reservoirs Using Horizontal Wells", paper SPE 37060 presented at the 2nd International Three-Day Conference on Horizontal Well Technology held in Calgary Alberta Canada, Nov. 16-20, 1996.

Vogel, J.V.: "Inflow Performance Relationships for Solution-Gas Drive wells", *Journal of Petroleum Technology* (January 1968), 83-92.

Von Schroeter, T., Hollaender, F., and Gringarten, A.C.: "Deconvolution of Well Test Data as a Nonlinear Total Least-Square Problem", *Society of Petroleum Engineers Journal* (Dec. 2004), pp. 375-390.

Wang, X., Indriati, S., Valko, P., and Economides, M.J.: "Production Impairment and Purpose-Built Design of Hydraulic Fractures in Gas-Condensate Reservoirs", paper SPE 64749 presented at the SPE International Oil and Gas Conference and Exhibition in China, Beijing, Nov. 7-10, 2000.

Wattenbarger, R.A. and Ramey Jr, H.J.: "An Investigation of Wellbore Storage and Skin Effects in Unsteady Liquid Flow: II. Finite Difference Treatment", Society of Petroleum Engineers Journal (September 1970), pp. 291-296.

Whitson, C.H. and Brulé M.R.: "Phase Behavior", SPE Monograph, Henry L.Doherty Series 20 (Jan. 2000).

Woods, R.W.: "Case History of Reservoir Performance of a Highly Volatile Type Oil Reservoir", paper SPE 378 presented at the AIME Annual Meeting held at Chicago, Feb. 13-17, 1955.

Yost II, A.B., Overby, W.K., Wilkins, D.A., and Locke, C.D.: "Hydraulic Fracturing of a Horizontal Well in a Naturally Fractured Reservoir: Gas Study for Multiple Fracture Design", paper SPE 17759 presented at the SPE Gas Technology Symposium held in Dallas, Texas, June 13-15, 1988.

Zheng, S.Y. and Corbett, P.: "Well Testing Best Practice", paper SPE 93984 presented at the SPE Europec/EAGE Annual Conference held in Madrid, Spain, June 13-16, 2005.

APPENDIX A

A-1 Composition of fluid sample A

Components	Fraction
CO2	0.009
N2	0.003
C1	0.5347
C2	0.1146
C3	0.0879
C4	0.0456
C5	0.0209
C6	0.0151
C7+	0.1692
M+	173
γ+	0.83648

A-2 Constant Composition Experiment (CCE) of fluid sample A at 176 °F

Pressure (psig)	Relative vol.
6000	0.9589
5500	0.9700
5000	0.9827
4900	0.9856
4800	0.9883
4700	0.9919
4600	0.9951
4500	0.9984
4460	1.0000
4443	1.0009
4305	1.0097
3900	1.0412
3531	1.0812
3132	1.1425
2769	1.2232
2422	1.3356
2128	1.4738
1880	1.6384
1660	1.8415
1351	2.2768
1061	2.9892

A-3 Constant Volume Depletion (CVD) for fluid sample A at 176 °F

Pressure (psig)	Vapour Z-factor	Moles recover
4460		0.0000
3600	0.798	0.0754
2800	0.783	0.1793
2000	0.788	0.3237
1200	0.843	0.4991
600	0.913	0.6397

A-4 Differential Liberation (DL) Experiment at 176 °F

Pressure (psig)	Oil rel. vol.	Gas-Oil Ratio (Mscf /stb)	Vapor Z-factor	Oil visc. (cp)	Gas visc. (cp)	Liquid density (lb /ft^3)	Gas gravity
4460	2.921	3.377		0.228	0.0000	33.087	
4000	2.343	2.351	0.825	0.290	0.0383	35.159	1.025
3492	2.059	1.814	0.788	0.338	0.0327	36.726	0.932
3003	1.886	1.471	0.772	0.380	0.0280	37.969	0.858
2514	1.756	1.205	0.773	0.440	0.0239	39.092	0.821
2004	1.645	0.970	0.790	0.515	0.0202	40.185	0.799
1534	1.550	0.775	0.816	0.602	0.0171	41.140	0.806
1001	1.464	0.573	0.856	0.748	0.0140	42.151	0.826
505	1.372	0.383	0.912		0.0120	43.325	0.888
209	1.298	0.245	0.958		0.0114	44.230	1.067
0	1.057	0.000	0.995	1.547	0.0109	48.775	1.767

A-5 Separator Test for fluid sample A

Saparator1

Temperature (F)	Pressure (psig)	Liquid density (lb /ft^3)	Vapor Mol. Wght.	Gas-Oil Ratio (Mscf /stb)
60	300		20.68	1.597
60	0	50.754		0.275
STVF	2.115			

Separator2

Temperature (F)	Pressure (psig)	Liquid density (lb /ft^3)	Vapor Mol. Wght.	Gas-Oil Ratio (Mscf /stb)
60	50		23.32	1.993
60	0	51.129		0.068
STVF	2.172			

A-6 Fluid Density at Bubble Point Pressure

Sat. pressure (psig)	Liquid density (lb /ft^3)
4460	33.01

A-7 Match of Tuning Experiment for Fluid Sample A

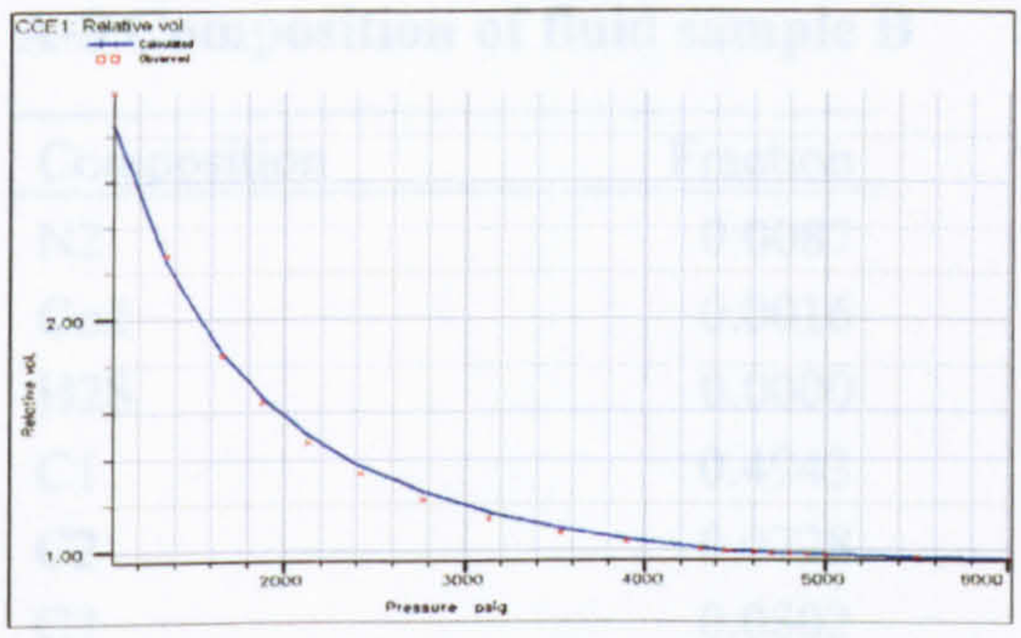

Figure A-7-1 CCE for Relative Volume Fluid A

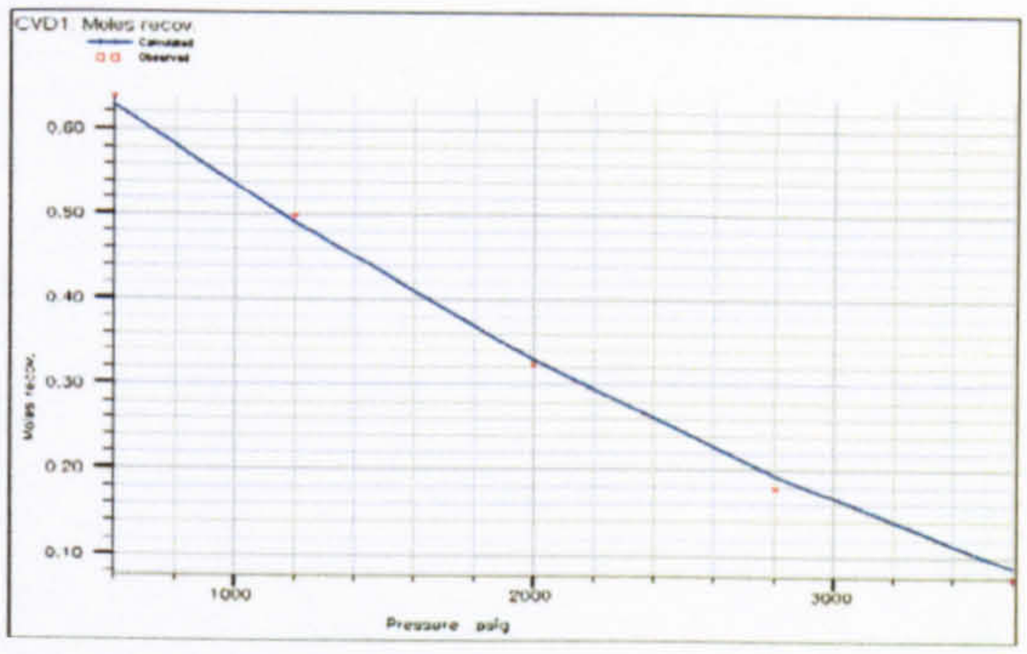

Figure A-7-2 CVD for Moles Recover Fluid A

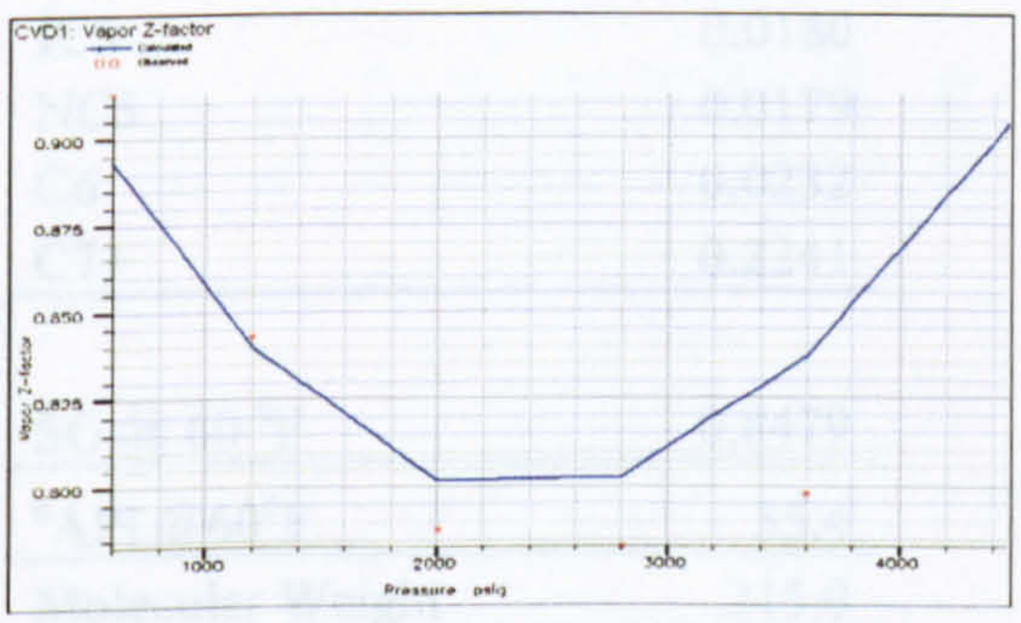

Figure A-7-3 CVD for Vap Z Factor Fluid A

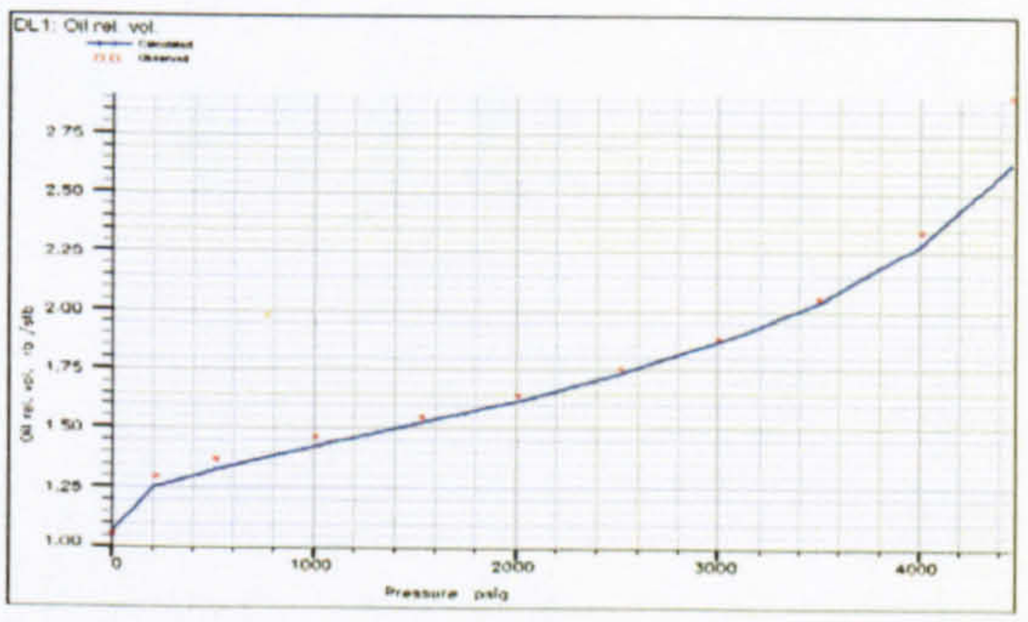

Figure A-7-4 DL for Oil Relative Vol. Fluid A

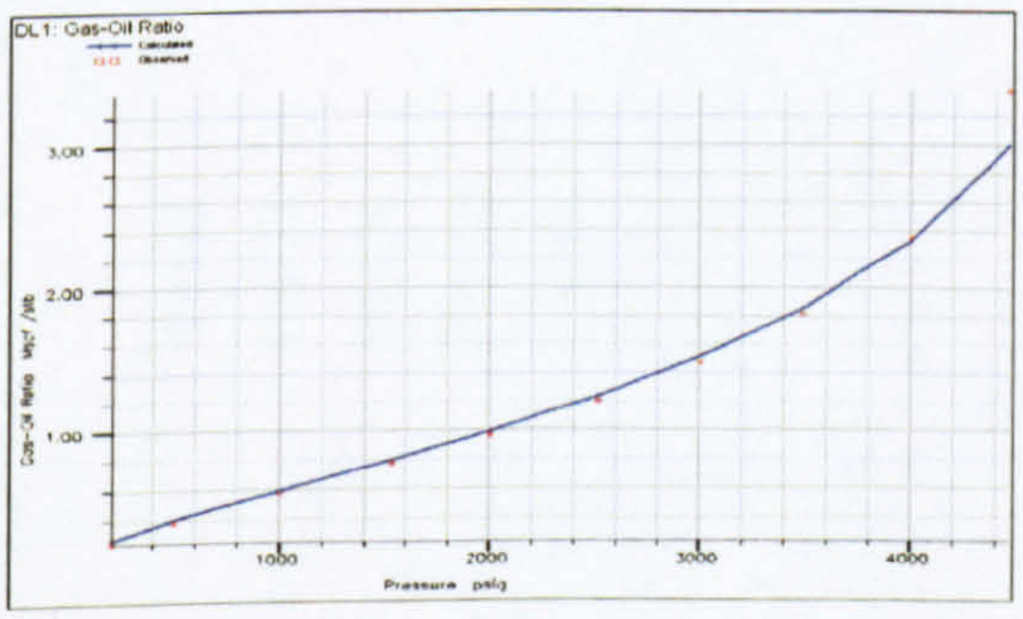

Figure A-7-5 DL for GOR Fluid A

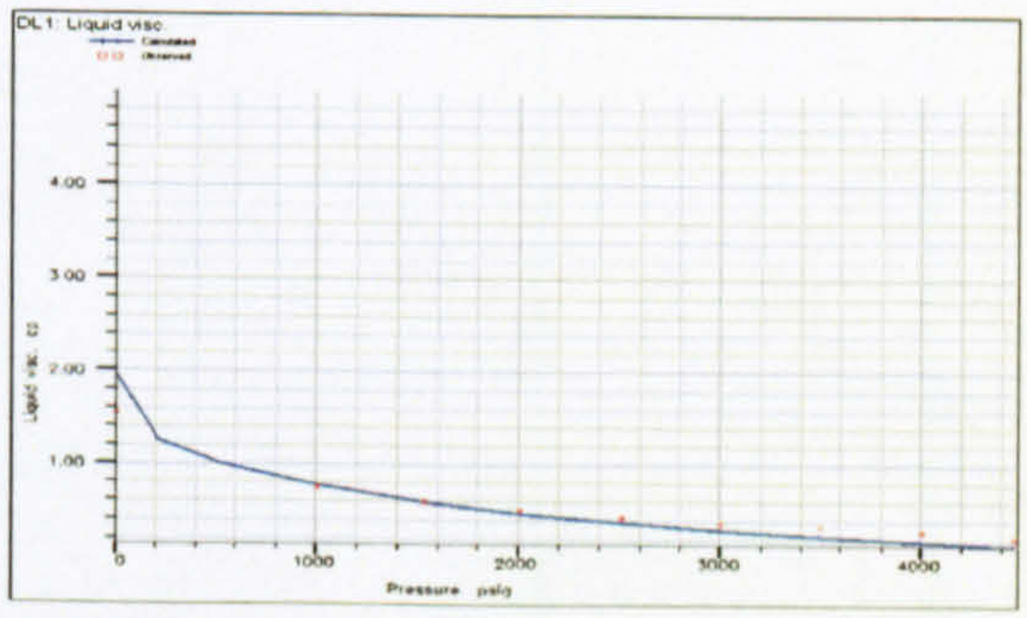

Figure A-7-6 DL for Liquid Viscosity. Fluid A

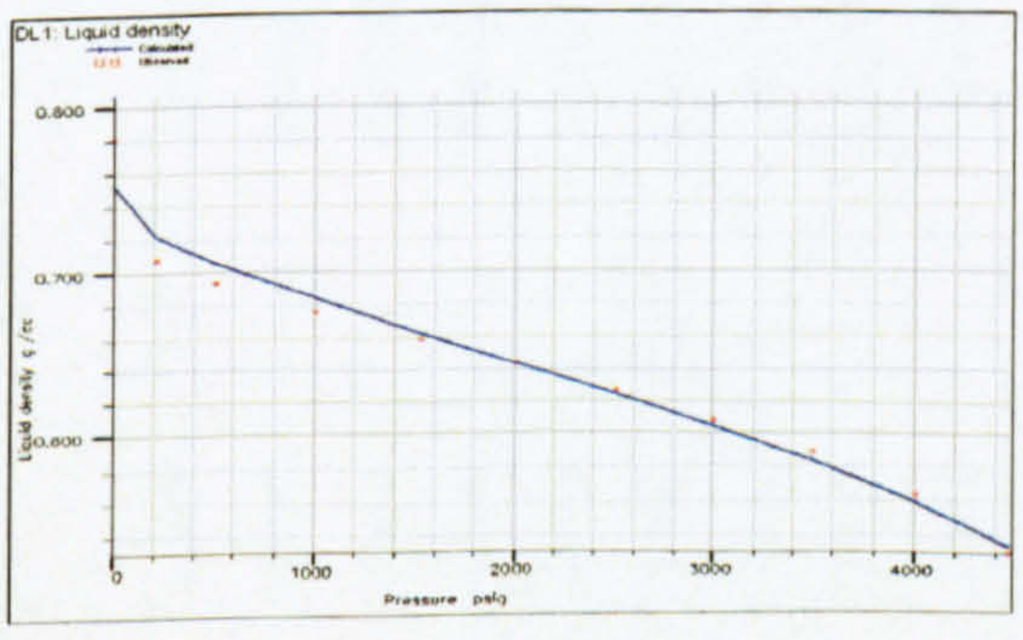

Figure A-7-7 DL for Liquid density Fluid A

A-8 Composition of fluid sample B

Composition	Fraction
N2	0.0087
Co2	0.0016
H2S	0.0000
C1	0.4943
C2	0.0728
C3	0.0802
IC4	0.0231
NC4	0.0361
IC5	0.0180
NC5	0.0179
C6	0.0232
C7+	0.2241

SG @ 60 °F	0.8479
°API @60°F	35.4
Molecular Weight	215.0

A-9 Constant Composition Experiment (CCE) of fluid sample B at 189 °F

Pressure (Psia)	Relative Volume (V/Vsat)*	Liquid Phase Density (gm/cm^3)	Y-Function $\frac{Psat^{-p}}{P(V/V_{sat}-1)}$	Lquid Phase Viscosity (cp)
5000	0.9804	0.6182		0.252
4700	0.9861	0.6146		0.247
4500	0.9902	0.6121		0.244
4300	0.9946	0.6094		0.241
4076	1.0000	0.6061		0.237
3700	1.0280		3.658	0.259
3300	1.0694		3.401	0.277
2900	1.1292		3.147	0.294
2500	1.2186		2.889	0.313
2100	1.3579		2.633	0.333
1700	1.5888		2.377	0.363
1300	2.0082		2.120	0.398
900	2.8949		1.864	0.461
500	5.4523		1.608	0.507
100	30.4446		1.351	0.653
15				1.434

A-10 Differential Liberation Experiment for fluid B at 189°F

Pressure (Psia)	Formation Volume factor	Gas Volume Facto (bbl/mscf)r	Gas Deviation Factor (Z=PV/NRT)	Solution Gas-Oil Ratio (Scf/stb)	Liberated Gas-Oil Ratio (scf/stb)	Specific Gravity of Librated Gas	Gas Viscosity (cp)	Liquid Phase Density (gm/cm3)
5000	1.9760							
4700	1.9870							
4500	1.9960							
4300	2.0050							
4076	2.0150			1786	0			0.6061
3700	1.8660	0.751	0.850	1513	273	0.8572	0.0394	0.6272
3300	1.7540	0.814	0.821	1296	490	0.8293	0.0361	0.6451
2900	1.6640	0.908	0.805	1113	673	0.8055	0.0330	0.6608
2500	1.5860	1.054	0.806	952	834	0.7855	0.0302	0.6759
2100	1.5170	1.274	0.818	808	978	0.7738	0.0280	0.6904

Continued on next page

Continued from previous Page (A-10 Differential Liberation Experiment for fluid B at 189°F)

Pressure (Psia)	Formation Volume factor (Bo)	Gas Volume Factor (bbl/mscf)	Gas Deviation Factor (Z=PV/NRT)	Solution Gas-Oil Ratio (Scf/stb)	Liberated Gas-Oil Ratio (scf/stb)	Specific Gravity of Librated Gas	Gas Viscosity (cp)	Liquid Phase Density (gm/cm3)
1700	1.4560	1.602	0.833	676	1110	0.7672	0.0262	0.7045
1300	1.3980	2.169	0.862	552	1234	0.7617	0.0247	0.7188
900	1.3420	3.220	0.886	433	1353	0.7862	0.0237	0.7336
500	1.2820	6.025	0.921	311	1475	0.8610	0.0228	0.7499
100	1.1760	31.665	0.968	125	1661	1.2824	0.0218	0.7738
15	1.0620	218.077	1.000	0	1786	2.1766	0.0208	0.8010

A-11 Separator Flash Liberation Experiment for fluid sample B at 189°F

Type of Liberation	Pressure (psig)	Temperature (°F)	First Stage	Stock Tank	Total	Formation Volume Factor (V_{sat}/V)[1]	Stock tank Oil (°API @ 60°F)	Seperator Gas Gravity (Air = 1.0000)
Flash	265	72	1212	216	1428	1.767	41.3	0.7113
Flash	0	72	1726		1726	1.952	37.3	0.9175
Flash	100**	72	1363		1469	1.786	40.7	0.7701
Differential		189			1786	2.015	37.1	0.9540

1 The volume of reservoir oil at the saturation pressure and temperature relative to stock tank oil @ 60°F

* First stage separator gas gravity

** Reservoir fluid flashed to 100 psig @ 72°F -> 45 psig @ 72°F->10 psig @72°F->0 psig @ 72°F.

A-12 Differential Liberation Experiment for fluid sample at 189°F

Pressure (Psia)	Formation Volume factor[1] (B_o)	Solution Gas-Oil Ratio[2] (Scf/stb)
5000	1.733	
4700	1.743	
4500	1.751	
4300	1.759	
+4076	1.767	1428
3700	1.637	1218
3300	1.538	998
2900	1.460	838
2500	1.391	696
2100	1.331	570
1700	1.277	454
1300	1.226	346
900	1.177	241
500	1.124	134
100	1.031	35
15	1.000	0

+ Reservoir pressure and bubble point pressure

[1] $B_o = B_{ofb}/B_{odb} - B_{od}$

[2] $R_s = R_{sp}-(R_L)_{st}B_{ofb}/B_{odb}$

A-13 Separator Test Experiment for fluid sample B

Separator Stage	1	0
Pressure (Psig)	265	0
Temperature (°F)	72	72
Gas-Oil Ratio (cfb)[1]	1212	216
Gas Specific Gravity (Air = 1.0000)	0.7113	1.3848

Component	Mole %	Mole %
Nitrogen	1.08	0.07
Carbon Dioxide	0.23	0.22
Hydrogen Sulfide	0.00	0.00
Methane	80.34	24.62
Ethane	9.26	16.98
PropaNe	6.32	31.41
i-Butane	1.03	8.45
n-Butane	1.15	11.20
i-Pentane	0.24	2.85
n-Pentane	0.17	2.08
Hexanes	0.09	1.10
Heptanes Plus	0.09	1.02
TOTAL	100.00	100.00

Total Gas-Oil Ratio (cfb).....1428
Stock Tank Oil Gravity (oAPI @60°F).....41.3
Bubble Point Formation Volume Factor (Vbp/Vsto)2.....1.767

[1]Gas-oil ratio in cubic feet of gas at 14.7 psia and 60°F per barrel of stock tank oil at 60°F

[2]Barrels of bubble point at 4076 psia and 189°F per barrel of stock tank

A-14 Match of Tuning Experiment for Fluid Sample B

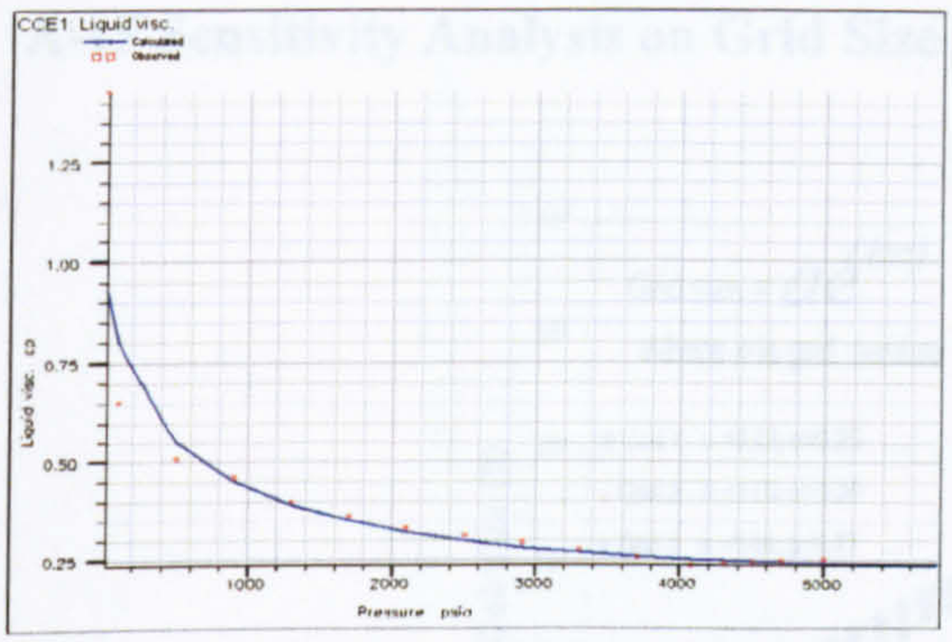

Figure A-14-1 CCE for Oil Viscosity Fluid B

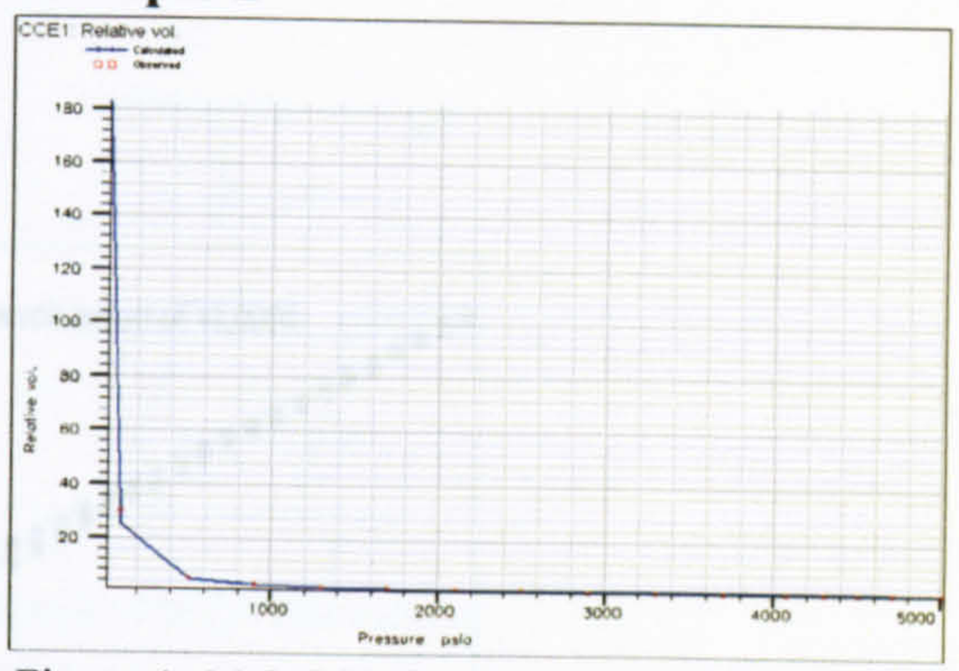

Figure A-14-2 CCE for Relative Vol. Fluid B

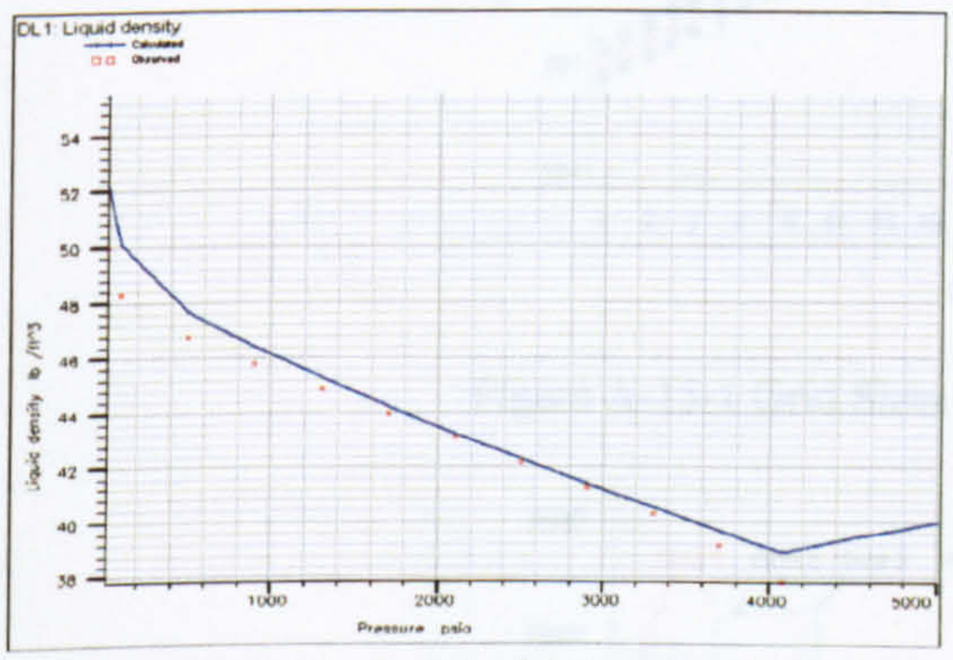

Figure A-14-1 DL for Liquid Density Fluid B

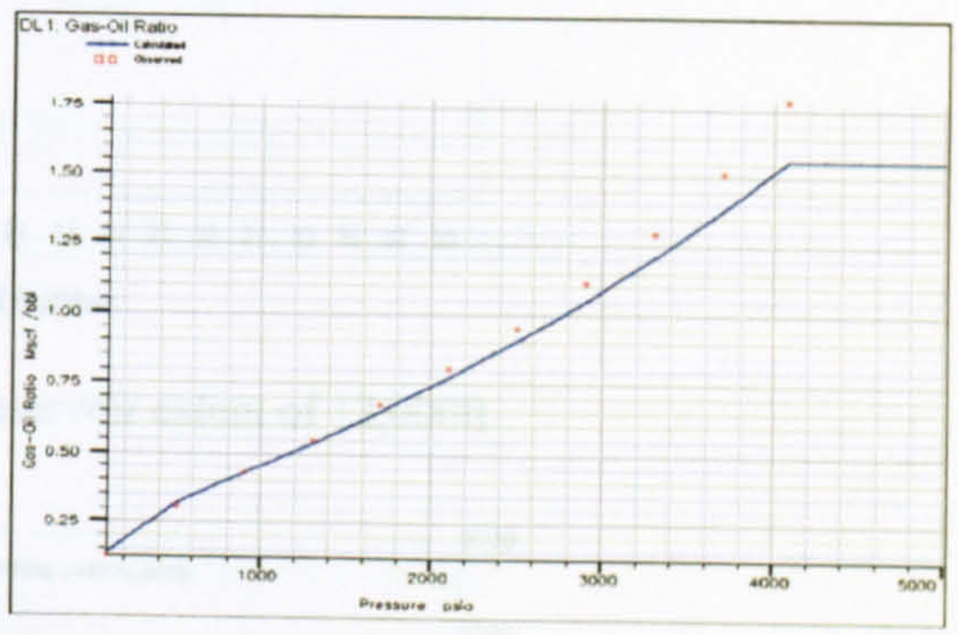

Figure A-14-2 DL for GOR Fluid B

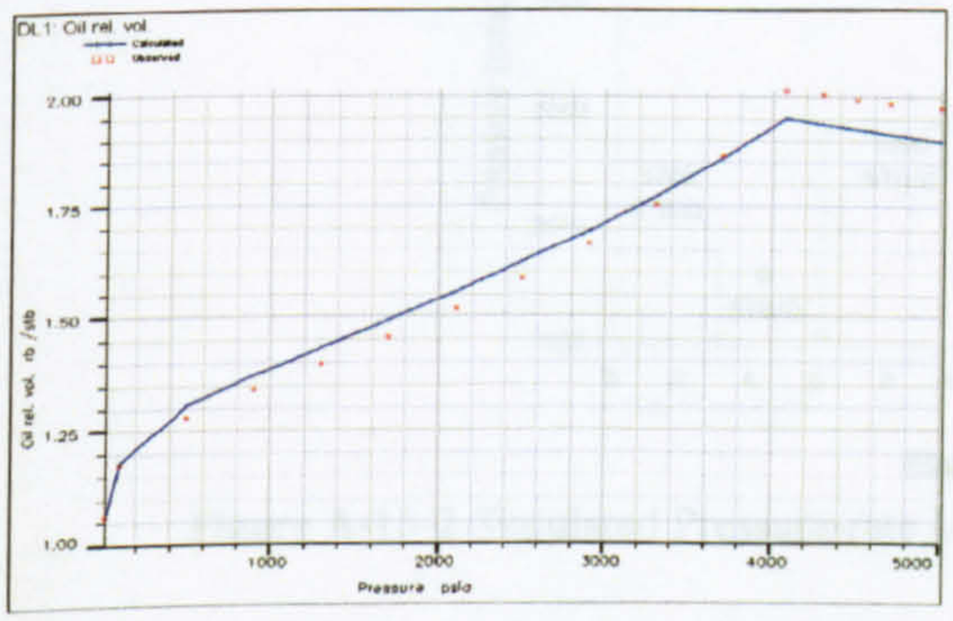

Figure A-14-1 DL for Oil Rel. Volume Fluid B

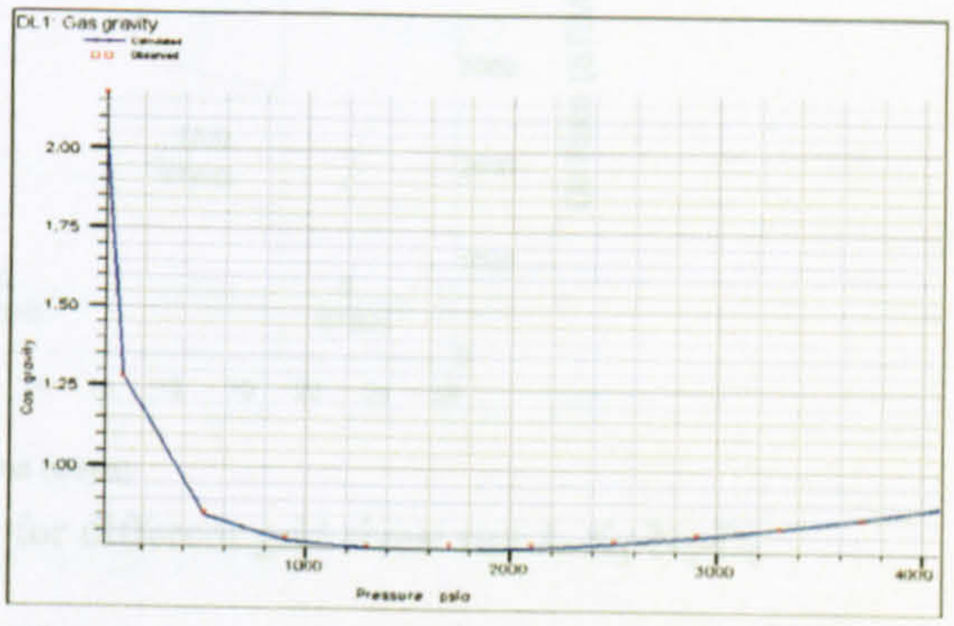

Figure A-14-2 DL for Gas Gravity Fluid B

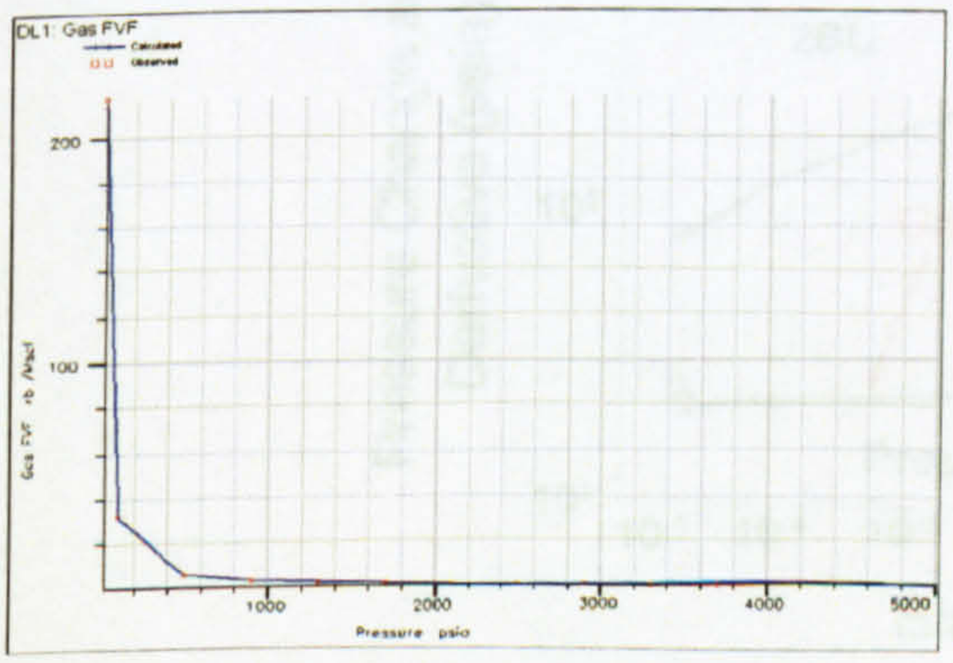

Figure A-7-1 DL for GAS FVF Fluid B

A-15 Sensitivity Analysis on Grid Size

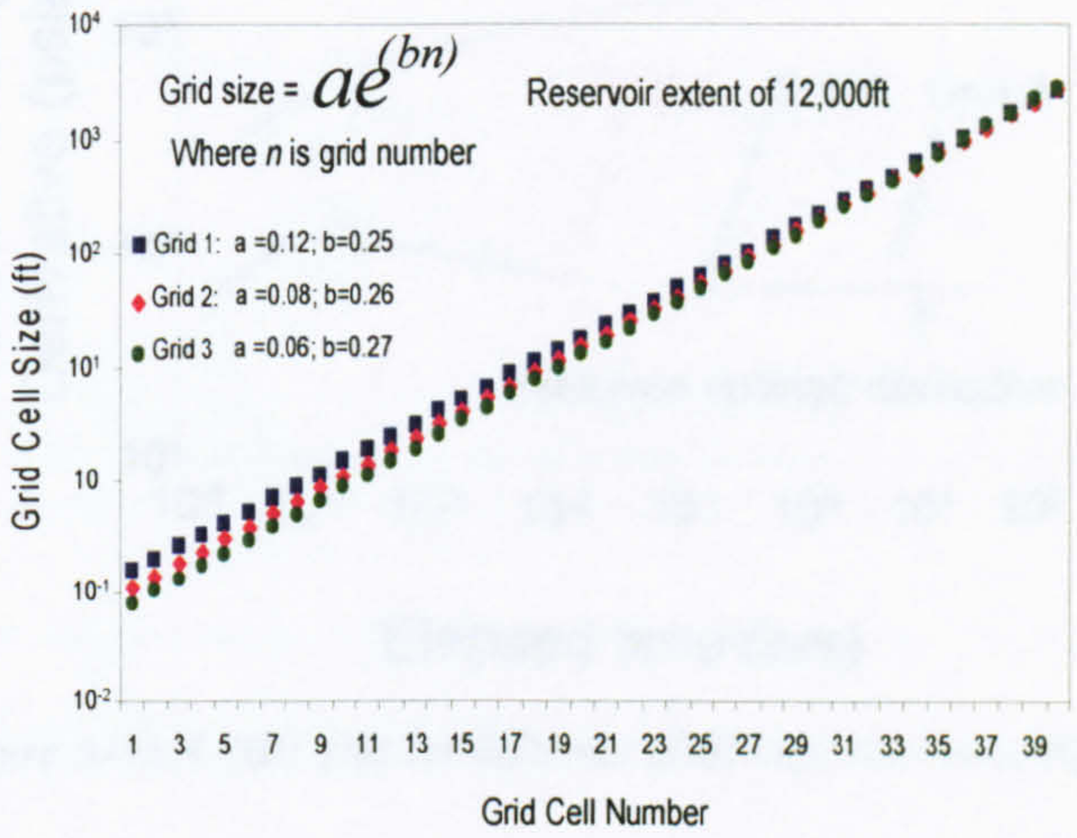

Figure A-15-1 Grid Sizes for reservoir extent of 12,000ft

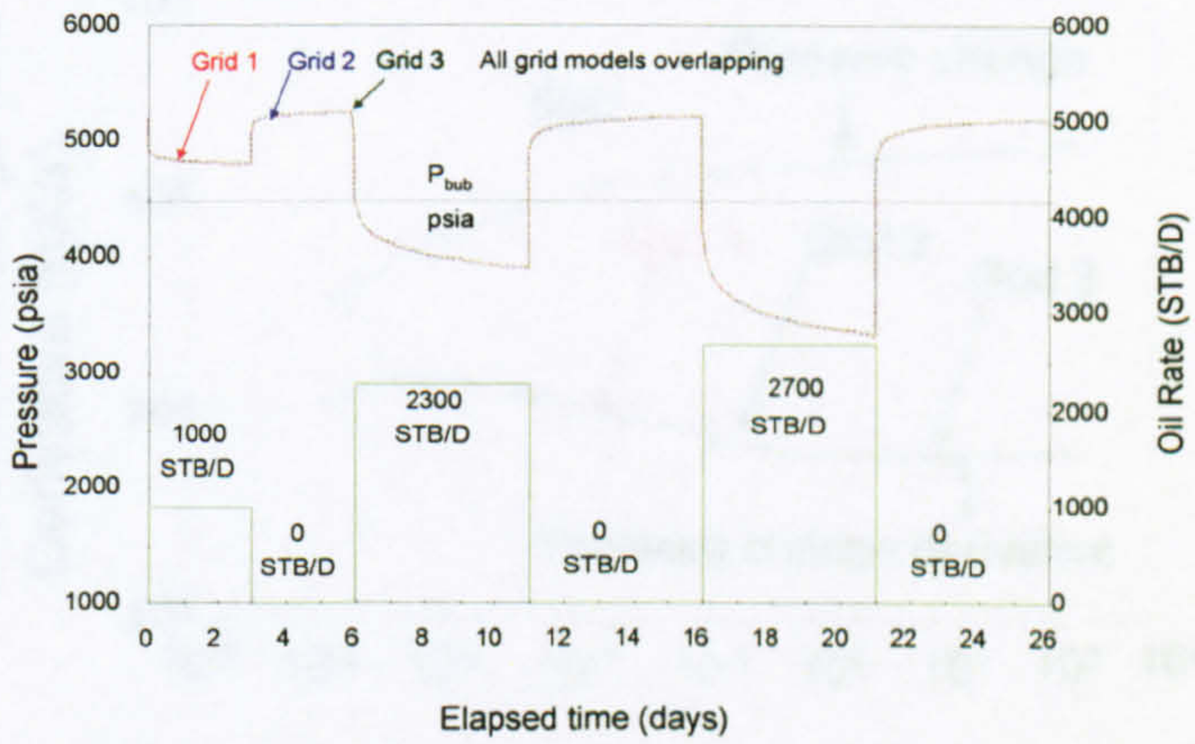

Figure A-15-2 Simulated Pressure-rate history for different grid sizes: run A-K_1-N_0-D_0

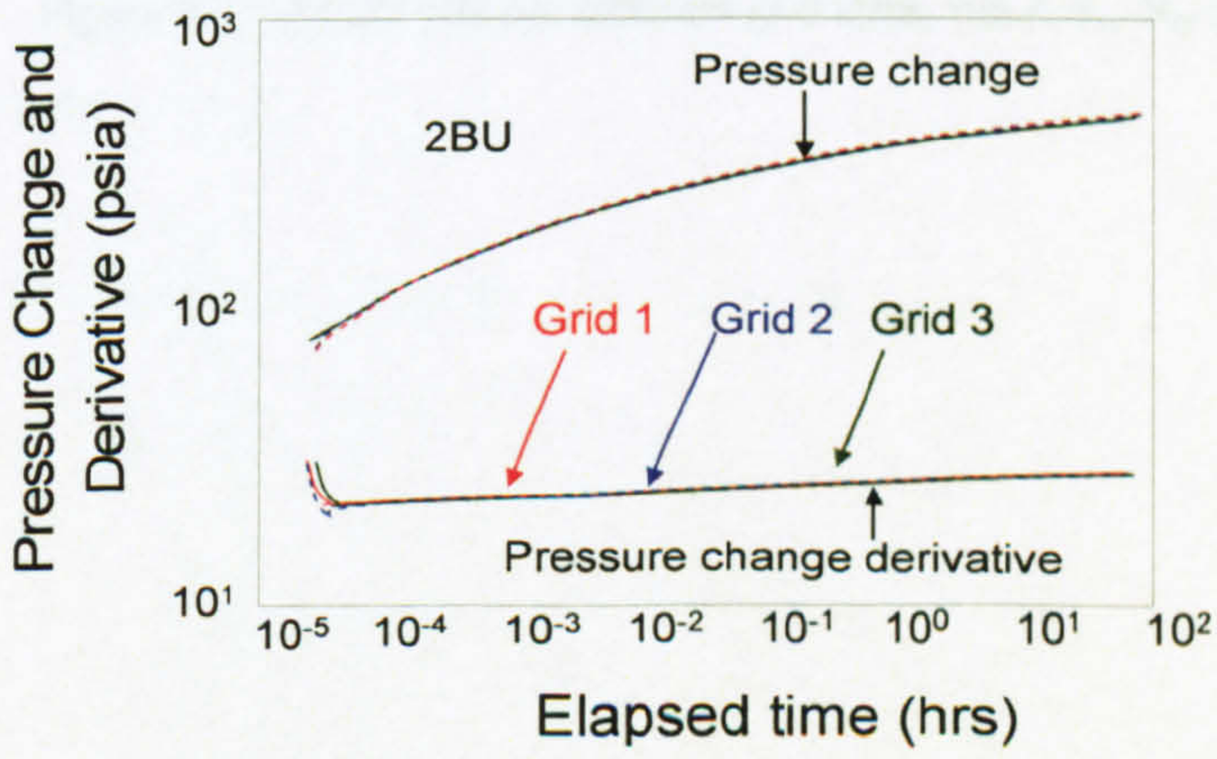

Figure A-15-3 2BU plot for different grid sizes: run A-K_1-N_0-D_0

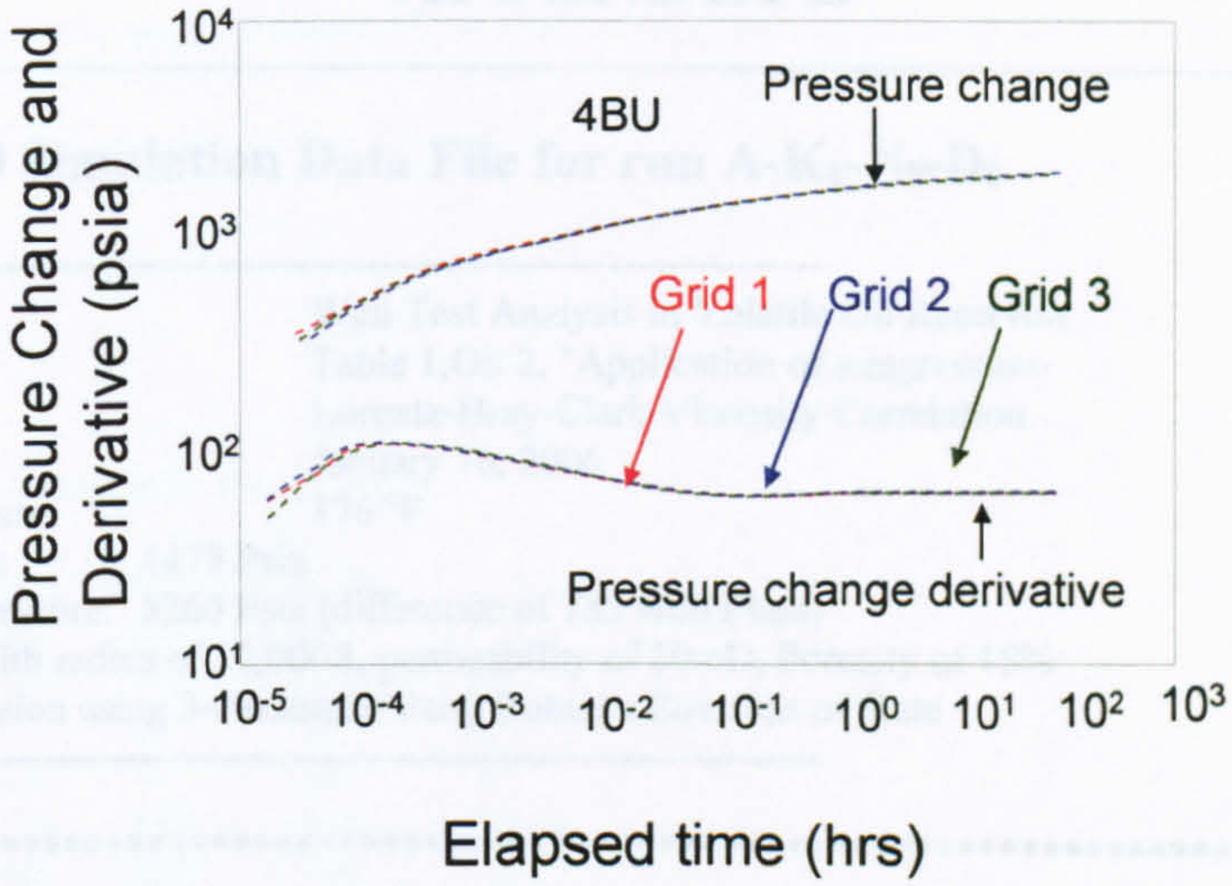

Figure A-15-4 4BU plot for different grid sizes: run A-K_1-N_0-D_0

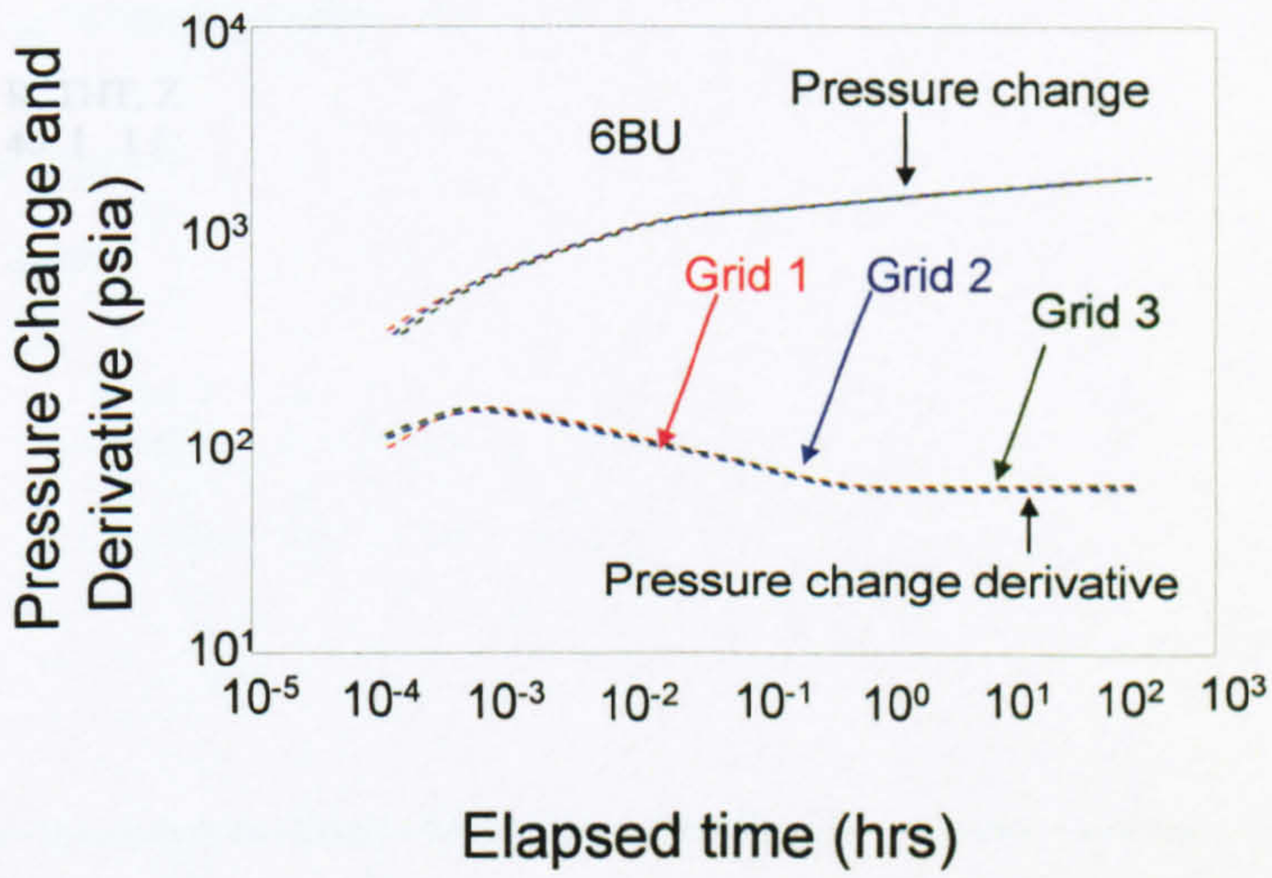

Figure A-15-5 6BU plot for different grid sizes: run A-K_1-N_0-D_0

APPENDIX B

B-1 Eclipse 300 Simulation Data File for run A-K_1-N_0-D_0

```
-- Title                          Well Test Analysis in Volatile Oil Reservoir
-- Fuid Sample A                  Table 1,Oil 2, "Application of a regression-
-- Viscosity Model                Lorentz-Bray-Clark Viscosity Correlation
-- Date:                          January 16, 2006
-- Resrvoir Temperature:          176 °F
-- Fluid Bubble Point:      4475 Psia
-- Initial Reservoir Pressure:  5260 Psia (difference of 785 with Pbub)
-- Radial Reservoir with radius of 12,000ft, permeability of 10mD, Porosity of 15%
-- Eclipse 300 Simulation using 3-Parameter Peng Robison Equation of State
----------------------------------------------------------------------

--**************************************************************************
RUNSPEC
--**************************************************************************

--NOSIM
FORMOPTS
HCSCAL /
DIMENS
-- Grid Dimensions
--                    R, THT, Z
                      40  1   1 /

-- Phases Present
OIL
WATER
GAS

RADIAL

--VELDEP
--1 1 0 1 /

-- Units
FIELD

EOS
PR3 /
PRCORR

-- Number of Components
COMPS
9 /

-- One stauration and PVT tables with 55 sat and pressure nodes 1 FIP region
TABDIMS
1 1 55 55 1 /

EQLDIMS
1 55 55 1 55 /

WELLDIMS
1 1* 1 5 /

UNIFIN
UNIFOUT
UNIFSAVE

START
01 JAN 2006 /
```

```
--*************************************************************************
GRID
--*************************************************************************

INIT
ECHO

-- Inner radius ft
INRAD
0.2 /

-- Vector of cell dimensions in R—direction
DRV
0.1         0.15    0.2     0.25    0.3
0.35        0.4     0.45    0.7     1
1.25        1.8     2.35    3.7     5
7           9       11      13      15
17          34      50      66      82
98          114     130     146     161.8
200         400     500     798     900
1000        1500    1800    1930    2000
/

-- Vector of cell dimensions in THT—direction
DTHETAV
360 /
-- Dimensions of cells in Z—direction 100 ft
DZV

-- Top of reservoir is at 10,000 ft
EQUALS
TOPS            10000 /
PERMR           10 /
PORO 0.15 /
/
RPTGRID
/
COPY
PERMR PERMZ /
/
MULTIPLY
PERMZ 0.1 /
/
--*************************************************************************
PROPS
--*************************************************************************
INCLUDE
FLUIDA.PVO /
-- Avg density at surface condition (14.7 psia)
DENSITY
1*                  63.100  1* /
--INCLUDE
--VELDEPPARA.txt /
-- Water PVT Properties
-- Ref Pres Ref FVF Compressibility Visc. Viscosibility

PVTW
14.7  1 2.7e-06 0.3 0 /
-- Rock Compressibility
ROCK
14.7                3.402e-6 /
--Relative permeability and capillary pressure data
--Water Relative Permeability
SWOF
--SW             KRW   KROW    PCOW
0.15            0     0.95    0
1               1     0       0
```

```
/
--Gas to Oil Relative Pemeability

INCLUDE
OilGasRelPerm.txt /
--*************************************************************************
REGIONS
--*************************************************************************
RPTREGS
--*************************************************************************
SOLUTION
--*************************************************************************
-- Mid depth = 10,050 ft, and WOC at 10,100 ft
EQUIL
10050 5259.8 10100 0.0 8000 0 3* 1 /

FIELDSEP
1 72 114.7 2 0 /
2 72 59.7  3 0 /
3 72 24.7  2 0 /
4 72 14.7  2 0 /
/
OUTSOL
RPTSOL
PRESSURE SWAT SOIL SGAS PSAT PBUB XMF YMF /
--*************************************************************************
SUMMARY
--*************************************************************************
WBHP
/
WOPR
/
WGPR
/
WWPR
/
--*************************************************************************
SCHEDULE
--*************************************************************************

RPTPRINT
7*0 1 5*0 /

RPTSCHED
TOTCOMP /
/
OUTSOL
TOTCOMP /
/
RUNSUM
-- Defining wells

-- Surface Separator Conditions
SEPCOND
SEP1 G1 1  72 114.7 2 0 /
SEP1 G1 2  72 59.7  3 0 /
SEP1 G1 3  72 24.7  4 0 /
SEP1 G1 4  72 14.7  0 0 /
/
WELSPECS
-- well group X Y BH-Dept phase others
Prod1 G1   1 1 10050 OIL /
/
--  Well Completion Data
COMPDAT
-- Name  I  J  K-up K-low flow-cond sat-table trans Dwell   Eff-Kh skin D-factor Penetration
Prod1 1  1   1 1   OPEN     2*        .2  1*  0 /
/
```

```
WSEPCOND
Prod1 SEP1 /
/
-- 1DD
WELLPROD
-- Name mode cntrl ORAT and others (BHP = 20 psia)
Prod1 OIL 1000 3* 20 /
/
INCLUDE
TIMESTEP3DAYS.txt /

-- 2BU
WELLPROD
-- Name mode cntrl ORAT and others (BHP = 20 psia)
Prod1 OIL 0 3* 20 /
/
INCLUDE
TIMESTEP3DAYS.txt /
-- 3DD
WELLPROD
-- Name mode cntrl ORAT and others (BHP = 20 psia)
Prod1 OIL 2300 3* 20 /
/
INCLUDE
TIMESTEP5DAYS.txt /

-- 4BU
WELLPROD
-- Name mode cntrl ORAT and others (BHP = 20 psia)
Prod1 OIL 0 3* 20 /
/
INCLUDE
TIMESTEP5DAYS.txt /

-- 5DD
WELLPROD
-- Name mode cntrl ORAT and others (BHP = 20 psia)
Prod1 OIL 2700 3* 20 /
/
INCLUDE
TIMESTEP5DAYS.txt /

-- 6BU
WELLPROD
-- Name mode cntrl ORAT and others (BHP = 20 psia)
Prod1 OIL 0 3* 20 /
/
INCLUDE
TIMESTEP5DAYS.txt /

END
/
```

B-2 Time Step for 3 Days

```
TUNING
1.1574E-6 1.1574E-1 1.1574E-7 1* 1.1 0.5 /
/
/
--TSCRIT
--0.25 0.000001  0.000010 /
TSTEP
-- LOG INCREASE IN TIME STEP

1.00E-06          49*1.83673469387755E-07          49*1.83673469387755E-06  49*1.83673469387755E-
05                49*1.83673469387755E-04
49*1.83673469387755E-03  49*1.83673469387755E-02  10*1.83673469387755E-01  1.63265306122451000E-
01                /
/
```

B-3 Time Step for 5 Days

```
TUNING
1.1574E-6 1.1574E-1 1.1574E-7 1* 1.1 0.5 /
/
/
--TSCRIT
--0.25 0.000001  0.000010 /

TSTEP
-- LOG INCREASE IN TIME STEP
1.00E-06          49*1.83673469387755E-07          49*1.83673469387755E-06  49*1.83673469387755E-
05                49*1.83673469387755E-04
49*1.83673469387755E-03  49*1.83673469387755E-02  21*1.83673469387755E-01  1.42857142857146000E-
01                /
/
```

APPENDIX C

C-1 Simulated Live oil PVT Properties (Dissolved Gas) for Fluid Sample A

Pressure Psig	Pressure Psia	GOR Mscf/Stb	Oil Vol Bbl/Stb	Rel Liq Visc Cpoise	Liq Dens gm/cc	Liq Z-Fac	Liquid Sat Frac	Rs Mscf/Stb
209	223.7	0.2687	1.255	1.2587	0.7225	0.0944	0.4122	0.09566
505	519.7	0.4039	1.3285	1.0166	0.7062	0.2026	0.5626	0.15986
1001	1015.7	0.5919	1.4237	0.7698	0.6843	0.3607	0.7234	0.27057
1534	1548.7	0.7954	1.5232	0.5909	0.6627	0.5062	0.8218	0.40452
2004	2018.7	0.9912	1.618	0.4746	0.6442	0.6177	0.8404	0.54024
2514	2528.7	1.2331	1.7351	0.3772	0.6241	0.7237	0.8617	0.71127
3003	3017.7	1.5085	1.8694	0.3037	0.6044	0.8124	0.9124	0.90457
3314.62	3329.32	1.7177	1.9727	0.2644	0.5913	0.8626	0.9824	1.04645
3375.1	3389.8	1.7625	1.9951	0.2573	0.5887	0.8718	0.9838	1.07588
3430.1	3444.8	1.8047	2.0162	0.251	0.5863	0.8801	0.9816	1.10340
3492	3506.7	1.8537	2.0409	0.2441	0.5835	0.8891	0.9856	1.13504
3540.1	3554.8	1.8931	2.0607	0.2388	0.5814	0.896	0.9833	1.16011
3595.1	3609.8	1.9397	2.0842	0.2329	0.5789	0.9038	0.9831	1.18947

Continued on next page

Continued from previous Page [Simulated Live oil PVT Properties (Dissolved Gas) for Fluid Sample A)

Pressure Psig	Pressure Psia	GOR Mscf/Stb	Oil Rel Vol Bbl/Stb	Liq Visc Cpoise	Liq Dens gm/cc	Liq Z-Fac	Liquid Sat Frac	Rs Mscf/Stb
3650.1	3664.8	1.9879	2.1086	0.2271	0.5764	0.9114	0.9829	1.21943
3705.1	3719.8	2.0379	2.134	0.2214	0.5738	0.9189	0.9826	1.25014
3760.1	3774.8	2.0899	2.1605	0.2158	0.5713	0.9262	0.9823	1.28164
3815.1	3829.8	2.144	2.1882	0.2103	0.5686	0.9334	0.982	1.31378
3870.1	3884.8	2.2004	2.2171	0.2049	0.566	0.9404	0.9816	1.34690
3925.1	3939.8	2.2593	2.2475	0.1996	0.5633	0.9473	0.9744	1.38072
4000	4014.7	2.3439	2.2912	0.1925	0.5595	0.9563	0.9876	1.42816
4035.1	4049.8	2.3855	2.3128	0.1893	0.5577	0.9605	0.9803	1.45097
4090.1	4104.8	2.4534	2.3482	0.1842	0.5549	0.9669	0.9797	1.48763
4145.1	4159.8	2.5249	2.3856	0.1793	0.552	0.9731	0.9791	1.52523
4200.1	4214.8	2.6005	2.4253	0.1744	0.549	0.9791	0.9784	1.56399
4255.1	4269.8	2.6806	2.4676	0.1695	0.5459	0.985	0.9776	1.60393
4310.1	4324.8	2.7657	2.5127	0.1648	0.5428	0.9907	0.9767	1.64508
4365.1	4379.8	2.8565	2.5611	0.1601	0.5396	0.9962	0.9757	1.68749
4420.1	4434.8	2.9539	2.6133	0.1554	0.5363	1.0015	0.9817	1.73139
4459.75	4474.45	3.0288	2.6536	0.1521	0.5339	1.0053	1	2.81520
4460	4474.7	3.0288	2.6536	0.1521	0.5339	1.0053	1	2.81520

Continued on next page

Continued from previous Page [Simulated Live oil PVT Properties (Dissolved Gas) for Fluid Sample A)

Pressure Psig	Pressure Psia	GOR Mscf/Stb	Oil Vol Bbl/Stb	Rel Liq Visc Cpoise	Liq Dens gm/cc	Liq Z-Fac	Liquid Sat Frac	Rs Mscf/Stb
4530.1	4544.8	3.0288	2.6477	0.1539	0.5351	1.0188	1	2.81520
4585.1	4599.8	3.0288	2.6432	0.1553	0.536	1.0294	1	2.81520
4640.1	4654.8	3.0288	2.6387	0.1567	0.5369	1.0399	1	2.81520
4695.1	4709.8	3.0288	2.6343	0.1582	0.5378	1.0505	1	2.81520
4750.1	4764.8	3.0288	2.63	0.1596	0.5387	1.061	1	2.81520
4805.1	4819.8	3.0288	2.6258	0.161	0.5395	1.0715	1	2.81520
4860.1	4874.8	3.0288	2.6216	0.1625	0.5404	1.082	1	2.81520
4915.1	4929.8	3.0288	2.6174	0.1639	0.5412	1.0925	1	2.81520
4970.1	4984.8	3.0288	2.6134	0.1654	0.5421	1.1029	1	2.81520
5025.1	5039.8	3.0288	2.6094	0.1668	0.5429	1.1134	1	2.81520
5080.1	5094.8	3.0288	2.6054	0.1683	0.5437	1.1238	1	2.81520
5135.1	5149.8	3.0288	2.6015	0.1697	0.5446	1.1343	1	2.81520
5190.1	5204.8	3.0288	2.5977	0.1712	0.5454	1.1447	1	2.81520
5245.1	5259.8	3.0288	2.5939	0.1726	0.5462	1.1551	1	2.81520

C-2 Simulated wet gas PVT Properties (Vaporised Oil) for Fluid Sample A

Pressure (Psia)	OGR (Stb/Mscf)	Gas FVF (Rb/Mscf)	Vap Visc(CP)	Vap Density gm/cc	Gas Grav	Vap Z-	Vapour Sat. Frac
209	0.00081	13.2399	0.0115	0.0176	1.0691	0.9250	0.5878
505	0.00063	5.4929	0.0124	0.0348	0.8781	0.8916	0.4374
1001	0.00097	2.6745	0.0137	0.0647	0.7945	0.8484	0.2766
1534	0.00197	1.6874	0.0155	0.0996	0.7715	0.8162	0.1782
2004	0.00374	1.2701	0.0178	0.1322	0.7711	0.8008	0.1596
2514	0.00714	1.0107	0.0209	0.1687	0.7828	0.7983	0.1383
3003	0.01240	0.8581	0.0244	0.2039	0.8035	0.8088	0.0876
3314.62	0.01708	0.7900	0.0270	0.2265	0.8215	0.8215	0.0176
3375.1	0.01812	0.7787	0.0275	0.2309	0.8254	0.8245	0.0162
3430.1	0.01912	0.7689	0.0280	0.2349	0.8292	0.8273	0.0184
3492	0.02029	0.7584	0.0286	0.2394	0.8336	0.8306	0.0144
3540.1	0.02124	0.7505	0.0290	0.2429	0.8371	0.8333	0.0167
3595.1	0.02238	0.7419	0.0295	0.2470	0.8413	0.8365	0.0169
3650.1	0.02356	0.7337	0.0300	0.2510	0.8456	0.8398	0.0171
3705.1	0.02479	0.7258	0.0306	0.2551	0.8501	0.8433	0.0174

Continued on next page

Continued from previous Page [Simulated wet gas PVT Properties (Vaporised Oil) for Fluid Sample A]

Pressure (Psia)	OGR (Stb/Mscf)	Gas FVF (Rb/Mscf)	Vap Visc(CP)	Vap Density gm/cc	Gas Grav	Vap Z-	Vapour Sat. Frac
3760.1	0.02607	0.7183	0.0311	0.2592	0.8548	0.8469	0.0177
3815.1	0.02741	0.7111	0.0317	0.2633	0.8596	0.8506	0.0180
3870.1	0.02882	0.7042	0.0322	0.2674	0.8647	0.8544	0.0184
3925.1	0.03028	0.6976	0.0328	0.2716	0.8699	0.8584	0.0256
4000	0.03238	0.6890	0.0336	0.2773	0.8773	0.8640	0.0124
4035.1	0.03341	0.6852	0.0340	0.2800	0.8809	0.8667	0.0197
4090.1	0.03508	0.6794	0.0346	0.2843	0.8868	0.8710	0.0203
4145.1	0.03684	0.6738	0.0353	0.2886	0.8929	0.8755	0.0209
4200.1	0.03868	0.6685	0.0359	0.2930	0.8993	0.8801	0.0216
4255.1	0.04062	0.6635	0.0366	0.2974	0.9060	0.8848	0.0224
4310.1	0.04265	0.6587	0.0373	0.3019	0.9130	0.8897	0.0233
4365.1	0.04480	0.6541	0.0381	0.3065	0.9203	0.8948	0.0243
4420.1	0.04706	0.6497	0.0389	0.3111	0.9280	0.9000	0.0183
4459.75	0.04878	0.6467	0.0394	0.3145	0.9338	0.9038	
4460	0.05200	0.6467					
4530.1	0.05471	0.6420					
4585.1	0.05760	0.6384					
4640.1	0.06070	0.6348					

Continued on next page

Continued from previous Page [Simulated wet gas PVT Properties (Vaporised Oil) for Fluid Sample A]

Pressure (Psia)	OGR (Stb/Mscf)	Gas FVF (Rb/Mscf)	Vap Visc(CP)	Vap Density gm/cc	Gas Grav	Vap Z-	Vapour Sat. Frac
4695.1	0.06405	0.6314					
4750.1	0.06768	0.6281					
4805.1	0.07165	0.6249					
4860.1	0.07604	0.6217					
4915.1	0.08095	0.6186					
4970.1	0.08655	0.6156					
5025.1	0.09311	0.6127					
5080.1	0.09574	0.6098					
5135.1	0.09574	0.6070					
5190.1	0.09574	0.6043					
5245.1	0.09574	0.6016					

C-3 Estimation of Compressibility from fluid properties for Fluid Sample A

Pressure (Psia)	Pmean	So/Bo[-dBo/dP+(dRs/dP*(Bg-RvBo)/(1-RsRv))]	Sg/Bg[-dBg/dP+(dRv/dP*(Bo-RsBg)/(1-RsRv))]	C_t=(1-Sw)xCoil-gas+SwxCw+Cf
223.7	111.85			
519.7	371.7	0.000957442	0.002084145	2.59E-03
1015.7	767.7	0.00041759	0.000587655	8.58E-04
1548.7	1282.2	0.000246797	0.000195616	3.80E-04
2018.7	1783.7	0.00016977	0.00011174	2.43E-04
2528.7	2273.7	0.000123219	7.00477E-05	1.68E-04
3017.7	2773.2	9.98299E-05	3.25013E-05	1.16E-04
3329.32	3173.51	9.54085E-05	5.08087E-06	8.92E-05
3389.8	3359.56	9.75425E-05	4.11706E-06	9.02E-05
3444.8	3417.3	9.57982E-05	4.5472E-06	8.91E-05
3506.7	3475.75	9.21031E-05	3.45761E-06	8.50E-05
3554.8	3530.75	9.13835E-05	3.94769E-06	8.48E-05
3609.8	3582.3	8.89284E-05	3.88029E-06	8.27E-05
3664.8	3637.3	8.63615E-05	3.81582E-06	8.05E-05
3719.8	3692.3	8.40118E-05	3.81327E-06	7.85E-05
3774.8	3747.3	8.18914E-05	3.7601E-06	7.66E-05
3829.8	3802.3	7.9351E-05	3.74849E-06	7.44E-05
3884.8	3857.3	7.77476E-05	3.75545E-06	7.31E-05
3939.8	3912.3	7.41229E-05	5.10575E-06	7.12E-05
4014.7	3977.25	7.24238E-05	2.43568E-06	6.74E-05
4049.8	4032.25	7.10054E-05	3.7344E-06	6.73E-05
4104.8	4077.3	6.79335E-05	3.82728E-06	6.48E-05
4159.8	4132.3	6.55874E-05	3.90711E-06	6.29E-05
4214.8	4187.3	6.31191E-05	3.93913E-06	6.08E-05

Continued on next page

Continued from previous Page [Estimation of Compressibility from fluid properties for Fluid Sample A]

Pressure (Psia)	Pmean	So/Bo[-dBo/dP+(dRs/dP*(Bg-RvBo)/(1-RsRv))]	Sg/Bg[-dBg/dP+(dRv/dP*(Bo-RsBg)/(1-RsRv))]	C_t=(1-Sw)xCoil-gas+SwxCw+Cf
4269.8	4242.3	6.00065E-05	3.98988E-06	5.82E-05
4324.8	4297.3	5.73323E-05	4.10977E-06	5.60E-05
4379.8	4352.3	5.37592E-05	4.26065E-06	5.31E-05
4434.8	4407.3	5.04425E-05	3.18647E-06	4.94E-05
4474.45	4454.625	4.90318E-05	0	4.55E-05
4474.7	4474.575	4.041E-05	0	3.81E-06
4544.8	4509.75	3.17881E-05	0	3.08E-05
4599.8	4572.3	3.09542E-05	0	3.01E-05
4654.8	4627.3	3.1007E-05	0	3.02E-05
4709.8	4682.3	3.03686E-05	0	2.96E-05
4764.8	4737.3	2.97269E-05	0	2.91E-05
4819.8	4792.3	2.9082E-05	0	2.85E-05
4874.8	4847.3	2.91286E-05	0	2.86E-05
4929.8	4902.3	2.91754E-05	0	2.86E-05
4984.8	4957.3	2.78286E-05	0	2.75E-05
5039.8	5012.3	2.78713E-05	0	2.75E-05
5094.8	5067.3	2.79141E-05	0	2.75E-05
5149.8	5122.3	2.7257E-05	0	2.70E-05
5204.8	5177.3	2.6597E-05	0	2.64E-05
5259.8	5232.3	2.66359E-05	0	0.00E+00

Formula for two-phase compressibility is given as:

$$C_t = (1-S_w)\left\{\frac{S_g}{B_g}\left[\frac{-dB_g}{dP}+\left(\frac{dR_v}{dP}\left(\frac{B_o-R_sB_g}{1-R_sR_v}\right)\right)\right]+\frac{S_o}{B_o}\left[\frac{-dBo}{dP}+\left(\frac{dR_s}{dP}\left(\frac{B_g-R_vB_o}{1-R_sR_v}\right)\right)\right]\right\}+S_wC_w+C_f$$

Estimated storativity ratio for A-K1-N0-D0: $(OCth)_{12}$ 4BU=2.5 and $(OCth)_{12}$ 6BU=3.2

Water compressibility (C_w) = 2.70E-06 1/psia; Irreducible Saturation (S_{wc}) = 0.15; Rock compressibility C_f= 3.40E-06 1/psia

Storativity ration for A-K_1-N_0: $(\emptyset C_t h)_{1/2}$ 4BU=2.5 and $(\emptyset C_t h)_{1/2}$ 6BU=3.2

APPENDIX D

D-1 Estimation of Compressibility from fluid properties for Fluid Sample B

Pressure (Psia)	P_{mean}	So/Bo[-dBo/dP+(dRs/dP*(Bg-RvBo)/(1-RsRv))]	Sg/Bg[-dBg/dP+(dRv/dP*(Bo-RsBg)/(1-RsRv))]	Ct=(1-Sw)xCog+SwxCw+Cf
15	7.5			
100	57.5	0.006548536	0.067472055	4.44E-02
500	300	0.001303004	0.003563985	2.93E-03
900	700	0.000493058	0.0004366	5.72E-04
1300	1100	0.000308718	0.000177608	3.06E-04
1700	1500	0.000218991	9.71424E-05	2.04E-04
2100	1900	0.000166182	6.11503E-05	1.50E-04
2150	2125	0.000171348	3.98848E-05	1.41E-04
2200	2175	0.000165097	4.01193E-05	1.37E-04
2250	2225	0.000158896	4.0364E-05	1.34E-04
2300	2275	0.000152743	4.06198E-05	1.30E-04
2350	2325	0.000146636	4.08872E-05	1.26E-04
2400	2375	0.000140575	4.11671E-05	1.23E-04
2450	2425	0.000134559	4.14602E-05	1.20E-04
2500	2475	0.000128587	4.17674E-05	1.16E-04
2550	2525	0.000137678	2.86836E-05	1.14E-04
2600	2575	0.000132864	2.88628E-05	1.11E-04
2650	2625	0.000128097	2.90486E-05	1.08E-04
2700	2675	0.000123374	2.92412E-05	1.06E-04
2750	2725	0.000118696	2.94411E-05	1.03E-04
2800	2775	0.000011406	2.96486E-05	1.00E-04
2850	2825	0.000109466	2.9864E-05	9.76E-05
2900	2875	0.000104913	3.00877E-05	9.50E-05

Continued on next page

Continued from previous Page [Estimation of Compressibility from fluid properties for Fluid Sample B]

Pressure (Psia)	P_{mean}	So/Bo[-dBo/dP+(dRs/dP*(Bg-RvBo)/(1-RsRv))]	Sg/Bg[-dBg/dP+(dRv/dP*(Bo-RsBg)/(1-RsRv))]	Ct=(1-Sw)xCog+SwxCw+Cf
2950	2925	0.000113478	2.14025E-05	9.49E-05
3000	2975	0.000109603	2.15544E-05	9.27E-05
3050	3025	0.000105772	2.17109E-05	9.04E-05
3100	3075	0.000101983	2.18723E-05	8.83E-05
3150	3125	9.82352E-05	2.20388E-05	8.61E-05
3200	3175	9.45274E-05	2.22105E-05	8.40E-05
3250	3225	9.08584E-05	2.23877E-05	8.19E-05
3300	3275	8.72271E-05	2.25705E-05	7.98E-05
3350	3325	9.3169E-05	1.64099E-05	7.97E-05
3400	3375	8.98899E-05	1.64278E-05	7.77E-05
3450	3425	8.66523E-05	1.64468E-05	7.58E-05
3500	3475	8.34547E-05	1.64669E-05	7.39E-05
3550	3525	8.02958E-05	1.64882E-05	7.20E-05
3600	3575	7.71742E-05	1.65107E-05	7.02E-05
3650	3625	7.40887E-05	1.65343E-05	6.83E-05
3700	3675	7.10379E-05	1.65592E-05	6.65E-05
3750	3725	8.18029E-05	1.08368E-05	6.95E-05
3800	3775	7.92392E-05	9.253E-06	6.71E-05
3850	3825	7.6669E-05	7.64321E-06	6.45E-05
3900	3875	7.40915E-05	6.0064E-06	6.20E-05
3950	3925	7.15061E-05	4.34149E-06	5.95E-05
4000	3975	6.89118E-05	2.64734E-06	5.69E-05
4050	4025	6.6308E-05	9.22781E-07	5.43E-05
4100	4075	0	5.64046E-09	1.40E-05
4150	4125	0	3.79114E-09	1.40E-05
4200	4175	0	2.54939E-09	1.40E-05
4250	4225	0	1.28583E-09	1.40E-05

Continued on next page

Continued from previous Page [Estimation of Compressibility from fluid properties for Fluid Sample B]

Pressure (Psia)	P_{mean}	So/Bo[-dBo/dP+(dRs/dP*(Bg-RvBo)/(1-RsRv))]	Sg/Bg[-dBg/dP+(dRv/dP*(Bo-RsBg)/(1-RsRv))]	Ct=(1-Sw)xCog+SwxCw+Cf
4300	4275	0	0	1.40E-05
4350	4325	0	0	1.40E-05
4400	4375	0	0	1.40E-05
4450	4425	0	0	1.40E-05
4500	4475	0	0	1.40E-05
4550	4525	0	0	1.40E-05
4600	4575	0	0	1.40E-05
4650	4625	0	0	1.40E-05
4700	4675	0	0	1.40E-05
4750	4725	0	0	1.40E-05
4800	4775	0	0	1.40E-05
4850	4825	0	0	1.40E-05
4900	4875	0	0	1.40E-05
4950	4925	0	0	1.40E-05
5000	4975	0	0	1.40E-05
5050				

Formula for two-phase compressibility is given as:

$$C_t = (1-S_w)\left\{\frac{S_g}{B_g}\left[\frac{-dB_g}{dP}+\left(\frac{dR_v}{dP}\left(\frac{B_o-R_sB_g}{1-R_sR_v}\right)\right)\right]+\frac{S_o}{B_o}\left[\frac{-dBo}{dP}+\left(\frac{dR_s}{dP}\left(\frac{B_g-R_vB_o}{1-R_sR_v}\right)\right)\right]\right\}+S_wC_w+C_f$$

Estimated storativity ratio for Fluid B (Well-DST15): $(\emptyset Cth)_{1/2}$ 2BU= 2.10; $(\emptyset Cth)_{1/2}$ 7BU=1.67 and $(\emptyset Cth)_{1/2}$ 16BU=2.52

Water compressibility (C_w) = 2.64E-05 1/psia; Irreducible Saturation (S_{wc}) = 0.40; Rock compressibility C_f= 3.40E-06 1/psia

Storativity ratio for Fluid B (Well-DST15): $(\emptyset C_th)_{1/2}$ 2BU= 2.10;$(\emptyset C_th)_{1/2}$ 7BU=1.67 and $(\emptyset C_th)_{1/2}$ 16BU=2.52

APPENDIX E

E-1 Conversion of Beta (β) from cm^{-1} to Forchheimer unit

$$\beta \approx \frac{0.005}{k^{0.5}\phi^{5.5}S^{5.5}} \text{ cm}^{-1} \text{ unit}$$

Estimating βin Forchheimer unit

$$\beta\left[F\left(\frac{1.01325E6cm^{-1}}{F}\right)\right] \approx \frac{0.005}{\phi^{5.5}\left[K\left(mD\frac{cm^2}{mD}\right)\right]^{0.5} 3.141533065E-6}$$

$$\beta\left[F\left(\frac{cm^{-1}}{F}\right)\right] \approx \frac{0.005}{1.01325E6 \times 3.141533065E-6 \times \phi^{5.5}\left[K\left(mD\frac{cm^2}{mD}\right)\right]^{0.5}}$$

$$\beta\left[F\left(\frac{cm^{-1}}{F}\right)\right] \approx \frac{0.005}{3.183158378 \times \phi^{5.5}\left[K\left(mD\frac{cm^2}{mD}\right)\right]^{0.5}}$$

$$\beta\left[F\left(\frac{cm^{-1}}{F}\right)\right] \approx \frac{1.570766957E-3}{\phi^{5.5}\left[K\left(mD\frac{cm^2}{mD}\right)\right]^{0.5}}$$

Therefore,

$$\beta = \frac{1.570766957E-3}{\phi^{5.5}K^{0.5}} \qquad \text{Forchheimer unit (Field unit)}$$

Appendix F

F-1 Formation petrophysical log properties-Well-3

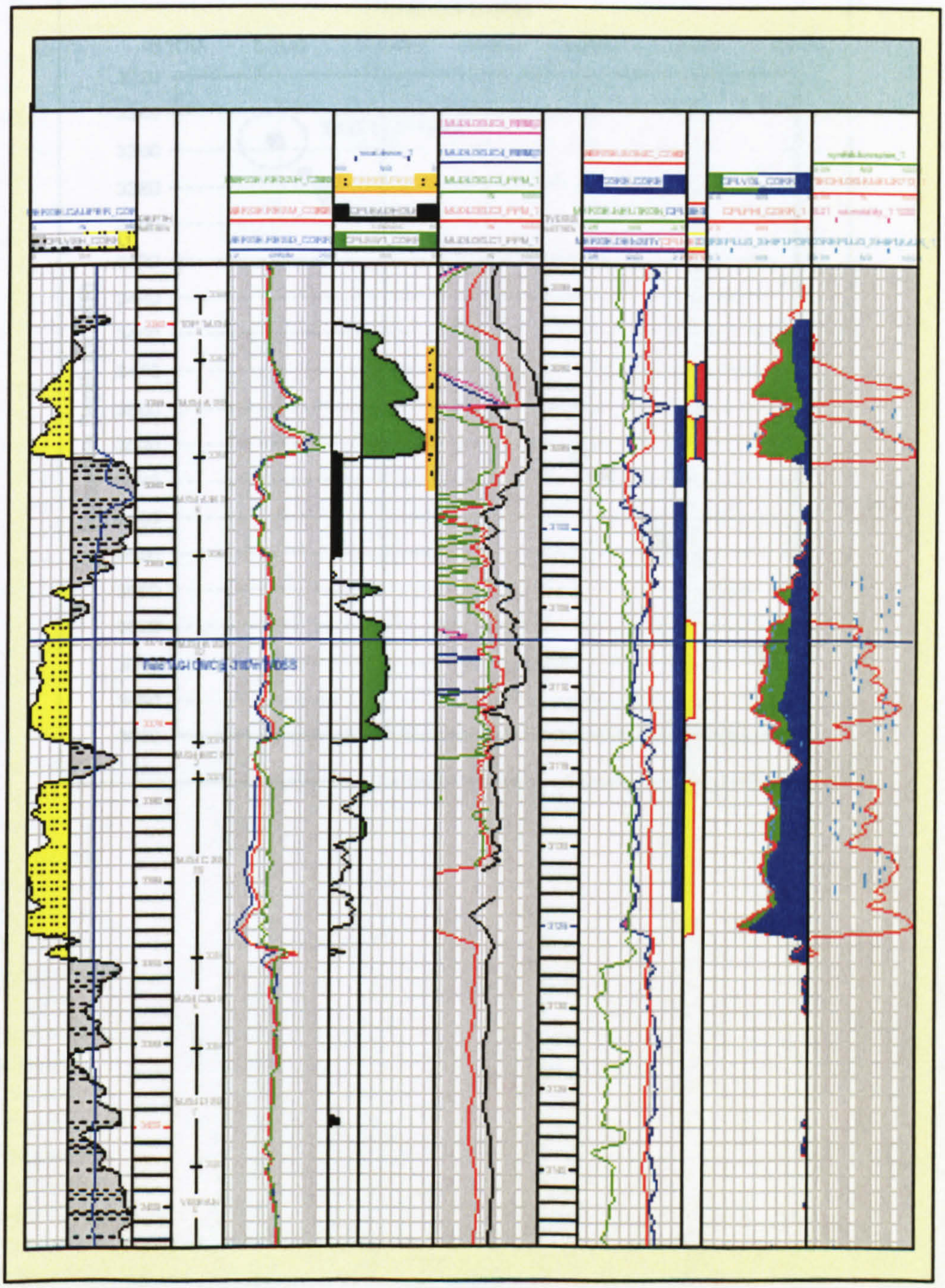

F-2 RFT from Well-3

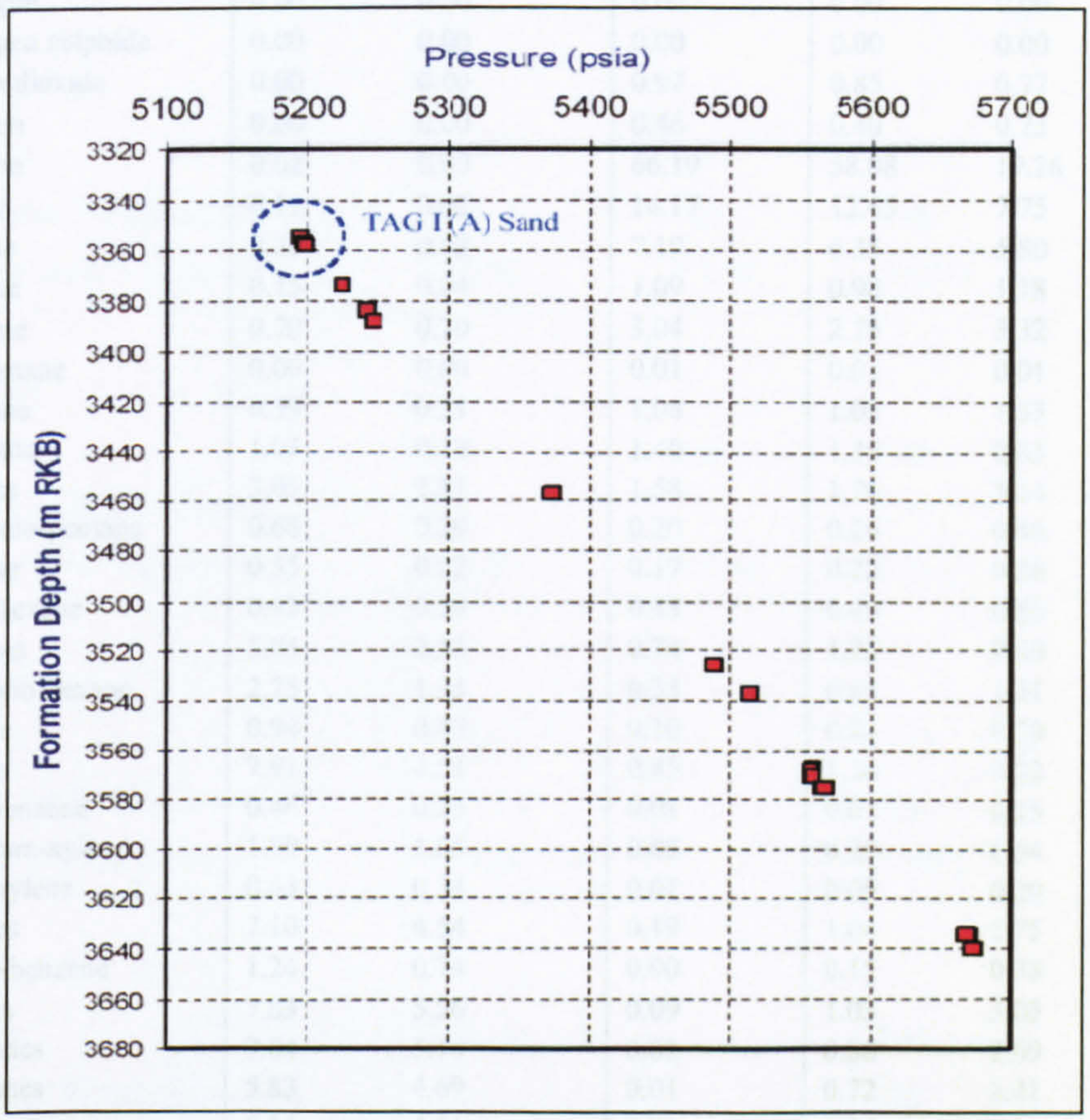

F-3 Composition of Well-3

Component	Flashed Liquid		Flashed Gas	Reservoir Fluid	
	Mole %	Weight %	Mole %	Mole %	Weight %
Hydrogen	0.00	0.00	0.00	0.00	0.00
Hydrogen sulphide	0.00	0.00	0.00	0.00	0.00
Carbon dioxide	0.00	0.00	0.97	0.85	0.77
Nitrogen	0.00	0.00	0.46	0.40	0.23
Methane	0.02	0.00	66.19	58.08	19.26
Ethane	0.11	0.02	14.17	12.45	7.75
Propane	0.36	0.08	7.19	6.35	5.80
i-Butane	0.15	0.04	1.09	0.98	1.18
n-Butane	0.70	0.20	3.04	2.75	3.32
neo-Pentane	0.00	0.00	0.01	0.01	0.01
i-Pentane	0.59	0.21	1.08	1.02	1.53
n-Pentane	1.05	0.38	1.40	1.36	2.03
Hexanes	3.05	1.31	1.58	1.76	3.14
Me-Cyclo-pentane	0.68	0.29	0.20	0.26	0.46
Benzene	0.55	0.22	0.17	0.22	0.36
Cyclo-hexane	0.93	0.39	0.43	0.49	0.85
Heptanes	5.05	2.53	0.74	1.25	2.60
Me-Cyclo-hexane	2.75	1.35	0.35	0.65	1.31
Toluene	0.94	0.43	0.10	0.21	0.39
Octanes	7.91	4.51	0.45	1.36	3.22
Ethyl-benzene	0.46	0.24	0.01	0.07	0.15
Meta/Para-xylene	1.99	1.05	0.05	0.29	0.64
Ortho-xylene	0.63	0.34	0.01	0.09	0.20
Nonanes	7.10	4.54	0.19	1.04	2.75
Tri-Me-benzene	1.24	0.74	0.00	0.15	0.38
Decanes	7.83	5.56	0.09	1.03	3.05
Undecanes	7.04	5.16	0.02	0.88	2.69
Dodecanes	5.83	4.69	0.01	0.72	2.41
Tridecanes	5.16	4.51	0.00	0.64	2.31
Tetradecanes	4.19	3.97	0.00	0.51	2.02
Pentadecanes	3.85	3.96	0.00	0.47	2.02
Hexadecanes	3.20	3.54	0.00	0.39	1.81
Heptadecanes	2.67	3.16	0.00	0.33	1.61
Octadecanes	2.43	3.04	0.00	0.30	1.55
Nonadecanes	2.17	2.84	0.00	0.27	1.45
Eicosanes	1.83	2.51	0.00	0.22	1.28
Heneicosanes	1.63	2.37	0.00	0.20	1.21
Docosanes	1.45	2.21	0.00	0.18	1.13
Tricosanes	1.26	2.00	0.00	0.15	1.02
Tetracosanes	1.12	1.85	0.00	0.14	0.94
Pentacosanes	1.07	1.85	0.00	0.13	0.94
Hexacosanes	0.87	1.55	0.00	0.11	0.79
Heptacosanes	0.81	1.51	0.00	0.10	0.77
Octacosanes	0.75	1.45	0.00	0.09	0.74
Nonacosanes	0.67	1.34	0.00	0.08	0.68
Triacontanes	0.61	1.26	0.00	0.07	0.64
Hentriacontanes	0.55	1.18	0.00	0.07	0.60
Dotriacontanes	0.48	1.07	0.00	0.06	0.55
Tritriacontanes	0.46	1.04	0.00	0.06	0.53
Tetratriacontanes	0.41	0.96	0.00	0.05	0.49
Pentatriacontanes	0.37	0.89	0.00	0.04	0.45
Hexatriacontanes plus	5.03	15.66	0.00	0.62	7.99
Totals	100.00	100.00	100.00	100.00	100.00

F-4 Hydrocarbon Analysis of Bottomhole Sample 1-12 to C36+: Well-3

Calculated Properties	Flashed Liquid	Flashed Gas	Reservoir Fluid
C7 plus			
Mole %	93.97	2.82	13.99
Molecular Weight (g mol-1)	209	100	190
Density at 60°F (g cm-3)	0.8332	0.7483	0.8235
C11 plus			
Mole %	55.91	0.03	6.88
Molecular Weight (g mol-1)	271	153	271
Density at 60°F (g cm-3)	0.8655	0.7940	0.8653
C20 plus			
Mole %	19.37		2.37
Molecular Weight (g mol-1)	422		422
Density at 60°F (g cm-3)	0.9058		0.9058
C36 plus			
Mole %	5.03		0.62
Molecular Weight (g mol-1)	625		625
Density at 60°F (g cm-3)	0.9375		0.9375

Calculated whole sample properties

Average mole weight (g mol-1)	201	27.0	48.3
Real relative density		0.938	
(Air = 1.000 at 14.73 psia and 60°F)			

NB : 0.00 means less than 0.005.

F-5 Match of Tuning Experiment for Fluid Sample from Well-3

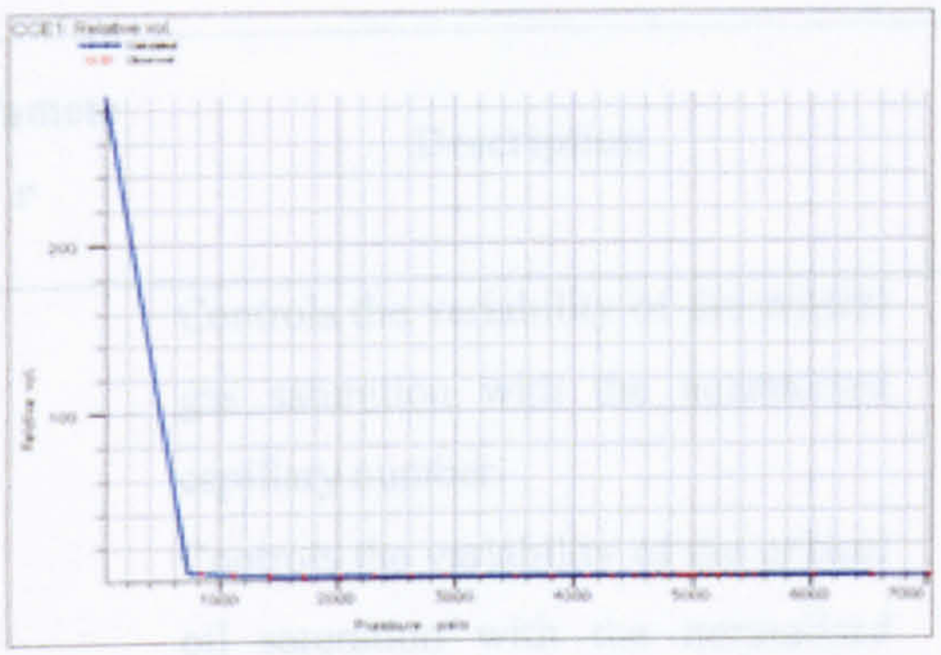

CCE for Relative Volume Fluid W3

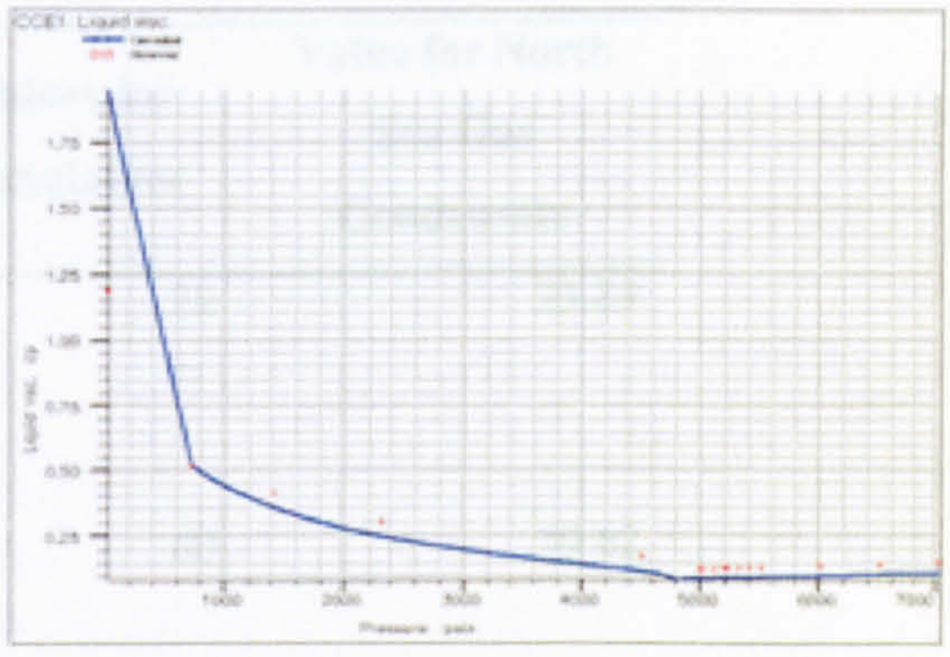

CCE for Liquid viscosity: Fluid W3

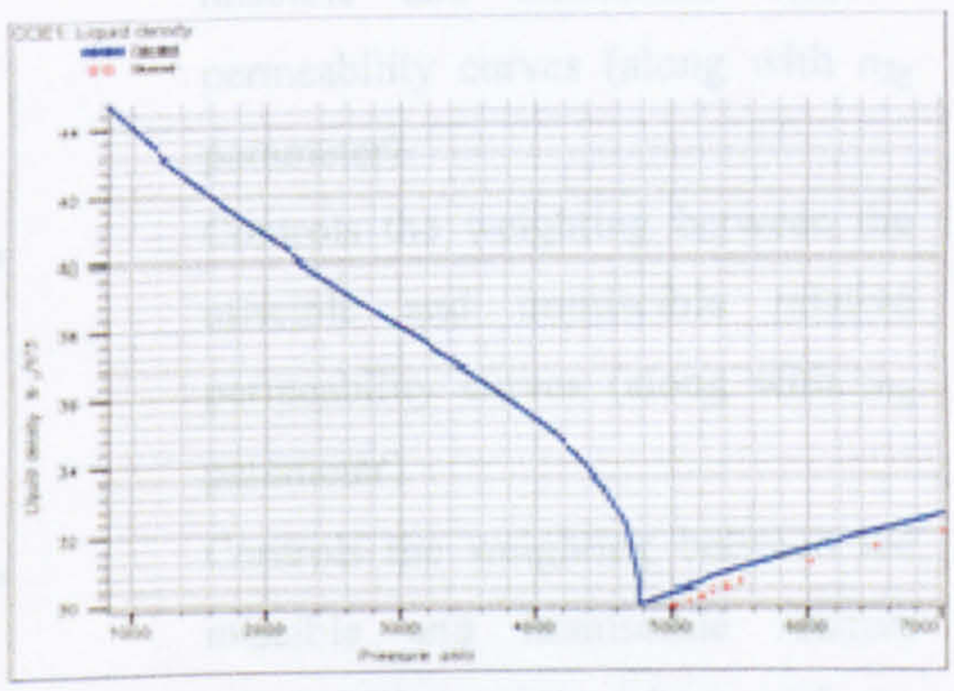

CCE Liquid Density: Fluid W3

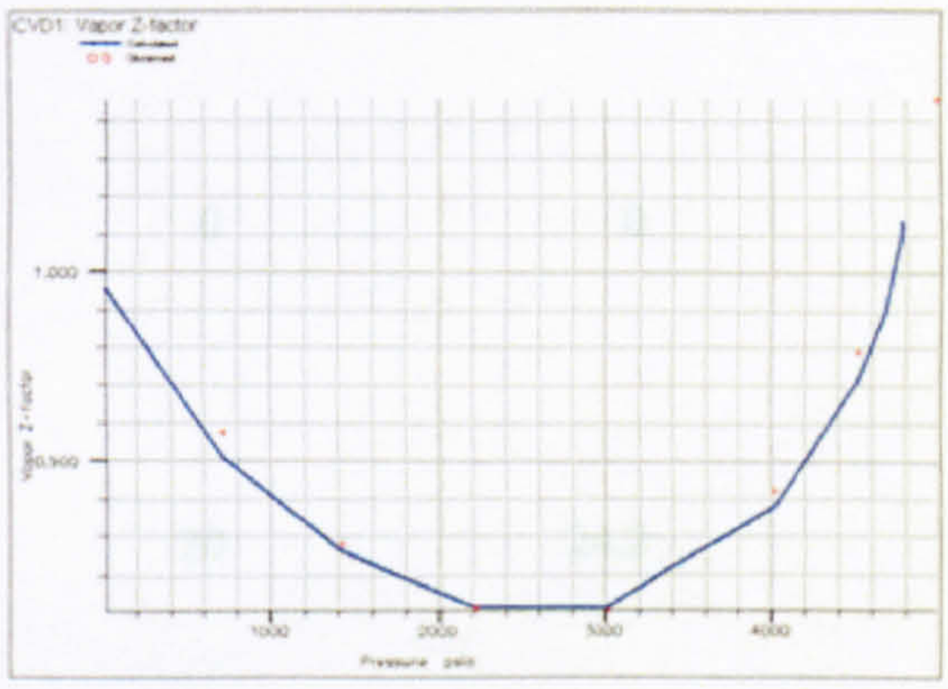

CVD for Vapour Z factor: Fluid W3

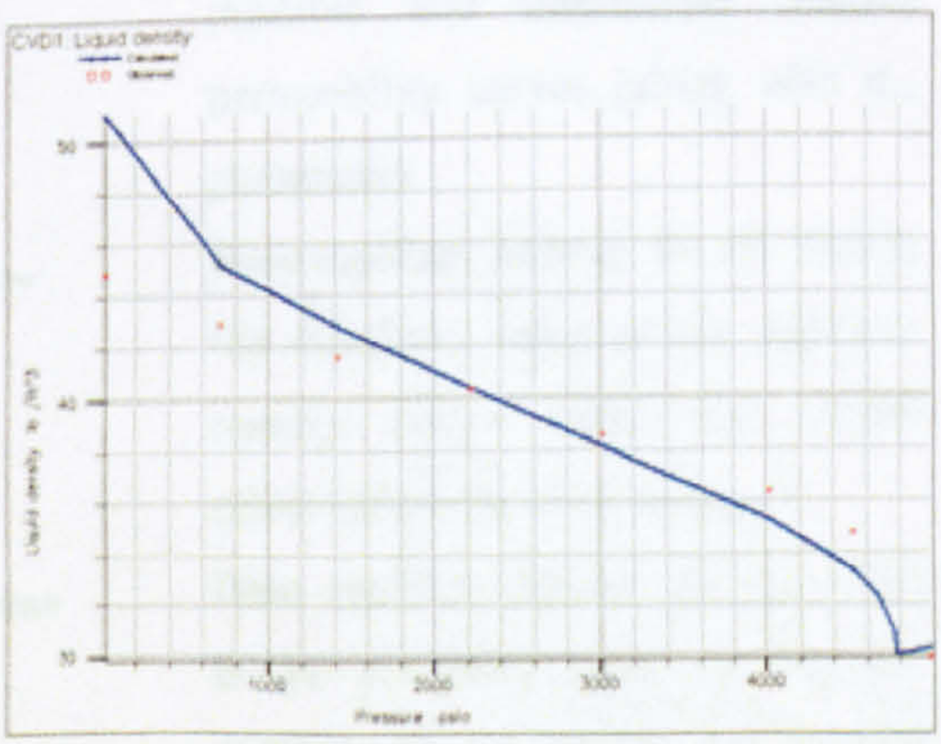

CVD for Liquid Density factor: Fluid W3

F-6 Input Parameter for Velocity-Dependent Relative Permeability Model: Well-3

Parameter	Description	Values for Simulation	Value for North Sea Gas Condensate
m_g	Controls the variability of the critical gas saturation with the normalised capillary number	23	23.89
m_o	Controls the variability of the critical oil saturation with the normalised capillary number	60	79.62
n_{1g}	Controls the weighting between the miscible and immiscible relative permeability curves (along with n_{2g} parameter)	5	6.23
n_{2g}	Controls the weighting between the miscible and immiscible relative permeability curves (along with n_{1g} parameter)	0	0
n_{1o}	Controls the weighting between the miscible and immiscible relative permeability curves (along with n_{2o} parameter)	20	24.2
n_{2o}	controls the weighting between the miscible and immiscible relative permeability curves (along with n_{1o} parameter)	0	0
N_{cbo}	Base capillary number for oil. This is the threshold value of the capillary number above which the VDRP effect is thought to be active.	1.0E-06	1.0E-06
$N_{cbg.n}$	Base capillary number for gas. This is the threshold value of capillary number above which the VDRP effect is thought to be active	1.0E-06	1.0E-06